STUDY ON HEAT AND MASS TRANSFER OF INTERNALLY HEATED LIQUID DESICCANT REGENERATION FOR SOLAR-ASSISTED AIR-CONDITIONING SYSTEM

QI RONGHUI

Ph.D

The Hong Kong Polytechnic University

2013

The Hong Kong Polytechnic University

Department of Building Services Engineering

Study on Heat and Mass Transfer of Internally Heated Liquid Desiccant Regeneration for Solar-assisted Air-conditioning System

Qi Ronghui

A thesis submitted in partial fulfillment of the requirements for the

Degree of Doctor of Philosophy

June, 2013

CERTIFICATE OF ORIGINALITY

I hereby declare that this thesis is my own work and that, to the best of my knowledge and belief, it reproduces no material previously published or written, nor material that has been accepted for the award of any other degree or diploma, except where due acknowledgement has been made in the text.

____________________ (Signed)

______Qi Ronghui________ (Name of student)

Department of Building Services Engineering

The Hong Kong Polytechnic University

Hong Kong SAR, China

June, 2013

ABSTRACT

Abstract of thesis entitled: Study on heat and mass transfer of internally heated liquid desiccant regeneration for solar-assisted air-conditioning system

Submitted by: Qi Ronghui

For the degree of: Doctor of Philosophy

At The Hong Kong Polytechnic University in June, 2013.

Traditional air-conditioning (AC) systems have several limitations, such as the poor humidity control, energy wastage, and the creation of wet surfaces that become breeding grounds for mildew and bacteria. The problems become more serious in warm or hot and humid climates. As an energy-saving and environmental-friendly alternative, the Liquid Desiccant AC System (LDAC) becomes a good solution to remove the extra moisture of air by desiccant absorption. Its major energy required is low-grade thermal energy, such as the solar thermal energy provided by solar collectors. To improve the system performance and to utilize the thermal energy efficiently, the internally cooled/heated dehumidifier/regenerator has drawn many attentions recently. Furthermore, due to its low possibility of droplets carried by the air and low pressure drop, the falling film dehumidifier/regenerator has become a promising type for liquid/gas contacting. As most energy consumes for regenerating

the solution, this research focused on the regeneration process. However, the study of literature shows that previous investigations on this system were insufficient.

This research aimed to investigate the heat and mass transfer of the internally heated liquid desiccant regeneration experimentally and theoretically by considering the change of wetted area, film thickness and mass transfer coefficient under the insufficient wetting conditions, and to develop a 3-D theoretical model for predicting the fluid characteristics and system performance more accurately. Based on the buildings' load profiles and weather data of Hong Kong, the dynamic operation performance of the whole Solar-assisted LDAC (SLDAC) was evaluated, and several system optimizations were proposed and studied to reduce the energy consumption.

The wetted area and mass transfer coefficient are key parameters affecting the system performance, and also indispensable parameters in the system evaluation. By testing a single channel internally heated regenerator, the influencing factors of wetted area, film thickness and mass transfer coefficient were investigated experimentally, as well as their effects on the mass transfer performance. The film sizes under different operation conditions were recorded by a thermal camera, and LiCl was chosen as the solution. The increase of wetted area benefits the mass transfer performance greatly, while the performance reduced with the increasing film thickness. The initial width of the film was affected by the solution distributor thickness most greatly, and changed significantly with the contact angle and solution mass flow rate. When the surface was pre-wetted to be hydrophilic, the initial width dramatically increased, and the contraction of falling film was effectively weakened. The film contraction was also reduced with the higher working surface temperature, while it was aggravated with the increase of solution temperature. Furthermore, under insufficient wetting conditions, the mass transfer coefficient decreased with the increase of solution mass flow rate. It also decreased with the increase of solution distributor thickness and solution temperature, and increased with the increasing air mass flow rate. Additionally, the contact angle of solution was experimentally found to be determined by the surface roughness, solution concentration and temperature.

Based on the experimental results, a theoretical model with an analytical solution was developed for accurately calculating the wetted area of the internally heated regeneration, by describing the transverse flow caused by the Marangoni effect. The model could be divided into three parts, including the model for initial wetted width, the model for contact angle and the model for contraction distance along the flow direction. The calculation results were compared with the experimental ones with small average errors of 8.8%, 12.3% and 10.8% respectively for the three parts. The film thickness, plate surface temperature, and solution temperature, concentration and contact angle were numerically found to significantly influence the wetted area. An empiric formula of mass transfer coefficient was also developed with the multi linear regression, showing an acceptable error compared with the experiments results.

Then, a 3-D model with a numerical solution of internally heated regeneration was developed for describing the heat and mass transfer among the air, solution and extra hot water in all three directions. The insufficient wetting condition, the change of film thickness due to the mass transfer and film deformation, and the effect of contact angle were considered. The calculation results were compared with those obtained by other existing theoretical models, and showed a closer trend to the experimental data, especially in the prediction of the influences of solution mass flow rate, hot water temperature and working plate surface temperature. The parameter study showed that the thickness of solution distributor has the greatest impact on the moisture removal rate, and the change of inlet solution temperature results in the most obvious change of the regeneration efficiency. The changes of solution concentration and hot water temperature also significantly affect the system performance. Though the increase of mass flow rates of solution, air and hot water benefits the mass transfer, the effect of excessive mass flow rates are slight. Although the model was developed based on the internally heated regeneration, it is also suitable for the adiabatic system by introducing of plate surface temperature. Furthermore, the new model could also be applied for the dehumidification process considering the similar heat and mass transfer mechanism between the dehumidification and regeneration of liquid desiccant.

Though the 3-D model could predict the system performance more accurately, it is complex and inconvenient for investigating the dynamic operation performance. A simplified numerical model of internally cooled/heated dehumidifier/regenerator was developed accordingly by defining three kinds of effectiveness, i.e. enthalpy effectiveness, moisture effectiveness, and temperature effectiveness. With the multi linear regression, the statistical correlations of effectiveness were developed by using the heat and mass driving forces and other related parameters as variables. The results were compared with those by the 3-D model with an acceptable error of 14.7% for dehumidifiers and 7.1% for regenerators.

With the simplified model, to evaluate the operation performance and energy potential, a dynamic simulation of the SLDAC was conducted by employing four nested iteration calculation loops. As a case study, the AC load profiles of three typical commercial buildings in Hong Kong were investigated. Results showed that only up to 12.5% of electricity consumption could be saved annually if the cooling tower is used as the only cooling source of the dehumidifier due to the high dehumidification demand in summer. But, by introducing an extra cooling coil for the dehumidifier and a heat exchanger for the regenerator, the electricity saving percentage could be significantly improved to 36.7%. Additionally, the energy consumption of solar-assisted systems is affected by the installation area of solar thermal collectors, and the energy saving could not be achieved until the area is larger than the minimum required value. For our case, the minimum installation area is 0.22

m^2/kW (peak load) for office buildings.

Academically, this research contributes a 3-D theoretical model for predicting the heat and mass transfer of falling film liquid desiccant system more accurately by employing the newly developed models for the wetted area and mass transfer coefficient during the dehumidification/regeneration process. It provides a useful reference for researchers and engineering to improve the wetted area, to enhance the heat and mass transfer, and to optimize the system performance. Furthermore, as the falling liquid film are widely employed in many industrial applications, such as vertical condensers, film evaporators, absorption towers and heat exchangers, our results could also be applied for the performance evaluation and optimization in these areas.

Keywords: heat and mass transfer; internally heated regeneration; liquid desiccant, air-conditioning system; wetted area; film thickness; mass transfer coefficient; experiment; model; simulation; operation performance

PUBLICATIONS DURING PHD STUDY

Journal papers arising from the thesis:

R.H. Qi, L. Lu, H.X. Yang, F. Qin, Investigation on wetted area and film thickness for falling film liquid desiccant regeneration system, Applied Energy, 112 (2013) :93–101.

R.H. Qi, L. Lu, H.X. Yang, F. Qin, Influence of plate surface temperature on the wetted area and system performance for falling film liquid desiccant regeneration system, International Journal of Heat and Mass Transfer, 64 (2013) :1003–1013.

R.H. Qi, L. Lu, H.X. Yang, Development of simplified prediction model for internally cooled/heated liquid desiccant dehumidification system, Energy and Buildings, 59 (2013): 133-142.

R.H. Qi, L. Lu, H.X. Yang, Quick performance prediction for internally cooled/heated liquid desiccant dehumidification system, Building Services Engineering Research & Technology, Published online before print, December 12, 2012, doi: 10.1177/0143624412468890.

R.H. Qi, L. Lu, H.X. Yang, Investigation on air-conditioning load profile and energy consumption of desiccant cooling system for commercial buildings in Hong Kong, Energy and Buildings, 49 (2012): 509-518.

R.H. Qi, L. Lu, H.X. Yang, Impact of climate change on ventilation load and energy use of air conditioning systems in buildings of Hong Kong, International Journal of Low-Carbon Technologies, 7 (4)(2012): 303-309.

R.H. Qi, L. Lu, H.X. Yang, Investigation on load profile of commercial buildings in Hong Kong, ZHONGNAN DAXUE XUEBAO(ZIRAN KEXUE BAN), 43 (1) (2012): 246-251 (In Chinese).

Conference papers arising from the thesis:

R.H. Qi, L. Lu, H.X. Yang, Y.M. Luo, Investigation on contact angle of LiCl for liquid desiccant air-conditioning system, Accepted by The 5th International Conference on Applied Energy 2013, Pretoria, South Africa, Paper ID: 494

R.H. Qi, L. Lu, H.X. Yang, A simplified model for counterflow internally cooled/heated dehumidifier/regenerator in liquid desiccant dehumidification system, A paper presented and collected by Healthy Buildings 2012, 8 - 12 July 2012, Brisbane, Australia.

R.H. Qi, L. Lu, H.X. Yang, Impact of climate change on ventilation load in buildings of Hong Kong, A paper presented and collected by 4th International Symposium on Heat Transfer and Energy Conservation, 6-9 January 2012, Guangzhou, China, Paper ID: TC-012

R.H. Qi, L. Lu, H.X. Yang, Investigation on Load Profile of Commercial Buildings in Hong Kong, A paper presented and collected by International Conference of WREC-Asia & SuDBE2011, 28-31 October 2011, Chongqing, China, Paper ID: DCW092

Other relevant publications:

R.H. Qi, C.Q. Tian, S.Q. Shao, M.S. Tang, L. Lu, Experimental investigation on performance improvement of electro-osmotic regeneration for solid desiccant, Applied Energy, 88 (8) (2011): 2816-2823

H.X. Yang, Y.T. Li, L. Lu, R.H. Qi, First order multivariate Markov chain model for generating annual weather data for Hong Kong, Energy and Buildings, 43 (9) (2011): 2371-2377

ACKNOWLEDGEMENTS

This thesis is the result of three-year hard work, and I feel deeply that my dissertation could not be completed without the help and support of many people. It is my pleasure to take this opportunity to express my grateful acknowledgements to all of them for their great help during my PhD study.

First and foremost, I would like to express my most sincere appreciation and gratitude to my chief supervisor, Dr. Lu Lin, for her expert guidance, continuous encouragement and constant support during my three years of the PhD study for my PhD. Her caring, encouraging and guidance provide an excellent foundation for my current thesis.

I wish to express my warm and grateful thanks to my co-supervisor, Prof. Yang Hongxing, for his insightful view and great help on my research and life. His constructive suggestions regarding my papers and thesis manuscripts were very much appreciated.

Furthermore, I would like to express my thanks to all the members in the Renewable Energy Research Group for their help and company during the PhD study, in particular Ms. Luo Yimo, Ms. Qin Fei and Mr. Peng Jinqing. I also would like to give my appreciation to the staffs and the technicians of the department.

I also appreciate The Hong Kong Polytechnic University and Hong Kong SAR Government for providing me with the Hong Kong PhD Fellowship. Without this financial support, it would not be possible to complete my PhD study in Hong Kong.

My heartfelt appreciation goes to my beloved parents, Prof. Qi Yaoguang and Ms. Liu Liping, for their love, patience and support, and the valuable advises and help on my experiment design and installation. Prof. Qi's inspiration and scientific attitude on research also deeply affects me.

Finally, I would like to give my special thanks to my husband, Mr. Huang Yu. He not only gives his fully support in my life, but also in my research work. Without him, I would never make it so far.

TABLE OF CONTENTS

CERTIFICATE OF ORIGINALITY I

ABSTRACT II

PUBLICATIONS DURING PHD STUDY VIII

ACKNOWLEDGEMENTS XI

TABLE OF CONTENTS XIII

LIST OF FIGURES XIX

LIST OF TABLES XXVII

NOMENCLATURE XXIX

CHAPTER 1 1

INTRODUCTION 1

1.1 Background of Liquid Desiccant Air-Conditioning System 1

1.2 Background of Solar-assisted Air-conditioning System 3

1.3 Objectives of the Thesis 5

1.4 Organization of the Thesis 8

CHAPTER 2 11

LITERATURE REVIEW AND RESEARCH METHOD 11

2.1 Introduction 11

2.1.1 Principles of desiccant dehumidification and regeneration 11

2.1.2 Potential application of LDAC in buildings 14
2.2 Regeneration methods for liquid desiccant air-conditioning system 15
2.2.1 Packed Regenerator 15
2.2.2 Open Cycle Solar Collector/regenerator 17
2.2.3 Electrodialysis Regenerator 20
2.2.4 Internally-heated Regenerator 22
2.2.5 Summary 24
2.3 Solution distribution methods for liquid desiccant air-conditioning system 25
2.4 Model and solutions for internally heated/cooled liquid desiccant system 26
2.4.1 Ren's Model and numerical solution 29
2.4.2 Mesquita's Model and numerical solution 35
2.4.3 Discussion 39
2.5 Investigation on wetted area of liquid desiccant system and other applications 43
2.5.1 Researches of wetted area of liquid desiccant dehumidification/regeneration 44
2.5.2 Researches of wetted area of other applications 45
2.6 Investigation of mass transfer coefficient of dehumidification/regeneration 47
2.7 Dynamic operation performance of SLDAC 52
2.7.1 Load profiles of buildings in Hong Kong 53
2.7.2 Quick prediction model for liquid desiccant systems 55
2.7.3 Dynamic operation performance of SLDAC 57
2.8 Limitations in the past studies 58
2.9 Methodology 60
CHAPTER 3 63

EXPERIMENT INVESTIGATION ON WETTED AREA OF LIQUID DESICCANT REGENERATION 63
3.1 Introduction 63
3.2 Description of experimental bench 64
3.3 Measurement of variables 70
3.4 Results 76
3.4.1 Influences of solution distributor, mass flow rate and concentration 77
3.4.2 Influences of plate surface temperature 82
3.4.3 Influence of solution inlet temperature 88
3.4.4 Influence of pre-wetting of working surface 91
3.4.5 Influencing factors of contact angle 96
3.5 Discussion 100
CHAPTER 4 102
MODEL DEVELOPMENT AND ANALYTICAL SOLUTION FOR WETTED AREA OF INTERNALLY HEATED REGENERATOR 102
4.1 Introduction 102
4.2 Model for Contact Angle 104
4.3 Model for Initial Wetted Width 108
4.4 Model for contraction distance along the flow direction 111
4.4.1 Model development for contraction distance along the flow direction 111
4.4.2 Model development for surface tension on the air/solution interface 116
4.4.3 Discussion 125
4.5 Summary 131

CHAPTER 5 138

EXPERIMENTAL INVESTIGATION ON MASS TRANSFER COEFFICIENT OF LIQUID DESICCANT REGENERATION 138

5.1 Introduction 138

5.2 Research method of mass transfer coefficient 139

5.2.1 Experimental condition 139

5.2.2 Theoretical analysis 141

5.3 Results 144

5.3.1 Influencing factors of mass transfer coefficient 144

5.3.2 Formulas of average overall mass transfer coefficient 151

5.3.3 Discussion 152

5.4 Summary 154

CHAPTER 6 156

3-D MODEL DEVELOPMENT FOR INTERNALLY COOLED/HEATED LIQUID DESICCANT SYSTEM 156

6.1 Introduction 156

6.2 3-D Model for internally cooled/heated liquid desiccant system 157

6.2.1 Governing equations and boundary conditions 160

6.2.2 Required Equations of the model 163

6.2.3 Numerical solution of the model 167

6.3 Verification and Comparison 172

6.4 Simulation result and parameter study 182

6.5 Summary 194

CHAPTER 7 197
MODEL DEVELOPMENT FOR OPERATION PERFORMANCE OF INTERNALLY COOLED/HEATED SLDAC 197
7.1 Introduction 197
7.2 Quick prediction model for internally cooled/heated LDAC 199
7.2.1 Simplified model development 199
7.2.2 Correlation development for three types of effectiveness.. 202
7.2.3 Correlations for ICHDR and Model verification 206
7.3 System modelling of internally cooled/heated SLDAC 212
7.3.1 Description of internally cooled/heated SLDAC 212
7.3.2 Simulation Models of System Components 214
7.3.3 Input and output parameters... 220
7.3.4 Iteration Loops 225
7.3.5 Simulation Procedure 229
7.4 Summary.. 232
CHAPTER 8 234
AIR-CONDITIONING LOAD ANALYSIS AND ENERGY PERFORMANCE OF SLDAC OF BUILDINGS IN HONG KONG.. 234
8.1 Introduction 234
8.2 Air-conditioning load analysis for commercial buildings in Hong Kong 236
8.2.1 Research method of load profile of commercial buildings 237
8.2.2 Annual AC load profiles and reheating ratio 241
8.2.3 Impact of climate change on ventilation load in buildings of Hong Kong 248

8.2.4 Summary 254

8.3 Operation performance of internally cooled/heated SLDAC in Hong Kong 255

8.3.1 Energy performance of internally cooled/heated SLDAC in Hong Kong 256

8.3.2 Problems of SLDAC applied in buildings of Hong Kong 259

8.4 Performance optimization of internally cooled/heated SLDAC in Hong Kong................ 261

8.4.1 Optimization of the addition of extra cooling coil 261

8.4.2 Optimization of the addition of auxiliary heat exchanger.. 266

8.4.3 Other optimization methods.. 270

8.4.4 Discussion 274

8.5 Summary.. 275

CHAPTER 9 278

CONCLUSIONS AND RECOMMENDATIONS FOR FUTURE WORK.............................. 278

9.1 Conclusions of Experimental Investigations 278

9.2 Conclusions of Theoretical Investigations 280

9.3 Conclusions of Numerical Investigations.. 282

9.4 Recommendations for Future Work 284

REFERENCES 286

LIST OF FIGURES

Fig. 2. 1 Flow chart of the desiccant cooling system 12

Fig. 2. 2 Schematic of typical liquid desiccant system 13

Fig. 2. 3 Schematic of the Regeneration Cycle 16

Fig. 2. 4 Schematic of the Direct Solar Collector/Regenerator 18

Fig. 2. 5 Internal Structure of the Solar Collector& Regenerator 18

Fig. 2. 6 Schematic of the electrodialysis regenerator 21

Fig. 2. 7 Schematic of the Internally-heated Regenerator 23

Fig. 2. 8 A differential element 30

Fig. 2. 9 Four different flow arrangements in internally cooled dehumidifier 31

Fig. 2. 10 Numerical model in the dehumidifier 34

Fig. 2. 11 Schematic diagram of the dehumidifier channel with notation 36

Fig. 2. 12 Schematic of grid with thickness change in the desiccant film 39

Fig. 2. 13 Schematic of coordinate system of liquid desiccant system 40

Fig. 2. 14 Simulation results of desiccant temperature during the dehumidification process 41

Fig. 2. 15 A flow chart of the methodology for experimental, theoretical and numerical studies 62

Fig. 3. 1 Schematic of working surface and coordinate system 65

Fig. 3. 2 Experimental design of the single channel liquid desiccant regenerator 67

Fig. 3. 3 Geometry of solution distributor 68

Fig. 3. 4 Figures of (a) Thermal camera imager; (b) Interface of image analysis software; (c) Contact angle goniometer; (d) PID controllers and (e) Laser optical interferometer 73

Fig. 3. 5 Examples of measurement image: (a) Thermal image during the regeneration process; (b) Contact angle and (c) Surface roughness ... 74

Fig. 3. 6 Changing of system performance with solution mass flow rate (a) Wetted area and (b) Moisture removal rate ... 80

Fig. 3. 7 Influencing factors of initial width of falling film (a) Changes with solution mass flow rate and distributor thickness and (b) Changes with solution concentration ... 81

Fig. 3. 8 Average film thicknesses of experiment groups 1-5 ... 82

Fig. 3. 9 Changing of system performance with plate surface temperature: (a) Moisture removal rate and (b) Wetted area ... 84

Fig. 3. 10 Outlet parameters of solution with different plate surface temperature (a) concentration and (b) temperature ... 85

Fig. 3. 11 Initial film width and $\overline{R_w}$ under different plate surface temperatures ... 86

Fig. 3. 12 Distribution of solution surface temperature along the x-axis ... 88

Fig. 3. 13 Changing of moisture removal rate with solution inlet temperature ... 89

Fig. 3. 14 Changing of wetted area with solution inlet temperature ... 90

Fig. 3. 15 Changing of system performance with solution inlet temperature (a) Initial wetted width and (b) Dimensionless hydraulic radius ... 91

Fig. 3. 16 Changing of wetted area with (a) solution inlet temperature and (b) plate surface temperature ... 93

Fig. 3. 17 Changing of initial wetted width with (a) solution inlet temperature and (b) plate surface temperature ... 94

Fig. 3. 18 Dimensionless hydraulic radius along the flow direction in both pre-wetting and dry conditions 94
Fig. 3. 19 Solution contact angle on the working surface under (a) dry condition and (b) pre-wetting condition 95
Fig. 3. 20 Changing of solution contact angle with surface profile roughness parameter 98
Fig. 3. 21 Changing of solution contact angle with solution concentration 99
Fig. 3. 22 Changing of solution contact angle with solution temperature 99
Fig. 4. 1 Comparison between calculation and experimental results of contact angle 106
Fig. 4. 2 Influencing factors of contact angle of LiCl 107
Fig. 4. 3 Comparison of initial width between calculation and experiment result 109
Fig. 4. 4 Influencing factors of initial wetted width during internally heated regeneration process (a) thickness of solution distributor, (b) solution mass flow rate and (c) solution concentration 110
Fig. 4. 5 Schematic of solution falling film and the y-z cross section 113
Fig. 4. 6 Changing of desiccant temperature on the interface with film thickness 118
Fig. 4. 7 schematic of mass transfer between air and liquid desiccant 119
Fig. 4. 8 Changing of parameters with film thickness (a) solution concentration on the interface and (b) equivalent concentration of air 122
Fig. 4. 9 Changing of solution concentration on the interface with (a) solution inlet temperature and (b) air inlet moisture content 123
Fig. 4. 10 Schematic of plate surface temperature during internally heated regeneration process 124
Fig. 4. 11 Comparison of Δx between calculation and experimental results 126

Fig. 4. 12 Influencing factors of Δx during internally heated regeneration process: (a) Plate surface temperature, (b) extra water temperature and (c)air temperature 129

Fig. 4. 13 Influencing factors of Δx during internally heated regeneration process: (a) solution inlet temperature, (b) solution inlet concentration, (c)air moisture content and (d) film thickness 129

Fig. 4. 14 Changing of Δx with solution contact angle and ε 130

Fig. 4. 15 Comparison of boundary of falling film between calculation and experimental results 132

Fig. 4. 16 Comparison of wetted area under different plate surface temperature between calculation and experimental results 133

Fig. 4. 17 Comparison of $\overline{R_w}$ between calculation and experimental results 134

Fig. 5. 1 Changing of system performance of G. 1 and 2 with the solution mass flow rate: (a) moisture removal rate, (b) wetted area and (c) mass transfer coefficient 147

Fig. 5. 2 Changing of system performance of G. 2 and 3 with the solution mass flow rate: (a) moisture removal rate, (b) wetted area and (c) mass transfer coefficient 148

Fig. 5. 3 Changing of system performance of G. 4 with the solution mass flow rate: (a) moisture removal rate, (b) wetted area and (c) mass transfer coefficient 149

Fig. 5. 4 Changing of mass transfer coefficient with plate surface temperature 150

Fig. 5. 5 Changing of mass transfer coefficient with air mass flow rate 151

Fig. 5. 6 Comparison of mass transfer coefficient between calculation and experimental results 152

Fig. 5. 7 Comparison of mass transfer coefficient between experimental results and previous simulation results 153

Fig. 6. 1 Schematic of one channel with different flow patterns of internally cooled/heated dehumidifier/regenerator........ 159

Fig. 6. 2 Geometry of one channel with notation 160

Fig. 6. 3 Schematic of simulation nodes along the flow direction........ 167

Fig. 6. 4 Schematic of an individual control element 168

Fig. 6. 5 Flow chart of numerical solution of 3-D model 172

Fig. 6. 6 Comparison between calculation results with 3-D model and experimental results.... 173

Fig. 6. 7 Comparison of experimental results, simulation results with 3-D model and with Khan’s model under different solution mass flow rate 175

Fig. 6. 8 Comparison of experimental results, simulation results with 3-D model and with Khan’s model under different water inlet temperature........ 176

Fig. 6. 9 Comparison of experimental results, simulation results with 3-D model and with Khan’s model under different solution inlet temperature........ 177

Fig. 6. 10 Comparison between simulation results with 3-D model and with Khan’s model in pre-wetting and dry conditions........ 178

Fig. 6. 11 Comparison between simulation results with 3-D model and with Khan’s model with different solution inlet concentration 179

Fig. 6. 12 Comparison between simulation results with 3-D model and with Khan’s model with (a) different air inlet temperature and (b) different air mass flow rate 180

Fig. 6. 13 Comparison between simulation results with 3-D model and experimental results: (a) film thickness along the flow direction; (b) thermal image of solution surface temperature in the experiment and (c) simulated solution surface temperature 181

Fig. 6. 14 Distribution of solution temperature during the internally heated regeneration process in (a) y-z section cross and (b) x-y plate.. 184

Fig. 6. 15 Distribution of solution concentration during the internally heated regeneration process in (a) y-z section cross and (b) x-y plate.. 185

Fig. 6. 16 Influence of solution mass flow rate on (a) moisture removal rate and (b) regeneration efficiency.. 186

Fig. 6. 17 Influence of solution inlet temperature on (a) moisture removal rate and (b) regeneration efficiency... 187

Fig. 6. 18 Influence of solution inlet concentration on (a) moisture removal rate and (b) regeneration efficiency... 188

Fig. 6. 19 Influence of hot water temperature on (a) moisture removal rate and (b) regeneration efficiency.. 189

Fig. 6. 20 Influence of hot water mass flow rate on (a) moisture removal rate and (b) regeneration efficiency... 189

Fig. 6. 21 Influence of air mass flow rate on (a) moisture removal rate and (b) regeneration efficiency.. 190

Fig. 6. 22 Influence of air inlet temperature on (a) moisture removal rate and (b) regeneration efficiency.. 191

Fig. 6. 23 Influence of air inlet moisture content on (a) moisture removal rate and (b) regeneration efficiency... 191

Fig. 6. 24 Influence of solution distributor thickness on (a) moisture removal rate and (b) regeneration efficiency 192

Fig. 7. 1 Comparison of six outlet parameters between prediction and simulation results 211

Fig. 7. 2 Comparison of composite errors between prediction and simulation results 212

Fig. 7. 3 Schematic diagram of system components of SLDAC 215

Fig. 7. 4 Schematic diagram of the links of the fluid temperatures 224

Fig. 7. 5 Iteration loops used in the simulation of SLDAC 228

Fig. 7. 6 Flow chart of the simulation procedure 231

Fig. 8. 1 Annual average external dry-bulb temperature from 1950 to 2007 240

Fig. 8. 2 Total air-conditioning load per area of three typical commercial buildings 243

Fig. 8. 3 Annual proportion of latent load for three commercial buildings 244

Fig. 8. 4 Proportions of load components in hotel and office buildings 245

Fig. 8. 5 Change of cooling ventilation load from 1950 to 2007 249

Fig. 8. 6 Vl and Vs in daytimes and nighttimes from 1950 to 2007 250

Fig. 8. 7 Annual cooling load of the hotel building per area from 1950 to 2007 251

Fig. 8. 8 Annual sensible and latent cooling load in daytimes and nighttimes 251

Fig. 8. 9 Change trend of (a) Electricity Consumption and (b) CO2 emission from 1950 to 2007 252

Fig. 8. 10 Annual average moisture content and RH of outdoor air from 1950 to 2007 253

Fig. 8. 11 Annual primary energy consumption of CVCS and LDAC 257

Fig. 8. 12 Annual electricity consumption of CVCS and LDAC 258

Fig. 8. 13 Energy saving percentages of LDAC with different solar collector areas 259

Fig. 8. 14 Comparison between the required dehumidification rate and actual one by LDAC .. 260

Fig. 8. 15 Schematic diagram of optimized SLDAC: Case 1 264

Fig. 8. 16 Monthly electricity consumption of the chiller in CVCS, LDAC and optimized LDAC 265

Fig. 8. 17 Annual primary energy consumption of CVCS, LDAC and optimized LDAC 1 265

Fig. 8. 18 Energy saving percentages of optimized SLDAC with different installed solar collector areas 266

Fig. 8. 19 Schematic diagram of optimized SLDAC: Case 2 268

Fig. 8. 20 Annual primary energy consumption of CVCS, optimized LDAC 1 and 2 269

Fig. 8. 21 Energy saving percentage of two optimized SLDAC with different installed solar collector areas 269

Fig. 8. 22 Schematic diagram of optimized SLDAC: Case 3 272

Fig. 8. 23 Schematic diagram of optimized SLDAC: Case 4 273

Fig. 8. 24 Annual primary energy consumption of CVCS, optimized LDAC 2, 3 and 4 274

LIST OF TABLES

Table 2. 1 Summary of experiments of previous research 48

Table 2. 2 Summary of experiments of previous research 49

Table 2. 3 Summary of mass transfer coefficient by different formulas 51

Table 3. 1 Summary of the measured parameters 68

Table 3. 2 Summary of the max measurement error 75

Table 3. 3 Experimental conditions of internally heated regeneration 78

Table 3. 4 Outlet parameters (selected) of internally heated regeneration 79

Table 3. 5 Experimental conditions of internally heated regeneration 83

Table 3. 6 Experimental conditions for different solution inlet temperature 88

Table 3. 7 Experimental conditions for different solution inlet temperature 92

Table 5. 1 Experimental conditions of internally heated regeneration 145

Table 6. 1 Values of maximum second derivative of variables 193

Table 7. 1 Summary of influencing parameters (including the changing range and initial value) 203

Table 7. 2 Significance Test for Linear Regression 207

Table 7. 3 Assumptions of individual component 220

Table 7. 4 Assumptions of initial parameters of working fluids 221

Table 7. 5 Summary of input and output variables of each component 222

Table 8. 1 Floor layouts and building façade of hotel building 237

Table 8. 2 Summary of weather data and simulation design variables of commercial buildings238

Table 8. 3 Comparison of related researches 241

Table 8. 4 Summary of reheat ratio in three typical buildings.. 247

Table 8. 5 Increasing rate and load change rate of external air temperature and moisture 254

NOMENCLATURE

A	area	m^2
A_w	wetting area	m^2
A_c	area of the collector	m^2
a	thermal diffusivity	m^2/s
a_D	mass transfer coefficient	$kg/m^2\ s$
a_H	heat transfer coefficient between desiccant and air	$kW/(m^2\ ^oC)$
a_w	heat transfer coefficient between desiccant and cooling/heating fluid	$kW/(m^2\ ^oC)$
b	constant parameter	-
c_p	specific heat capacity	$kJ/(kg\ ^oC)$
D	mass diffusion coefficient	m^2/s
D_r	width of rim part	m
E_i	measurement error of individual device	-
$e_{i,\max}$	the maximum relative error of individual parameter	%
H	height of dehumidifier/regenerator	m
h	enthalpy	kJ/kg
h	convection heat transfer coefficient between solution and air	$kW/ (m^2\ ^oC)$
L	length of dehumidifier/regenerator	m
$\dot{m}$	mass flow rate	kg/s

n	number of data	-
Nu	Nusselt number	-
P	individual outlet parameter	-
Q_c	cooling load	kJ
Ra	profile roughness parameter	nm
r_{ab}	latent heat of water vapourization	kJ/kg
R_W	hydraulic radius of falling film	m
$\overline{R_w}$	dimensionless hydraulic radius	-
RH	relative humidity	%
Sh	Sherwood number	-
t	temperature	℃
th	thickness of air channel	m
u	flow velocity in the y axis	m/s
wf	wetting factor	-
W	width	m
Δx	contraction distance of solution film in the transverse direction	m

Greek symbols

α	indicator of whether the plate is uniformly pre-wetted or not	-
$\delta_{\max,i}$	thickness of solution distributor	m

δ	thickness	m
ε	effectiveness	-
γ_s	kinematic viscosity	m^2/s
κ	deformation indicator of solution film	-
λ	thermal conductivity	kW/(m °C)
μ	dynamic viscosity	Pa s
v	flow velocity in the z axis	m/s
θ	contact angle	°
ρ	density	kg/m^3
σ	surface tension	N/m
ω	moisture content	kg/kg
τ	transmissivity of the cover glass upon the solar collector	-
ζ	concentration of desiccant solution	%

Subscripts

a	air
cen	central part
d	design parameter of dehumidifier/regenerator
e	environment
i	initial

I	interface between air and solution
in	inlet
max	maximum
m	moisture
out	outlet
p	plate
rim	rim part
s	solution
f	heating fluid
w	wetting
de	dehumidifier
re	regenerator
da	Outdoor fresh air
hot	hot fluid
cold	cold fluid

CHAPTER 1

INTRODUCTION

1.1 Background of Liquid Desiccant Air-Conditioning System

A person will spend about 70–90% of his/her life time inside the built environment (Liang et al. 2010), so the comfort indoor air quality becomes a big concern. Due to the significant improvement of living and working standards, the number of air-conditioned buildings has been increasing greatly with the increasing energy consumption in these buildings in recent years. However, several limitations of the traditional vapour compression air-conditioning (AC) system has been addressed by researchers (Liu et al. 2006, Yu et al. 2009, Liu et al. 2009, Ge et al. 2011), such as the energy wastage, poor humidity control, and wet surfaces that become breeding grounds for mildew and bacteria. The large energy demand of the AC system highly depends on the fossil fuel, and the over use of chlorofluorocarbons also becomes a potential threat. Furthermore, the increasing frequent breakout of infectious diseases, such as avian influenzas H5N1 and H7N9, has raised the risk of the application of the conventional AC system.

Regarded as an energy-saving and environmental-friendly alternative, the liquid desiccant AC system is an effective solution for handling the sensible and latent loads separately and dealing with the extra moisture with desiccant absorption. The systems can also significantly increase the coefficient of performance (COP) of the combined refrigeration system with vapour compression chillers. To re-concentrate the liquid desiccant for applying it repeatedly, the major energy consumed in the system occurs in the regenerator, which is usually the low-grade thermal energy provided by the waste heat or renewable energy.

To avoid the pollution on the supply air, the carryover of desiccant droplets with the process air is an important concern of the liquid desiccant AC system (Jain et al. 2000). Due to its low possibility of droplets carried by the air and low pressure drop, the falling film dehumidifier/regenerator has become a promising type for effective liquid/gas contacting (Yin et al. 2008). It is also widely used in industrial applications (Ali et al. 2010). In adiabatic liquid desiccant applications, the heat and mass transfer happens only between the air and the desiccant, so the performance decays quickly because of the change of temperature and concentration gradients (Dai et al. 2001). Different from adiabatic applications, the internally cooled/heated dehumidifier/regenerator could maintain the thermal and mass transfer performance as it is cooled or heated synchronously by introducing the extra cooling/heating fluid. In addition, the system dimensions could also be minimized (Yin et al. 2010).

In practical falling film liquid desiccant systems, researchers found that the working surface is usually found to be wetted very incompletely by the desiccant, which would significantly impact the heat and mass transfer between air and solution (Howell et al. 1987, Park et al. 1994, Jain et al. 2000, Pietruschka et al. 2006). The wetted area and film thickness are also indispensable parameters in theoretical models. However, previous investigations on the wetted area, which changes with the operation and design parameters of the falling film system, is limited and insufficient, especially in the area of liquid desiccant dehumidification/regeneration (Liu et al. 2007, Ren et al. 2007, Yin et al. 2008, Yin et al. 2010). This problem would seriously affect the accuracy of the simulation and evaluation for the performance of liquid desiccant AC system.

Furthermore, though there are several widely accepted theoretical models for predicting the performance of internally cooled/heated dehumidification/regeneration, some limitations have been observed in previous researches (Kessling et al. 1998, Mesquita et al. 2006, Ren et al. 2007). The main reason is that the actual dehumidification/regeneration process among the air, desiccant and extra fluid is three-dimensional, which means that the heat and mass transfer occurs in the direction of all three axis. However, most of the existing models only have two dimensions, assuming that either the heat and mass transfer in the thickness direction or the insufficient wetting condition on the working plate could be neglected. These assumptions may cause large deviations between simulation and experiment results.

1.2 Background of Solar-assisted Air-conditioning System

Compared with other forms of energy, the solar energy is clean and the most abundant renewable energy. Solar energy is mainly used to generate electricity or provide thermal energy. Compared with the solar photovoltaic technology, the solar collector has higher conversion efficiency (70-90% of collector, 10-15% of PV), lower initial cost and higher reliability, and is suitable for different domestic and industrial uses. There are many applications of solar water heating system, such as to heat up the air and water, to reheat the overcooled air, to operate heat engines and pumps.

For the purpose of energy saving and environmental friendly, it is natural to make people think of utilizing the solar energy to deal with the heavy energy consumption of air-conditioning system in buildings, especially in the subtropical or tropical areas suffering the long cooling season and enjoying the abundant solar radiation at the same time. Many processes for the transformation of solar radiation in cooling have been investigated in recent years, including the photovoltaic driven vapour compression system, the thermally driven adsorption/absorption chillers, the thermally driven desiccant dehumidification and the steam driven thermo mechanical cycles (Henning, 2007). Considering the system COP, practicability, safety and solar utilization efficiency, the desiccant dehumidification is a promising type of solar-assisted air-conditioning system by handling the air moisture separately and consuming the thermal energy to regenerate the desiccant.

The solar-assisted system mainly consisted of the cooling and dehumidification system, the solar collector, the energy storage system and the auxiliary thermal system. Each sub-system has several energy consuming components such as fans, pumps, chillers and so on. To evaluate the energy consumption and economic efficiency of the whole system, the dynamic operation performance under different load profiles and operation conditions was investigated by many researchers with both numerical and experimental methods (Khalid Ahmed et al. 1997, Rane et al. 2002, Chen et al. 2003, Liu et al. 2006, Li et al. 2007, Alizadeh et al. 2007). However, due to a large number of variables involved in the simulation, limitations of previous researches on operation performance of solar-assisted air-conditioning system were observed, especially for the warm or hot and humid areas.

Additionally, to simulate the operation performance of solar-assisted air-conditioning system, it is necessary to choose a case building in a certain area, to obtain the required climatic data and building's air-conditioning load profiles.

1.3 Objectives of the Thesis

For the air-conditioned buildings, the solar-assisted liquid desiccant air-conditioning system is an effective alternative to the traditional vapour compression technology to approach more accessible, economical, and cleaner air processing while attenuating the reliance on the fossil fuel energy sources. To improve the system performance and to utilize the thermal energy efficiently, the internally cooled/heated dehumidifier/regenerator has drawn many attentions recently. Due to its low possibility of droplets carried by the air and low pressure drop, the falling film dehumidifier/regenerator has become a promising type for liquid/gas contacting. However, the common insufficient wetting condition in practical systems would seriously impact the heat and mass transfer of the falling film liquid desiccant system, and the limitations of previous researches make it difficult to predict the actual wetted area and mass transfer coefficient under different design and operation conditions. Furthermore, as the heat and mass transfer occurs in all three dimensions rather than two dimensions, the existing theoretical models should be improved with the consideration of the effect of wetted area and film thickness to evaluate the system performance more accurately.

Furthermore, by utilizing the solar energy to directly handle the sensible and latent loads separately, the solar-assisted liquid desiccant air-conditioning system is considered as an energy efficient and environment friendly solution. To evaluate the energy potential of the system, the operation performance and energy consumption should be simulated and compared with conventional systems. However, due to the complex of the solar-assisted system, the previous numerical and experimental researches have their limitations, especially for the warm or hot and humid areas where this kind of application is suitable.

Accordingly, this thesis will focus on resolving the existing problems of the falling film liquid desiccant air-conditioning system and prompting the wide application of the solar-assisted system for the cooling load dominated buildings. As most energy consumes for regenerating the solution, this research focused on the internally heated regeneration process. The specific objectives of this thesis are summarized as follows:

(1) To develop a model of the wetted area during the internally heated regeneration process experimentally and theoretically by considering the effects of different operation and design influencing factors, including the thickness of solution distributor, film thickness, the inlet parameters of solution, air and extra heating fluid, the plate surface

temperature and the pre-wetting of working surface. Additionally, an empiric formula for the contact angle of liquid desiccant, which is significant in the model, should be also developed with the experimental results;

(2) To develop a model for the mass transfer coefficient during the regeneration by employing the actual wetted area and mass transfer rate under different operation conditions;

(3) To develop a 3-D theoretical model with a numerical solution of internally heated regenerator for describing the heat and mass transfer among the air, solution and extra hot water in all three directions, by taking the insufficient wetting condition and change of film thickness due to the mass transfer and film deformation into account. The model should be verified with other existing theoretical models and the experimental data;

(4) To develop a computer program of the solar-assisted liquid desiccant air-conditioning system by linking the model of individual component with four nested iteration loops. To simplify the simulation, a quick prediction model for the internally cooled/heated dehumidifier/regenerator should be developed first;

(5) To investigate the energy potential and operation performance of the solar-assisted liquid desiccant air-conditioning system by choosing a typical building in Hong Kong as a case study. According to simulation results, several optimal design methods are provided.

1.4 Organization of the Thesis

For investigating the internally heated regenerator, the wetted area is found to be a key parameter. In Chapter 3, by building and testing a single channel internally heated regenerator, the influencing factors of the wetted area of falling film regeneration were investigated experimentally, as well as their effects on the mass transfer performance. The factors mainly include the thickness of solution distributor, solution mass flow rate, solution concentration, solution temperature, plate surface temperature and the pre-wetting of working surface. Additionally, the influencing factors affecting the contact angle, which was found to play a significant role in the wetted area of falling film, were also experimentally investigated, including the concentration and temperature of desiccant, and the roughness of the surface.

Then, in Chapter 4, based on the experimental results, a theoretical model was developed for accurately calculating the wetted area of the internally heated regenerator. The model could be divided into three parts, including the model for initial wetted width, the model for contact angle and the model for the contraction distance along the flow direction. To verify the model, the results were compared with those obtained from experiments. Furthermore, with this new model, the change of wetted area with different parameters was simulated numerically. For enhancing the mass transfer performance, some suggestions were given to improve the film area of the internally heated liquid desiccant system.

Besides the wetted area, the mass transfer coefficient is the other important parameter for evaluating and predicting the system performance. Therefore, in Chapter 5, the impacts of operation parameters of the coefficient under actual wetted area were investigated experimentally. Based on the test data, an empiric formula was developed with the multi linear regression, and the prediction results were verified with experimental results.

With the experimental and theoretical studies in Chapter 3, 4 and 5, a 3-D model with a numerical solution of internally heated regenerator was developed in Chapter 6 for describing the heat and mass transfer among the air, solution and extra hot water in all three directions. The insufficient wetting condition, the change of film thickness due to the mass transfer and film deformation, and the effect of contact angle were taken into account. The calculation results were compared with both those obtained by other existing theoretical models and the experimental results. Furthermore, with this new model, the system performance was simulated numerically under different operation conditions. A parameter study was conducted to show the effect of different inlet parameters on the moisture removal rate and regeneration efficiency. Though the model was developed based on the regeneration process, the model could also be applied for the dehumidification process with the similar heat and mass transfer mechanism between dehumidification and regeneration.

Though the 3-D model could predict the system performance more accurately, this method is complex which is inconvenient for predicting the dynamic operation performance. In Chapter 7, firstly, a simplified numerical model for the internally cooled/heated dehumidifier/regenerator was developed by defining three kinds of effectiveness, i.e. enthalpy effectiveness, moisture effectiveness, and temperature effectiveness. Based on the numerical simulation and linear regressions, the statistical correlations of three types of effectiveness were developed, by using the heat and mass driving forces and other related parameters as variables. Then, the dynamic simulation model of the whole system was developed, to evaluate the energy potential and operation performance of the solar-assisted liquid desiccant air-conditioning system. By performing the physical characteristics of different components simultaneously, all units could be linked together to form a complete system with four nested iteration loops, and outlet parameters of all fluids and the energy consumption of individual component could be obtained.

To evaluate the energy potential of the system, the buildings in Hong Kong, which are suitable for applying solar-assisted air-conditioning system, were chosen as the case study. The Chapter 8 first investigated the AC load profiles of three typical commercial buildings in Hong Kong, and studied the main problems of the application of traditional AC system in these buildings. Then, the dynamic operation performance and energy consumption of the solar-assisted liquid desiccant air-conditioning system employed in the building was simulated and compared with the conventional system. To reduce the consumption, several optimization methods were proposed and compared.

CHAPTER 2

LITERATURE REVIEW AND RESEARCH METHOD

2.1 Introduction

2.1.1 Principles of desiccant dehumidification and regeneration

The aim of dehumidification/regeneration process is to transfer the water vapour between the process air and the desiccant, including the liquid and solid one. The solution starts to exchange moisture with the surrounding air when they reach the equilibrium. When the vapour pressure at the desiccant surface is less than that of air, the desiccant absorbs or adsorbs moisture. After that, this moisture can be removed from the desiccant to a regeneration process air stream, by heating the desiccant to 50~260℃. The desiccant releases the moisture when its vapour pressure is greater than that of air. The desiccant is then cooled so that it could absorb or adsorb the moisture again.

In a desiccant air-conditioning system, the desiccant circulates between a dehumidifier and a regenerator in the same way as in an absorption/adsorption refrigeration system. The main difference is that the equilibrium temperature of liquid desiccant is determined by the partial pressure of water in the humid air to which the solution is exposed instead of the total pressure. The flow chart of desiccant cooling is shown in Fig. 2.1.

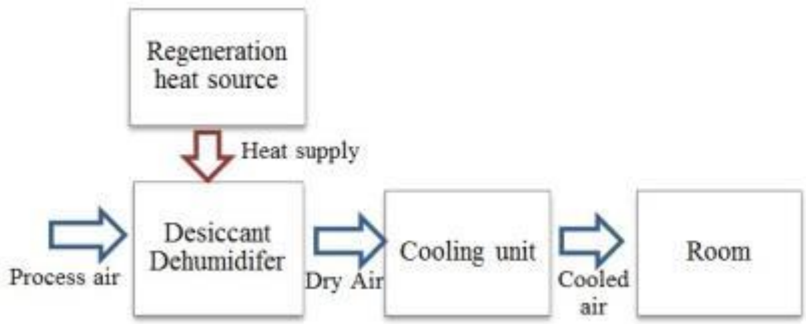

Fig. 2. 1 Flow chart of the desiccant cooling system

The major advantages of desiccant system include: a) only air and water are required as working fluids. CFCs and HCFCs, which may have serious impacts on the ozone layer, are no longer required; b) various kinds of low-grade thermal energy can be applied as heat sources in the regeneration, such as solar energy, waste heat and natural gas; c) with higher COP, the electrical energy requirement could be reduced compared with conventional refrigeration systems; and d) since the desiccant system is operated near the atmospheric pressure, the maintenance and construction are simplified. However, there are some limits of its application: a) the initial cost is higher than the conventional air-conditioning system; b) the condensation heat, which includes the sorption heat, is large and needs more cooling water to take away.

Due to its high dehumidification capacity, thermal energy efficiency and reliability, the Liquid Desiccant Air-Conditioning System (LDAC) has drawn increasing attentions. A typical liquid desiccant system is shown in Fig. 2.2, with two important parts, i.e. dehumidifier and regenerator. In the dehumidifier, the concentrated solution is sprayed or fell down while the ambient or return air is blown across the stream. Then, the diluted solution from the dehumidifier is contacted with the air in the regenerator, where the moisture is taken away from the solution. The resulting concentrated solution is collected and hot humid air is rejected to the ambient. To improve the COP, a recuperative heat exchanger is usually applied to preheat the cool diluted solution from the dehumidifier using the hot concentrated solution from the regenerator.

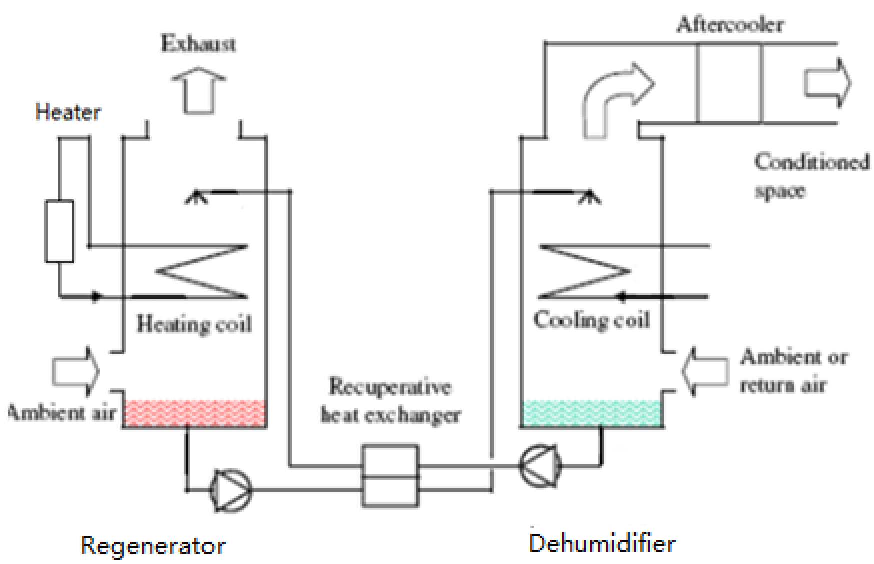

Fig. 2. 2 Schematic of typical liquid desiccant system

For re-concentrating the solution to apply it repeatedly, the major energy consumed in the liquid desiccant system occurs in the regenerator. Therefore, this research focused on the heat and mass transfer in the regenerator, but results can extend to dehumidification process due to the similar heat and mass transfer mechanism of the dehumidification and regeneration of liquid desiccant.

2.1.2 Potential application of LDAC in buildings

Due to the application of conventional vapour compressor AC system, the most common complaint of the indoor thermal comfort is the low indoor air temperature within air-conditioned buildings, especially for buildings in humid climate, such as Hong Kong. Besides, the conventional system has other disadvantages, such as limited humidity control, energy wastage, and occurrence of wet surface which may become a breeding ground for mildew and bacteria (Ge et al. 2011). These problems may be more serious in humid climate. As the low-grade thermal energy could be used to drive the system, the Solar-Assisted Liquid Desiccant Cooling AC system (SLDAC), which could handle the sensible and latent loads separately, is considered as an energy efficient and environment friendly solution.

However, there are limited researches on energy performance of LDAC in buildings. Fong et al. (2011) developed a detailed research on solar-assisted solid desiccant cooling system, and found that the system could save energy in office buildings. However, the solid desiccant could not be applied for thermal storage, which was found to be very important in our research, and the heat loss of the system is higher than that of liquid desiccant system. Li et al. (2010) studied the energy consumption of a liquid desiccant system with solar Collector/Regenerator (C/R) in a typical room. But, they only considered a room rather than the whole building, and no efficient solution for preventing dusts from being blown into the regenerator was proposed.

As a modern society, most commercial buildings in Hong Kong are air-conditioned, and consume significant sector-wide electricity because of the high indoor thermal requirement and local warm and moist weather in the past 20 years. Fortunately, with abundant solar radiation (Hui, 2000), Hong Kong is suitable for developing solar energy applications, and can have good potentials for applying the SLDAC in buildings.

2.2 Regeneration methods for liquid desiccant air-conditioning system

Liquid desiccant regeneration occurs in the regenerator, and the heat is furnished to the desiccant solution with the air being concurrently blown to carry away the moisture desorbed by the heat. Therefore, the regeneration process consumes most energy in the liquid desiccant system, and different structures of the regenerator were investigated by many researchers.

In this section, several current types of regenerators were introduced and discussed, including the packed tower regenerator, open cycle solar collector/regenerator, electrodialysis regenerator and internally heated regenerator. The performances and limitations of these methods were compared.

2.2.1 Packed Regenerator

Providing larger contact surface area and extending contact time between the solution and air, the packed tower regenerator has been researched widely in these years. As shown in the Fig.

2.3, the weak solution is firstly heated by the heat exchanger and then sent into the regenerator. The desiccant was distributed over the packings by spray heads evenly, and the heat and mass transfer occurs in the interspaces of packings. The packings are usually made by polypropylene, which could supply a large specific surface area. The packings have two major types, namely random and regular. The regular packings offer a relative low pressure drop of the air stream, but with high installation expense. The random packed towers could facilitate more mass transfer by providing larger area in a relatively smaller volume.

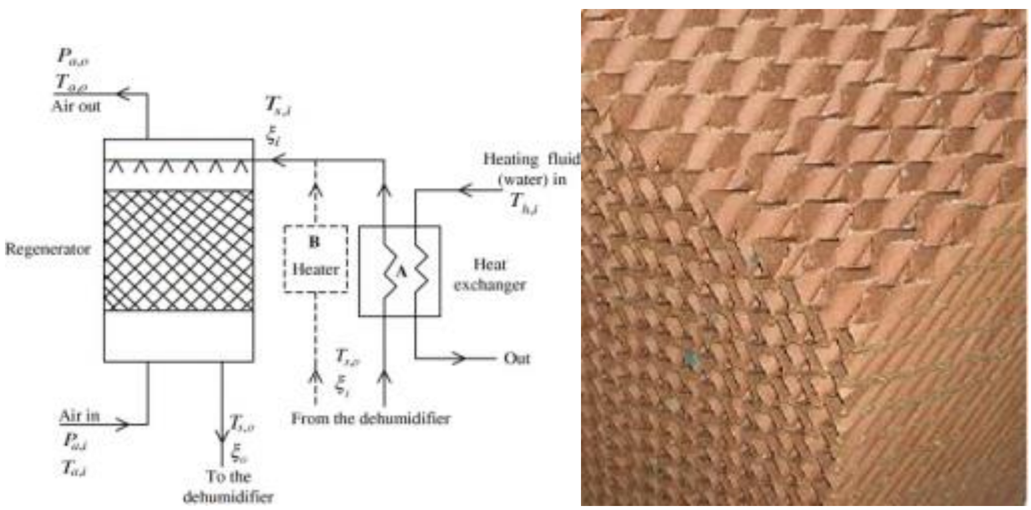

Fig. 2. 3 Schematic of the Regeneration Cycle

Factor and Grossman(Factor and Grossman 1980) compared the experimental and theoretical model of a packed regenerator using LiBr and pre-heated air. Etras et al. (Ertas, Gandhidasan et al. 1994) investigated the influence of different variables on the performance of packed regenerators. Potniz et al. (1996) tested a packed regenerator using random polypropylene and structured packing, and found that the evapouration rate was 130–300% greater than the structured packing bed. Longo (2004) experimentally studied the sorption/desorption liquid desiccant system using H_2O/LiBr and H_2O/KCOOH. Kakabayev (Gandhidasan 2005) investigated the influence of heating source on the evapouration rate of a packed bed regenerator.

The advantages of the packed regenerator include: a) contact surface area and contact time are larger because of the packings, which leads to good regeneration efficiency and smaller volume; and b) the system could easily change to the auxiliary heat resource, such as electricity and natural gas (for renewable energy system).

However, it also has several disadvantages: a) because of the relative high flow rate, the carryout of liquid desiccant droplets is a serious problem, which would lead to air pollution and equipment corrosion; b) the solution temperature drops seriously from the top to bottom of the regenerator; c) the solution is heated indirectly by the heat source, which may cause heat loss.

2.2.2 Open Cycle Solar Collector/regenerator

The open cycle solar collector/regenerator (C/R) is just like a flat plate type of solar thermal collector for water heating. The difference is that its two ends are open to the ambient environment and the working fluid is the liquid desiccant, as shown in Fig. 2.4. The liquid desiccant solution runs down from the top on the surface of the absorber plate. At the same time, the ambient air flows over in the channel between the absorber plate and glass cover. The air and solution can be arranged either as parallel flow or counter flow, as shown in Fig. 2.5.

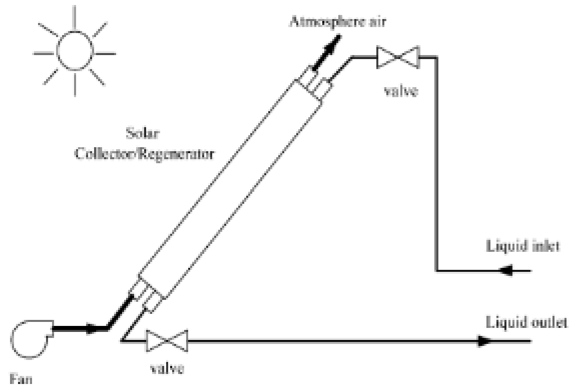

Fig. 2. 4 Schematic of the Direct Solar Collector/Regenerator

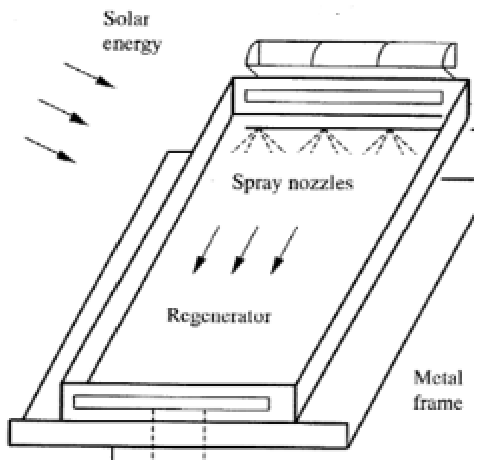

Fig. 2. 5 Internal Structure of the Solar Collector& Regenerator

The concept of the open cycle absorption solar cooling system was first reported in 1969 (Kakabayev A. 1969). Then, Kakabayev et al. (1976)investigated the regeneration of LiCl solution with an open surface, and Alizadeh and Saman (Alizadeh and Saman 2002)investigated a forced parallel flow type solar C/R using LiCl as the absorbent solution and found that the air and solution mass flow rate and climatic conditions have impacts on the regenerator's performance in 2002. Kabeelet al. (2005) investigated the regeneration process using cross flow of the air on the surface of a solar C/R.

According to the previous research, parameters, including the initial concentration, flow rate and temperature of solution, and the velocity, inlet temperature, humidity ratio of regeneration air, and the solar intensity, have been identified as the influential factors on the performance of solar C/R. The air status (especially the air moisture content) and the inlet temperature of the solution have significant effect on the water evapouration rate. Besides, the solar radiation is another important weather variable that dominates the system performance. Latest studies of solar C/R are mostly focused on enhancing the performance by improving the above influential parameters. Peng and Zhang (Peng and Zhang, 2009) introduced an air pre-treatment unit, in which the regeneration air could be pre-heated and dehumidified with a slice of concentrated solution with low temperature, and presented an increment of solution outlet concentration of about 70% by the experiment.

The advantages of the solar C/R include: a) the energy gained is directly used to heat the liquid desiccant without any energy transfer, so the heating efficiency is higher because of low heat loss; b) the solution spray to the environment is reduced because of the lower flow rate; and c) the structure of solar C/R is relatively simple. As the collector and the regenerator are combined together, the occupied area of the structure is small and usually installed on the roof.

However, due to its open structure, the solar C/R also has several inevitable disadvantages: a) the dust of the process air enters the solar C/R easily, so the filter requires frequent maintenance. If the surrounding air is used as the regeneration air, the impact of air conditions, such as pollution and windstorm, should be considered; b) when the solar radiation is insufficient, changing into the auxiliary heat resource is difficult. Similarly, if the radiation is excessive, the heat storage from the system is also difficult; and c) the liquid desiccant, such as LiCl and LiBr, would cause serious corrosion of the absorber plate of the collector, which is usually made by metal.

2.2.3 Electrodialysis Regenerator

The technique of electrodialysis regenerator is based on the transport of ions through selective membranes under the influence of an electrical field. It is a novel regeneration method of the liquid desiccant, and both the concentrated desiccant solution and pure water can be obtained after the regeneration (Li and Zhang 2009). As shown in Fig. 2.6, when a potential difference is applied between electrodes, the cations move towards the cathode, and anions move towards the anode. The cations go through the cation membrane, which have fixed groups with negative charges, and are retained by the anion-exchange membrane. Furthermore, the anions circulate through the anion-exchange membranes, which have fixed groups with positive charges, and are retained by the cation-exchange membranes. This movement produces rise in the ions concentration in some compartments (concentrate compartments) and decrease in the adjacent ones (dilute compartments). So, the concentrated desiccant solution and pure water can be generated by repeating the circles several times. The electrical field required is low voltage DC, which could be supplied by renewable energy such as solar or wind power generation.

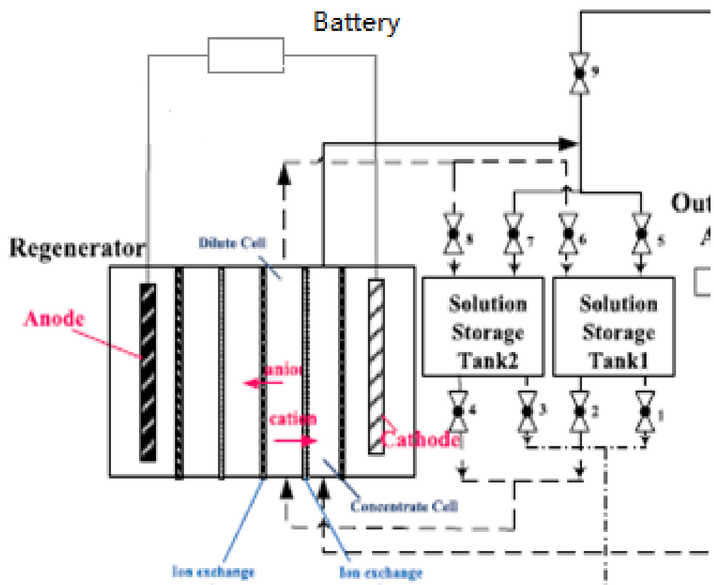

Fig. 2. 6 Schematic of the electrodialysis regenerator

Al-Farayedhi et al. (Al-Farayedhi, Gandhidasan et al. 1999) proposed the RO (reverse osmosis) regeneration method by using membrane technology. The work has been extended (Al-Sulaiman, Gandhidasan et al. 2007) with the analysis of a liquid desiccant based two-stage evapourative cooling system using MFI zeolite membrane, which shows that this new method could be an alternative for liquid desiccant regeneration as most commissioned liquid desiccants are electrolyte solutions. Compared to the conventional thermal regeneration method, this potential method gets rid of the heat supply of the regeneration process, and prevents the droplets of desiccant solution from spraying into the atmosphere.

However, up to now, the technology is far from the practical application as it requires several circles for regenerating the solution and blocks the dehumidification process from continuous operation. The maintenance and initial cost are predicted to be extremely high compared to the conventional regenerator, as well as the energy consumption.

2.2.4 Internally-heated Regenerator

The internally heated regenerator has drawn increasing attentions these years. The regenerator is usually composed by a plate or plate-fin heat exchanger, which contains several passages for the heating fluid, i.e. hot water and air. Between two neighbouring plates, it is recommended to put several layers of fin side by side inter-crossing, which can provide more contacting area for desiccant solution and air. As shown in Fig. 2.7, the desiccant solution enters the internally heated regenerator from the top and contacts with the counter-current air blown from the bottom. The solution would be dispersed to the fins by a distributing unit between the plates due to the gravity. The heating fluid flows horizontally and carries out heat transfer with the crossed air/solution.

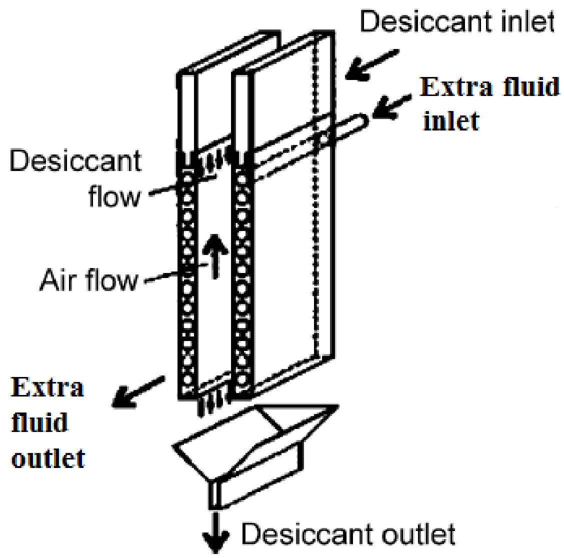

Fig. 2. 7 Schematic of the Internally-heated Regenerator

In the packed regenerator, there is no extra heat transferred into the regenerator, so the desiccant temperature would become lower and lower in the progress of regeneration. This problem could be solved by this internally heated regenerator. As the solution is heated by the hot fluid and regenerated by the unsaturated air at same time, the internally heated regenerators could provide more heat and mass transfer gradients and have the possibility to make regenerators miniaturization. In 1998, Khan and Martinez numerically studied the performance of an internally cooled counter flow absorber using thin plate heat and mass exchanger with LiCl as desiccant, and found that the number of mass transfer units had great effect on the enthalpy and humidity effectiveness(Khan 1998). Khan also investigated an internally cooled dehumidifier using the tube–fin exchanger with the cross-flow air(Khan and Martinez 1998). Then, Jain et al. investigated a liquid desiccant system, which consisted of a packed bed regenerator and an internally cooled dehumidifier(Jain, Dhar et al. 2000). In the same year, Mesquita et al.

investigated the internally cooled dehumidifier which could be used as a solar regenerator(Mesquita, Harrison et al. 2006). In theoretical studies, Ren et al. developed an analytical model for internally cooled or heated system, which was agreed well with the numerical model(Ren, Tu et al. 2007). Recently, Yin et al. presented a model of internally cooled dehumidifier, which was developed with their experimental results (Yinet al. 2008, 2009, and 2010)

This kind of regenerator has many advantages, including: a) the higher efficiency; b) good alternative to avoid the carryout of desiccant droplets as the regenerator could provide comparable performance at low solution flow rate; and c) easy changer-over between solar thermal energy and other auxiliary heat resource, such as electricity and natural gas. The superfluous energy storage can be applied, and d) the system could provide larger heat/mass transfer area per unit volume. Besides, the heating fluid is heated by the supplied energy and then transported into the regenerator with heat loss, but the heat loss is small compared to that of the packed regenerator.

2.2.5 Summary

In this section, several types of regenerators were reviewed and discussed, including the packed tower regenerator, open cycle solar collector/regenerator, electrodialysis regenerator and internally heated regenerator. Generally, the common regenerator could be divided into the two main types. If the heat and mass transfer happens only between the air and desiccant and there is no extra heat transferred into the regenerator, it could be defined as the adiabatic one. The other kind of regenerator, namely the internally heated one, could maintain the surface vapour pressure of desiccant by introducing the extra cooling/heating fluid.

According to the analysis, an ideal regenerator should have several characteristics as below:

a) Large contact surface area and long contact time for air/solution contacting;
b) Low solution flow rate (in the same regeneration efficiency);
c) Suitable for using renewable energy, and changing over to an auxiliary heat resource easily;
d) Small heat loss of the heating resource;

Therefore, the internally heated regenerator with renewable energy supply (e.g. solar thermal energy) can be considered as a better option for the liquid desiccant air-conditioning system in buildings.

2.3 Solution distribution methods for liquid desiccant air-conditioning system

The solution distributor is used to feed the liquid desiccant into the dehumidifier or regenerator, and there are two types, i.e. spray one and falling film one. To avoid the corrosion of ventilation system and potential pollution of indoor air, little carryover of desiccant with the air stream in liquid systems is expected. The air pressure drop through the absorber/desorber should also be reduced.

In the spray type of solution distribution, with the help of nozzles in the spray chamber, the solution has been broken into small droplets to provide a large surface area (Jain et al. 2007). Although the method is well known for its simplicity, low cost and compact size, its efficiency is not high, and other problems exist, including extremely high chance of liquid carryover and large pressure drops on liquid side (Pesaran et al. 1995, Chung et al. 2000).

For the falling film distribution, the desiccant flows down by gravity with a thin film over the vertical surfaces, such as tubes or plates. The entering air contacts with the surface of flowing liquid film. This distribution type has a low pressure drop and low initial cost, and also provides high contact area per unit volume. Such system has been studied widely (Elsarrag 2006, Pietruschka et al. 2006), but the incomplete wetting of the surface with solution film is usually observed in practical applications.

Therefore, due to its low pressure drop and low possibility of solution droplets carried by air, the falling film becomes a promising type for better liquid/gas contacting, attracting wide investigations and industrial applications.

2.4 Model and solutions for internally heated/cooled liquid desiccant system

In traditional adiabatic liquid desiccant systems, only the air and desiccant exchange heat and mass, so the efficiency may reduce quickly because of the latent heat of water vapourization.

With the extra cooling/heating fluid, the internally cooled/heated liquid desiccant system can maintain the low surface vapour pressure on the solution as it is cooled or heated synchronously. This configuration can improve the thermal performance, and miniaturize the system dimensions. It can also reduce the possibility of solution droplets carried by the process air. However, due to the addition of extra fluid, the thermal process of the internally heated regeneration is more complicated, including the heat and mass transfer among the air, solution and fluid. Until now, most researchers investigated on the theoretical model and solution of dehumidifier process. As the fundamental and physical model of dehumidifier and regenerator are similar, this section reviewed the theoretical studies of the heat and mass transfer process of internally cooled dehumidifier.

Although there are several practical types of internally cooled units, i.e. coil-type and plate type exchangers, the composition is usually simplified as the double plate in theoretical models. The distribution method of liquid desiccant is also simplified as the falling film, and the thermal and mass transfer exchange between dispersed desiccant droplets and air is ignored. The development of physical model could be divided into five stages.

1) In the early models of 1980s, the heat and mass transfer resistance between the bulk solution film and its surface was neglected, and the thickness of the solution film was then neglected as well (Queiroz, Orlando et al. 1988; Kessling, Laevemann et al. 1998).

2) In Hellmann and Grossman’s models (Hellmann and Grossman 1995), the heat and mass transfer resistances of solution film were included in the equations. The outer surface of

the tube or plate was assumed to be uniformly wetted and the Lewis factor was assumed to be equal to unity. The conditions of non-unity values of Lewis factor and incomplete surface wetting conditions were not contented.

3) The effect of incomplete surface wetting area was brought into several differential models, such as the model from Peng and Howell (Peng and Howell 1981). The influences of non-unity values of Lewis factor and fin efficiency factor were also considered in a combined parameter. However, compared to experiment results, the simulation results could be correlated with the measured data only if a very small fraction of the surface was supposed to be wetted by the desiccant solution.

4) Recently, the incomplete surface wetting condition was taken into consideration. By comparing the model predictions with the experimental data, Jain et al. (2000) suggested two wetting factors to account for the effect of improper wetting. Then, a general two-dimensional model was developed by Ren et al. (2007), with the consideration of the effect of solution film heat and mass transfer resistances, non-unity values of Lewis factor and incomplete surface wetting conditions. One disadvantage of the models is that the boundary conditions have to be similar for both phenomena, and an isothermal boundary condition has to be accompanied by a uniform concentration condition. Besides, the heat and mass transfer inside the desiccant film and air in the thickness direction was not calculated in these models.

5) Focusing on the un-uniform distribution of thermal properties in the thickness direction, Ali et al. (2004) analyzed the dehumidification process by assuming the constant film thickness. The model was further improvement by Mesquita et al (2006), who introduced variable film thickness along the flow direction due to the moisture movement between the air and liquid desiccant.

Two representative models of the internally cooled dehumidification, i.e. by Ren et al. (2007) and by Mesquita et al. (2006), which are widely accepted and commonly used by researchers, were decrypted in details in the following sections.

2.4.1 Ren's Model and numerical solution

In this steady-state model, firstly, to obtain a set of differential equations of energy and mass conservation, a differential element has been chosen, as shown in Fig. 2.8. A set of differential equations can be obtained by principles of energy and mass balance.

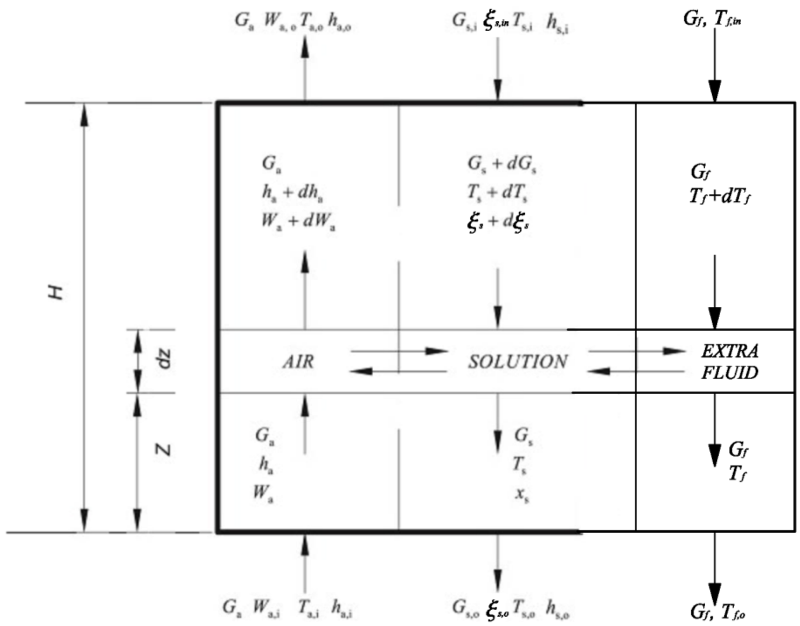

Fig. 2. 8 A differential element

where $\dot{m}$ and t stand for the mass flow rate and temperature, respectively. ζ means the concentration of solution, and W is the moisture content of process air. h stands for the enthalpy The subscripts a, s, f indicate the conditions of air, solution and fluid, respectively.

The four kinds of direction profile are shown in the Fig. 2.9. δ_a and δ_f stand for the flow directions for air and cooling fluid streams, respectively, and are set to equal to ± 1. Besides these profiles, due to its simple structure, the cross-flow profile of cooling fluid is also widely used in practical applications.

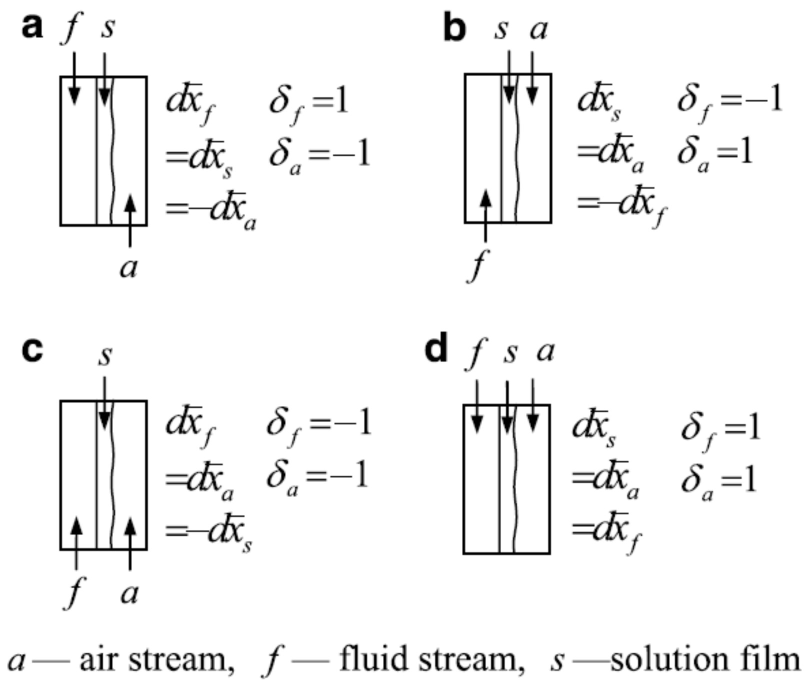

Fig. 2. 9 Four different flow arrangements in internally cooled dehumidifier

Several assumptions are adopted in this model, including: a) The properties of water, desiccant solution and air are considered uniform within the control volume; b) The surface wet ability along the height of exchanger was constant; c) The desiccant and air are assumed to be well mixed in the cross-section area of their flow direction, which means that gradients for each fluid only exist in their respective flow directions; d) The cooling fluid is assumed to distribute evenly and completely on the surface; e) There is no heat transfer to the surroundings; and f) Local wall temperature of the heat exchanger is equal to the local water temperature.

The model consists of mass and energy balance equations. Firstly, the energy balance equations include:

Air: $$\dot{m}_a dh_a = [a_{H,a} A(t_I - t_a) + r_{V,I} a_{D,a} A_w (\omega_I - \omega_a)] dx_a \quad (2.\ 1)$$

Solution-air interface: $$a_{H,s} A(t_s - t_I) = a_{H,a} A(t_I - t_a) + r_{ab,I} a_{D,a} A_w (\omega_I - \omega_a) \quad (2.\ 2)$$

Fluid stream: $$\dot{m}_f c_{pf} dt_f = a_w A_f (t_s - t_f) dx_f \quad (2.\ 3)$$

Whole differential element: $$d(\dot{m}_s h_s) + \dot{m}_f c_{p,f} dt_f \cdot \delta_f + \dot{m}_a dh_a \cdot \delta_a = 0 \quad (2.\ 4)$$

Then the mass balance equations include:

Solution–air interface: $$-a_{D,s} A_w (\zeta_s - \zeta_I) = a_{D,a} A_w (\omega_I - \omega_a) \quad (2.\ 5)$$

Solution: $$\frac{\partial(\dot{m}_s \zeta_s)}{\partial x} = 0 \quad (2.\ 6)$$

Whole differential element: $$d\dot{m}_s = -\delta_a \dot{m}_a d\omega_a \quad (2.\ 7)$$

Where, m refers to the mass flow rate, and h is the enthalpy. The A, A_m and A_f mean the total area, wetting area(contact area between air and solution film) and cooling area(contact area between solution film and cooling fluid) during the dehumidification process. a_w stands for the thermal conductivity between solution film and cooling fluid, and a_H and a_D mean the heat and mass transfer coefficients between solution film and air, respectively. $r_{ab,I} = r_{V,I} - \hat{r}_{W,I}$, is the heat of absorption or desorption at the interface. The subscript a, s, f, I stand for air, solution, extra fluid, and the interface between air and solution.

To complete the equations, several equations are also needed.

For the specific enthalpy of moist air: $$h_a = (c_{p,da} + \omega_a c_{pv})t_a + \omega_a h_{fg,0} \quad (2.8)$$

For the energy change of desiccant solution, the Gibbs equation applies:

$$d(\dot{m}_s h_s) = \dot{m}_s c_{ps} dt_s + \hat{h}_{W,S} d\dot{m}_s \quad (2.9)$$

Eqs. (2.1)- (2.9) should be integrated subjecting to the following boundary conditions:

$$\begin{cases} t_a = t_{a,i}, \omega_a = \omega_{a,i} \ for\ x_a = 0 \\ t_s = t_{s,i}, \zeta_s = \zeta_{s,i}, \dot{m}_s = \dot{m}_{s,i} \ for\ x_s = 0 \\ t_f = t_{f,i} \ for\ x_f = 0 \end{cases} \quad (2.10)$$

The enthalpy and humidity ratio of equilibrium state between air and solution could be calculated with the function of solution temperature and concentration. So, with the numerical integration or analytical solution, the equation set could be solved. Most researchers recommended the first solution by employing the finite difference method due to its higher accuracy and lower complexity. By integrating the Eq. (2.1-10), the governing equations could be solved by the numerical finite difference method with the following steps (Luo et al. 2011).

1) Determining the equations for the Nusselt number and Sherwood number. The heat transfer coefficient for the forced convection can be obtained by:

$$a_H = \frac{Nu \cdot \lambda}{d} \quad (2.11)$$

The mass transfer coefficient can be obtained by the following equations:

$$a_D = \frac{Sh \cdot D}{d} \tag{2. 12}$$

2) Setting the zero point of the z axis, e.g. the bottom of the dehumidifier, and dividing the whole area into n parts averagely. The numerical zones are shown in Fig. 2.10.

.

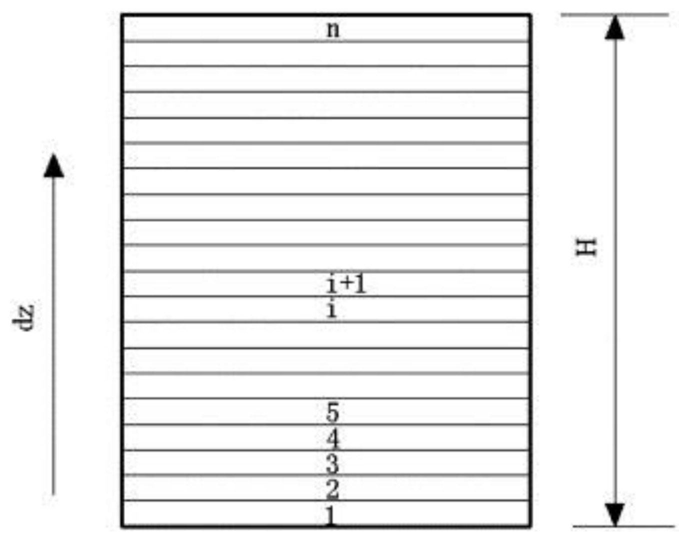

Fig. 2. 10 Numerical model in the dehumidifier

3) With the boundary equations, the parameters of the first microelement could be calculated by Eq. (2.1-12). Then, by repeating the calculation until i = n−1, the inlet or outlet parameters of the dehumidifier can be obtained;

4) Comparing the parameters with previous simulation results until the difference between recent and previous results are smaller enough, e.g. $<10^{-4}$.

2.4.2 Mesquita's Model and numerical solution

In this model, to simplify the mathematical analysis, the following assumptions are made: a) the wall is considered isothermal, i.e., the change of cooling water temperature being neglected; b) the flow is laminar and fully developed for the liquid-desiccant and air, and there is thermodynamic equilibrium at the desiccant/air interface; c) the desiccant flow is smooth (not wavy); d) the physical properties are constant, and no shear forces are exerted on the desiccant by the air; e) the body force in the air, diffusion in the direction of the flow, species thermo-diffusion and diffusion-thermo effects are negligible; and f) the velocity of desiccant in the transverse direction is negligible.

The geometry of the internally cooled dehumidifier channel is presented in Fig. 2.11, where δ_s is the thickness of liquid desiccant falling film and δ_c means the half thickness of air channel. The governing momentum, energy and species equations are listed.

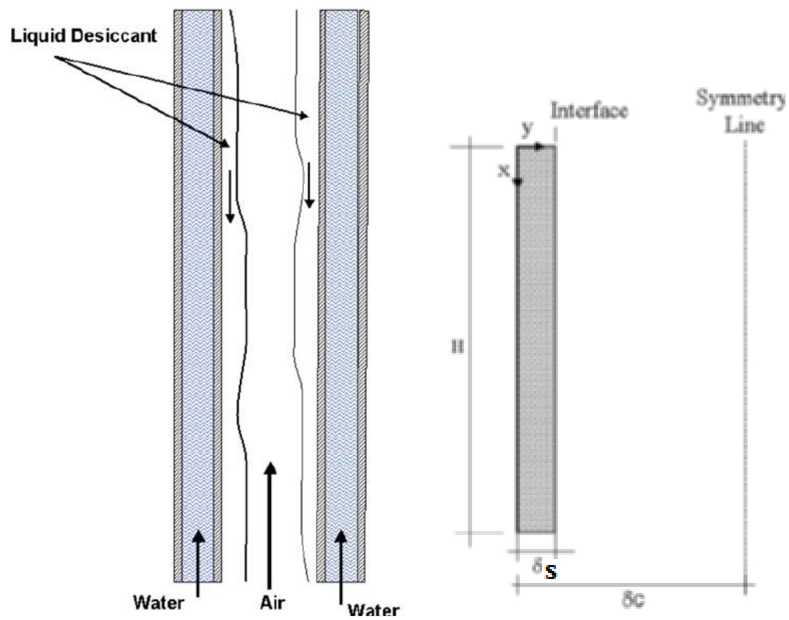

Fig. 2. 11 Schematic diagram of the dehumidifier channel with notation

For the liquid desiccant film:

$$\gamma_s \frac{\partial^2 u_s}{\partial y^2} + \rho_s g = 0$$
$$a_s \frac{\partial^2 t_s}{\partial y^2} = u_s \frac{\partial t_s}{\partial x} \qquad (2.\ 13)$$
$$D_s \frac{\partial^2 \zeta_s}{\partial y^2} = u_s \frac{\partial \zeta_s}{\partial x}$$

For the air:

$$u_a \frac{\partial^2 u_a}{\partial y^2} = \frac{\partial P}{\partial x}$$

$$a_a \frac{\partial^2 t_a}{\partial y^2} = u_a \frac{\partial t_a}{\partial x} \qquad (2.\ 14)$$

$$D_a \frac{\partial^2 \omega_a}{\partial y^2} = u_a \frac{\partial \omega_a}{\partial x}$$

The boundary conditions are:

$$x = 0 \quad t_s = t_{s,in};\ t_a = t_{a,in};\ \zeta_s = \zeta_{s,in};\ \omega_a = \omega_{a,in};$$

$$y = 0 \quad t_s = t_f;\ \frac{\partial \zeta}{\partial y} = 0;\ u_s = 0;$$

$$y = \delta_s \quad t_s = t_a;\ u_s = -u_a;\ \omega_a = \omega_e;\ \frac{\partial u_s}{\partial y} = 0;\ \frac{\partial u_a}{\partial y} = 0; \qquad (2.\ 15)$$

$$y = \delta_c \quad \frac{\partial t_a}{\partial y} = 0;\ \frac{\partial \omega_a}{\partial y} = 0;\ \frac{\partial u_a}{\partial y} = 0;$$

The velocity profile for the liquid desiccant could be obtained by:

$$u_s = \frac{g}{\gamma_s}(\delta_s y - \frac{y^2}{2}) \qquad (2.\ 16)$$

Then, the film thickness could be calculated with the following equation. It should be noticed that the $\overline{m}_s$ means the mass flow rate of desiccant per unit length ($kg/(s \cdot m)$).

$$\delta_s = (\frac{3\overline{m}_s \gamma_s}{\rho_s g})^{1/3} \qquad (2.\ 17)$$

The velocity profile for the air stream can be calculated also through the momentum and continuity equations for the air stream, where the $\bar{m}_a$ is the air mass flow rate per unit length ($kg/(s \cdot m)$).

$$
\begin{aligned}
u_a &= u_s + \frac{dp}{dx}\frac{1}{\mu_a}[\frac{1}{2}(y^2 - \delta_s{}^2) + (\delta_c - y)] \\
\frac{dp}{dx} &= 3\mu_a[\frac{u_s}{(\delta_s - \delta_c)^2} + \frac{\bar{m}_a}{2\rho_a(\delta_s - \delta_c)^3}]
\end{aligned}
\qquad (2.\ 18)
$$

To solve the problem, the energy and species balances at the air/desiccant interface could be calculated by the additional equations.

$$
\begin{aligned}
h_s \frac{\partial t_s}{\partial y} &= h_a \frac{\partial t_a}{\partial y} + \rho_a D_a h_{fg} \frac{\partial \omega_a}{\partial y} \\
\rho_s D_s \frac{\partial \zeta}{\partial y} &= \rho_a D_a \frac{\partial \omega_a}{\partial y}
\end{aligned}
\qquad (2.\ 19)
$$

Where *D* is diffusion coefficient, and ω is the moisture content and *m* is the mass flow rate. γ_s and ρ_s stand for the kinematic viscosity and density of solution respectively, which are decided by the solution temperature and concentration. h is the convective heat transfer coefficient. u is the flow velocity. The subscripts*a, s, f* stand for the air, solution and extra fluid, and *in* and *out* mean the inlet and outlet characteristics.

Therefore, by combining the Eqs. (2.13 – 2.19), the government equations could be solved using the finite-difference method. The differential elements for the numerical simulation are shown in

Fig. 2.12. The interface between the last node in the desiccant side and the first node in the air side was represented by an additional node. This interface node has no volume, but provides heat and mass exchange between the air and desiccant. The number of nodes in the flow direction varied according to the height of the channel.

The variable thickness of falling film along the flow direction due to the change of moisture content of desiccant is considered in this model. To reduce the computational time, the change in the airflow velocity profile was neglected as the changes in film thickness are small.

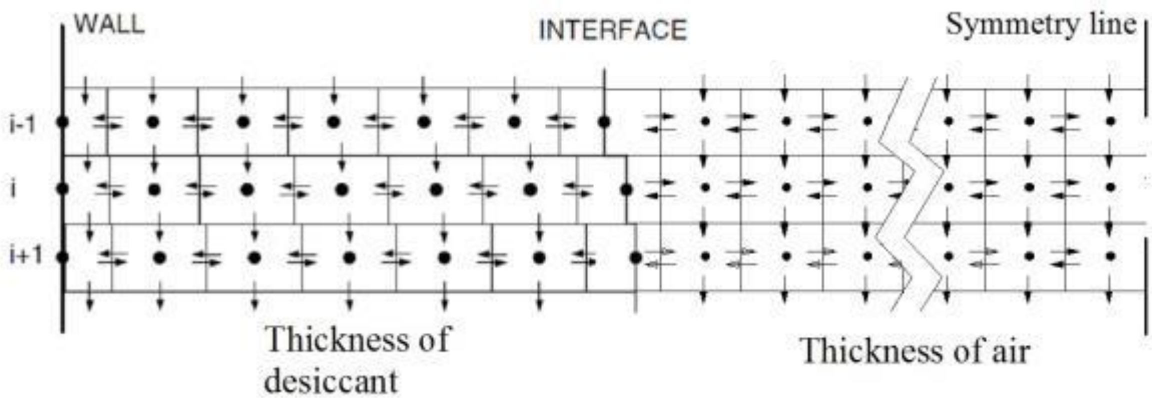

Fig. 2. 12 Schematic of grid with thickness change in the desiccant film

According to Mesquita's investigation, the simulation results by this model with variable thickness of falling film were closer to the experimental data (Kessling et al. 1998) than the results from other theoretical models, especially for low desiccant flow rates.

2.4.3 Discussion

Although the above two models are widely used to predict the performance of internally cooled dehumidification, both of them have limitations. The main reason is that the actual dehumidification process among the air, desiccant and extra fluid is three-dimensional, and the heat and mass transfer occurs in the direction of all three axis, as shown in Fig. 2.13. However, both of the described models only consider two dimensions, and their assumptions may cause large deviations between simulation and experimental results, which were observed in previous researches. To show the properties and limitations of these models, the distribution of solution temperature was simulated under the similar conditions, as shown in Fig. 2.14. The operation conditions were also indicated in this figure.

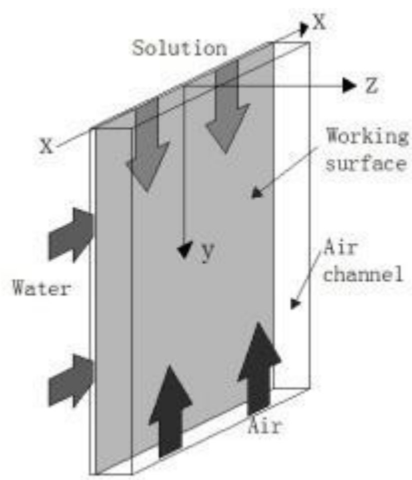

Fig. 2. 13 Schematic of coordinate system of liquid desiccant system

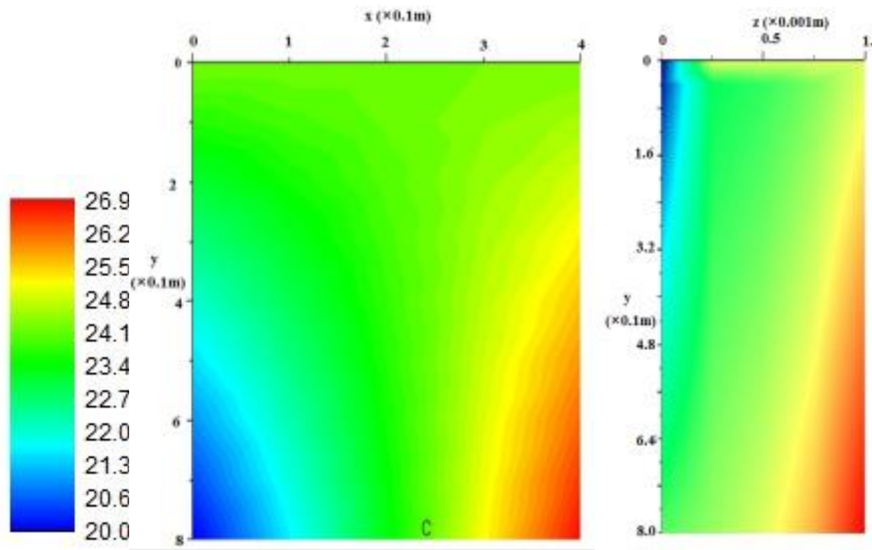

(a) By Ren's model (b) By Mesquita's model

$t_{s,in}$ (°C)	$\zeta_{s,in}$ (%)	$m_{s,in}(kg/s)$	$t_{a,in}$ (°C)	$\omega_a(g/kg)$	$m_a(kg/s)$	$t_{f,in}$ (°C)	$m_f(kg/s)$
25	35	0.5	25	9.5	1	20	0.5

Fig. 2. 14 Simulation results of desiccant temperature during the dehumidification process

For Ren's model, the change of physical parameters in the x-y plane could be numerically simulated. In Fig. 2.14(a), a simulation result of the desiccant temperature is showed as an example. In this case, the liquid desiccant film is exchanging the heat and moisture with the counter-flow air by direct contact, and also exchanging the thermal energy with the cross-flow water by indirect contact. The wetting factor was set as 0.7. From the figure, the temperature of liquid desiccant in most area increases a little along the flow direction due to the combined impacts of latent heat of vapourization and the cool water. Besides, the solution temperature is relatively low in the side part of water entering. The average outlet temperature of solution could be calculated as 24.8°C. The limitations of this model could be summarized as:

a) The heat and mass transfer inside the desiccant film and air in the thickness direction, and it through the air/desiccant interface were ignored in this model;
b) Although the incomplete wetting condition is considered in this model, it assumed that a part of every differential element was wetted by desiccant and the other part was dry, which was different from the practical condition. Actually, several elements should be totally wetted, and others are totally dry; So in Fig. 2.14 (a), the simulation results showed the solution was covered uniformly on the working plate, which was different from the practical condition;
c) The change of film thickness along the flow direction was ignored, which was proved to have a significant impact on the calculation results (Mesquita, 2006);
d) The isothermal boundary condition between desiccant and air has to be accompanied by a uniform concentration condition.

In terms of Mesquita's model, we could predict the variation of different parameters inside the desiccant film and air in y-z plane, and the change of film thickness along the flow direction was also considered. As shown in Fig. 2. 14(b), the results of solution temperature were obtained under the similar condition in Fig. 2.14(a). As shown in the figure, during the internally cooled dehumidification, the average outlet temperature of desiccant decreased a little, which means that the latent heat of vapourization could be carried out by the extra water. The solution temperature near the surface was much lower, as the working surface was cooler than the desiccant. The calculated average outlet temperature of solution was 25.3℃, which is different with the results from Ren's model. The main reason may be that in this model, the incomplete wetting condition in the dehumidification was ignored, and the film thickness was calculated by the design size of dehumidifier, which may be different from the real wetted width of falling film. The limitations of this model could be summarized as:

a) The incomplete wetting condition in the dehumidification was ignored;
b) The film thickness was calculated by the design size of dehumidifier rather than the actual wetted area;
c) This model is not suitable for the cross-flow pattern of extra fluid or air, which means that the change in the x-axis could not be calculated in this model.

In conclusion, there are several limitations in existing models, which cause a deviation between simulation and experimental results. To predict the performance of liquid desiccant air-conditioning systems more accurately, a 3-D model needs to be developed, which could describe the heat and mass transfer in all three axis. Furthermore, the incomplete wetting condition, the change of film thickness, and the variation of parameters in three directions should be considered.

2.5 Investigation on wetted area of liquid desiccant system and other applications

As mentioned before, the wetted area is an indispensable parameter in theoretical models, which significantly influence the accuracy of simulation result. Without an acceptable value for the wetted area, the Lewis Number during the dehumidification/regeneration process could not be obtained accurately, and the large deviations between previous simulations and experiment results may be caused. However, in practical falling film liquid desiccant systems, the working surface is usually found to be wetted very incompletely by the desiccant. Therefore, how to determine the wetted area and mass transfer coefficient in a reasonable way attracts interests of researchers all over the world.

Besides the liquid desiccant dehumidification or regeneration, the falling film of chemical solution or water is also widely used in other applications, such as the vertical condenser, absorption tower and evapourator. The system efficiency is reduced by the serious incomplete wetting, and the wetted area also a key parameter. Many researchers worked on the prediction of wetted area under different conditions experimentally and theoretically.

Researches of wetted area for liquid desiccant dehumidification/regeneration were reviewed, and the investigation results on the wetted area in other applications were also summarized.

2.5.1 Researches of wetted area of liquid desiccant dehumidification/regeneration

The wetted area can be represented by the wetting factor, which is defined as the ratio between the wetting area and total area. Howell et al. (1987) investigated a counter flow absorber built by a falling film fin-tube exchanger. He found that the experimental data could be correlated with the prediction by theoretical models only if a very small fraction of the exchanger surface was supposed to be wetted by the desiccant solution. By comparing the simulation and experiment results, in 1994, Park et al. indicated that a large part of fin surface was not wetted in their experiments. Kessling et al. (1998) developed and tested an internally cooled dehumidifier with a parallel plate exchanger. They found that it is difficult to achieve adequate wetted surfaces, button detailed analysis on the wetted area is discussed.

Then, Jain et al. (2000) experimentally studied a falling film tubular absorber and a falling film plate regenerator of liquid desiccant. They found that the actual wetting factors were about 0.2 to 0.6 in a falling film dehumidifier and regenerator of liquid desiccant. Besides, the error of the simulation with theoretical model was too large to be accepted, about 30-50%. Yin et al. (2007) tested an internally cooled/heated dehumidifier/regenerator using plate–fin heat exchanger. The wetting area of both dehumidification and regeneration was set at 0.7 based on the experimental results. In their theoretical study, Pietruschka et al. (2006) modelled a liquid desiccant cooling system, and indicted that there is no appropriate model to predict the wetting area, which depends on the heat and mass transfer conditions. Liu et al. (2006, 2007) assumed the wetting factor to be 0.8 in the simulations, but the changes of wetted factor under different conditions were neglected.

2.5.2 Researches of wetted area of other applications

According to the investigations on vertical condenser and absorption tower, when the working surface temperature is different with the liquid, the heat transfer would change the properties of falling film (Goussis et al. 1987, Wilson et al. 2002). These variations lead to an uneven distribution of surface tension upon the liquid-vapour interface, which could induce a fluid flow in the transverse direction (Kabov, 2002). This effect, namely the Marangoni effect, could significantly influence the wetted area and flow dynamics, and the heat and mass transfer of the falling film dehumidifier/regenerator as well.

Wasden et al. (1990), Yoshimura et al. (1996) and Park et al. (2004) investigated the caused film deformation and contraction waves by the inherently instability experimentally. In 2002, Chang and Demekhin summarized the properties of waves on the solution surface, and discussed the theoretical models. However, most of these works only considered the Marangoni effect and film deformation in the stream-wise direction, and the fluid instability in the transverse direction was ignored. In 2001, Geng et al. experimentally found that the wetted width of falling film was changed with the surface temperature, and water was used as the working fluid. Then, Zhang et al. (2006) developed a model to predict the contraction distance of water film, and found that the uneven distribution of surface tension in the transverse direction was much higher than that in the stream-wise one.

Furthermore, the minimum wetting rate, which is related to the wetted area, has also been studied by many researchers. With an experimental study of laminar liquid films on an inclined plate, Moran et al. (1997) investigated the film thickness and wetting rate, and found that the previous models showed under-prediction results. Then, by building several near-identical milk evaporators, Broome et al. (2005) investigated the liquid distribution on the evapourator tube, and developed a semi-empirical formula for minimum wetting rates. Based on their experimental and theoretical investigations, Morison et al. (2006[1], 2006[2] and 2006[3]) tested the influence of distributor of industrial evapourator tubes, and improved the model for the wetting rate. In 2005, Zhang et al. found that the size of the opening of water distributor could influence the wetted area greatly, but the detailed effect was not obtained. Besides, the studies of contact angle of liquid on the working surface, which shows an impact on the wetted area, were also reviewed. An equation was applied by Al-Farayedhi et al. (2002) for predicting the contact angle of liquid desiccant. The studies of contact angle were summarized and discussed by Luo et al. (2007). But, the results of current predictions can't agree with the experimental results well.

In conclusion, the wetted area and wetting factor were previously assumed to be constants without considering the influences of different operation parameters. Furthermore, the assumed values by different researchers differ greatly. Therefore, it is necessary to investigate the changing characteristics of wetted area, and to develop a model for accurately predicting the wetting factor for falling film liquid desiccant system.

2.6 Investigation of mass transfer coefficient of dehumidification/regeneration

The mass transfer coefficient is a very important parameter during the internally cooled/heated dehumidification/regeneration process. Without an effective calculation method of the coefficient, the performance simulation and predication could not be conducted. Until now, the mass transfer coefficient is usually obtained by empiric formulas, which were developed according to the experiment results with the Eq. (2.20) or Reynold's analogy.

$$a_D = \frac{\dot{m}_a \cdot (\omega_{a,in} - \omega_{a,out})}{\rho_a(\omega_a - \omega_I) \cdot dA} = \frac{\dot{m}_s \cdot \zeta_{in} \cdot (\frac{1}{\zeta_{in}} - \frac{1}{\zeta_{out}})}{\rho_a(\omega_a - \omega_I) \cdot dA} = \frac{\dot{m}_{s,out} - \dot{m}_{s,in}}{\rho_{air}(\omega_a - \omega_I) \cdot dA} \tag{2. 20}$$

In this section, several common formulas of mass transfer coefficient are reviewed.

a) In Kessling's (1998) research, the mass transfer coefficient in the dehumidifier has been determined directly by experiment results. The operation conditions during their experiments were listed in Table 2.1.

Table 2. 1 Summary of previous experiments

Type	Size (m^2)	Size of the channel (m^3)	Solution flow rate (g/s)	Air flow rate (g/s)	Solution/air flow pattern
Regeneration	0.46×0.98	$0.46 \times 0.98 \times 0.0055$	0.235	6.36-24.8	Counter-flow
Dehumidification	0.46×0.98	$0.46 \times 0.98 \times 0.0055$	0.116-1.242	12.64	Counter-flow

Results showed that the coefficient was in a range from 0.024-0.3 kg/m^2 s. It was found that when the air to solution mass ratio was smaller than 50, the coefficient decreased lineally with the decrease of solution flow rate when the air flow rate was constant. But, the coefficient was almost constant when the ratio was larger than 50. The mass transfer coefficient was also found to be linear with the air velocity within the channel. This method for determining the mass transfer coefficient is not practical because of without considering the influences of input parameters.

b) In Yin's research (2007), an empirical formula has been gained according to the experiment results, as shown in Eq. (2.21-22). The operation conditions during their experiments were listed in Table 2.2.

Table 2. 2 Summary of previous experiments

Type	Size (m^2)	Size of the channel (m^3)	Solution flow rate (g/s)	Air flow rate (g/s)	Solution/air flow pattern
Regeneration	0.298×0.6	0.298×0.6×0.012	8.33-10	10.0-12.4	Counter-flow
Dehumidification	0.298×0.6	0.298×0.6×0.012	10.36	12.2	Counter-flow

In dehumidification:

$$Sh = 4.513\times10^{-3}\cdot k\cdot \mathrm{Re}^{1.56}\, Sc^{0.33}$$
$$k = 76.456T_s^{-2.991} \quad (2.\ 21)$$

In regeneration:

$$Sh = 4.676\cdot k\cdot \mathrm{Re}^{1.55}\, Sc^{0.33}$$
$$k = 5.52T_s^{-3.36}$$

(2. 22)

The impacts of the air flow rate, solution temperature and size of the dehumidifier/regenerator have been considered. However, other significant influencing parameters are not discussed in these equations, such as the solution flow rate, air absolute humidity. Furthermore, as shown in Eq. (2.21) and (2.22), the coefficient decreases dramatically with the increase of solution temperature. It is inconsistent with the fact that higher solution temperature leads to higher regeneration efficiency.

c) In Liu's simulation research (Liu et al. 2006, 2007), the *Le* was set to be equal to 1, which means that the mass transfer coefficient is proportional to the heat transfer coefficient by the following equation.

$$a_D = a_H / c_{p,m} \tag{2. 23}$$

This method neglected the difference between heat and mass transfer, and the mass transfer coefficient is the function of *Re* which is decided by the air flow rate.

d) In many studies, the mass transfer coefficient is obtained by the Reynold's analogy. There are two common approaches of the analogy, and the first one is:

$$a_D = a_H / (c_{p,m} \times Le^{2/3}), \quad \text{where } Le = Sc / \mathrm{Pr}_a \tag{2. 24}$$

The second one is:

$$a_D = a_H / (c_{p,m} \times \left(\frac{k_a}{D_a} \right)^{2/3}) \tag{2. 25}$$

where k_a is the heat conduction coefficient of air.

In this method, the mass transfer coefficient is mainly determined by the air flow rate and air temperature. The influences of solution flow rate, solution temperature, air humidity and other parameters are ignored.

Therefore, in current researches, at least five kinds of semi-empirical formulas were used to estimate the mass transfer coefficient during the liquid desiccant dehumidification/regeneration process. To compare these formulas, with the operation conditions indicated in the literature (Yin et al. 2008), the coefficient with different formulas was calculated. As shown in Table 2.3, the results varied greatly under the same conditions. Results of Eq. (2.23-25) are similar, as the mass transfer coefficient is a function of heat transfer coefficient in all these formulas all. However, large deviations were found among other equations. The result from Kessling's was even about 10 times larger than that of Eq. (2.25).

Table 2. 3 Summary of mass transfer coefficient by different formulas

	Operation Conditions	Mass transfer coefficient of different formulas (×10^{-2} kg/m^2 s)				
		Kessling's	Eq. (2.21-22)	Eq. (2.23)	Eq. (2.24)	Eq. (2.25)
Dehumidification	$\dot{m}_s = 10g/s, \dot{m}_a = 10g/s$ $t_{s,in} = 25.3°C, t_{a,out} = 30.3°C$	7.6	5.1	0.91	1.02	1.04
Regeneration	$\dot{m}_s = 10g/s, \dot{m}_a = 10g/s$ $t_{s,in} = 74.3°C, t_{a,out} = 34.1°C$	8.8	2.8	0.92	1.04	1.06

It is very hard for researchers or engineers to choose a suitable formula to evaluate the performance of liquid desiccant dehumidifier/regenerator. The mean reason of the differences, in my opinion, is lack of the effective value of wetted area during the heat and mass transfer process. Therefore, developing a new method of calculating the mass transfer coefficient, which could take all significant input parameters into account and give acceptable results in different operation conditions, is of great importance. The wetted area has to be determined firstly, and then an acceptable mass transfer coefficient could be gained experimentally and theoretically.

2.7 Dynamic operation performance of SLDAC

In traditional vapour compression air-conditioning system, the air has to be cooled below the dew point to remove the moisture and then reheated to a comfortable temperature. The low evapourating temperature of the chiller caused poor COP value and high energy consumption of the system. Due to the higher cooling and dehumidification load, these problems would be more serious for buildings in warm or hot and moist districts. However, if the liquid desiccant system could be integrated with the cooling system, the problem may be avoided. By employing the solar energy, the SLDAC system is considered as a good alternative for energy saving and indoor air quality improvement. Therefore, to evaluate the energy consumption and economic efficiency of the whole system, the simulation of dynamic operation performance under different load profiles and operation conditions is necessary.

The whole system includes the liquid desiccant system, solar thermal system, cooling/heating system, energy storage system and auxiliary thermal system. Each sub-system has many energy consuming components, such as fans, pumps, chillers, and so on. In the liquid desiccant system, the dehumidifier and regenerator are the most critical components. Due to a large number of variables involved in theoretical heat and mass transfer models, the simulation method is complex and usually requires thousands of iterative calculations, which is inconvenient for researchers and engineers, especially those investigating the dynamic operation performance of the system. Therefore, the quick prediction model for liquid desiccant systems should be developed. Furthermore, many researchers are devoted themselves to optimizing the cooperation of sub-systems for a higher COP and a lower initial cost of the SLDAC system.

Most building in Hong Kong are air-conditioned with high energy use, and the SLDAC should be suitable. The building in Hong Kong is chosen as a case study to investigate the operation performance and system optimization of SLDAC system under real weather conditions. Understanding the characteristics of the AC load profile of buildings in Hong Kong is a basis and significant part.

In this section, firstly, the studies of the AC load profiles of buildings in Hong Kong and the responses to the climate change were reviewed, and the quick prediction model for liquid desiccant systems as well. The related researches of dynamic operation performance of the whole SLDAC were also summarized and analysed.

2.7.1 Load profiles of buildings in Hong Kong

To evaluate the performance of the LDAC system, understanding the characteristics of the AC load profile of buildings in Hong Kong is significant. The climate change is also a vital reason for the increasing energy consumption in Hong Kong. The increasing consumption of electricity for air-conditioning leads to large greenhouse gas emissions and in turn exacerbates the climate change. Therefore, it is also important to analyse how the AC load in these buildings responds to the local climate change.

The load profile of commercial buildings in Hong Kong has been investigated by local researchers. By survey, Yu and Chow (2001) derived the annual chiller-loads of 20 commercial office buildings. Deng (2003) analysed the total electrical load in existing hotels. Since Hong Kong has introduced several building energy codes in recent years, simulations have been proved as a reliable method for analysing the thermal processes and energy consumptions in buildings. Yik et al. (2001) calculated the cooling load profiles of a typical room. Zhang et al. (2001) simulated the ventilation load in buildings, and found that the dehumidification load took a significant position. Bojić et al. (2005) simulated the space cooling load for high-rise residential buildings. Lam et al. (2010) investigated the relationship among the cooling load, heating load and total load by simulation.

Furthermore, the climate change impact on AC load has been investigated only in recent years. Lam et al. (2010) developed a simple model to predict the AC electricity use for commercial sectors based on local meteorological data, and also investigated the trends of heat and cold stresses, which means the human discomfort, under the local subtropical climates in the same year. Wan et al. (2010) conducted energy simulations for air-conditioned office buildings in five cities including Hong Kong, and predicted the trends of buildings' total load to 2100. They estimated the impact of climate change on total energy use in office buildings and analysed the potentials of different measures in 2011. Most researches of local UHI focus on the generation and the effect on external micro urban temperature. Memon et al. (2009) found that an UHI can well reflect urban heating during night-time and early morning and evaluated the reliability. In 2010, this group investigated the impact of the important environmental variables on urban heating in Hong Kong from 1990 to 2005.

Most previous studies investigated the total or part of AC load in buildings, and there is little research on comprehensive load profile analysis of different types of commercial buildings in Hong Kong. Furthermore, the research on the response of the local AC load to the climate change is limited.

2.7.2 Quick prediction model for liquid desiccant systems

Previous studies investigated the quick prediction model for liquid desiccant systems, and most focused on the adiabatic ones. For dehumidifiers, a correlation, developed by Chung and Luo (1994) based on their experimental works, is widely accepted to determine the outlet air moisture content and moisture removal rate. In 2004, Abdul-Wahab et al. improved the correlation with the experiment data of different structured packing densities. In the same year, Gandhidasan et al. (2004) developed a prediction model to obtain the packed dehumidification performance, by introducing dimensionless vapour pressure and temperature difference ratios. In their research, the ratios were assumed to be constants, and the influences of design variables and operation conditions were ignored. In terms of regenerators, investigation of packed bed regenerators using heated air was carried out by Gandhidasan (1990). In a later study, Gandhidasan (2005) presented a simplified model in which the desiccant could be heated by heating fluid or electricity, but where the ratios were assumed as constants. These assumptions caused the results of system performance independent with the omitted inlet parameters, which disagreed with the theoretical models, and limited the model's applicability.

However, due to the complex configuration, research on ICHLD systems is limited compared to those on adiabatic ones. The impact of flow patterns in internally cooled dehumidifiers was investigated by Liu et al. (2009), and it was discovered that the performance of different patterns was similar within a difference of 5%. There is even less research on the internally heated regenerators. In their experiments, Yin et al. (2008, 2010) found that the internally heated regenerator has higher effectiveness, and investigated the effect of several inlet variables of different fluids. In 2012, Gao et al. experimentally analysed the moisture removal rate in a regenerator using evapourative condenser, and derived an empirical formula with regressions. But, only few influencing parameters were tested and included in this formula.

According to the literature review, until now, there is no direct way to obtain the outlet parameters, and the heat and mass transfer performance of dehumidifiers and regenerators in LDAC systems, especially for internally cooled/heated systems. Most previous prediction correlations could only predict the outlet moisture content of air and solution rather than the whole outlet parameters. Furthermore, these correlations would only be valid in the specific system due to the missing of influences of several variables such as design variables and inlet parameters of air. Because of these limitations, it is necessary to find a quick and accurate way to calculate the outlet characteristics and to predict the system performance of LDAC system, through which the influences of all design variables and operation parameters should be considered.

2.7.3 Dynamic operation performance of SLDAC

Researchers had investigated the dynamic operation performance of SLDAC has numerically and experimentally. In 1995, Lowenstein et al. presented the summer performance of a liquid desiccant system, and indicated that 52% of building's cooling demand could be met by the system. Khalid Ahmed et al. (1997) studied a hybrid vapour absorption combined with the liquid desiccant system. The COP of this system is about 50% higher than that of a traditional absorption system. Rane et al. (2002) simulated a combined system with the liquid desiccant system and compression chiller, and found that COP increased by 45% compared to a conventional system. In 2003, Chen et al. analysed the summer performance of a multi-stage liquid desiccant system driven by hot water under the climate of Beijing with the average COP of 1.1. Liu et al. (2006) established a liquid desiccant system process by recovering energy from the exhaust air. They adopted the electrical and thermal COP to evaluate the system performance, and found that the primary energy consumption and operating cost of liquid desiccant system are 78% and 75% of the conventional system in summer.

For the applications in Hong Kong and other similar hot areas, Li et al. (2007) investigated a SLDAC with the solar C/R, and found that under the Hong Kong's weather conditions, the energy consumption of the system was 25–50% less than the conventional system. Alizadeh et al. (2007) tested a SLDAC in the tropical climate, and the overall electrical COP was approximately six. In 2008, Katejanekarn and Kumar simulated the operation performance of a solar-regenerated liquid desiccant ventilation system. The results indicated that the solar radiation, ventilation rate, and desiccant solution concentration play significant roles. Then, they installed and operated a real system for a period of nine months in a hot and humid climate (Thailand) in 2009, and found that the system could reduce the humidity level by about 11% RH when the temperature was kept same with the ambient air. In 2011, Judah et al. investigated the feasibility of using a solar-powered liquid desiccant system to dehumidify the supply air and produce fresh water under the humid climate. After optimizing the heat sink temperature and regeneration temperature, the monthly energy cost of the novel system was predicted to be about 1/3 of the conventional system.

In conclusion, until now, researchers mainly investigated the operation performance of the packed-bed or solar collector/regenerator liquid desiccant system, but the research on dynamic performance and influencing parameters of the solar-assisted internally cooled/heated system is limited. The research on optimizing operation parameters to improve the efficiency or reduce the system cost under hot climate district, such as Hong Kong, is also limited.

2.8 Limitations in the past studies

This chapter presents a comprehensive literature review on the mechanism and application of liquid desiccant system, especially the regeneration system. The researches of load profiles of

Hong Kong were also summarized. The existing models of dehumidification/regeneration have many limitations, and hardly predict the wetted area and mass transfer coefficient accurately. In summary, we have the following observations:

a) The existing two-dimensional theoretical models cannot describe the actual three-dimensional heat and mass transfer of dehumidification/regeneration process among the air, desiccant and extra fluid. Furthermore, the assumptions, such as the use of wetting factor, also cause some problems.

b) The wetted area of liquid desiccant, as a key factor affecting the system performance, is usually determined by simple assumptions without considering the influences of different operation parameters. Furthermore, the assumed values by different researchers vary greatly, which cause a large deviation between simulation and experimental results.

c) The results of different existing formulas of mass transfer coefficient vary greatly under same conditions. It is hardly to find a suitable formula to evaluate the performance of liquid desiccant dehumidifier/regenerator.

d) The research on the operation characteristics and energy consumption of the whole SLDAC system is limited, especially in the warm and humid districts such as Hong Kong.

2.9 Methodology

Based on the literature review in Chapter 2, the wetted area and mass transfer coefficient are key parameters affecting the performance evaluation and simulation of LDAC. By building and testing a single channel internally heated regenerator, the influencing factors of wetted area and system performance under different conditions are investigated, as well as the change of mass transfer coefficient with the actual wetted area. Details of the experimental method can be found in Chapter 3 and 5. Based on the experimental results, a theoretical model with an analytical solution is developed for accurately calculating the wetted area of internally heated regeneration, as given in Chapter 4. Additionally, an empiric formula of the mass transfer coefficient during the regeneration process is developed in Chapter 5.

Based on these studies, in Chapter 6, a 3-D model with a numerical solution of internally heated regenerator is developed and verified, for describing the heat and mass transfer among the air, solution and extra hot water in all three directions. The insufficient wetting and change of film thickness due to the mass transfer and film deformation were taken into account. With the new model, a parameter study has been done numerically to show the effect of inlet parameters on the moisture removal rate and regeneration efficiency.

As the 3-D model is inconvenient for investigating the dynamic operation performance, a simplified numerical model of internally cooled/heated dehumidifier/regenerator is developed, by defining three kinds of effectiveness, i.e. enthalpy effectiveness, moisture effectiveness, and temperature effectiveness. The statistical correlations of effectiveness are developed with the multi linear regression. With the simplified model, a dynamic simulation of the whole SLDAC system, including solar thermal system, liquid desiccant regenerator/dehumidifier, cooling system, energy storage system and auxiliary heating system, is conducted. Detail of the simplified prediction model and dynamic simulation method can be found in Chapter 7.

To evaluate the operation performance and energy potential of the system, with the AC load profiles of three typical commercial buildings and weather data of Hong Kong as a case study, the annual energy consumption and system performance is simulated and compared with conventional systems, as indicated in Chapter 8. Several optimization configurations are also proposed to improve the system performance and save the energy.

A flow chart summarizing the methodology is shown in Fig. 2.15.

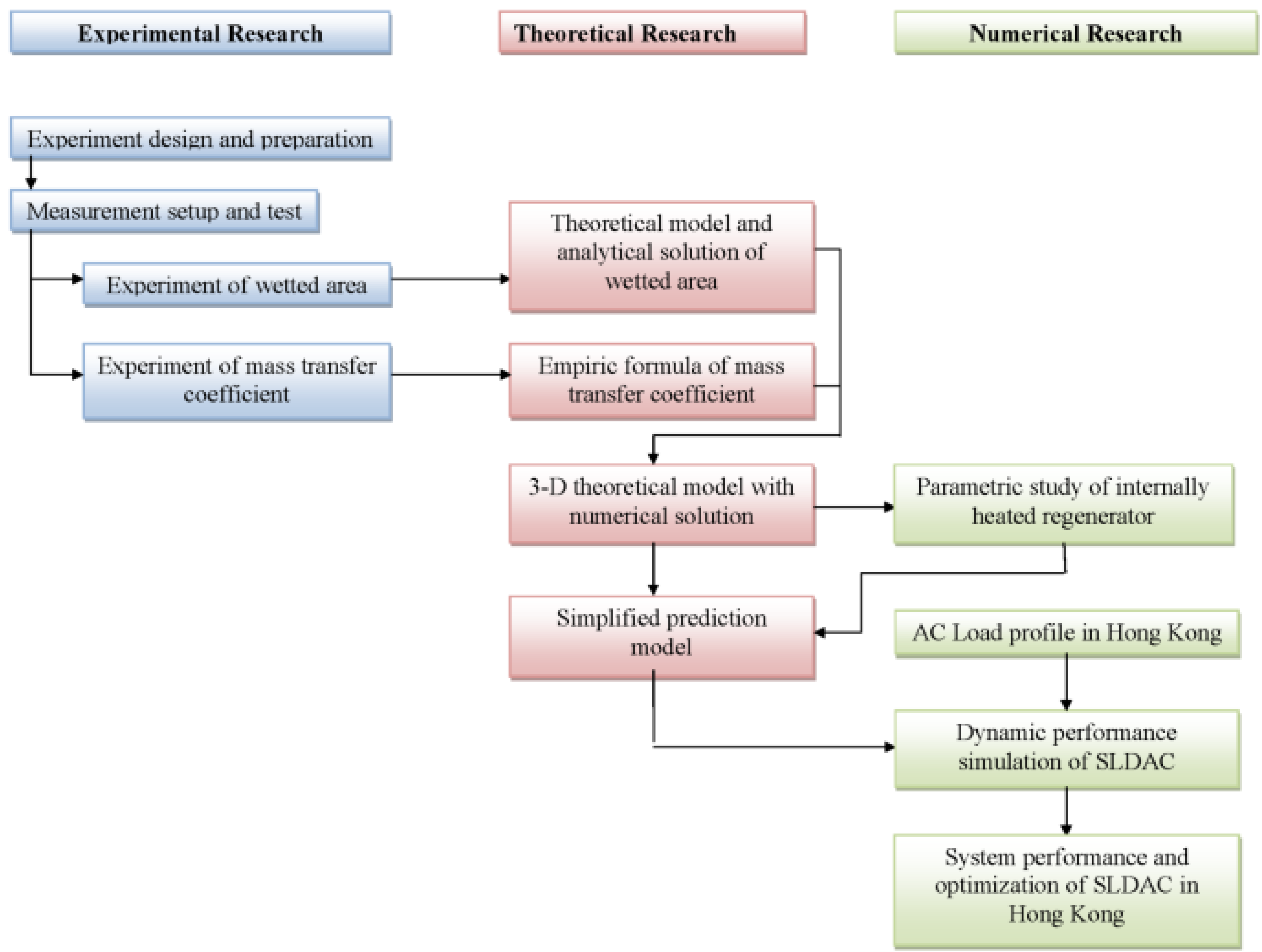

Fig. 2. 15 A flow chart of the methodology for experimental, theoretical and numerical studies

CHAPTER 3

EXPERIMENT INVESTIGATION ON WETTED AREA OF LIQUID DESICCANT REGENERATION

3.1 Introduction

The wetted area is found to be a key parameter for investigating the mass transfer efficiency and operation performance of falling film liquid desiccant system. Without an acceptable value of the area, the performance could not be evaluated and simulated accurately. However, the previous investigations on the wetted area were very insufficient. Therefore, it is necessary to investigate the changing characteristics of wetted area and system performance under different operation conditions experimentally for the falling film liquid desiccant system. As most energy is consumed in the regeneration process, this research focused on the heat and mass transfer in the regenerator.

Referring to the literature review in the chapter 2, many researchers have done the experiments for the same purpose, such as Howell et al. (1987), Park et al. (1994), Kessling et al. (1998), Jain et al. (2000), Yin et al. (2007) for the internally cooled/heated dehumidifier/regenerator, and Geng et al. (2001), Zhang et al. (2005, 2006) for the water flow. However, previously, the wetted area was usually assumed to be constant without considering the influences of operation parameters. Furthermore, the assumed values by different researchers differ greatly. To fill those gaps in the aforementioned experimental studies, following aspects will be investigated in this experiment:

(1) By building and testing a single channel internally heated regenerator, the effects of influencing factors on the wetted area and film thickness of falling film liquid desiccant system were investigated experimentally, as well as the mass transfer performance. The factors included the thickness of solution distributor, solution mass flow rate, solution concentration, solution temperature, plate surface temperature and the pre-wetting of working surface;
(2) The detailed influencing factors affecting the contact angle, which was found to play a significant role in the wetted area of falling film, were experimentally investigated, including the concentration and temperature of desiccant, and the roughness of the surface.

3.2 Description of experimental bench

As mentioned earlier, most energy consumed in practical applications is for re-concentrating the liquid desiccant. Therefore, in our experiments, the regeneration process was conducted and analysed. To investigate the influences of different operation parameters, a single channel experimental setup was fabricated. The experimental rig was designed to allow the liquid desiccant film to flow down along the vertical test surface by gravity, exchanging the moisture and heat with the counter-flow air by direct contact and exchanging heat with the cross-flow water by indirect contact simultaneously. The desiccant solution was distributed on the working surface through the solution distributor. The lithium chloride (LiCl) aqueous solution was used as the desiccant.

As shown in Fig. 3. 1, the working surface, with the area of 750×650 mm (length × width), was made of the polished stainless steel (Type 316) with a thickness of 1.2 mm. The average profile roughness parameter of the working surface was 608 nm. The directions of x, y and z axis were also indicated.

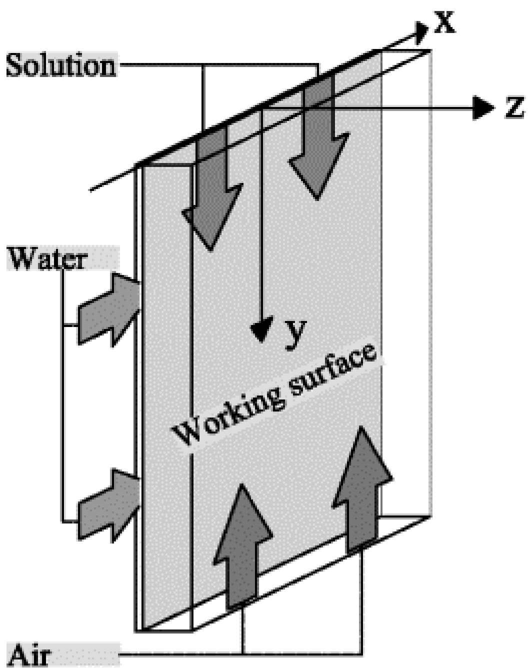

Fig. 3. 1 Schematic of working surface and coordinate system

The setup consists of a solution distribution system, an air handling system and a water handling system, as shown in Fig. 3. 2. The solution system consists of two solution tanks, a solution pump, a solution valve and an anti-corrosion electricity heater. To prevent the corrosion, the PVC tubes and plastic pumps were applied to transport the desiccant. The two tanks, i.e., the inlet tank and outlet one, could avoid the change of inlet temperature and concentration of desiccant solution. The air handling system includes a filter, a heater, two sampling devices, a main fan and a wind damper. To avoid the uneven distribution in the wind tunnel, the air from 5 points at the same cross section was mixed in the sampling device, which included a sampling duct, an extra fan and a mixing box, and was measured inside the box. The process air was driven in a counter-flow direction of the desiccant, with the main fan on the top of the bench. The flow rate of the air was adjusted by the wind damper under the fan.

The supply water was pumped to circulate in copper pipes inside the double plates in cross current to an upward air flow and a downward solution flow. As the cross-flow pattern of water could save the pump energy consumption and simplify the system composition, it is commly used in industrial applications. Besides, according to Liu's research (Liu et al. 2009), by comparing with different flow patterns of water, the difference of performance of liquid desiccant system was slight, which is less than 5%. So, in our experimental research, the cross-flow pattern of water was employed. The water temperature was increased by the electricity heater, and a blender was used to fully mix the water in the tank. The air channel upon the working surface, with an adjustable width from 3 cm to 10 cm, was made of 5 mm transparent material. The outer sides of working surface, wind tunnels and water/solution pipes were all well insulated by the 20 mm neoprene foam to reduce the heat loss. Besides, In order to obtain the steady-going air state, the experimental setup was placed in a psychrometric room with stable air temperature and relative humidity.

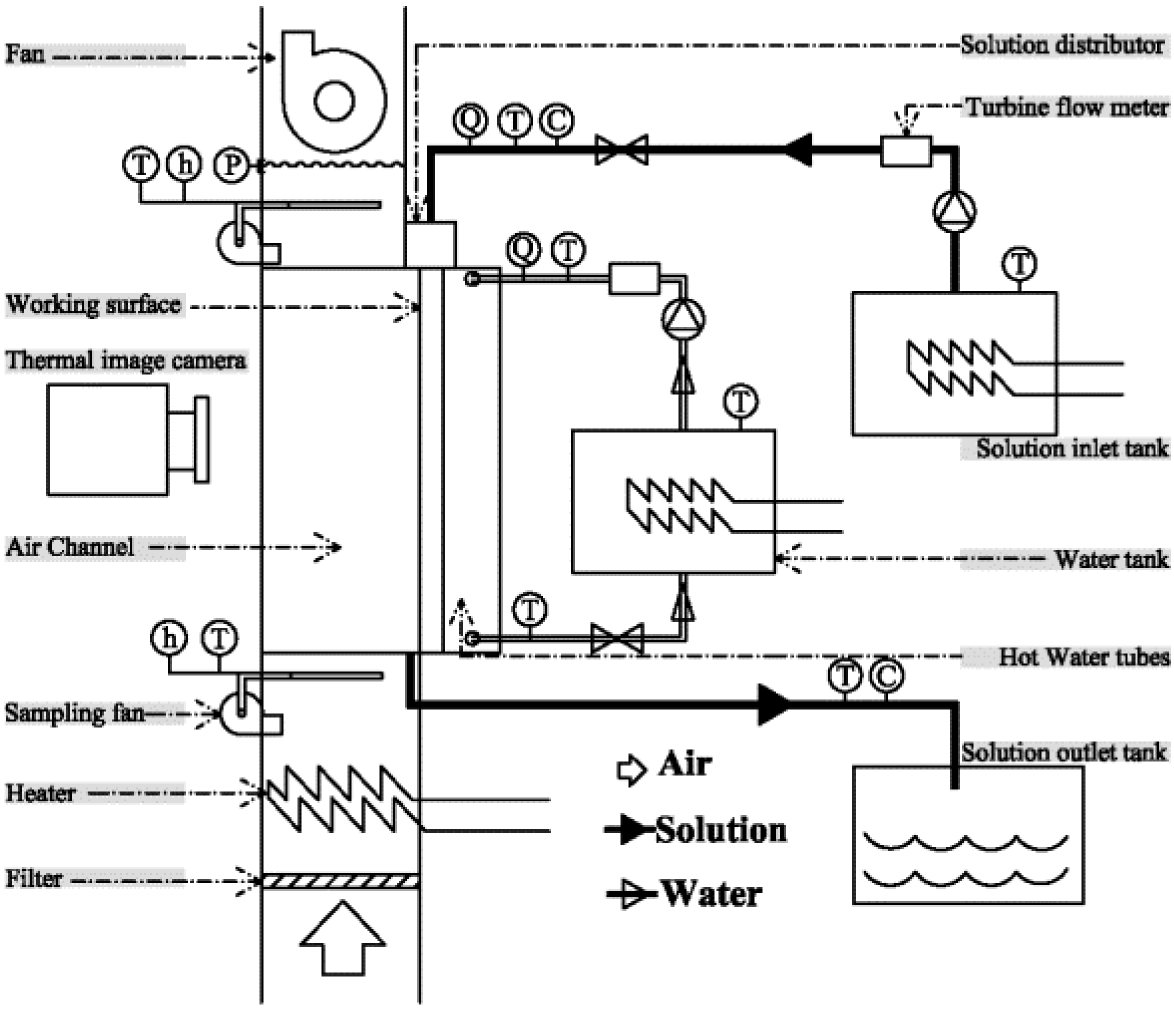

Fig. 3. 2 Experimental design of the single channel liquid desiccant regenerator

To find out the influence of solution distributor, as shown in Fig. 3.3, a package of distributors with different slit thicknesses was made, with the same material to the working surface. In this thesis, the thickness of solution distributer indicated the width of open slit of the distributer.

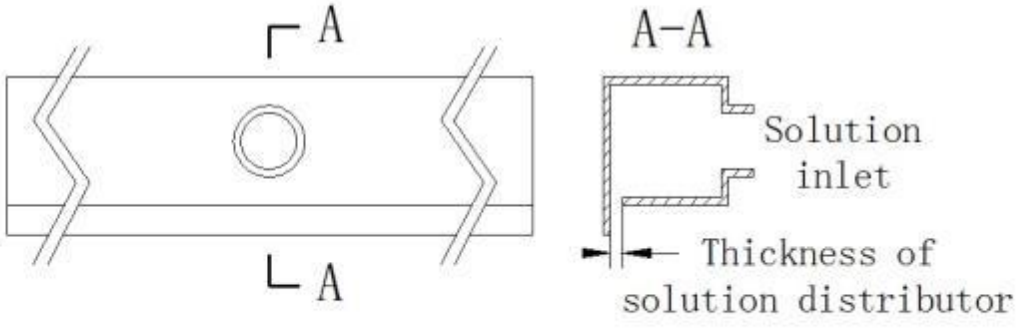

Fig. 3. 3 Geometry of solution distributor

According to the common working conditions of internally heated regeneration, the initial inlet values of operation parameters in our experiments were selected, as listed in Table 3.1. The changing ranges were also given. During the experiments, by changing one parameter and keeping other parameters as constants with initial values, the film size, surface temperature and inlet/outlet parameters under different operation conditions could be obtained. All measurements were conducted after the states of air, desiccant and water were approaching steadily.

Table 3. 1 Summary of the measured parameters

Parameters	Symbols	Range	Initial value
Inlet mass flow rate of solution (kg/s)	$m_{s,in}$	0.02-0.2	0.035
Inlet temperature of solution (℃)	$t_{s,in}$	25-60	45
Inlet concentration of solution (%)	$\zeta_{s,in}$	25-35	28
Thickness of solution distributor (10^{-3} m)	δ_{max}	1.0-2.0	1.0
Mass flow rate of air (kg/s)	m_a	0.05-2.50	1

Inlet temperature of air (°C)	$t_{a,in}$	20-40	25
Inlet moisture content of air (g/kg dry air)	$\omega_{a,in}$	5-15	9.87 (RH: 50%)
Thickness of air channel (10^{-3} m)	δ_a	10-100	50
Inlet flow rate of hot water (kg/s)	$m_{f,in}$	0.05-0.2	0.13
Inlet temperature of hot water (°C)	$t_{f,in}$	25-60	55

To investigate the influence of different operation parameters on the wetted area and system performance, the experiment was conducted following the listed steps:

a) The fan was started to make the process air with the set temperature and RH flow through the wind tunnel;

b) The water pump was started to make the hot water flow through the hot water tubes with a given mass flow rate and temperature;

c) The data was observed when the steady states of the air and surface temperatures were reached;

d) The plate surface temperature was measured with the thermal image camera;

e) The solution pump was started to make the solution flow down the working surface with a given mass flow rate and temperature;

f) The data was observed when the steady states of air and solution were reached;

g) The wetted area and surface temperature of the solution were measured with the thermal image camera, and the inlet/outlet parameters of all fluids were recorded;

h) One of the parameters, i.e. solution temperature or concentration, was changed and steps a) to g) were repeated.

The steady state condition was obtained if the maximum deviations of the following variables were within the given limits: air temperature ±0.2℃, air flow rate ±5%, solution temperature ±0.2 ℃, and water temperature ±0.1 ℃.

Choosing the regeneration process as our experiment type also has other advantages. The changing ranges of inlet temperature of water, solution and process air of regenerators are larger compared to those of dehumidifiers, and more operation conditions could be provided. For example, as extra heat source is applied in the regeneration, the solution temperature was changed from 25 to 60℃ during our experiments, while the changing range is usually set as 20-30℃ for the dehumidification (Yin, 2008).

3.3 Measurement of variables

The tested parameters include the inlet and outlet temperatures of all fluids, flow rates of all fluids, air humidity, solution concentration, contact angle between solution and working surface and the surface roughness. The thermal image of the working area was recorded by the highly sensitive Thermal Camera Imager, to obtain the film size and surface temperature of working plate and solution. The maximum error of the surface temperature was 0.1℃. According to the difference of temperature and reflectivity between the dry and wet areas, the image was firstly processed with the supporting software InsideIR to identify the film area, and then resized and pixelated with the Photoshop. Afterwards, with the software AutoCAD, the film width and area could be measured. Considering the width of an individual pixel in the image and the minimum observed values during our experiment, the maximum relative errors of the film size and wetted area were 0.7% and 1.1%, respectively.

Several Pt-RTDs were used to obtain the inlet and outlet temperatures of solution, water and air, with the accuracy of 0.1℃. A specific gravity hydrometer, with the accuracy of 1 kg/m^3, was applied to obtain the density of solution for determining the solution concentration with the temperature. The calculated error for the solution concentration is about 0.147 %. The flow rates of solution and water were measured by the turbine flow-meter, with the maximum error of about 1.6 L/h. The humidity of air was calculated with the data recorded by the dry and wet-bulb thermometer inside the box. The maximum error for temperature was 0.1℃ and the error for the absolute humidity was about 0.16 g/kg. To improve the accuracy of the measured humidity, the flow velocity around the thermometer should be higher than 2.5 m/s. The temperature and flow rate of all fluids could be adjusted to the pre-set values with the PID controllers. The data of operation parameters were recorded automatically by data logger once per second.

The contact angle of desiccant, which is measured through the liquid when a solution/air interface meets a solid surface, was recorded by the contact angle goniometer with an accuracy of 0.05°. To measure the angle, a solution droplet was automatically dripped on the test plane and stayed for about 30-60 seconds to approach the stable condition. Then the angle was recorded by the goniometer. To improve the experimental accuracy, every test with different parameters was repeated 4-5 times to obtain the average contact angle. The roughness of working plate was recorded by the Veeko laser optical interferometer, with an accuracy of 0.01 nm. All the data were recorded by a data acquisition system, namely the Agilent 34970A. The figures of the thermal camera imager, the interface of image analysis software, the contact angle goniometer, the laser optical interferometer and the PID controllers were shown in Fig. 3. 4.

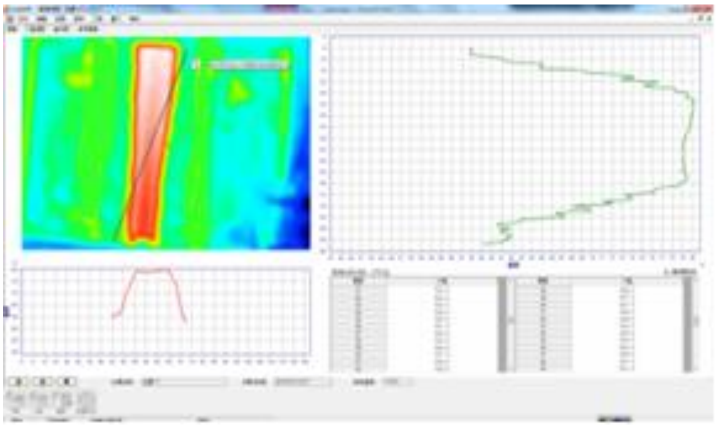

(a) Photo of Thermal Camera Imager (b) Interface of image analysis software

(c) Photo of Contact Angle Goniometer (d) Photo of PID controllers

(e) Photo of Laser optical interferometer

Fig. 3. 4 Figures of (a) Thermal camera imager; (b) Interface of image analysis software; (c) Contact angle goniometer; (d) PID controllers and (e) Laser optical interferometer

Several measurement images were shown in Fig. 3. 5, including the thermal image during the regeneration process, the image of contact angle and the image of surface roughness.

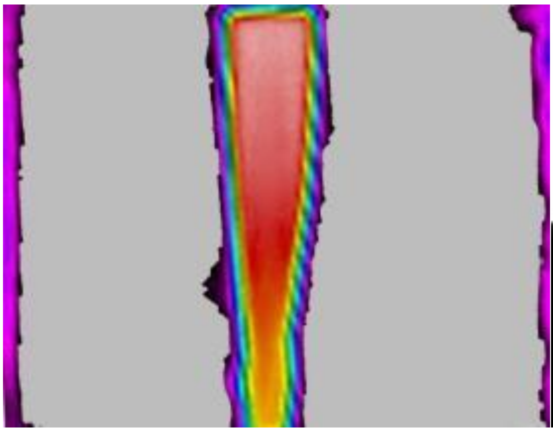

(a) (b)

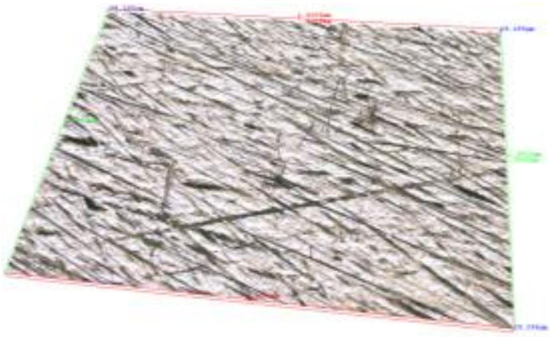

(c)

Fig. 3. 5 Examples of measurement image: (a) Thermal image during the regeneration process; (b) Contact angle and (c) Surface roughness

With the following equation, the maximum relative error of individual parameter could be calculated.

$$e_{i,\max}(\%) = \frac{E_i}{P_{\min}} \qquad (3.\ 1)$$

where E_i means the measurement error of individual device, such as the RTD and flow meter. $P_{\min}$ is the minimum value of the measured parameter, where the maximum relative error occurs.

Knowing the changing range and error of different measurement devices, the maximum relative errors of measurement could be calculated, which was summarized in Table 3.2. To reduce the random error, the result employed in our analysis was obtained with the average of the measured data of 1 minute.

Table 3. 2 Summary of the max measurement error

Parameters	Symbols	Max measurement error (%)
Mass flow rate of solution (kg/s)	m_s	2.7
Temperature of solution (°C)	t_s	0.4
Concentration of solution (%)	ζ_s	0.6
Density of solution (kg/m^3)	ρ_s	0.09
Contact angle of solution (°)	θ	0.1
Thickness of solution distributor (10^{-3} m)	δ_{max}	2.0
Mass flow rate of air (kg/s)	m_a	1.1
Temperature of air (°C)	t_a	0.5
Moisture content of air (g/kg dry air)	ω_a	1.7
Thickness of air channel (10^{-3} m)	δ_a	0.2
Flow rate of hot water (kg/s)	m_f	0.9
Temperature of hot water (°C)	t_f	0.4

The mass transfer performance of the experiments could be represented as the moisture removal rate, as shown in Eq. (3.2). By combining the error of individual parameter, its accumulated measurement error could be calculated to be 2.44%.

$$\dot{m}_{removal} = \dot{m}_a(\omega_{a,out} - \omega_{a,in}) \tag{3. 2}$$

where ω is the moisture content and *m* is the mass flow rate. The subscripts, *a* stand for the air, and *in* and *out* mean the inlet and outlet characteristics.

With the film wetted width observed during the experiments, the film thickness could be calculated with the following equation, by assuming the constant thickness in the x-axis:

$$\delta_s = (\frac{3m_s\mu_s}{W_s(y)\rho_s^2 g})^{1/3} \tag{3. 3}$$

where W_s stands for the width of solution film, which changed along the flow direction due to the film contraction. Additionally, the accumulated measurement error of the calculated film thickness was derived to be 0.62%.

The dimensionless hydraulic radius of solution falling film, which is defined as the ratio between the half of wetted width and the initial film width, could be calculated with Eq. (3.4). It should be noticed that $\overline{R_w}$ is different along the flow direction.

$$\overline{R_w} = \frac{W_i - \Delta x}{2W_i} \tag{3. 4}$$

where Δx is the contraction distance during the falling film process.

During our experiments, it was found that the air flow showed a small impact on the wetted area or film thickness of solution. Compared to the desiccant, the effect of hot water flow rate was also minor. The results of unimportant parameters were not listed and discussed.

3.4 Results

Before investigating the influences factors of the wetted area, the mass and energy balance of the measured data should be checked firstly, to verify the test procedure.

As shown in Eq. (3.5) and (3.6), in ideal internally heated liquid desiccant systems, the moisture added to the process air ($\dot{m}_1$) should be equal to that removed from the solution ($\dot{m}_2$), and the change of energy in solution and air ($\dot{e}_1$) should be equal to the change in the hot water ($\dot{e}_2$).

$$\begin{aligned} \dot{m}_1 &= m_a(\omega_{a,out} - \omega_{a,in}) \\ \dot{m}_2 &= m_{s,in}\zeta_{s,in}\left(\frac{1}{\zeta_{s,in}} - \frac{1}{\zeta_{s,out}}\right) \end{aligned} \qquad (3.\ 5)$$

$$\begin{aligned} \dot{e}_1 &= (m_{s,in}h_{s.in} - m_{s,out}h_{s.out}) + (m_a h_{a.in} - m_a h_{a.out}) \\ \dot{e}_2 &= m_f t_{f,in} - m_f t_{f,out} \end{aligned} \qquad (3.\ 6)$$

where h stands for the enthalpy, and m is the mass flow rate. ζ_s is the concentration of solution. t means the temperature. The subscripts *a*, s, f stand for the air, solution and extra fluid.

In our experiments, the average deviation between $\dot{m}_1$ and $\dot{m}_2$ was found to be 5.38%, and that between $\dot{e}_1$ and $\dot{e}_2$ was 8.78%, which were acceptable. So, the measured data were acceptable for the further analysis. The errors were mainly caused by the systematic error and statistical error from multiple sensors and multiple readings.

3.4.1 Influences of solution distributor, mass flow rate and concentration

To investigate the influence of solution distributor, mass flow rate and concentration on the wetted area, the five experiment groups with variables operation parameters were conducted, as listed in Table 3.3. Each group had eight tests with different mass flow rates, so the effect of solution flow rate could be observed and analyzed. As the solution mass flow rate affected the wetted area and system performance significantly, to make the result more convincingly, its influences were tested under different operation conditions. Then, by comparing the results from G.1 and G.3, and the results from G.2 and G.4, the impacts of solution distributor thickness, $\delta_{\max}$, could be investigated. Furthermore, the effect of solution concentration were studied with the experiment G.1 (ζ_{in}=25.3℃), G.2 (ζ_{in}=28.2℃) and G.5 (ζ_{in}=37.1℃).

Furthermore, as a reference, the outlet parameters were listed in Table 3.4. These tests were selected for the similar mass flow rate or temperature of desiccant.

Table 3. 3 Experimental conditions of internally heated regeneration

Group No.	$\delta_{\max}$ (mm)	m_s (kg/s)	$t_{s,in}$ (℃)	ζ_{in} (%)	$t_{w,in}$ (℃)	$m_{w,in}$ (kg/s)	$t_{a,in}$ (℃)	$\omega_{a,in}$ (g/kg)
1	1.0	0.025, 0.054, 0.069 0.096, 0.097, 0.123 0.139, 0.158	45.1	25.3	55.4	0.131	24.1	9.34
2	1.0	0.025, 0.056, 0.088 0.105, 0.126, 0.118 0.146, 0.161	44.8	28.2	55.4	0.132	23.8	9.26
3	1.25	0.029, 0.051, 0.065 0.084, 0.099, 0.103 0.119, 0.131	45.2	25.2	55.5	0.130	23.7	9.20
4	1.25	0.023, 0.044, 0.050	44.7	28.0	55.3	0.125	23.7	9.47

		0.066, 0.092, 0.112 0.127, 0.147						
5	1.0	0.037, 0.079, 0.091 0.113, 0.117, 0.120 0.144, 0.150	45.2	37.1	54.9	0.126	24.1	9.50

Table 3. 4 Outlet parameters (selected) of internally heated regeneration

No. (Group No.-Test No.)	$t_{s,out}$ (℃)	ζ_{out} (%)	$t_{w,out}$ (℃)	$t_{a,out}$ (℃)	$\omega_{a,out}$ (g/kg)
1-2	41.0	25.8	53.4	25.4	13.3
2-2	41.6	28.6	53.0	26.4	12.4
3-2	41.3	25.6	53.1	25.9	13.2
4-3	42.1	28.4	52.4	25.4	12.3

As shown in Fig. 3.6, due to the larger thickness of solution distributor in groups 3 and 4, the wetted area decreased significantly compared to those in groups 1 and 2. By comparing with the groups with similar solution concentration, the wetted areas in G. 1 were about twice of those in G. 3, and G. 1’s moisture removal rates were much higher than those of G. 3 by about four times. The comparison between groups 2 and 4 showed the similar trend. Under the same operation condition, the removal rate was found to be approximately proportional to the square of wetted area, which means the increase of wetted area would lead to an obvious increase of mass transfer efficiency. Furthermore, both the wetted area and moisture removal rate increased with the solution mass flow rate. Although the increase of solution concentration seriously weakened the mass transfer between air and solution, its impact on the wetted area is insignificant. Therefore, increasing the wetted area is an effective method to increase the performance of falling film liquid desiccant system.

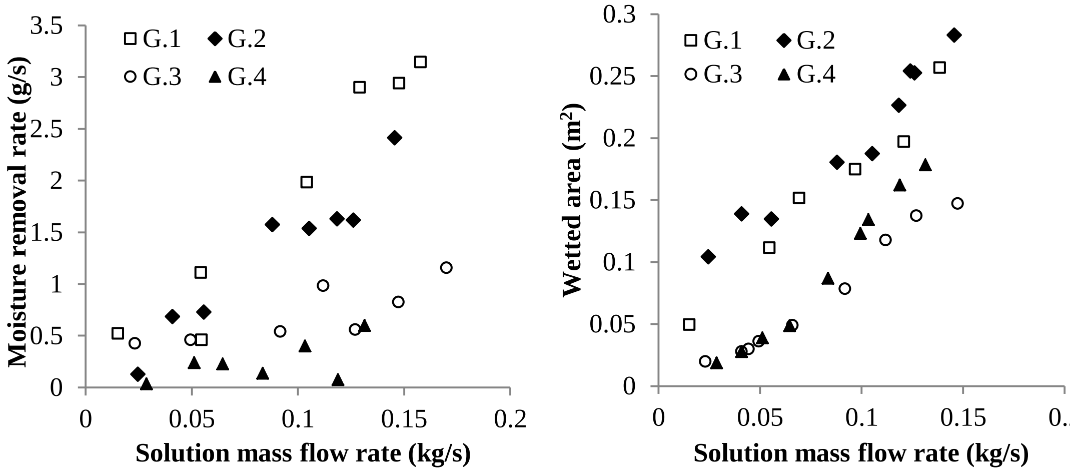

(a) (b)

Fig. 3. 6 Changing of system performance with solution mass flow rate (a) Moisture removal rate and (b) Wetted area

The initial film width, W_i, which means the width of falling film at the top of the working surface, is an important factor on solution wetted area. The changing trend of W_i with several influencing parameters could be found in Fig. 3.7. From Fig. 3.7 (a), when the thickness of solution distributer reduced from 1.25 to 1.0 mm, the film thickness reduced and the initial width increased significantly about 1.5 to 3 times. The width was also found to increase almost proportional to the solution mass flow rate under the similar solution mass flow rate, which would significantly increase the wetted area. As demonstrated in Fig. 3.7 (b), with the increase of solution concentration, W_i increased slightly. The shrinkage of the falling film along the flow direction was also observed in our experiments.

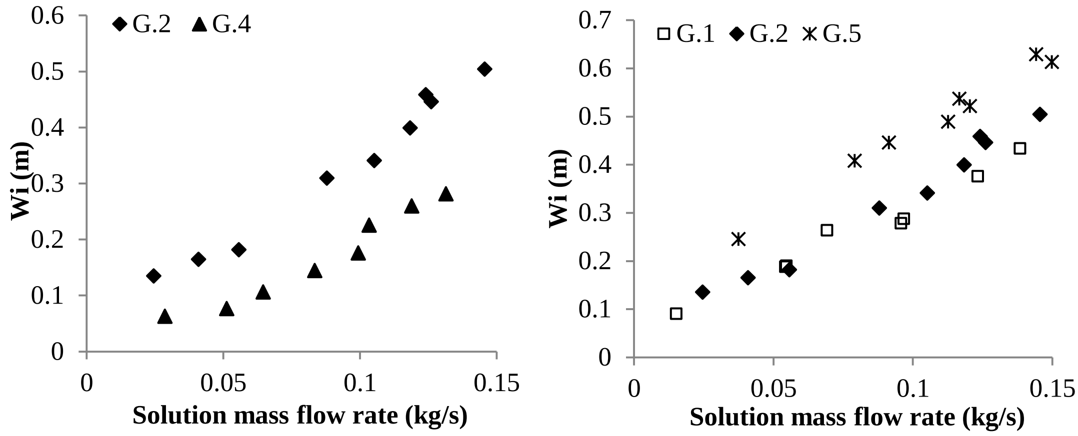

(a) (b)

Fig. 3. 7 Influencing factors of initial width of falling film (a) Changes with solution mass flow rate and distributor thickness and (b) Changes with solution concentration

As found in our experiments, the typical flow shape of solution falling film was a symmetrical tongue type, in which the central surface temperature is higher than that of the edge part. With the film wetted width observed during the experiments, the film thickness could be calculated with the following equation, by assuming the constant thickness in the x-axis (Mesquita, 2006):

$$\delta_s = \left(\frac{3m_s\mu_s}{W_s(y)\rho_s^2 g}\right)^{1/3} \quad (3.\ 7)$$

As shown in Fig. 3.8, the average film thicknesses recorded in five experiment groups were found to be about two thirds of the thickness of solution distributor, $\delta_{\max}$, with an acceptable average error of 9.74%. Besides, the solution temperature, concentration and mass flow rate show little impact on the average film thickness.

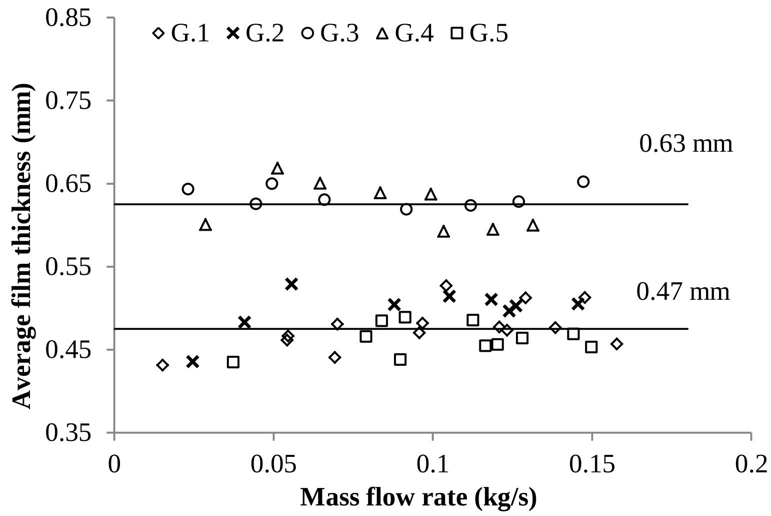

Fig. 3. 8 Average film thicknesses of experiment groups 1-5

3.4.2 Influence of plate surface temperature

Although the parameters of air and extra hot water show a relatively small impact on the wetted area, they could influence the temperature of the plate working surface. As the working surface is usually wetted by the desiccant incompletely, in this study, the plate surface temperature was defined as the surface temperature of dry area, which could impact the heat and mass transfer during the whole dehumidification/regeneration process. In practical applications, we found that the plate surface temperature was usually lower than the solution temperature, due to the air and surrounding temperature was commonly much lower (Air temperature: 20-30℃, Solution temperature: 50-60℃). Therefore, in our experiments, the effects of different plate surface temperature were investigated. To make the analysis more complete, the tested changing range of surface temperature should be large enough, which means the temperatures in several tests were larger than the solution temperature and the others were smaller.

To investigate the influence of plate surface temperature, the experiments with various operation parameters were conducted, as listed in Table 3.4. The experiments could be divided into three groups, and each group had nine tests with different surface temperatures. The surface temperature used in our analysis is the average temperature of the whole plate before the desiccant flowing down, which was assumed to be equal to the surface temperature of dry area during the regeneration process. The thickness of the solution distributor was chosen as 1 mm.

Table 3. 5 Experimental conditions of internally heated regeneration

Group No.	$m_{s,in}$ (kg/s)	$t_{s,in}$ (℃)	ζ_{in} (%)	t_p (℃)	m_w (kg/s)	$t_{a,in}$ (℃)	$\omega_{a,in}$ (g/kg)
6	0.034	46.6	30.0	29.1, 31.8, 33.4 36.3, 38.0, 38.9 41.1, 46.4, 48.8	0.131	24.1	9.34
7	0.054	46.4	30.0	29.5, 30.8, 34.0 36.3, 39.0,40.8 44.0, 47.5, 50.1	0.129	23.8	9.26
8	0.062	46.1	29.5	26.6, 29.0,31.5 36.5, 39.0, 31.9 45.5, 47.3, 49.4	0.130	23.7	9.20

As shown in Fig. 3.9 (a), with the increase of plate surface temperature, the moisture removal rate of desiccant solution increased significantly, which means that the surface temperature plays an important role in the heat and mass transfer during the regeneration process. From Fig. 3.9 (b), it could be found that the wetted area of falling film was also significantly increased. When the plate surface temperature increased from 29.1 to 46.4°C, the wetted area of G.6 increased about 1.5 times, with a growth rate of 2.17×10^{-3} m^2/°C. The trends of G.7 and G.8 were similar, while the improvement of wetted area (about 1.87 and 1.74×10^{-3} m^2/°C respectively) was not as obvious as that of G.6.

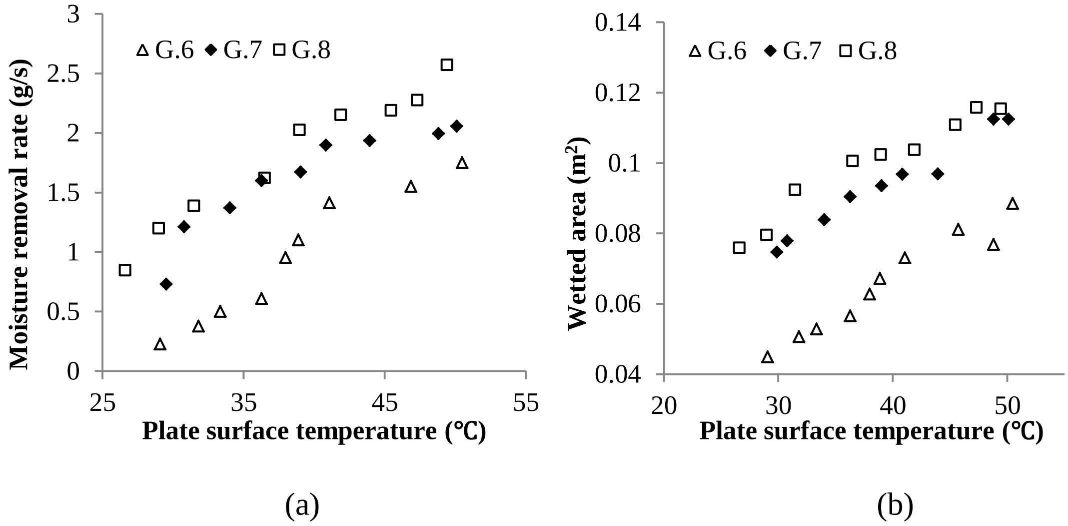

Fig. 3. 9 Changing of system performance with plate surface temperature: (a) moisture removal rate and (b) wetted area

The outlet parameters of solution during our experiments are shown in Fig. 3.10. From Fig. 3.10(a), with the increase of plate surface temperature, as the moisture removal rate increased, the outlet concentration of solution increased accordingly. So, with the higher plate surface temperature, the regeneration performance of solution could be improved. As shown in Fig. 3.10(b), due to the latent heat of vapourization in the regeneration process, the outlet solution temperature was not as high as the inlet one when it flowed over the plate and exchanged heat and mass with the air. With the increase of plate surface temperature, the outlet solution temperature also increased, and the trend became more obvious for the small mass flow rate of solution.

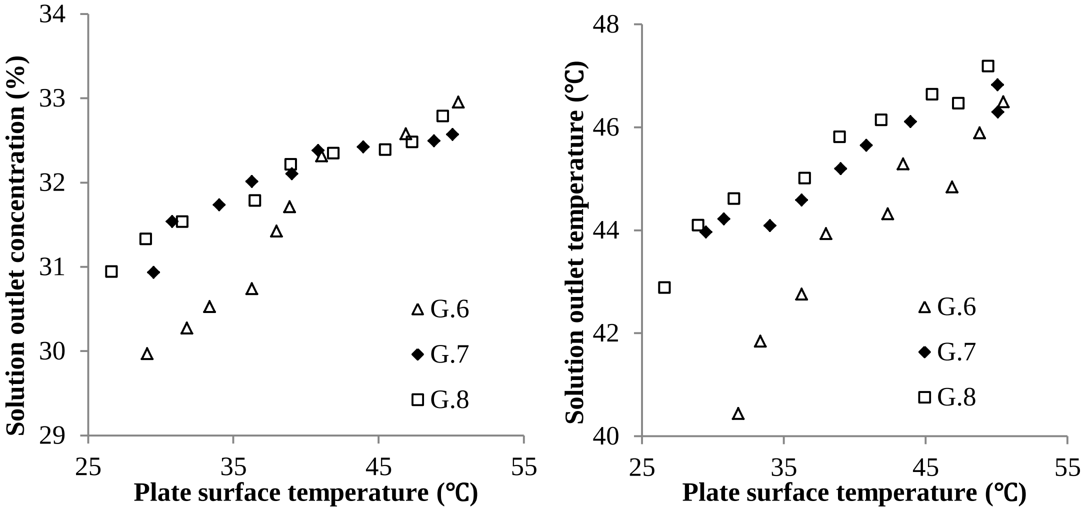

(a) (b)

Fig. 3. 10 Outlet parameters of solution with different plate surface temperature (a) concentration and (b) temperature

Therefore, the effect of plate surface temperature was more crucial at low solution mass flow rate. With the increasing plate surface temperature, the system performance could be effectively enhanced, because of the increased wetted area for heat and mass transfer and the reduced temperature difference between solution and plate. Besides, the moisture removal rate and wetted area also increased with the solution mass flow rate, which was discussed in Section 3.4.1.

The wetted area of falling film is mainly decided by two parameters, the initial film width and the wetted width along the flow direction, which were found to be determined by the characteristics of solution and working surface. The influences of the plate surface temperature on both parameters were investigated. From Fig. 3.11 (a), it could be found that the initial width of falling film rarely changed with the plate surface temperature. Therefore, the increase of wetted area was mainly caused by the weakened contraction of falling film in the transverse direction. With the thermal image camera, the size of falling film under different conditions could be recorded. Taking the experiment G.6 as an example, the $\overline{R_w}$ along the flow direction under different plate surface temperature was shown in the Fig. 3.11 (b).

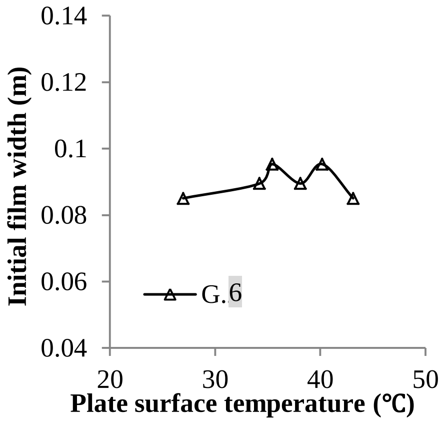

(a)

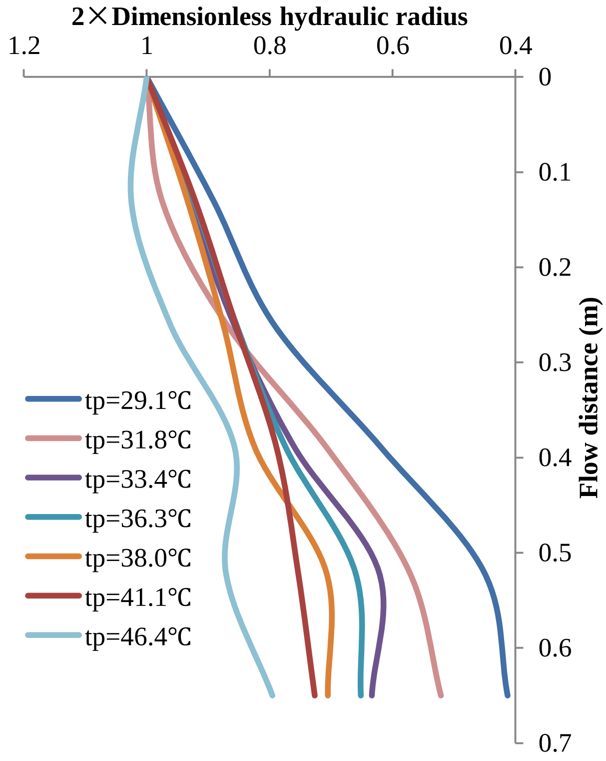

(b)

Fig. 3. 11 Initial film width and $\overline{R_w}$ under different plate surface temperatures

From Fig. 3.12 (b), with the increase of flow distance, the $\overline{R_w}$ of most conditions was reduced, but the reduction was smaller when the plate surface temperature was higher. When the surface temperature increased from 29.1 to 46.4℃, the $\overline{R_w}$ at the bottom of the working surface (when y=0.65 m) doubled, from around 0.2 to 0.4, and the wetted area increased about 1.5 times, as can be seen in Fig. 3.9 (b). The increase of the wetted width could decrease the thickness of the falling film, which could reduce the average solution velocity and increase the contact time between the air and the liquid desiccant. The enhancement of the heat and mass transfer area and time could cause a significant increase of the moisture removal rate of the regenerator. Besides, the $\overline{R_w}$ was found to be higher than 0.5 on the upper part of the working surface when the plate surface temperature was higher than the solution temperature, which means the film expanded rather than contracted in this situation.

The solution falling film was found to be divided into two parts. A horizontal temperature distribution of a test in G.6 was chosen as an example. As shown in Fig. 3.12, the surface temperature of the solution in the central part was almost unchanged along the x-axis, while that in the rim part it changed dramatically. The widths of both parts were found to be changed with the solution mass flow rate and flow distance. It was due to the change of film thickness in the rim part. The experimental conditions and the value of y-coordinate are also listed in this figure.

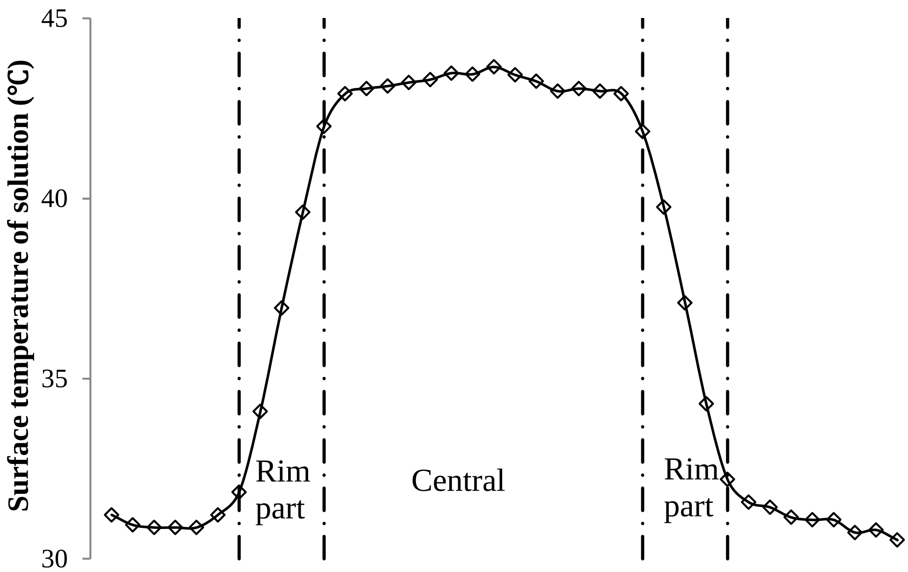

y (m)	m_s (kg/s)	$t_{s,in}$ (°C)	ζ_{in} (%)	t_p (°C)	$t_{w,in}$ (°C)	$m_{w,in}$ (kg/s)	$t_{a,in}$ (°C)	$\omega_{a,in}$ (g/kg)
0.325	0.034	46.6	30.0	29.1	51.2	0.131	24.1	9.34

Fig. 3. 12 Distribution of solution surface temperature along the x-axis

3.4.3 Influence of solution inlet temperature

To investigate the influence of solution inlet temperature, the experiments with different operation parameters were conducted, as listed in Table 3.5. The experiments could be divided into three groups, and eight tests with various solution inlet temperatures were conducted for each group. The thickness of the solution distributor was chosen as 1 mm.

Table 3. 6 Experimental conditions for different solution inlet temperature

Group No.	δ_{max} (mm)	m_s (kg/s)	$t_{s,in}$ (°C)	ζ_{in} (%)	$t_{w,in}$ (°C)	$m_{w,in}$ (kg/s)	$t_{a,in}$ (°C)	$\omega_{a,in}$ (g/kg)
9	1.0	0.037	35.5,37.3, 41.3 44.8,47.3, 49.9 52.7, 56.2	27.9	55.2	0.129	23.2	9.45
10	1.0	0.064	39.4,42.9, 45.7 49.2,52.1, 53.9 56.3,59.2	28.0	55.5	0.130	23.8	9. 41
11	1.0	0.092	35.6,39.5, 44.0 48.0,49.5, 52.0 53.3, 55.3	28.0	54.7	0.130	22.9	9.37

As indicated in Fig. 3.13, the mass transfer rate during the regeneration process increased significantly with the solution temperature. The effect was caused by the decrease of the equilibrium pressure above the solution because of the higher temperature and the increase of wetted area, as shown in Fig. 3.14.

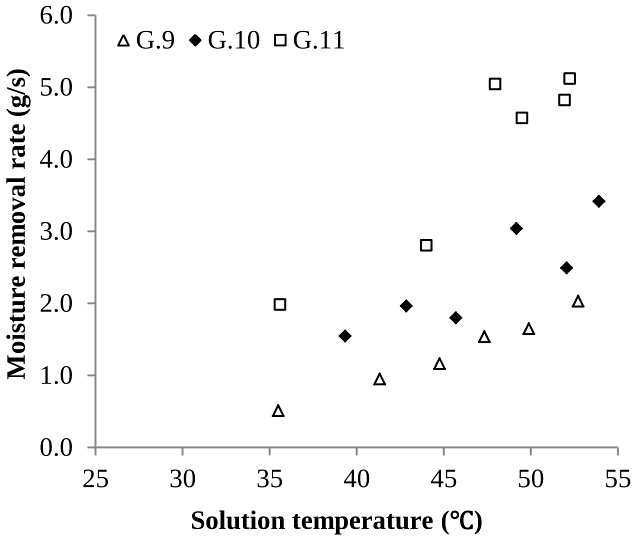

Fig. 3. 13 Changing of moisture removal rate with solution inlet temperature

It could be found that the wetted area of three experiments increased obviously with the solution temperature. The rising rate of G. 9 to 11 was about 1.6, 1.2 and 1.0×10^{-3} m^2/℃, respectively, which gives that the improvement of area was more effective in the small mass flow rate of solution. The similar result was also found in the experiment of plate surface temperature. Compared to the experiments in 3.3.2, the rising rate with the solution temperature was not as high as that with the plate surface temperature at the similar mass flow rate. As mentioned earlier, the increase of wetted area could increase the contact time between air and solution. The improvement of heat and mass transfer area and time could cause a significant increase of the regeneration efficiency.

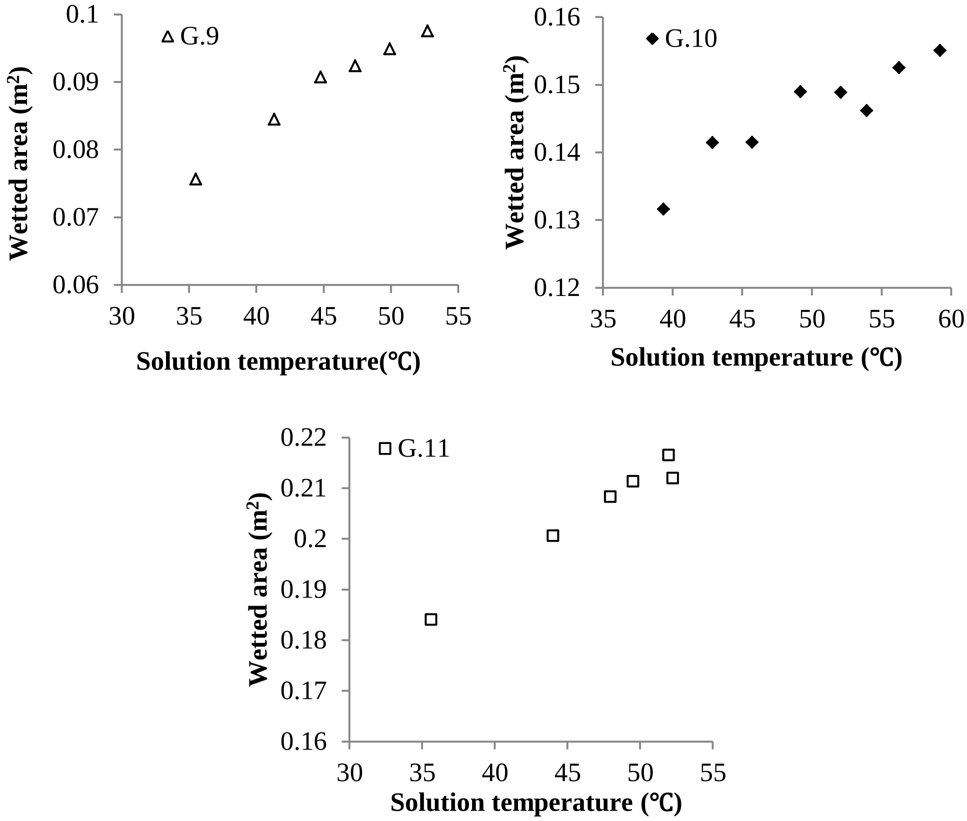

Fig. 3. 14 Changing of wetted area with solution inlet temperature

The influence of the solution temperature on wetted area could be divided into two parts. The experiment G. 10 was used as an example. As shown in Fig. 3.15 (a), with the increase of solution temperature, the initial film width, W_i, increased with the rate of about 1.4 $\times 10^{-3}$ m/℃. However, it could be found that the film contraction in the transverse direction aggravated with the higher solution temperature in most conditions. The $\overline{R_w}$ along the flow direction under different solution temperatures was shown in the Fig. 3.15 (b). Fortunately, the enlargement of film contraction or the decrease of $\overline{R_w}$ was not serious. For example, when the temperature increased from 42.9 to 59.2℃, the $\overline{R_w}$ at the middle of the working surface (when y=0.325 m) decreased from about 0.4 to 0.38, and the average decreasing ratio was only about

0.37 %/℃. The effect of film contraction on the wetted area was offset by that of the initial film width, so the area increased with the solution temperature. It also explained the reason that the rising rate of the area with solution temperature was not as high as that with the plate surface temperature.

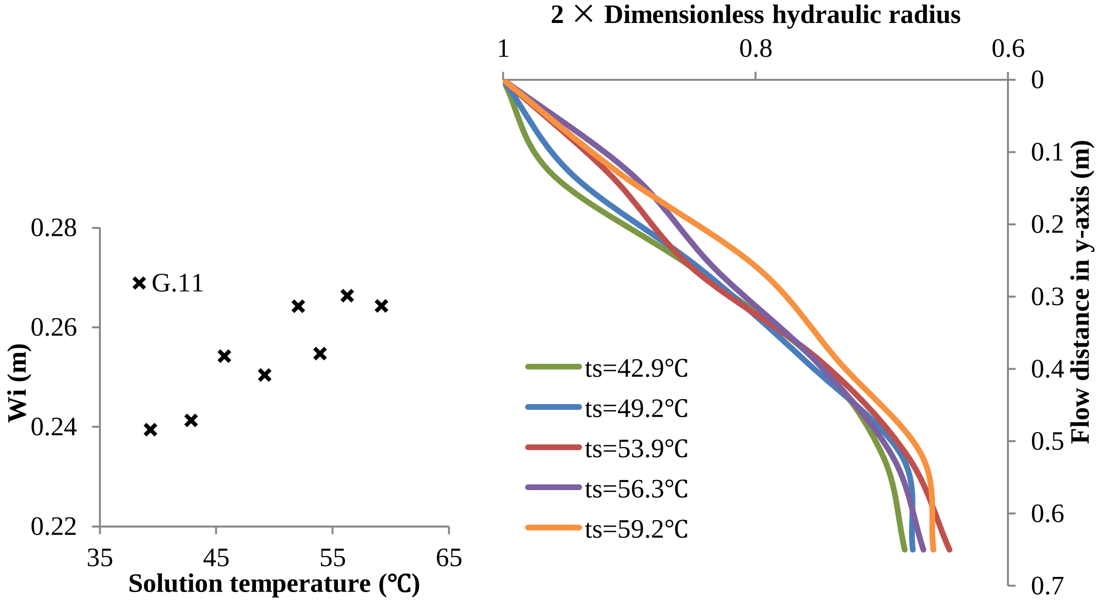

(a) (b)

Fig. 3. 15 Changing of system performance with solution inlet temperature (a) Initial wetted width and (b) Dimensionless hydraulic radius

3.4.4 Influence of pre-wetting of working surface

During our experiments, it was found that the pre-wetting of working surface could benefit the regeneration performance. To find the detail impacts of the pre-wetting, four groups of experiments were conducted, and each group includes 6-7 individual tests with various plate surface temperatures or solution temperatures. The thickness of the solution distributor was chosen as 1 mm. At the beginning of each test, for G.

12 and 14, the whole working surface was cleaned with the water and alcohol, and was then carefully blew with the hot air, to make the whole surface as dry as possible. In terms of G. 13 and 15, the desiccant with the same temperature of working surface was applied to flow down for 1-2 minutes, to make the whole surface wetted as completely as possible. The surface temperature used in our analysis is the average temperature of the whole plate.

Table 3. 7 Experimental conditions for different solution inlet temperature

Group No.	m_s (kg/s)	$t_{s,in}$ (°C)	t_p (°C)	ζ_{in} (%)	$m_{w,in}$ (kg/s)	$t_{a,in}$ (°C)	$\omega_{a,in}$ (g/kg)
12	0.062	37.4,42.1,45.3 49.0,52.8,55.4 57.2	35.4	27.9	0.129	23.8	9.45
13	0.064	39.4,42.9,45.7 49.2,52.1,56.3 59.2	35.5	28.0	0.130	23.8	9. 41
14	0.062	44.8	26.9,30.5,33.7 37.8,41.4,43.5	27.9	0.128	22.7	9.56
15	0.063	44.5	27.0,34.2,35.4 38.1,40.2,43.1	28.0	0.125	21.2	9.22

It could be found that the moisture removal rates in the pre-wetting conditions were significantly higher than those in the dry ones, due to the enhancement of wetted area. As shown in Fig. 3.16, the wetted area increased obviously when the surface was uniformly pre-wetted. The increasing ratio of the area was about 30-40% by comparing with G. 12 and 13. In terms of G. 14 and 15, the ratio was even higher, about 45-60%. As mentioned before, the increase of wetted area could importantly improve the regeneration efficiency of the internally heated regenerator.

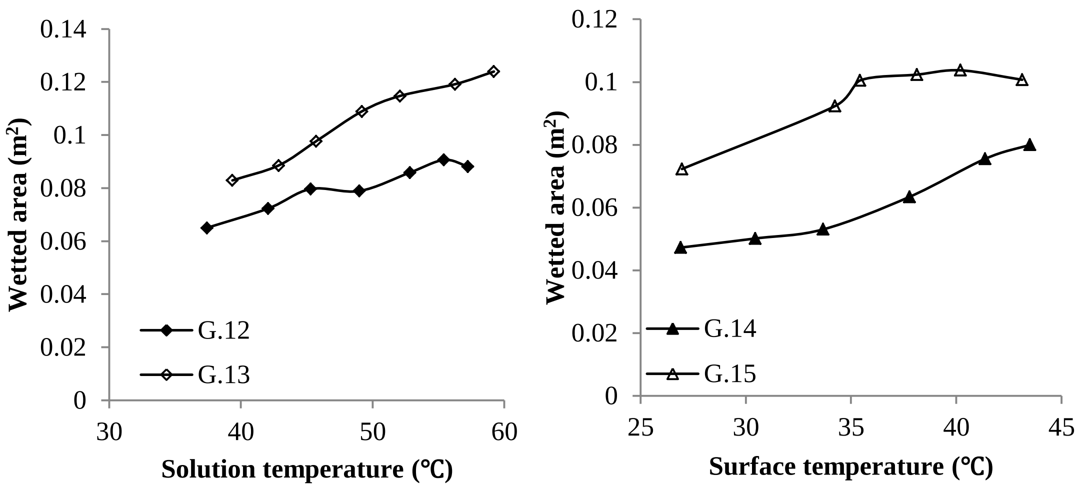

Fig. 3. 16 Changing of wetted area with (a) solution inlet temperature and (b) plate surface temperature

From Fig. 3.17, when the surface was pre-wetted, the initial width of falling film was obvious enlarged for 1-2 times. Furthermore, the film contraction was found to be effectively restrained during the pre-wetting conditions. Two tests with almost similar experimental conditions, one from G. 12 and one from G. 13, were chosen as examples. As shown in Fig. 3.18, along the flow direction, the $\overline{R_w}$ of the pre-wetted test was about 1.5 to 2 times of that of the dry one, and the effect was more obvious when y was larger (the flow distance was longer). Therefore, with the combined effect of enlarged initial width and weakened film contraction, the wetted area was dramatically enhanced during the pre-wetting conditions. The experimental conditions of the two tests are also listed in this figure.

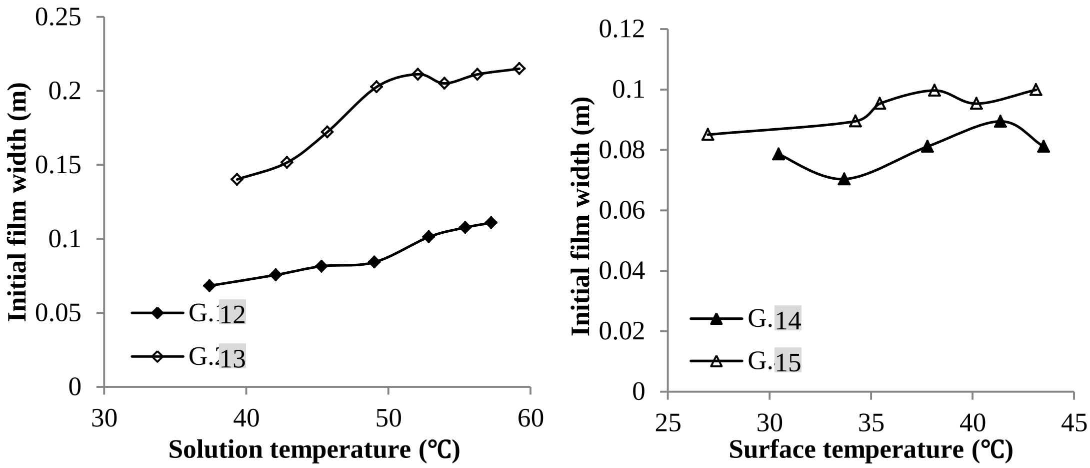

Fig. 3. 17 Changing of initial wetted width with (a) solution inlet temperature and (b) plate surface temperature

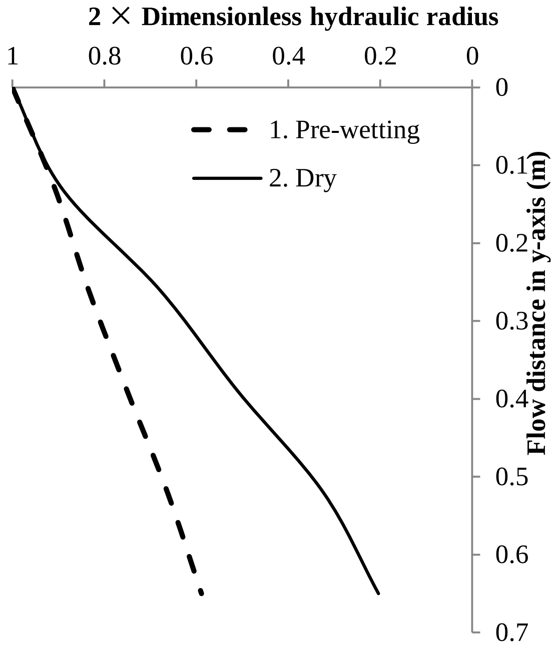

No.	m_s (kg/s)	$t_{s,in}$ (℃)	ζ_{in} (%)	t_p (℃)	$m_{w,in}$ (kg/s)	$t_{a,in}$ (℃)	$\omega_{a,in}$ (g/kg)
1	0.062	44.8	27.9	37.8	0.128	22.7	9.56
2	0.063	44.5	28.0	38.1	0.125	21.2	9.22

Fig. 3. 18 Dimensionless hydraulic radius along the flow direction in both pre-wetting and dry conditions

The solution contact angle on the working surface is found to affect the wetted area play critically. With the goniometer, the contact angle and surface properties could be observed and recorded. The two tests from G. 14 and G. 15 were still chosen as examples. From Fig. 3.19 (a), the surface was plain if it was totally dry, and the contact angle was about 65 °. However, when the surface was uniformly pre-wetted, in Fig. 3.19 (b), small liquid desiccant droplets would spread above the surface, which made the surface hydrophilic, so the contact angle significantly reduced. Additionally, the solution contact angle was changed with the solution and surface characteristics, which will be discussed in the next section.

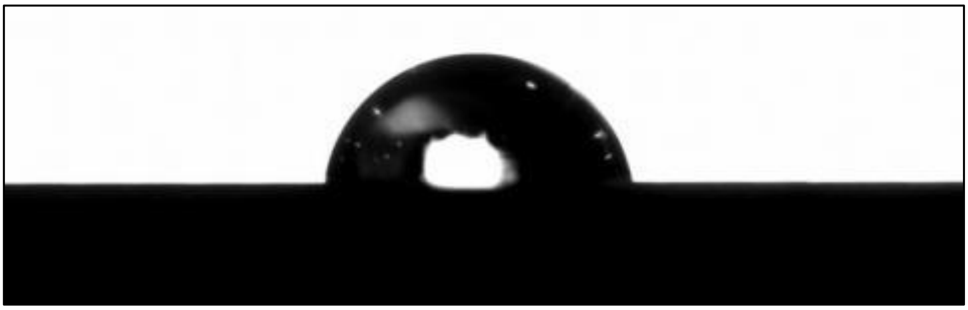

(a)

(b)

Fig. 3. 19 Solution contact angle on the working surface under (a) dry condition and (b) pre-wetting condition

The pre-wetting of working surface is the simplest way to make it hydrophilic, but it is difficult to make the surface completely wetted and the effect may not be stable in industrial applications. Many manufacture processes, such as self-cleaning coating and surface roughness, could also be applied to reduce the contact angle of the working surface.

3.4.5 Influencing factors of contact angle

According to our experimental results, the contact angle of the desiccant showed a significant impact on the wetted area of falling film liquid desiccant regeneration system. As indicated in previous researches, this angle changes with the characteristics of solution and working surface. However, the research on the contact angle during the regeneration process is very limited. To predict the wetted area of falling film accurately, the influencing factors affecting the contact angle were experimentally investigated, including the concentration and temperature of desiccant, and the roughness of the surface.

The widely used LiCl was chosen as the liquid desiccant in this research. Four test plates made by stainless steel (Type 316, similar to the working surface applied in our experiments) with different surface roughness were produced. The contact angles with different parameters were obtained by the contact angle goniometer, with an accuracy of 0.05°. The temperature was measured by the thermal camera imager, with a maximum error of 0.1 ℃. The profile roughness parameter, Ra, of the plates was recorded by the Veeko laser optical interferometer, with an accuracy of 0.01 nm. To measure the angle, a solution droplet was dripped on a test plane, and stayed for about 30-60 seconds to approach the stable condition. Then, the angle was recorded by the goniometer automatically. To improve the experimental accuracy, every test was repeated 4-5 times to obtain the average contact angle.

As the droplet of solution was small, its temperature was assumed to be equal to the temperature of test plate surface. The surface temperature used in our analysis is the average temperature of the whole test plate. During our experiments of internally heated regeneration, as the contact angle occurs at the edge of the falling film, which was thin, the solution temperature could be also assumed to be equal to the temperature of plate surface.

The effect of surface roughness on the contact angle was firstly investigated. The Ra of the four test plates was 551.7, 393.8, 287.9 and 171.5 nm, respectively. As shown in Fig. 3.20, with the increase of Ra, the contact angle increased at first and then decreased. The trends of the tests with different solution concentrations were similar. By fitting the data with the least square method, the maximum angle could be predicated to occur in the Ra of 369.1 nm. Therefore, the higher or smaller surface roughness is useful to reduce the contact angle, which could benefits the wetted area of falling film. During the tests, the temperature of the test plates and solution was kept as 24.5℃.

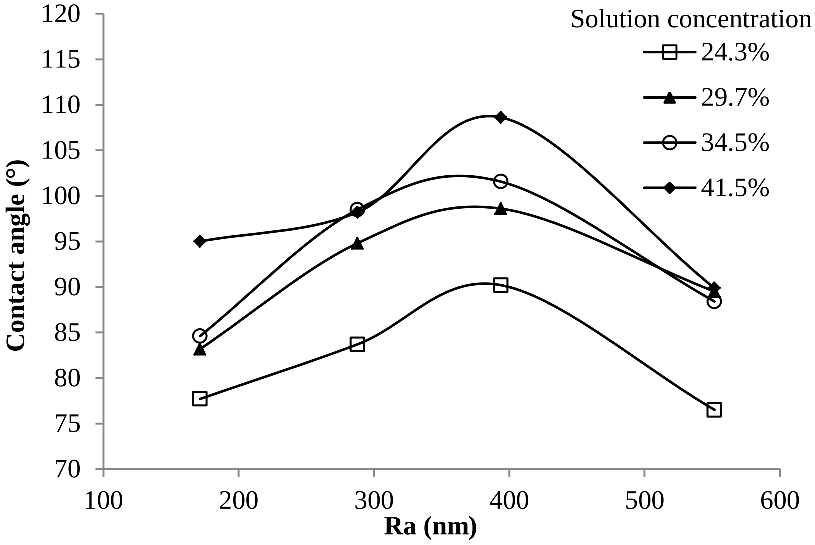

Fig. 3. 20 Changing of solution contact angle with surface profile roughness parameter

Then, the contact angle of solution with different concentrations on the same test plate (Ra=287.9 nm) was investigated. As shown in Fig. 3.21, the angle was found to increase with the concentration, with an increasing rate of about 0.89 °/%. Due to the increase of contact angle, as shown in Fig. 3.6(b), the wetted area decreased with the solution concentration. Besides, during the tests, the temperature of the test plates and solution was kept as 24.5℃.

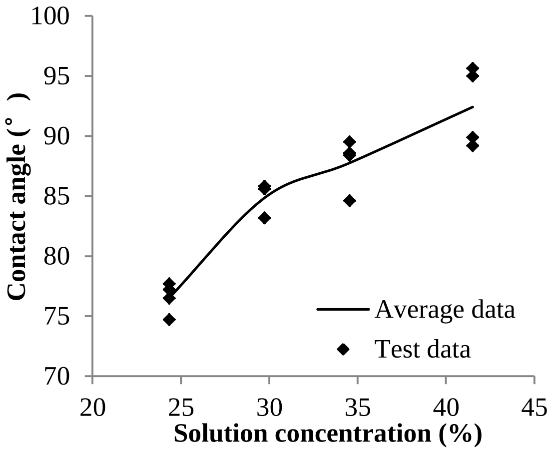

Fig. 3. 21 Changing of solution contact angle with solution concentration

Then, the influence of solution temperature was studied experimentally. As shown in Fig. 3.22, the contact angle decreased almost proportionally with the solution temperature. But the change was relatively minor, with the rate of about 0.52 °/℃. During the tests, the solution concentration was the 34.5%, and the Ra of test plate was 287.9 nm.

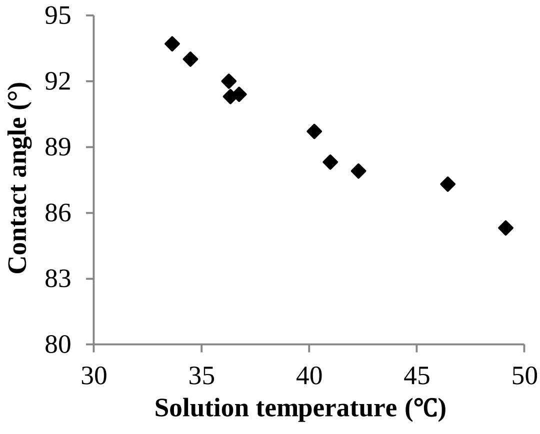

Fig. 3. 22 Changing of solution contact angle with solution temperature

3.5 Discussion

In the falling film regeneration system, the wetted area is a key parameter. In this chapter, by building and testing a single channel internally heated regenerator, the influencing factors affecting the wetted area were investigated experimentally, as well as their effects on the mass transfer performance.

The increase of wetted area could significantly improve the moisture removal rate of regenerator. In incomplete wetting conditions, the typical flow shape of solution falling film was a symmetrical tongue type, and the film contracted along the flow direction. The film area was mainly decided by two parameters, i.e. the initial film width and the wetted width along the flow direction, which are determined by the characteristics of solution and working surface. Air and hot water affected slightly compared to the properties of desiccant.

The initial film width was affected most greatly by the thickness of solution distributor. When the working surface was pre-wetted to reduce the desiccant contact angle, the width could be dramatically increased. Another significant influencing factor of the initial width was the mass flow rate of solution, with which the width increased almost proportionally. With the increase of solution temperature, the initial width also increased, with a relatively slow growth rate. The effect of solution concentration was minor. Furthermore, the contraction of falling film could be effectively weakened when the surface was pre-wetted to make it hydrophilic, so the film width along the flow direction increased significantly. The increase of plate surface temperature could also reduce the film contraction in transverse direction especially at low solution mass flow rate. The contraction was found to be aggravated with higher solution temperature but slightly. Both the initial width and film width along the flow direction were affected by the solution contact angle, which was experimentally found to be determined by the surface roughness, solution concentration and temperature.

Therefore, the wetted area of falling film is mainly influenced by the parameters of liquid desiccant, working surface and operation conditions. To evaluate the performance of falling film regeneration system accurately, it is necessary to develop a theoretical model for simulating the wetted area by considering the comprehensive effect of different parameters.

CHAPTER 4

MODEL DEVELOPMENT AND ANALYTICAL SOLUTION FOR WETTED AREA OF INTERNALLY HEATED REGENERATOR

4.1 Introduction

As the working surface is usually wetted incompletely by the desiccant in practical applications, the wetted area is a critical factor affecting the system performance of falling film liquid desiccant regeneration system. In Chapter 3, the impacts of different influencing factors on the wetted area were investigated experimentally, by testing a single channel internally heated regenerator. It concludes that the wetted area is determined by many parameters, such as the characteristics of liquid desiccant, working surface, solution distributor, etc.

As summarized in Chapter 2, most previous studies of the wetted area focused on the applications of vertical condenser, evapourator or absorption tower. The minimum wetting rate, which is related to the initial film width, has been studied experimentally by Moran et al. (1997), Broome et al. (2005) and Morison et al. (2006). Furthermore, Wasden et al. (1990), Yoshimura et al. (1996) Chang et al. (2002) and Park et al. (2004) investigated the film deformation led by the inherently instability experimentally and theoretically, but most works only considered the effect on the stream-wise direction. Geng et al. (2001) and Zhang et al. (2006) observed the uneven film characteristics in the transverse direction and developed a model to predict the contraction distance of water film. In addition, the studies of contact angle were summarized and discussed by Luo et al. (2007). But there are gaps between current predictions and experimental results. Therefore, the research on the wetted area under different operation and design parameters was insufficient, especially in the area of liquid desiccant dehumidification/regeneration. To obtain an acceptable value of the area, a model should be developed to predict the size of falling film. With the model, the heat and mass transfer process could be evaluated and simulated more accurately.

In this chapter, based on the experimental results, a theoretical model was developed for accurately calculating the wetted area of falling film liquid desiccant system. As discussed earlier, the wetted area is mainly determined by two parameters, i.e. the initial film width, and the wetted width along the flow direction. The contact angle also affects the wetted area by influencing the two parameters. The model could be divided into three parts, including the model for initial wetted width, the model for contact angle and the model for the contraction distance along the flow direction. To verify the model, the results were compared with the experimental findings.

With this new model, the change of wetted area with different conditions of the regeneration process was simulated numerically. For enhancing the mass transfer performance, some suggestions were given to enlarge the film area of the internally heated liquid desiccant system. Although the model was developed under the regeneration process, as the similar heat and mass transfer mechanism between dehumidification and regeneration, it could also be applied for the dehumidification process of liquid desiccant system.

4.2 Model for Contact Angle

By affecting the wetted area, the contact angle of desiccant is important in the falling film liquid desiccant system. The change of contact angle could change both the initial width and the width along the flow direction of the solution film. Therefore, to predict the wetted area of falling film, it is necessary to develop a model for calculating the contact angle under different parameters. The widely used LiCl was chosen as the liquid desiccant in this research. The working surface is made of stainless steel, which is applied in most practical applications and our experiment.

In our experiment, it could be found that the contact angle of LiCl increased with the solution concentration and decreased with the temperature. Furthermore, when the roughness of the surface increased, the angle firstly increased and then decreased, showing a maximum value. Based on the experimental result, the angle is supposed to be the function of the surface tension, which is decided by the solution concentration and temperature, and the roughness of working surface. With the test data of different conditions, the function could be obtained by the multiple linear regressions, as shown in Eq. (4.1).

$$\lg(\theta) = 4.55 \cdot f(Ra) + 17.37 \cdot \sigma(T_s, \zeta) - 1.58 - 0.314 \cdot \alpha \qquad (4.1)$$

Based on our experimental data, the $f(Ra)$ and α could be obtained by the following equation.

$$\begin{aligned} & f(Ra) = -3.51 \times 10^{-7} \cdot Ra^2 + 2.59 \times 10^{-4} \cdot Ra \\ & \alpha = \begin{cases} 1 & \text{if the working surface is properly pre-wetted} \\ 0 & \text{if the working surface is dry} \end{cases} \end{aligned} \qquad (4.2)$$

Besides, the surface tension could be calculated by (Conde, 2004):

$$\begin{aligned} \sigma(T_s, \zeta) = & (2.36 - 1.47 \cdot (1 - \frac{T_s}{647.3}))(1 + 2.76\zeta - 12.01\zeta(\frac{T_s}{647.3}) \\ & + 14.75\zeta(\frac{T_s}{647.3})^2 + 2.44\zeta^2 - 3.15\zeta^3)(1 - \frac{T_s}{647.3})^{1.26} \end{aligned} \qquad (4.3)$$

where θ is the contact angle of the solution/air interface on the working surface, with the unit of rad. Ra is the profile roughness parameter, which stands for the surface roughness of the plate, with the unit of nm. σ means the surface tension of solution, which is determined by T_s, the absolute temperature, and ζ, the concentration of liquid desiccant. α stands for whether the plate is uniformly pre-wetted or not.

To verify the newly developed equation, the experiment results under about 55 different conditions were compared with the calculation ones by Eq. (4.1-4.3). The

Average Relative Deviation (ARD) between our prediction result and experimental result could be calculated by the following equations.

$$ARD = \frac{1}{n}\sum_{i=1}^{n}\left|\frac{W_{\exp eriment,i} - W_{prediction,i}}{W_{\exp eriment,i}}\right| \times 100\% \qquad (4.\ 4)$$

where n is the number of data.

As shown in Fig. 4.1, compared to the experiment ones, the calculated result of contact angle showed an acceptable difference of less than ±25%, with a small ARD of 12.3%. Therefore, the equation could be employed to calculate the contact angle of LiCl on the stainless steel surface.

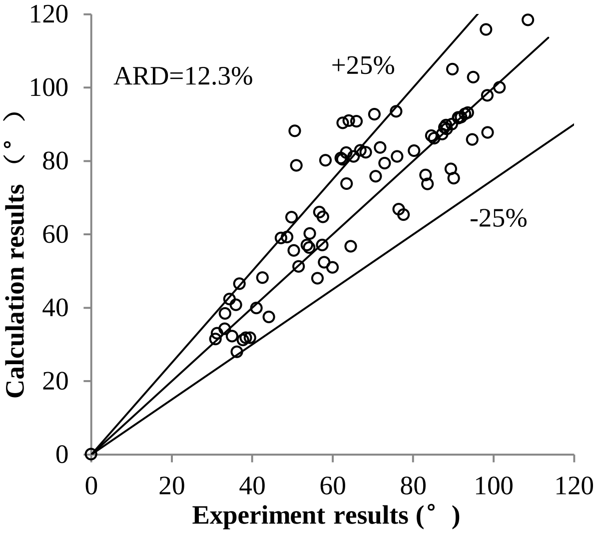

Fig. 4. 1 Comparison between calculation and experimental results of contact angle

With the equation, the impacts of influencing factors of contact angle of LiCl were discussed. The pre-set initial values for the simulation were: t_s=50℃, $\zeta_{in} = 30\%$ and

Ra=600 nm. By changing one parameter and keeping others as constant, the contact angle under different operation conditions could be calculated numerically.

As indicated in Fig. 4.2, the contact angle increased almost proportionally with the surface tension of solution. As the surface tension is the function of solution temperature and concentration, the contact angle could be considered to increase with the concentration and decrease with the temperature of liquid desiccant. According to the function of surface tension, the change rate of angle with the concentration is much higher than that with the solution temperature. Furthermore, with the increase of surface roughness, the contact angle increased at first and then decreased, and showed the maximum value when the Ra was around 379 nm.

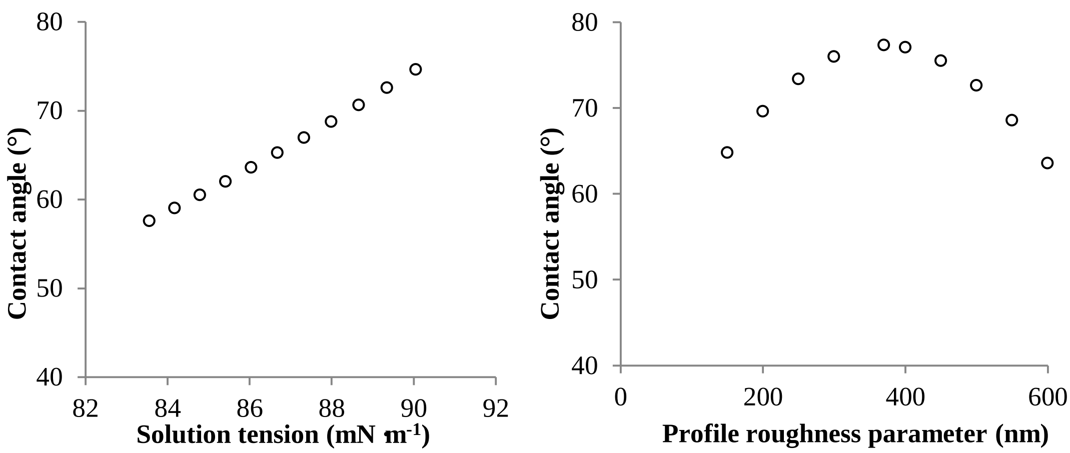

Fig. 4. 2 Influencing factors of contact angle of LiCl

The small contact angle of solution benefits the wetted area of falling film regeneration system, as well as the mass transfer performance. Therefore, to reduce the angle, making the surface rougher or smoother is helpful, and decreasing the solution surface tension is also effective.

4.3 Model for Initial Wetted Width

An important factor on the solution wetted area is the initial film width, W_i, which means the width of falling film at the top of the working surface. According to our experiment, under incomplete wetting conditions, the thickness of solution distributor greatly affected the wetted width. It also increased almost proportionally with the mass flow rate of solution. With the increase of temperature or the decrease of concentration of desiccant, the initial width increased but insignificantly. Besides, the impact of air and hot water could be neglected compared to the properties of desiccant.

Based on our experimental data and previous research (Moran et al., Broome et al., Morison et al., and Zhang et al.), a semi-theoretical formula for calculating the initial wetted width was developed, as shown in Eq. (4.5).

$$W_i = \frac{2.53 \times 10^{-4} \cdot m_s \gamma_s^{0.2}}{{\delta_{\max}}^3 \rho_s g (1-\cos\theta)^{0.6}} \tag{4. 5}$$

where $\delta_{\max}$ means the thickness of solution distributor, and m_s is the mass flow rate of solution. γ_s and ρ_s stand for the kinematic viscosity and density of solution respectively, which are decided by the solution temperature and concentration

(Manuel et al., 2009). θ is the contact angle of solution/air interface on the working surface.

To verify the equation, the measured initial film widths of more than 50 experiments were compared with the result obtained by Eq. (4.5). As shown in Fig. 4.3, the calculated result of initial width showed an acceptable difference of less than ±20%, with a small ARD of 8.76%. Therefore, the equation can be employed to calculate the initial film width of liquid desiccant system.

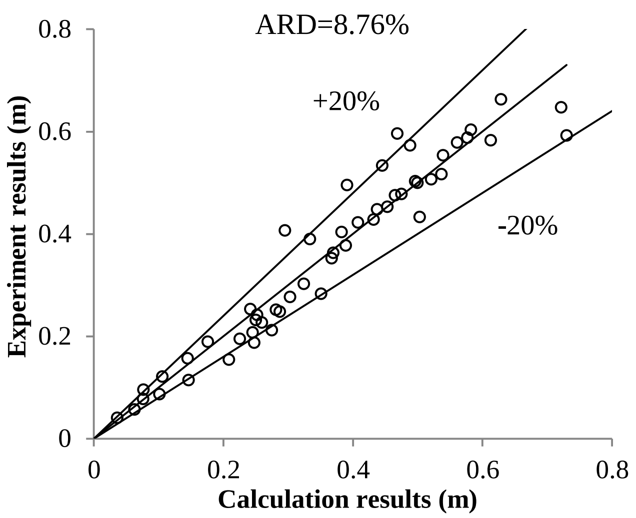

Fig. 4. 3 Comparison of initial width between calculation and experiment result

With the equation, the impact of different parameters could be investigated numerically. The pre-set initial values for the simulation were: t_s=50℃, $\zeta_{in} = 30\%$, Ra=600 nm, m_s=0.05 kg/s and δ_{max} =1 mm. As shown in Fig. 4.4 (a), the W_i decreased dramatically with the thickness of solution distributor. The smaller the thickness is, the higher change rate of W_i . From Fig. 4.4 (b), W_i increased proportionally with the solution mass flow rate. As shown in Fig. 4.4 (c), the impact of solution concentration is slight, and it could be expressed as the change of density, viscosity and contact angle of liquid desiccant.

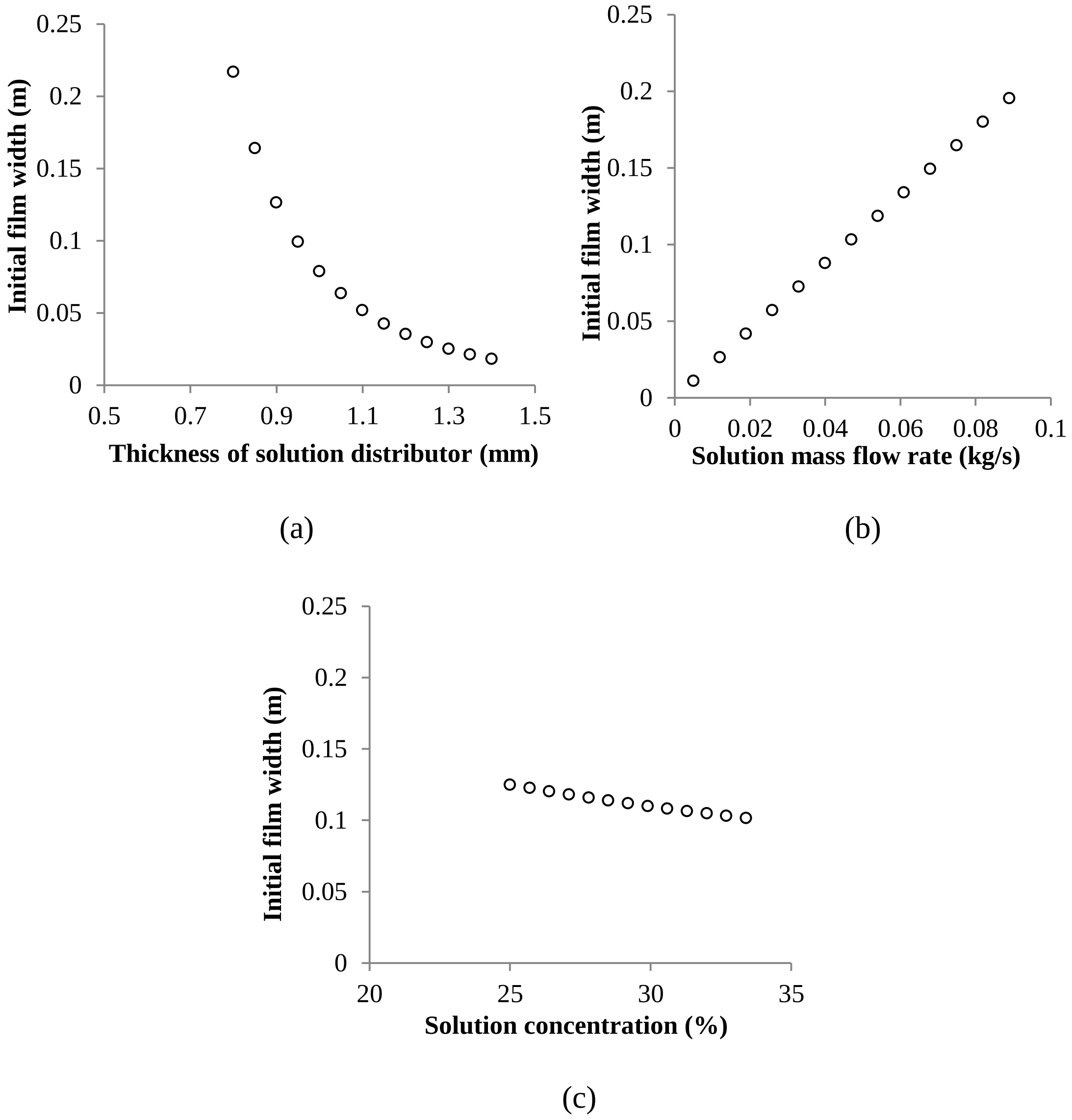

Fig. 4. 4 Influencing factors of initial wetted width during internally heated regeneration process (a) thickness of solution distributor, (b) solution mass flow rate and (c) solution concentration

Therefore, to increase the initial film width for larger wetted area, reducing the thickness of solution distributor is the most effective way, and the increase of solution mass flow was also useful.

4.4 Model for contraction distance along the flow direction

4.4.1 Model development for contraction distance along the flow direction

From the experiment, in incomplete wetting conditions, the typical flow shape of solution falling film was symmetrical, and the film was contracted along the flow direction. But in several conditions, the film was expanded. The contraction distance, which is the difference between the initial and local film wetted width, were found to be influenced by the fluids and working surface comprehensively. With the increase of plate surface temperature or the decrease of solution temperature, the film contraction in transverse direction was found to be reduced especially at low solution mass flow rate. If the surface is pre-wetted to be hydrophilic, the contraction could also be effectively weakened. Besides, the film width along the flow direction was affected by the solution contact angle.

The contraction of falling film is mainly caused by small fluid flow in the transverse direction. When the working surface is cooled/heated by the extra fluid, the heat transfer would change the properties of falling film (Goussis et al. 1987; Wilson et al. 2002). These variations lead to an uneven distribution of surface tension upon the liquid-vapour interface, which could induce a fluid flow in the transverse direction (Kabov et al. 2002). This effect, namely the Marangoni effect, could significantly influence the wetted area and flow dynamics, and the heat and mass transfer of the falling film dehumidifier/regenerator as well.

To simplify the problem, based on our experimental result (as described in Section 4.4.2), the falling film could be divided into two parts: a central part with an almost uniform solution temperature and a rim part with a dramatically changed temperature. The surface tension gradient in the rim part is considered to be the main reason for bringing about the contraction of the internally heated falling film. The surface tension gradient would be caused by not only the temperature difference, but also the solution concentration gradient in the rim part. Fig. 4.5 shows a schematic of the uppermost section of the solution falling film, which is symmetric to the y-axis. The central and rim part were indicated in this figure, and D_r stands for the width of rim part. σ_{cen} and σ_{rim} mean the surface tension of the sides of rim part. The velocity profile of y-z cross section was also shown. t_p and $t_{s,in}$ mean the plate surface temperature and the inlet temperature of falling film, respectively. Δx stands for the film deformation distance, which is a positive value when the film contracts and a negative value when the film expands. It should be noticed that Δx would be changed with the flow distance of the falling film.

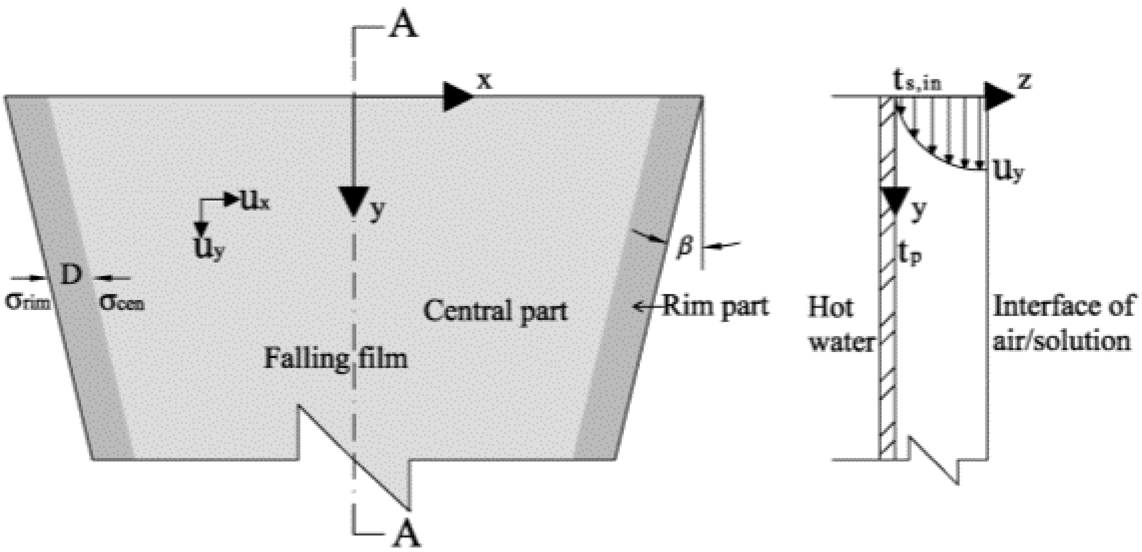

Fig. 4. 5 Schematic of solution falling film and the y-z cross section

The following assumptions were made: 1) the flow of falling film was laminar, and both solution and air flow were fully developed; 2) the desiccant flow was smooth, which means the film waves were neglected; 3) the thermodynamic equilibrium was approached immediately on the desiccant/air interface; 4) the change of solution velocity and temperature gradient in z-direction was neglected; 5) the effect of gravity and inertia force in x axis was neglected; 6) at the edge of falling film, the solution temperature was equal to the plate temperature of working surface, and the film thickness was equal to the thickness of boundary layer; and 7) Two-Film Theory was applied to solve the problem.

The film contraction is caused by the difference of surface tension, which leads to a solution flow in the transverse direction, u_x . For the rim part, the momentum equation and boundary conditions in the z-direction could be obtained by:

$$\mu_s \frac{\partial^2 u_x}{\partial z^2} = 0$$

Boundary conditions

$$z = 0 \qquad u_x = 0 \tag{4. 6}$$

$$z = \delta_x \qquad \mu_s \frac{\partial u_x}{\partial z} = \frac{\partial \sigma}{\partial x} \cos\beta$$

where the β is the angle indicated in Fig. 4.5.

By integrating the momentum equation in the film thickness direction and considering the Marangoni flow rate in the previous research (Kabov et al. 2002), the transverse flow velocity on the liquid/air interface could be expressed as the following equation:

$$\mu_s \frac{u_x}{\delta_x} = \frac{\partial \sigma}{\partial x} \cos\beta = \frac{(\sigma_{cen} - \sigma_{rim})}{4D_r} \frac{u_{y,m}}{\sqrt{u_{y,m}^{\ 2} + u_x^{\ 2}}} \tag{4. 7}$$

Therefore, solving the Eq. (4.7), the u_x could be obtained:

$$u_x = \frac{\sqrt{2}}{2} u_{y,m} [(1 + \frac{4(\frac{\delta_{cen}(\sigma_{cen} - \sigma_{rim})}{4\mu_s D_r})^2}{u_{y,m}^{\ 2}})^{1/2} - 1]^{1/2} \tag{4. 8}$$

where $u_{y,m} = \frac{1}{2} \frac{\rho_s g}{\mu_s} \delta_{cen}^{\ 2}$, means the maximum flow velocity in y-direction. δ_{cen} stands for the film thickness at the position of the central side of the rim part. μ_s, ρ_s

and σ stand for the dynamic viscosity, density and surface tension of solution respectively, which are decided by the solution temperature and concentration.

The value of D_r could be calculated with the following equation (Zhang et al. 2005).

$$D_r = \frac{\kappa \delta_{cen} \sin\theta}{1-\cos\theta} + \delta_{cen}\sqrt{\frac{2\kappa(\kappa-1)}{1-\cos\theta} - (\kappa-1)^2} \tag{4. 9}$$

where θ means the contact angle of the solution on the specific working surface. κ stands for the deformation of solution film in the transverse direction, which changes with the flow distance.

Therefore, by integrating the Eq. (4.7), the contraction distance during the internally heated regeneration process could be obtained by Eq. (4.10).

$$\begin{aligned}
&\Delta x = 2\cdot\int_0^{y/u_{y,m}} u_x dt = \sqrt{2}u_{y,m}\frac{|\sigma_{rim}-\sigma_{cen}|}{\sigma_{rim}-\sigma_{cen}}\int_0^y [(1+\frac{\delta_{cen}{}^2(\sigma_{cen}-\sigma_{rim})^2}{4u_{y,m}{}^2\mu^2 D_r{}^2})^{1/2}-1]^{1/2}dy \\
&\text{let } f(y) = [(1+\frac{\delta_{cen}{}^2(\sigma_{cen}-\sigma_{rim})^2}{4u_{y,m}{}^2\mu^2 D_r{}^2})^{1/2}-1]^{1/2} \\
&\Delta x = \sqrt{2}u_{y,m}\frac{|\sigma_{rim}-\sigma_{cen}|}{\sigma_{rim}-\sigma_{cen}}\int_0^y f(y)dy
\end{aligned} \tag{4. 10}$$

In this equation, the surface tension in the central side, σ_{cen}, is decided by the temperature and concentration of the solution/air interface of falling film in the same position, $t_s(x, y, \delta_{cen})$ and $\zeta_s(x, y, \delta_{cen})$. Furthermore, the surface tension at the edge of falling film, σ_{rim}, is the function of the plate temperature of working surface and the solution concentration on the interface at the edge of falling film, t_p and $\zeta_{s,p}$. δ_{cen} stands for the film thickness at the position of central side of the rim part.

From Eq. (4.10), the function $f(y)$ was extremely complicated and difficult to be integrated. By the numerical simulation, it could be found that the function increases monotonically. Therefore, to obtain the analytical solution, the Eq. (4.10) could be solved with the mean value theorem of integrals, as shown in Eq. (4.11).

$$\Delta x \approx \sqrt{2} u_{y,m} \frac{\left|\sigma_{rim} - \sigma_{cen}\right|}{\sigma_{rim} - \sigma_{cen}} f(\frac{y}{2}) y$$
$$\text{where } f(y) = [(1 + \frac{\delta_{cen}{}^2 (\sigma_{cen} - \sigma_{rim})^2}{4 u_{y,m}{}^2 \mu^2 D_r{}^2})^{1/2} - 1]^{1/2} \tag{4. 11}$$

It could be found that the surface tension on the solution/air interface plays a significant role in this equation. To obtain the distance, an analytical solution for the surface tension should be developed firstly.

4.4.2 Model development for surface tension on the air/solution interface

As the surface tension of liquid desiccant is determined by both temperature and concentration, to solve the Eq. (4.11), the formulas of $t_s(x, y, \delta_{cen})$, t_p , $\zeta_s(x, y, \delta_{cen})$ and $\zeta_{s,p}$ should be obtained, which are discussed in the following sub-sections.

1) **Solution of desiccant temperature on the desiccant/air interface**

The desiccant temperature on the desiccant/air interface, $t_s(x,y,\delta_{cen})$, could be obtained with the following governing equations and boundary conditions.

$$\mu\frac{\partial^2 u_y}{\partial z^2}+\rho g=0$$
$$u_y\frac{\partial t_s}{\partial y}=a_s\frac{\partial^2 t_s}{\partial z^2}$$

Boundary conditions

$$z=0 \qquad u_y=0,\ t_s(x,y,0)=t_p;$$
$$z=\delta_x \qquad \frac{\partial u_y}{\partial z}=0,\ \frac{\partial t_s(x,y,\delta)}{\partial z}=-\frac{h}{\lambda}(t_s(x,y,\delta)-t_a);$$
$$y=0 \qquad t_s(x,0,z)=t_{s,in}; \tag{4. 12}$$

where h is the convection heat transfer coefficient between solution and air. λ is the thermal conductivity of solution. u means the flow velocity. a_s means the thermal diffusivity of solution. δ is the thickness of falling film. The subscript *s*, *a* and *p* stand for the solution, air and plate surface, respectively.

By solving the equations, the distribution of solution temperature on the film surface could be expressed as:

$$t_s(x,y,\delta)=\left(t_{s,in}-\frac{\frac{h}{\delta c_s\rho_s}t_a+\frac{a_s}{\delta^2}t_p}{\frac{h}{\delta c_s\rho_s}+\frac{a_s}{\delta^2}}\right)e^{-\frac{12\left(\frac{h}{\delta c_s\rho_s}+\frac{a_s}{\delta^2}\right)}{5u_{y,m}}y}+\frac{\frac{h}{\delta c_s\rho_s}t_a+\frac{a_s}{\delta^2}t_p}{\frac{h}{\delta c_s\rho_s}+\frac{a_s}{\delta^2}} \tag{4. 13}$$

It could be found that the surface temperature of solution is mainly determined by the inlet temperature of solution, the local temperature of air and working surface, and the thickness of falling film. By assuming t_a=25 ℃, t_p=35℃ and $t_{s,in} = 50^{\circ}\mathrm{C}$, the change trend of solution surface temperature could be found in the following figures. As the temperature would change with the flow distance, y was set as 0.325 m. From Fig. 4.6, with the increase of film thickness, the surface temperature of liquid desiccant increased, with the desiccant inlet temperature as the upper limit. When the film thickness was thick, the surface temperature was stable, which is a little smaller than the temperature of working surface.

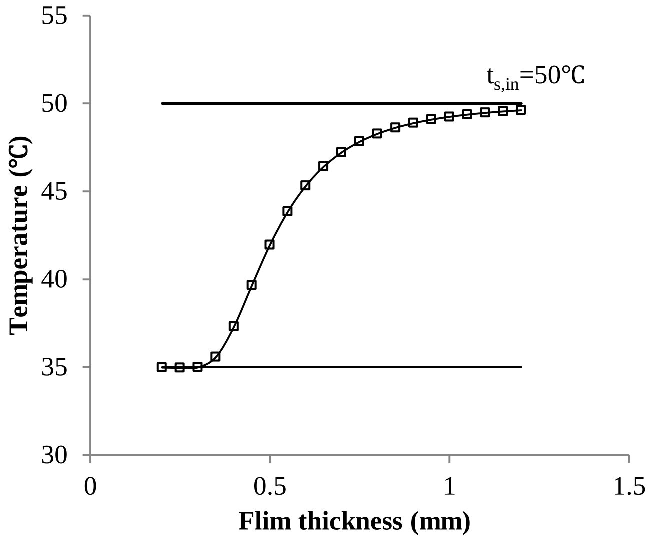

Fig. 4. 6 Changing of desiccant temperature on the interface with film thickness

2) Solution of desiccant concentration on the desiccant/air interface

As the mass transfer between air and liquid desiccant is very complex, the Whitman's Two-film theory (Whitman, 1923) was used to develop the model of the desiccant concentration on the desiccant/air interface. Although it contents many assumptions, this theory is widely accepted for the mass transfer between gas and liquid (Zhou et al. 2005). It considers thin boundary films existing on both sides of the air and desiccant on their interface. Under the influence of concentration difference, the component molecules move through the bulk gas phase to the films on the interface and then to the bulk liquid phase, as known as the mass transfer. These films are assumed as stagnant with a fixed thickness, and provide the main resistances of mass transfer. The schematic diagram of the mass transfer between air and liquid desiccant is shown in Fig. 4.7.

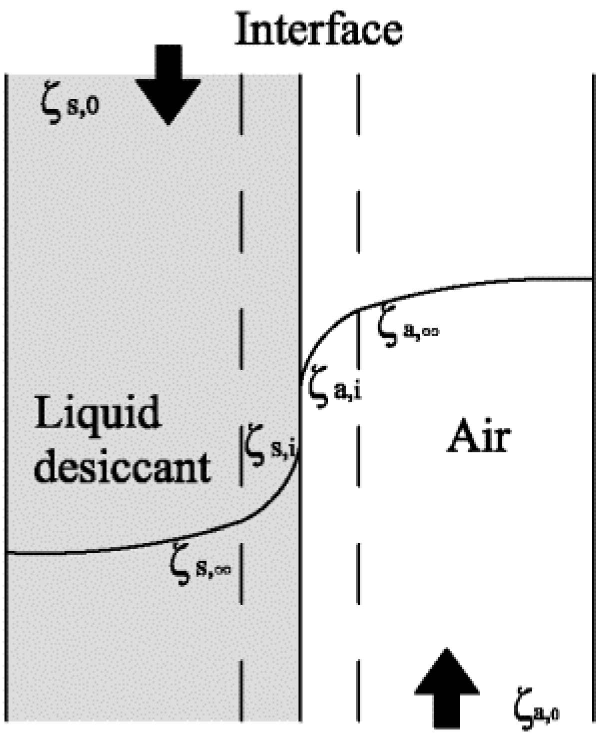

Fig. 4. 7 schematic of mass transfer between air and liquid desiccant

Therefore, the desiccant concentration on the desiccant/air interface, $\zeta_s(x, y, \delta_{cen})$, could be obtained with the following governing equations and boundary conditions.

$$\mu \frac{\partial^2 u_y}{\partial z^2} + \rho g = 0$$

$$u_y \frac{\partial \zeta_s}{\partial y} = D_s \frac{\partial^2 \zeta_s}{\partial z^2}$$

Boundary conditions:

$$\begin{aligned}
&z = 0 \qquad u_y = 0 \\
&z = \delta - \delta_{sf} \qquad \zeta_s = \zeta_{s,\infty}; \\
&z = \delta \qquad \frac{\partial u_y}{\partial z} = 0;\ t_a = t_s;\ D_s \frac{\partial \zeta_s}{\partial z} = -k_s(\zeta_s - \zeta_{a,i}); \\
&y = 0 \qquad \zeta(x, 0, z) = \zeta_{s,in};
\end{aligned} \tag{4. 14}$$

where $\zeta_{s,\infty}$ is the concentration of the bulk solution phase. $\zeta_{a,i}$ means the equivalent concentration of air on the interface, which is the function of air temperature and moisture content. k_s is the convection mass transfer coefficient between solution and air. δ_{sf} means the thickness of assumed thin boundary film on the desiccant side on the air/solution interface, which can be calculated by $\delta_{sf} = \frac{D_s}{k_s}\delta$. The subscripts, *a* and *i* stand for the solution, air and interface, respectively.

By solving the equations, the distribution of solution concentration on the film surface could be expressed as:

$$\zeta_s(x, y, \delta) = \frac{\frac{k_s \delta_{sf}}{\delta^2}(\zeta_{s,in} - \zeta_{a,i})}{\frac{D_s}{\delta^2} + \frac{k_s \delta_{sf}}{\delta^2}} e^{\frac{-\frac{D_s}{\delta^2} - \frac{k_s \delta_{sf}}{\delta^2}}{\frac{5}{12}u_m + \frac{u_m}{3}\frac{(\delta - \delta_{sf})^3}{\delta^3} - \frac{2u_m}{3}\frac{(\delta - \delta_{sf})}{\delta} - \frac{u_m}{12}\frac{(\delta - \delta_{sf})^4}{\delta^4}} y} + \frac{\frac{D_s}{\delta^2}\zeta_{s,in} + \frac{k_s \zeta_{a,i} \delta_{sf}}{\delta^2}}{\frac{D_s}{\delta^2} + \frac{k_s \delta_{sf}}{\delta^2}}$$

(4. 15)

From Eq. (4.15), besides the properties of solution and air, the solution concentration on the film surface is mainly the function of the inlet desiccant concentration, the equivalent concentration of air on the interface, and the film thickness. On the air/solution interface, the air temperature is considered as to be equal to the solution temperature. So, to obtain the equivalent concentration of air on the interface, the solution temperature on the film surface should be calculated firstly by Eq. (4.15).

With Eq. (4.13) and (4.15), the influencing factors of the solution concentration on the film surface were investigated numerically. The initial value of the parameters required was set: $t_{s,in} = 50^{\circ}\mathrm{C}$, $\zeta_{s,in} = 30\%$, t_a=25 ℃, $\omega_a = 9.5 g/kg$, t_p=35 ℃ and δ =0.5 mm. As shown in Fig. 4.8 (a), with the increase of film thickness, the solution concentration on the air/solution interface first increased and then decreased dramatically. To explain this phenomenon, the equivalent concentration of air was also indicated. From Fig. 4.8 (b), due to the liquid desiccant regeneration process, the air concentration was higher than that of solution, to make the moisture transfer from the liquid to the gas. When the film thickness was thin, the air temperature on the air/solution interface, which was considered to be equal to the solution temperature, was almost equal to the plate surface temperature (as mentioned in Fig. 4.6). So, the relative low air temperature led to a low air concentration. With the increase of film thickness, because of the increased interface temperature, the air concentration increased significantly. However, the rising rate of air concentration gradually reduced, and the concentration approached almost steady when the film thickness was large. Therefore, firstly, with the increase of film thickness, due to the larger concentration gradient between air and solution, the desiccant on the film surface was regenerated effectively and its concentration increased dramatically. Then, with the further increase of film thickness, the increase of difference of air/desiccant concentration became slower. But, the flow velocity of liquid desiccant, which was proportional to the square of film thickness, increased dramatically. A serious decrease of the contact time of air and desiccant was caused. Therefore, the desiccant concentration on the film surface decreased due to the insufficient mass transfer between air and liquid desiccant.

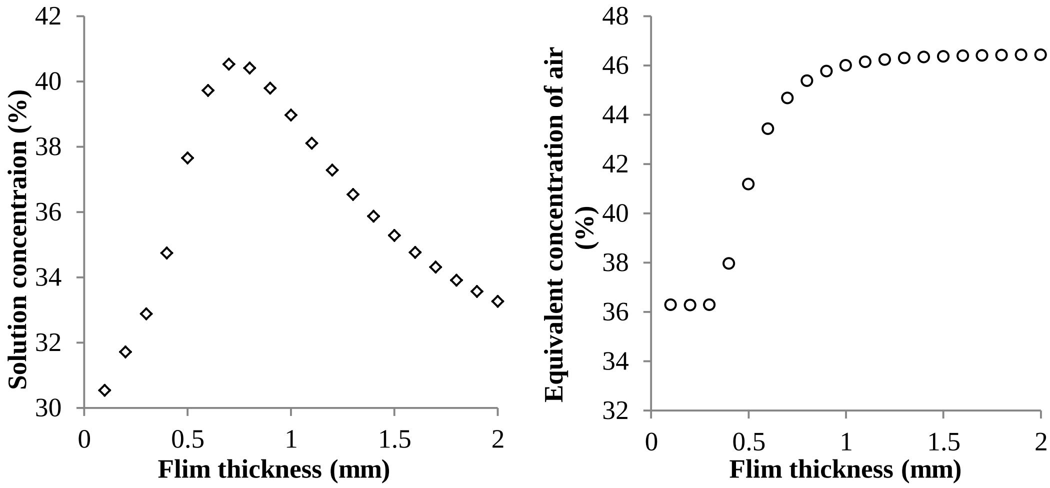

(a) (b)

Fig. 4. 8 Changing of parameters with film thickness (a) solution concentration on the interface and (b) equivalent concentration of air

The influence of solution inlet temperature was shown in Fig. 4.9 (a). As the water vapour pressure of desiccant increased with the temperature, the difference of moisture content between air and desiccant increased, which benefits the mass transfer, and the solution concentration on the air/desiccant interface increased. From 4.10 (b), the increase of inlet moisture content of air, which reduced the drive force of mass transfer, caused a decrease of solution concentration on the film surface, but the impact was not as obvious as other parameters discussed before. Besides, the impact of solution inlet concentration and air temperature were minor.

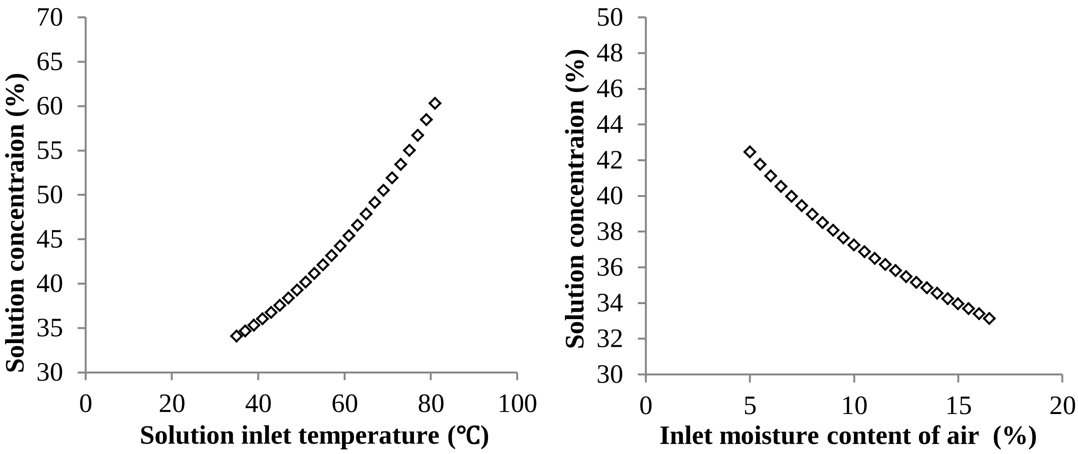

Fig. 4. 9 Changing of solution concentration on the interface with (a) solution inlet temperature and (b) air inlet moisture content

3) Solution of plate temperature on the working surface

As the working surface is usually wetted by the desiccant incompletely, the plate surface temperature could be observed as the surface temperature of dry area, which could impact the heat and mass transfer during the whole dehumidification/regeneration process. As shown in Fig. 4.10, the plate surface temperature is determined by the temperature of air and extra hot fluid, the heat transfer coefficient of working surface, the thermal resistance of insulation and the surrounding temperature of the regenerator. By certain assumptions, the temperature of working surface could be calculated with the equations of heat transfer by conduction and convection. From Eq. (4.10), it could be found that by influencing the solution temperature in the rim part of falling film, the plate surface temperature presents a significant effect on the wetted area and system performance. Therefore, as the rim part is very thin, the plate surface temperature at this position could be assumed as to be equal to the surface temperature of the dry area, which means the influence of solution temperature could be neglected.

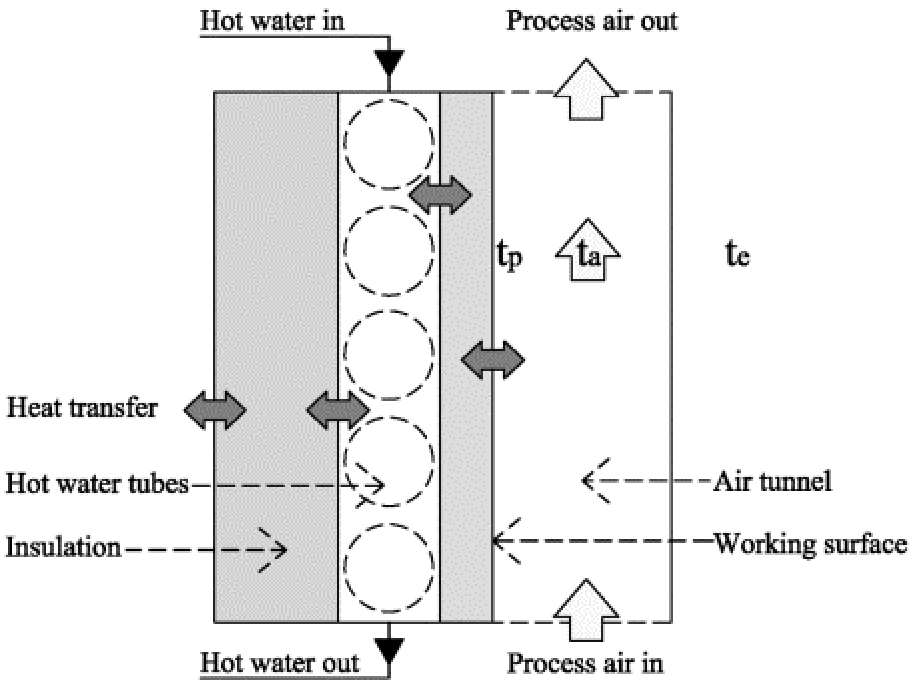

Fig. 4. 10 Schematic of plate surface temperature during internally heated regeneration process

The following assumptions were made: a) the hot water tubes and air tunnel were perfectly insulted, and the impact of environment temperature could be ignored; and b) the convective heat transfer between hot water tubes and working plate was neglected. Therefore, the temperature of working surface could be obtained with Eq. (4.16).

$$t_p = (\frac{\lambda_p}{\delta_p} t_w + h_p t_a) / (\frac{\lambda_p}{\delta_p} + h_p) \tag{4. 16}$$

where h_p is the convection heat transfer coefficient between working surface and air. λ_p and δ_p are the thermal conductivity and thickness of working plate, respectively. The subscript *w*, *a* and *p* stand for the hot water, air and plate surface, respectively.

From Eq. (4.16), besides the characteristics of working plate, the plate surface temperature is mainly determined by the hot water temperature and air temperature. As the water/air temperature changes along the flow direction, the local temperature at the certain flow distance should be used in this equation.

4.4.3 Discussion

By substituting the Eq. (4.13), (4.15) and (4.16) into Eq. (4.11), the contraction distance along the flow direction of the falling film liquid desiccant system could be calculated. As the analytical solution of surface tension of desiccant was developed, no iteration was required, and the distance could be calculated directly with the inlet parameters and physical properties of air, liquid desiccant and extra heating fluid. The design parameters such as the physical properties of working plate and the thickness of solution distributor are also required. Therefore, with the newly developed model, the contraction distance under different operation conditions could be predicted. To verify the model, the results were compared with those obtained from experiment of the internally heated regeneration.

As shown in Fig. 4.11, as the contraction distance increased with the value of y-axis, the Δx under five different positions (where y=0.13, 0.26, 0.39, 0.52, 0.65 m) along the flow direction of each test was calculated and compared with those recorded by the thermal image camera. The majority of the simulation result showed an acceptable difference of less than ±25%, with an ARD of 10.8%. Therefore, the model could be employed to calculate the contraction distance of falling film liquid desiccant regeneration system.

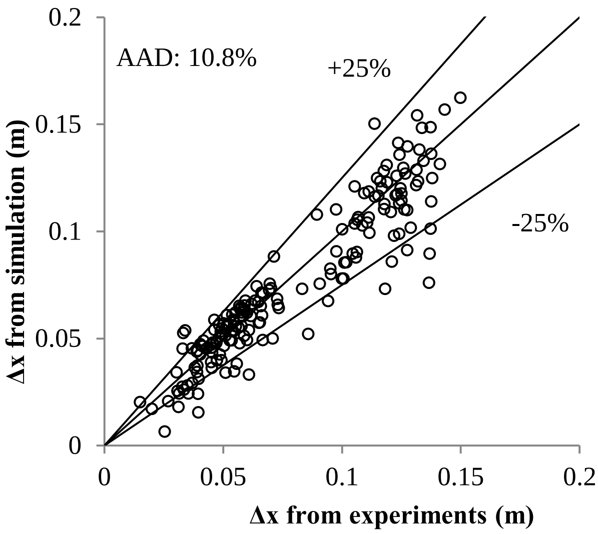

Fig. 4. 11 Comparison of Δx between calculation and experimental results

The errors may be caused by: 1) the slight irregularity or uneven roughness of the working surface due to the industrial processing; 2) the measurement uncertainty of individual parameter during the experiment; and 3) the assumptions made for developing the model, such as the employment of the Two-Film Theory.

With the new model, the influencing factors of the contraction distance during the falling film regeneration could be investigated numerically. The pre-set initial values for the simulation were m_s=0.04 kg/s, $t_{s,in}$=55℃, $\zeta_{in} = 30\%$, t_p=45 ℃, $t_{a,in}$=25 ℃, $\omega_a = 9.5 g/kg$, δ=1 mm and $\kappa = 1.5$. The properties and area of working surface were same as the surface in our experiment. As the Δx changed with the flow direction of falling film, only the result at y=0.35 m were listed and analysed.

From Fig. 4.12 (a), the increase of temperature on the working surface reduced the contraction distance, which caused an increase of film wetted area. With the further increase of plate surface temperature, the shape of film would turn from contraction into expansion, which was also observed in our experiment in the previous chapter. As mentioned before, if the liquid desiccant system was well insulated, the plate surface temperature was mainly decided by the temperature of hot water and air, and the influences were indicated in the Fig. 4.12 (b) and (c).

As shown in Fig. 4.13 (a), with the increase of inlet temperature of desiccant, the Δx increased with an increasing growth rate. The Δx was lower than zero when the inlet temperature of desiccant was low, which means the wetted width along the flow direction would be larger than the initial one. Therefore, the falling film could expand rather than contract during the dehumidification process. The expanded film could improve the wetted area and enhance the heat and mass transfer. Furthermore, when the solution concentration increased, in Fig. 4.13 (b), the Δx increased, mainly because of the change of solution contact angle. However, the impact of the moisture content of air, which is shown in Fig. 4.13 (c), was not as significant as other parameters.

Besides the physical properties of air, solution and water, the film thickness also showed a significant influence on the contraction distance, as indicated in Fig. 4.13 (d). The Δx increased dramatically with the thickness of solution film. When the falling film was thin enough, the Δx was less than zero, which was also observed by previous researchers.

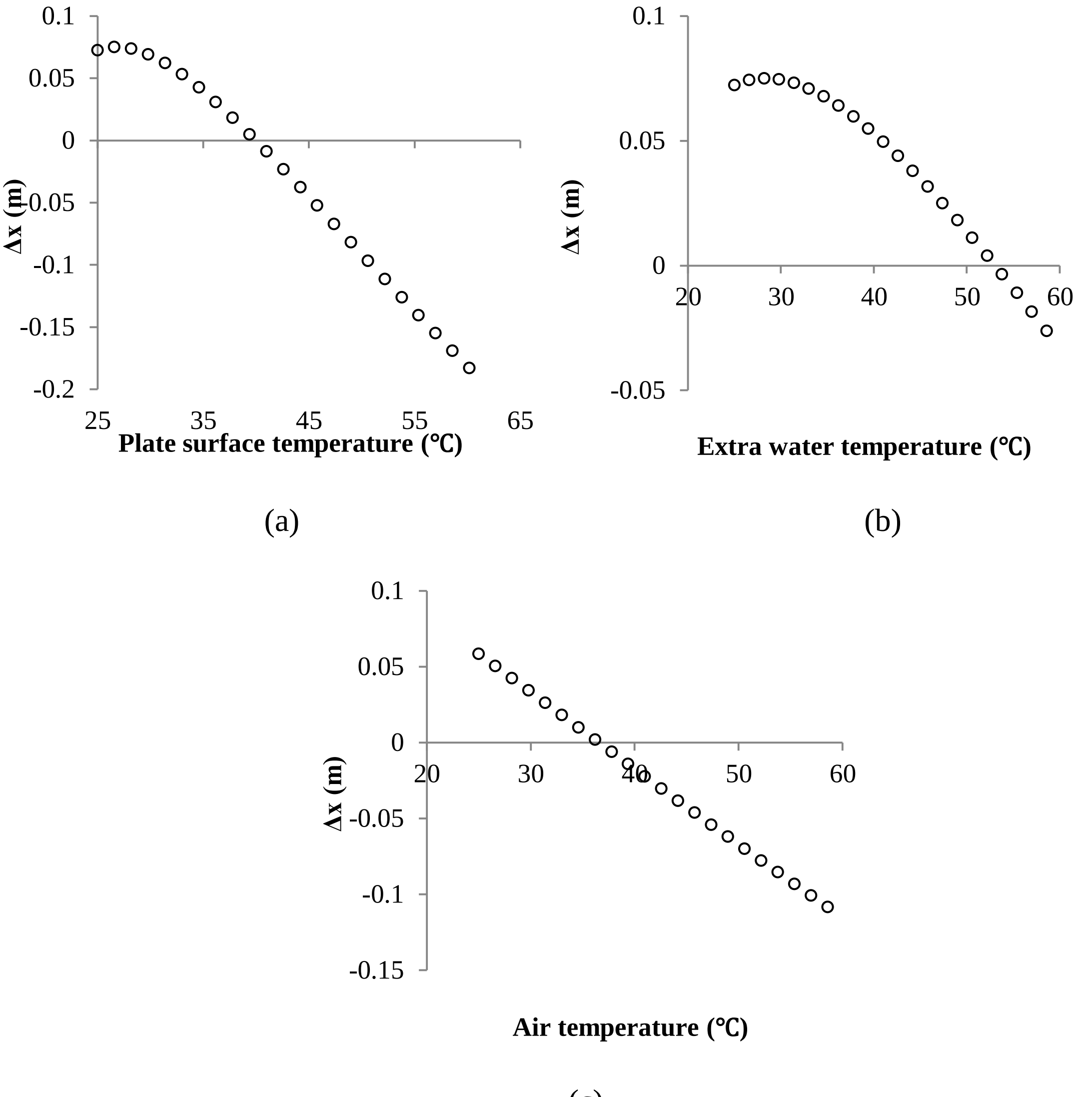

(c)

Fig. 4. 12 Influencing factors of Δx during internally heated regeneration process: (a) Plate surface temperature, (b) extra water temperature and (c)air temperature

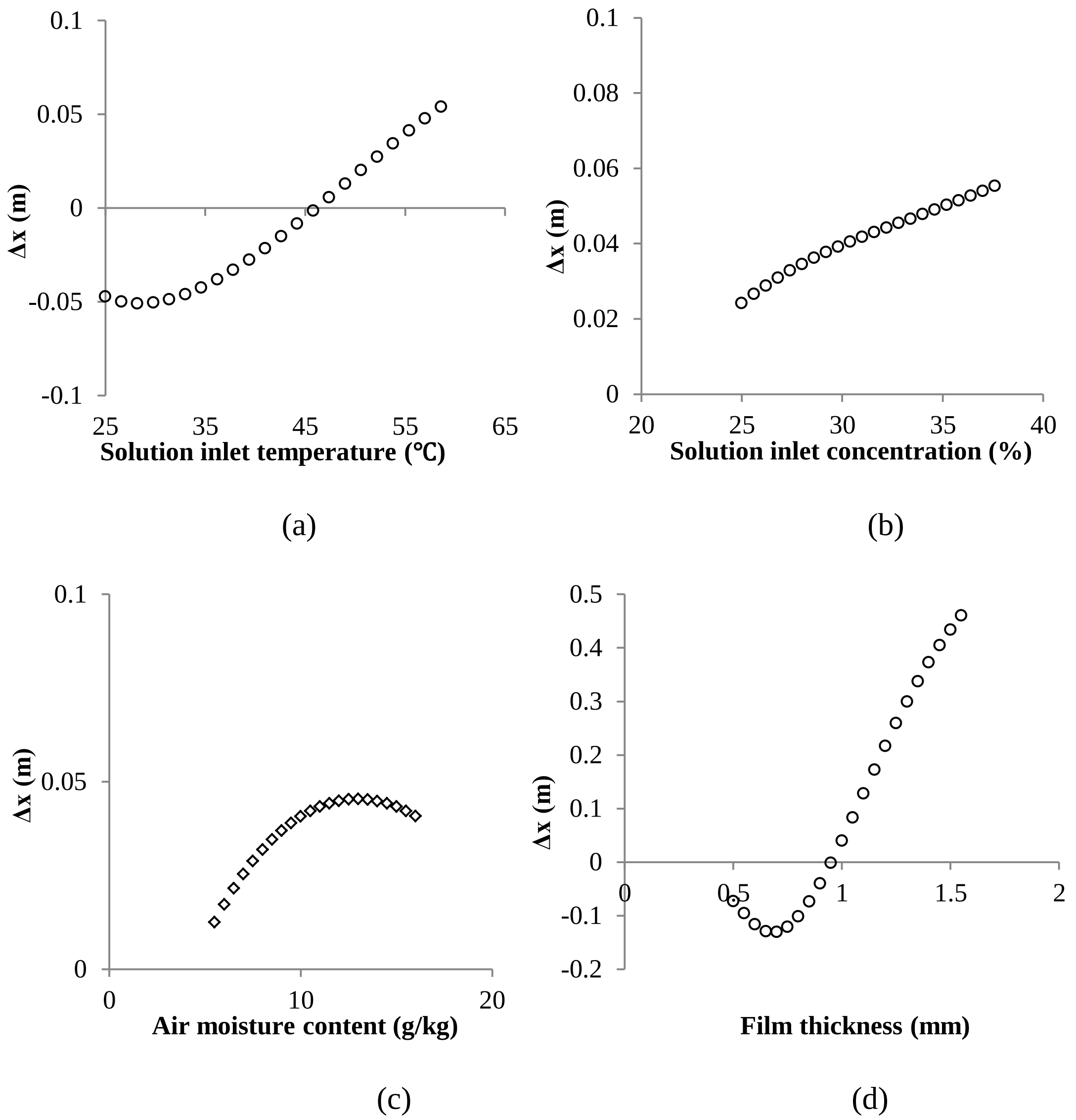

Fig. 4. 13 Influencing factors of Δx during internally heated regeneration process: (a) solution inlet temperature, (b) solution inlet concentration, (c)air moisture content and (d) film thickness

Furthermore, as shown in Fig. 4.14, the Δx was also found to increase with the contact angle of desiccant, and the rising rate increased dramatically with the decrease of the value of κ , especially when κ is close to 1. With the increase of κ , the Δx decreased, but the reducing rate was regularly slow. As shown in our experiment of falling film regeneration, with higher solution mass flow rate, the contraction in the transverse direction could be reduced. Therefore, κ could be predicted to increase with the mass flow rate of desiccant.

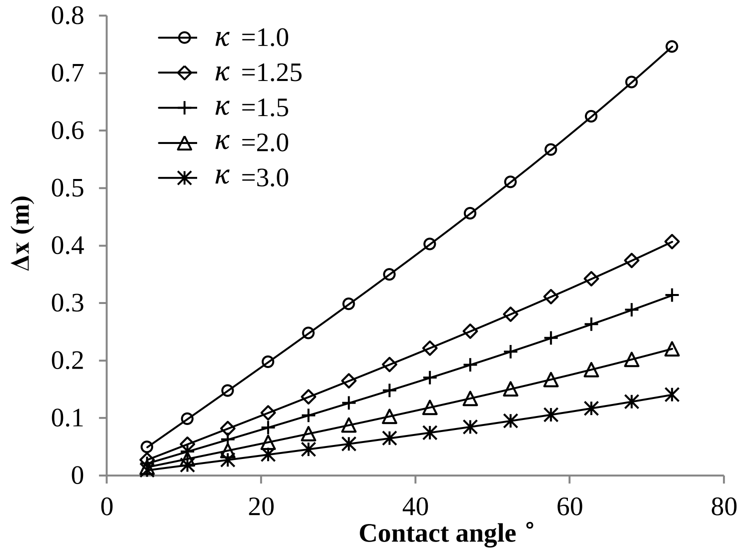

Fig. 4. 14 Changing of Δx with solution contact angle and ε

Therefore, the increase of plate surface temperature, which is caused by the increase of extra water temperature or air temperature, could decrease the contraction distance and enlarge the wetted area of falling film during the liquid desiccant regeneration. Therefore, in practical applications, the insulation for the hot water tank and wind tunnel is necessary. The provision of insulation could not only prevent the temperature reduction of desiccant but also increase the wetted area for better heat and mass transfer. In terms of intermittent operation systems, during the stopover period, the system should be well insulated to prevent the surface being cooled by the surrounding air. Before the operation, the regenerator should be pre-heated with the hot water indirectly or hot air directly, to improve the plate surface temperature. Furthermore, the reduction of film thickness with the solution distributor could also increase the wetted area effectively. Besides, as the decrease of contact angle could increase the wetted area effectively, several methods could be employed to make the working surface more hydrophilic, such as changing the properties of working surface or adding proper additives into the desiccant.

4.5 Summary

For predicting the wetted area of falling film liquid desiccant system, a new model was developed, including the empirical formula for contact angle of desiccant (Eq. (4.1-4.2)), the model for initial wetted width (Eq. (4.5)) and the theoretical model for the contraction distance along the flow direction (Eq. (4.8-11)) with analytical solutions of several required parameters (Eq. (4.13), (4.15) and (4.16)). Therefore, the whole wetted area of the falling film could be calculated with the following equation.

$$A_w = \int_0^y (W_i - \Delta x)dy \tag{4. 17}$$

The dimensionless hydraulic radius of the solution falling film, which is defined as the ratio between the half of the wetted width and the initial film width, could be calculated with Eq. (4.18). It should be noticed that $\overline{R_w}$ is different along the flow direction.

$$\overline{R_w} = \frac{W_i - \Delta x}{2W_i} \tag{4. 18}$$

To verify the newly developed model of wetted area, the results were compared with those obtained from experiment of internally heated regeneration. Taking a test in Section 3.4.2 as an example, as shown in Fig. 4.15, the calculated film boundary was close to the experimental one recorded by the thermal camera. The experiment conditions were also listed in this figure.

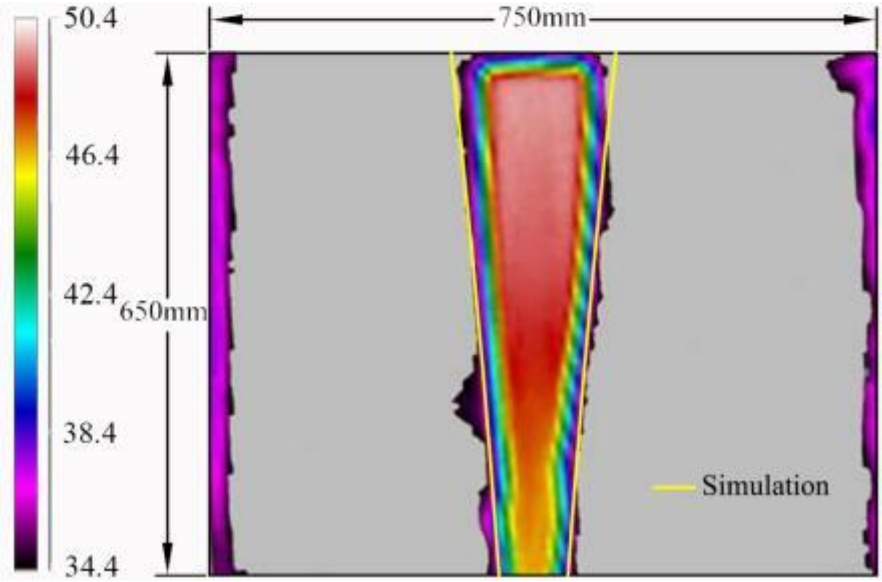

m_s (kg/s)	$t_{s,in}$ (°C)	ζ_{in} (%)	t_p (°C)	$t_{w,in}$ (°C)	$m_{w,in}$ (kg/s)	$t_{a,in}$ (°C)	$\omega_{a,in}$ (g/kg)
0.034	46.6	30.0	33.4	51.2	0.131	24.1	9.34

Fig. 4. 15 Comparison of boundary of falling film between calculation and experimental results

For the whole wetted area of liquid desiccant falling film, the experiment G. 6-7 from Section 3.4.2 and G. 14-15 from Section 3.4.4 were chosen for the comparison. From Fig. 4.16, the trends of wetted area obtained from simulation and experiment were similar and both areas increased with the plate surface temperature.

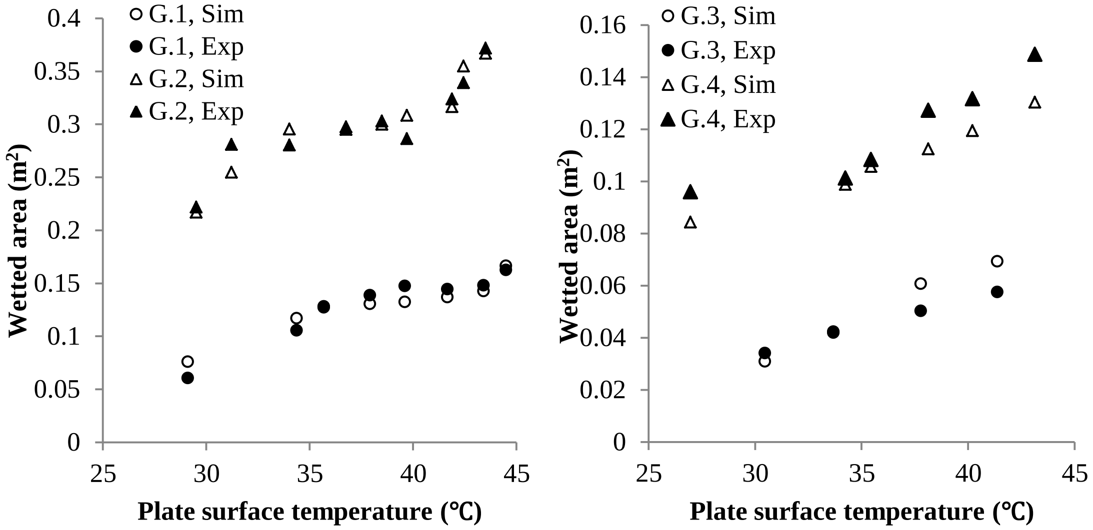

Fig. 4. 16 Comparison of wetted area under different plate surface temperature between calculation and experimental results

Furthermore, as shown in Fig. 4.17, the $\overline{R_w}$ under five different positions (where y=0.13, 0.26, 0.39, 0.52, 0.65 m) along the flow direction of each test were calculated and compared with those recorded in our experiments. The majority of the simulation results showed an acceptable difference of less than ±25%, with an ARD of 11.2%. Therefore, the model could be employed to calculate the contraction distance and wetted area of falling film liquid desiccant regeneration system.

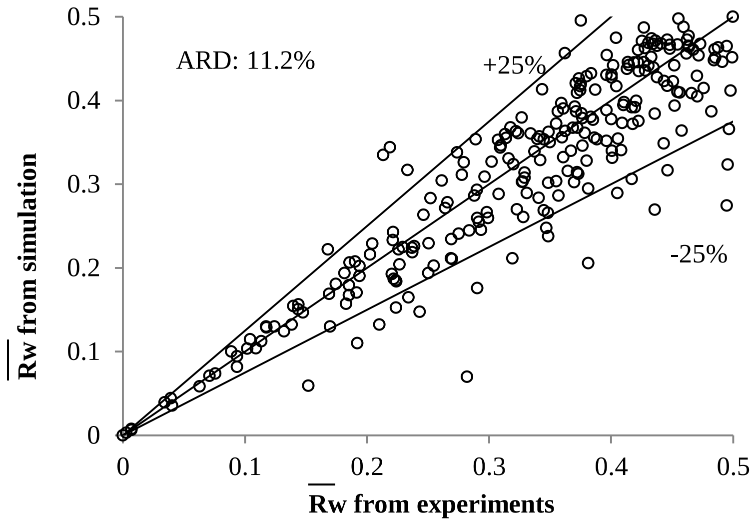

Fig. 4. 17 Comparison of $\overline{R_w}$ between calculation and experimental results

The effects of different parameters on the wetted area during our experiments could be explained physically and theoretically based on the model developed in this chapter. As shown in Fig. 3.6, with the increase of solution mass flow rate, the wetted area of falling film and moisture removal rate was found increased significantly, while they decreased dramatically with the solution distributor thickness. The main reason of the improved wetted area is: a) as obtained with Eq. (4.5), with the increase of solution mass flow rate, the initial film width increased proportionally, which leads to a enlargement of wetted area. However, with the increase of solution distributor thickness, the initial width reduced dramatically ($Wi \sim \frac{1}{\delta_{\max}{}^{3}}$). b) As shown in Fig. 4.13 (d) simulated with the theoretical model described in Chapter 4.4, the film contraction distance increases with the film thickness. Therefore, with the increase of solution mass flow rate, the film thickness decreased, as well as the contraction distance, but the effect was not obvious. However, as the film thickness increased significantly with the solution distributor thickness, the contraction distance increased and the film width reduced accordingly. Therefore, during our experiments, the wetted area increased with the solution mass flow rate, but decreased obviously with the solution distributor thickness.

As shown in the Fig. 3.9, we experimentally observed that the wetted area and system performance increased obviously with the plate surface temperature. For the wetted area, it is mainly because, as indicated in Eq. (4.10), the solution surface tension at the edge of falling film, σ_{rim}, decreased with the plate surface temperature. So, the difference between the surface tension in the both sides of the rim part of falling film was reduced, which led to a decrease of contraction distance. Therefore, the film width along the flow direction increased significantly. Besides, according to Eq. (4.5), the initial film width was not changed with the surface temperature. So, with the higher film wetted width, the wetted area increased obviously.

As shown in 3.14, the wetted area was observed to increase with the solution temperature. But compared to the experiments in Chapter 3.3.2, the rising rate was not as high as that with the plate surface temperature at the similar mass flow rate. Based on Eq. (4.5), as the change of solution temperature would change the kinematic viscosity, density and contact angle of solution, it could be calculated that the initial film width increased with the solution temperature. As described in Chapter 4.4.1-2, the surface tension in the central side, σ_{cen}, is decided by the temperature and concentration of the solution/air interface of falling film. With the increase of solution temperature, the temperature of the solution/air interface increased, while its concentration also increased. Therefore, the solution surface tension σ_{cen} decreased, but the effect was not obvious. The difference between σ_{cen} and σ_{rim} increased accordingly, as well as the contraction distances, which would lead to a decrease of film wetted width. So, with the combined effect of initial width and film width along the flow direction of the falling film, with the increase of solution temperature, the wetted area increased, but the changing rate was not as obvious as that of plate surface temperature.

Furthermore, as shown in Fig. 3.17, with the increase of solution contact angle, the initial film width decreased significantly, which could also be predicted with the semi-theoretical model in Chapter 4.3. From Fig. 3.18 we could found, the smaller contact angle benefited the film width along the flow direction effectively, which could also be explained by the theoretical model in Chapter 4.4.1. As obtained in Eq. (4.9), the value of D_r increased with the decrease of solution contact angle. From Eq. (4.10), it could be calculated that the contraction distance decreased significantly with the increase of D_r. So, with the smaller contact angle, the contraction distance was proved to decrease significantly, which could improve the film width. Therefore, as both the initial width and film width along the flow direction increased with the smaller contact angle, the wetted area could be enlarged significantly.

From this new model, it could be found that the wetted area of falling film is changed with the parameters and physical properties of liquid desiccant, air, extra heating fluid and the working plate. The results are also suitable for the adiabatic liquid desiccant system by introducing plate surface temperature. Furthermore, as the similar heat and mass transfer mechanism between dehumidification and regeneration of liquid desiccant, the newly developed model could also be applied for the dehumidification process. With this newly developed model, the value of wetted area required in theoretical models could be predicted accurately, which could significantly improve the accuracy of performance evaluation and simulation of liquid desiccant air-conditioning systems.

CHAPTER 5

EXPERIMENTAL INVESTIGATION ON MASS TRANSFER COEFFICIENT OF LIQUID DESICCANT REGENERATION

5.1 Introduction

In the internally cooled/heated liquid desiccant system, the mass transfer coefficient is a significant parameter to evaluate the moisture exchange between air and solution. Without an effective calculation method of the coefficient, the performance simulation and predication could not be conducted.

Referring to the literature review in Chapter 2, many researchers had carried out the theoretical analysis and experimental tests on the system performance of internally cooled/heated liquid desiccant system, and built several empiric formulas to predict the mass transfer coefficient (Kessling et al. 1998, Yin et al. 2007). The coefficient was also obtained by the Reynold's analogy in some studies, and mainly determined by the air flow rate and temperature (Liu et al. 2006, 2007). By comparing the prediction results of different formulas, large deviations were found. As most experimental conditions were insufficiently wetted by the liquid desiccant, lack of data of actual wetted area during the heat and mass transfer process is the mean reason causing the big differences. Therefore, developing a new empiric formula of mass transfer coefficient, which could take all significant influencing factors into account, is of great important.

In this chapter, firstly, the impacts of different influencing factors on the mass transfer coefficient under real wetted area were investigated experimentally. Then, based on the test data, an empiric formula for the insufficient wetting conditions was developed with the multi linear regression. To verify the formula, the prediction results were compared with those obtained from experiments. By comparing with the formula from previous research, the application of coefficient obtained in our investigation was discussed.

5.2 Research method of mass transfer coefficient

5.2.1 Experimental condition

To develop the empiric formula of mass transfer coefficient, the experiments under different operation conditions were conducted. The detailed information of the experiment rig, measurement method, operation condition and other related issues could be referred to Chapter 3.

In our experiments, the thermal image of the regeneration process was recorded by the thermal camera imager, and then was processed with the image analysis software. Several Pt-RTDs were used to obtain the inlet and outlet temperatures of solution, water and air, with the accuracy of 0.1℃. A specific gravity hydrometer, with the accuracy of 1 kg/m^3, was applied to obtain the density of solution for determining the solution concentration with the temperature. The flow rates of solution and water were measured by the turbine flow-meter, with the maximum error of about 1.6 L/h. The humidity of air was calculated with the recorded data by the dry and wet-bulb thermometer, with the maximum error of about 0.16 g/kg.

During the internally heated regeneration process, the inlet temperature of liquid desiccant was around 35.4 to 53.7℃, and the mass flow rate was changed from 0.03 to 0.15 kg/s. The inlet solution concentration was about 25.9% to 30.7%. The moisture content of process air was around 9.8 to 18.2 g/kg dry air, and its velocity during the tests was 0.3–1.5 m/s. Besides, during the experiments, due to the effect of extra hot water, the temperature of working surface was changed from 26.9 to 44.1℃. The mass transfer performance of the experiments could be represented by the moisture removal rate, as shown in Eq. (5.1).

$$\dot{m}_{removal} = \dot{m}_a(\omega_{a,out} - \omega_{a,in}) \tag{5. 1}$$

where ω is the moisture content and *m* is the mass flow rate. The subscripts, *a* stands for the air, and *in* and *out* mean the inlet and outlet characteristics.

5.2.2 Theoretical analysis

To obtain the coefficient under different experimental conditions, the two-film theory was employed. There are mainly three mass-transfer resistances in the moisture transfer between the gas phase and the liquid phase, which are gas-phase resistance, liquid-phase resistance and interface resistance. As the interface resistance is relatively small, it could be neglected (Bird et al. 1960). Therefore, the local moisture removal rate could be expressed as:

$$\begin{aligned} d\dot{m}_{removal} &= a_{D,a}(\omega_{a,bulk} - \omega_{a,I})dZ \\ d\dot{m}_{removal} &= a_{D,s}(\xi_{s,bulk} - \xi_{s,I})dZ \end{aligned} \tag{5. 2}$$

where $a_{D,a}$ and $a_{D,s}$ stand for the mass transfer coefficient of the gas and liquid phase, respectively. The subscripts *a, s, I* mean the air, solution and the solution/air interface.

However, the parameters on the interface are difficult to be recorded. Instead of using the single-phase coefficients, an overall mass transfer coefficient was introduced to evaluate the mass transfer between air and desiccant. The coefficient is defined by the following equation.

$$\frac{1}{a_D} = \frac{1}{a_{D,a}} + \frac{1}{\varphi a_{D,s}} = \frac{1}{\omega_{a,bulk} - \omega_I}\frac{d\dot{m}_{removal}}{dZ} \tag{5. 3}$$

where φ is a function of temperature and concentration of the bulk liquid desiccant (Zhang et al. 2010).

Therefore, the average overall mass transfer coefficient could be given as:

$$\bar{a}_D = \frac{\dot{m}_{removal}}{(\omega_{a,bulk} - \omega_e)A_w} \tag{5. 4}$$

where A_w means the actual wetted area of falling film recorded in the experiments, which is influenced by the parameters of air, solution, extra fluid and plate surface.

According to previous researches, the mass transfer coefficient is represented by three dimensionless quantities: the Sherwood number, Reynolds number, and Schmidt number. The mass transfer coefficient correlation obtained from the dimensional analysis is given as:

$$\bar{a}_D(\frac{\delta_a}{D_a \rho_a}) = Sh = b_1 \mathrm{Re}_a^{b_2} \mathrm{Sc}_a^{b_3} \mathrm{Re}_s^{b_4} \mathrm{Sc}_s^{b_5} \tag{5. 5}$$

where δ_a stands for the thickness of air channel. The D and ρ mean the diffusion coefficient and the density.

Therefore, with the experimental data, the mass transfer coefficient under different conditions could be obtained by Eq. (5.4). With the multi linear regression, the value of b_1~b_5 in Eq. (5.5) could be estimated, with the following steps.

a) Let

$$y_i = \ln Sh,\ x_{1i} = \ln(\mathrm{Re}_a)_i,\ x_{2i} = \ln(\mathrm{Sc}_a)_i,\ x_{3i} = \ln(\mathrm{Re}_s)_i,\ x_{4i} = \ln(\mathrm{Sc}_s)_i\ \ (i = 1,2,3,...,n, n > 3)$$

$$\text{and } Y = \begin{bmatrix} y_1 \\ y_2 \\ y_3 \\ . \\ . \\ . \\ y_n \end{bmatrix} \quad X = \begin{bmatrix} 1 & x_{11} & ... & x_{41} \\ 1 & x_{12} & ... & x_{42} \\ 1 & x_{13} & ... & x_{43} \\ . & . & & . \\ . & . & & . \\ . & . & & . \\ 1 & x_{1n} & ... & x_{4n} \end{bmatrix} \quad B = \begin{bmatrix} \ln b_1 \\ b_2 \\ . \\ . \\ b_5 \end{bmatrix} \quad \sigma = \begin{bmatrix} \ln \sigma_1 \\ \sigma_2 \\ . \\ . \\ \sigma_5 \end{bmatrix} \tag{5. 6}$$

where n is the number of statistical data. σ is the independent normally distributed random error with equal weighting of the rates.

b) Eq.(5.6) became:

$$Y = XB + \sigma \tag{5. 7}$$

c) Make the equation of linear regression approximation, Eq.(5.8)

$$\widehat{Y} = X\widehat{B} \tag{5. 8}$$

d) Use the linear least squares estimate to get the coefficient matrix, as shown in Eq. (5.9). With the coefficient matrixes, the mass transfer coefficient correlation could be obtained by Eq. (5.8).

$$\widehat{B} = (X^T X)^{-1} X^T Y \tag{5. 9}$$

e) To verify the coefficients obtained by linear regressions, an F test has to be conducted. The F-ratio required for the test could be calculated by Eq. (5.10).

$$
\begin{aligned}
F &= \frac{\sum_{regression}/m}{\sum_{residuals}/(n-m-1)} \\
\sum_{residuals} &= \sum (\varepsilon_i - \widehat{\varepsilon}_i)^2 \\
\sum_{regression} &= \sum (\widehat{\varepsilon}_i - \overline{\varepsilon})^2 \qquad i = 1, 2, 3, \ldots n
\end{aligned}
\tag{5. 10}
$$

where n is the number of statistics, and m is the number of variables.

As the accuracy of linear regressions would significantly increase with the quantity of independent statistical data, an adequate amount of data is necessary.

5.3 Results

5.3.1 Influencing factors of mass transfer coefficient

To investigate the influencing factors of mass transfer coefficient, six experiment groups were conducted, as listed in Table 5.1. Each group had six to nine tests with different operation conditions. The variables included the mass flow rate of solution or air, inlet temperature of solution, temperature of working surface and the inlet humidity of air. As discussed before, the impact of extra hot water and air temperature were indirect, and their results were not listed. It could be found that by comparing with G.1 and G. 2, the effect of solution distributor thickness, $\delta_{\max}$, could be observed, as well as the influence of solution mass flow rate. Then, by comparing with G.2 and G. 3, as only the solution concentrations were different, the impact of concentration could be investigated. Furthermore, G.4 and G.5 was conducted to obtain the influence of solution temperature and plate surface temperature, respectively.

Additionally, with G.6, the influence of air mass flow rate was tested.

Table 5. 1 Experimental conditions of internally heated regeneration

No.	δ_{max} (mm)	m_s (kg/s)	$t_{s,in}$ (℃)	$\zeta_{s,in}$ (%)	t_p (℃)	$\omega_{a,in}$ g/kg	m_a (kg/s)
1	1.0	0.025,0.056 0.088,0.105 0.126,0.118 0.146, 0.041	44.8	28.2	38.1	9.26	0.11
2	1.25	0.023,0.044 0.050,0.066 0.092,0.112 0.127, 0.147	44.7	28.0	37.8	9.47	0.11
3	1.25	0.029,0.051 0.065,0.084 0.099,0.103 0.119, 0.131	45.2	25.2	36.9	9.20	0.11
4	1.0	0.037	35.5,37.3 41.3,44.8 47.3,49.9 52.7, 56.2	27.9	38.0	9.45	0.11
5	1.0	0.034	46.6	28.1	29.1, 31.8, 33.4 36.3, 38.0, 38.9 41.1, 46.4, 48.8	9.34	0.11
6	1.0	0.036	46.0	28.2	37.9	9.37	0.03, 0.058 0.077,0.110 0.131,0.155

As shown in Fig. 5.1 (a), with the increase of solution mass flow rate, the moisture removal rate increased almost proportionally. Synchronously, the wetted area also increased, as shown in Fig. 5.1 (b), due to the increase of initial wetted width and the reduction of film contraction, as described in Chapter 3 and 4. Therefore, as indicated in Fig. 5.1 (c), the overall average mass transfer coefficient actually decreased with the solution mass flow rate. When the solution mass flow rate was higher, the reduction rate of the coefficient regularly slowed down. However, this change trend in our experiments was quite different to the previous results in the literature. The possible reason is that under the insufficient wetting conditions, with the increase of solution mass flow rate, the rising rate of wetted area is larger than that of moisture removal rate, which led to the decrease of mass transfer coefficient.

According to our investigations, the thickness of solution distributor significantly influenced the performance of internally heated regeneration, by influencing the film thickness of liquid desiccant. When the film thickness was enlarged, the moisture removal rate and wetted area seriously reduced at the same solution mass flow rate, by comparing G. 1 and 2 in Fig. 5.1 (a) and (b). The mass transfer coefficient in G. 2 was also found smaller than that of G. 1. As the flow velocity of desiccant increased significantly with the film thickness, the contact time between air and solution decreased, which reduced the mass transfer performance and the coefficient accordingly.

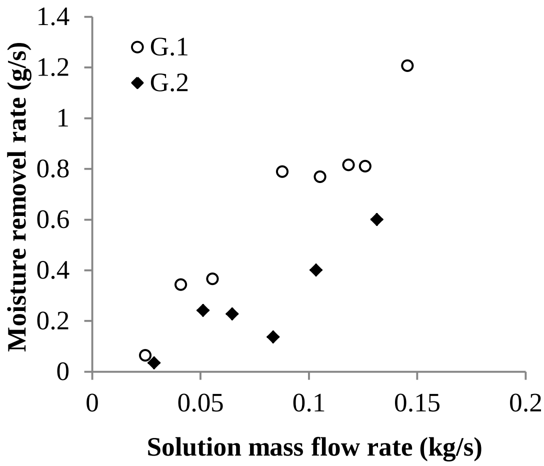

(a)

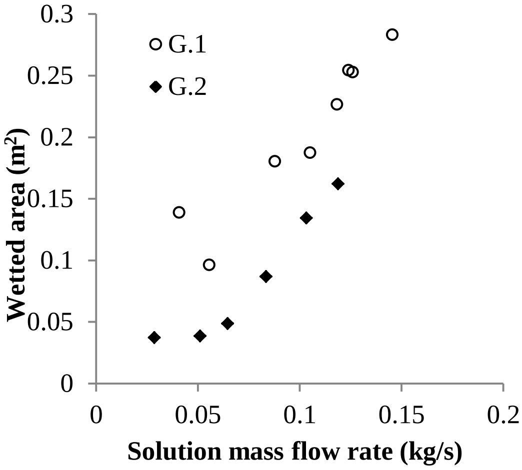

(b)

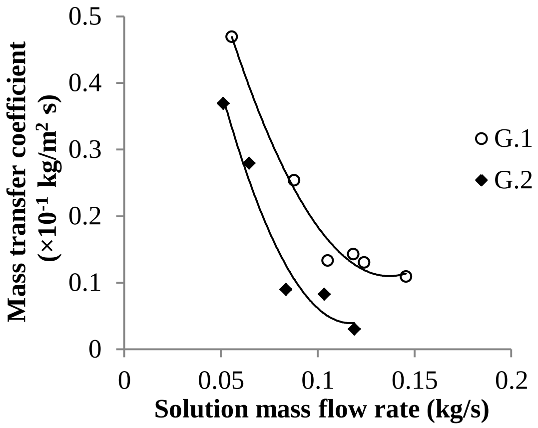

(c)

Fig. 5. 1 Changing of system performance of G. 1 and 2 with the solution mass flow rate: (a) moisture removal rate, (b) wetted area and (c) mass transfer coefficient

The influence of inlet solution concentration was shown in Fig. 5.2. Comparing with the G. 2 ($\zeta_{s,in}$ =28.0%), the moisture difference between air and solution was improved in G. 3 ($\zeta_{s,in}$ =25.2%), as well as the mass transfer driving force. Therefore, from Fig. 5.2(a), the moisture removal rate in G. 3 was higher. However, with the increase of solution concentration, the wetted area increased a little, mainly due to the change of solution contact angle. So, as shown in Fig. 5.2 (c), it was found that the $\bar{a}_D$ was decreased, but the effect was insignificant compared to other influencing factors.

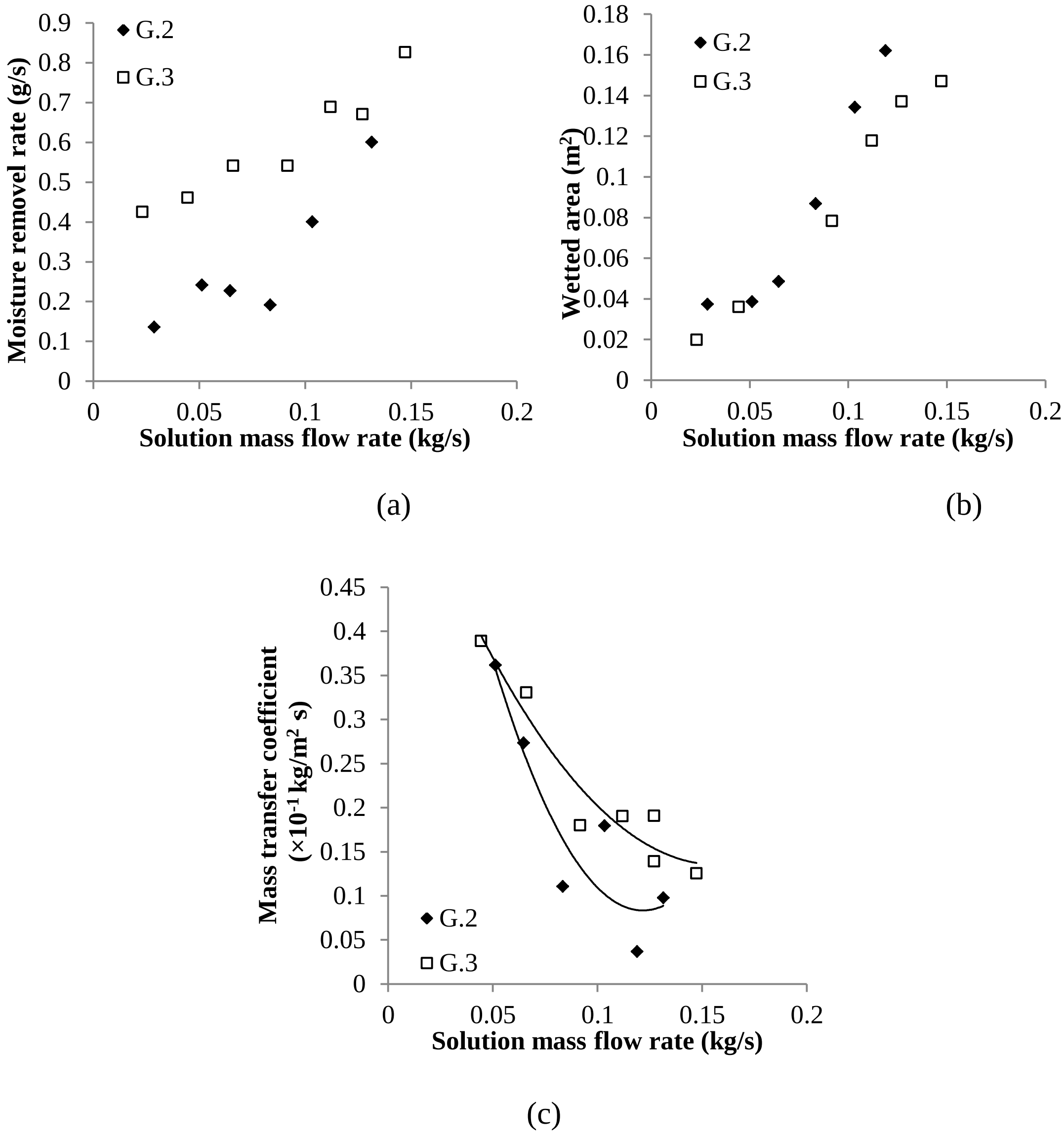

Fig. 5. 2 Changing of system performance of G. 2 and 3 with the solution mass flow rate: (a) moisture removal rate, (b) wetted area and (c) mass transfer coefficient

Furthermore, with the experimental results in Fig. 5.3, the impact of solution inlet temperature on the system performance was investigated. As shown in Fig. 5.3 (a), the increase of solution temperature could effectively improve the mass transfer during the regeneration process. The higher solution temperature also led to an increasing difference of equilibrium moisture content between the solution/air interface and air. Synchronously, due to the enhancement of initial wetted width, the wetted area increased. Therefore, from Fig. 5.3 (c), the mass transfer coefficient calculated with Eq. (5.4) decreased with the increase of inlet temperature of solution.

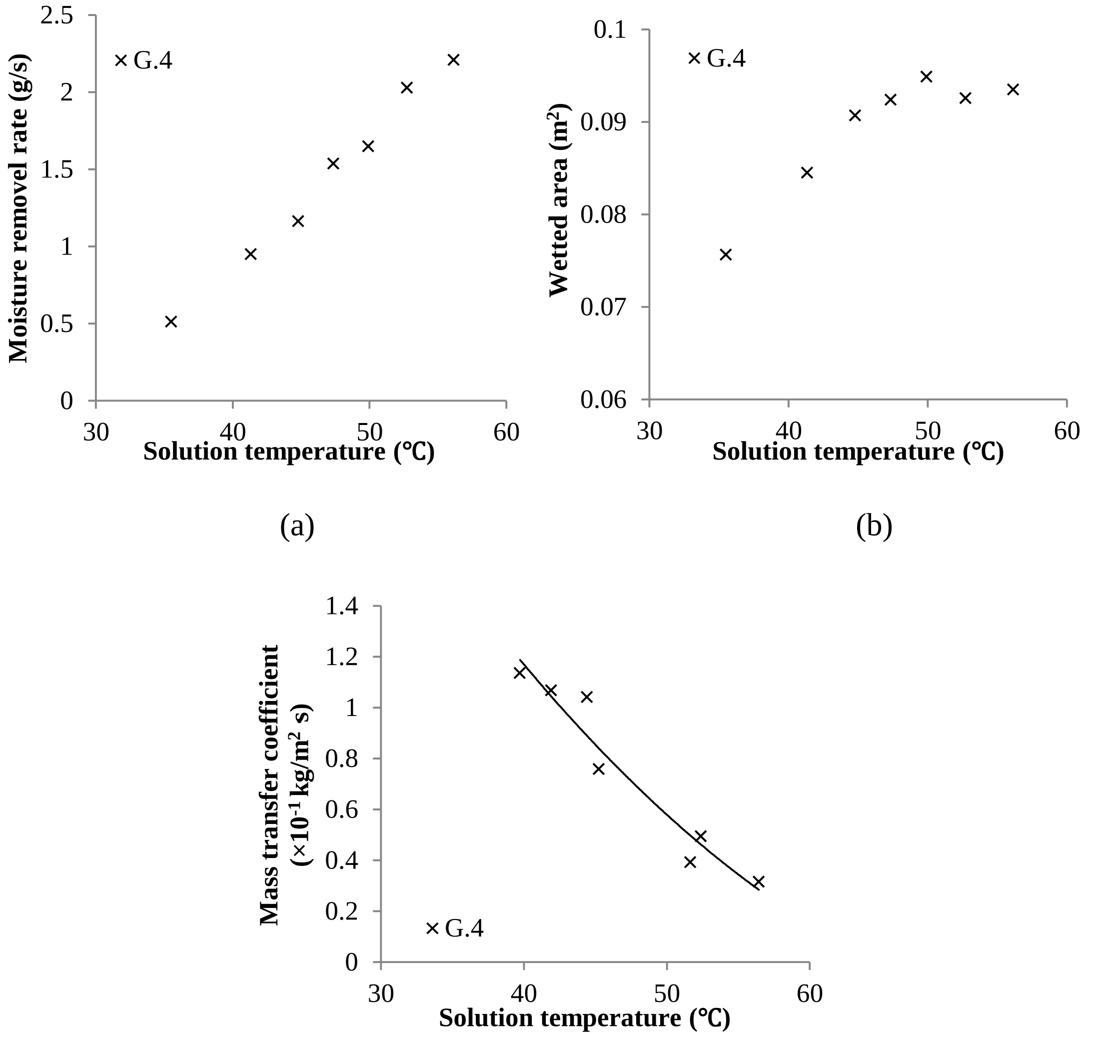

(c)

Fig. 5. 3 Changing of system performance of G. 4 with the solution mass flow rate: (a) moisture removal rate, (b) wetted area and (c) mass transfer coefficient

As shown in Fig. 5.4, the change of working surface temperature rarely influenced the mass transfer coefficient between solution and air. As indicated in Chapter 3, the moisture removal rate and wetted area both increased with the plate surface temperature, and same rising rates were found. Therefore, the mass transfer coefficient obtained from the experiment results almost kept unchanged.

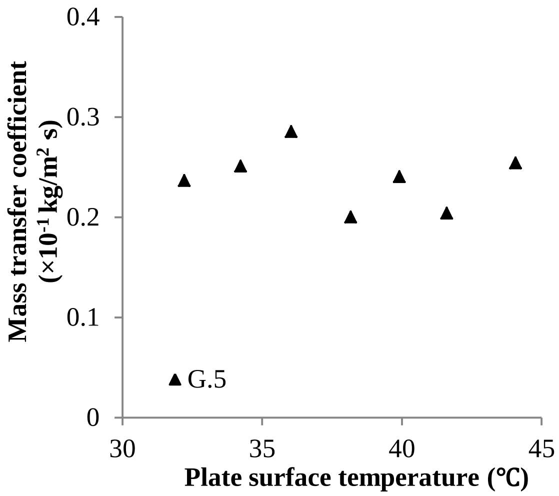

Fig. 5. 4 Changing of mass transfer coefficient with plate surface temperature

Besides the parameters of desiccant solution, the mass transfer coefficient also varied with the air mass flow rate. As shown in Fig. 5.5, with the increase of mass flow rate of air, the average mass transfer coefficient increased. As discussed before, the influence of air velocity on the wetted area could be neglected. Therefore, the change trend of $\overline{a}_D$ in our experiments was found similar to the previous research (Zhang et al. 2010).

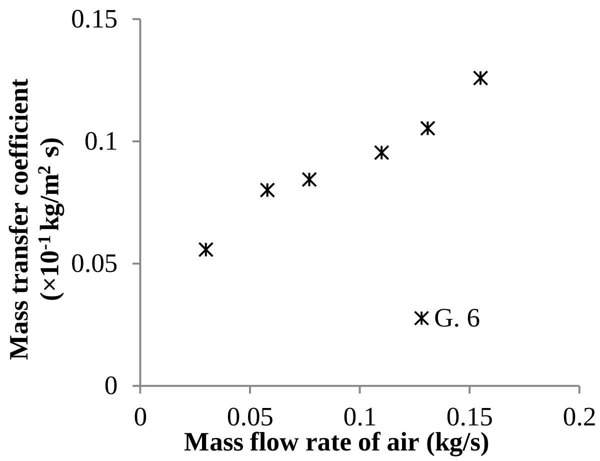

Fig. 5. 5 Changing of mass transfer coefficient with air mass flow rate

5.3.2 Formula of average overall mass transfer coefficient

With the experimental data, the constants b_1 to b_5 of Eq. (5.5) could be obtained by the multi linear regression. The correlation of the mass transfer coefficient of the internally heated regeneration is:

$$\bar{a}_D\left(\frac{\delta_a}{D_a\rho_a}\right) = Sh = 3.2\times10^{-4}\,\mathrm{Re}_a^{0.37}\,\mathrm{Sc}_a^{0.33}\,\mathrm{Re}_s^{0.47}\,\mathrm{Sc}_s^{0.33} \quad (5.\ 11)$$

As shown in Fig. 5.6, the deviations between the predicted and our experimental values for the regeneration process were approximately ±30%. Therefore, the obtained correlation could be used to predict the mass transfer coefficient for the insufficient wetted internally heated regenerator using the lithium chloride solution as the desiccant. The data were obtained when the mass concentration and temperature of the lithium chloride solution were in the ranges of 25–30% and 30–50℃, respectively, and the temperature and humidity ratio of the air were in the ranges of 25–50 ℃ and 0.005–0.015 kg/kg dry air, respectively.

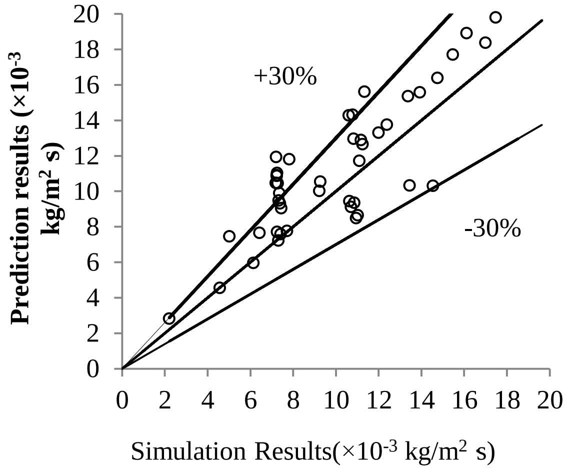

Fig. 5. 6 Comparison of mass transfer coefficient between calculation and experimental results

5.3.3 Discussion

By comparing with the correlations of mass transfer coefficient in previous researches (Zhang et al., Yin et al.), the equation developed in our research presents a similar form with the existing correlations, which was all represented using the dimensionless quantities: the Sherwood number, Reynolds number, and Schmidt number. However, in previous studies, as the solution film thickness was usually predicted with the assumption of wetted area, the flow velocity, which was determined by the thickness, could not be calculated accurately. In our equation, the actual wetted width of desiccant film under different conditions was employed, so the coefficient could describe the mass transfer more accurately.

In our research of the regeneration process, in most situations, the change trend of mass transfer coefficient was observed to be different with the previous results. The influence of solution mass flow rate was chosen as an example. As shown in Fig. 5.7, the coefficients calculated by the Yin's correlation (Yin et al. 2007) were smaller than the experimental ones at the small mass flow rate of solution. Meanwhile, with the increase of solution mass flow rate, the simulation data would exceed the test results. Furthermore, the coefficient was found to decrease with the mass flow rate of solution in our experiment, and an opposite trend was observed in the simulation results.

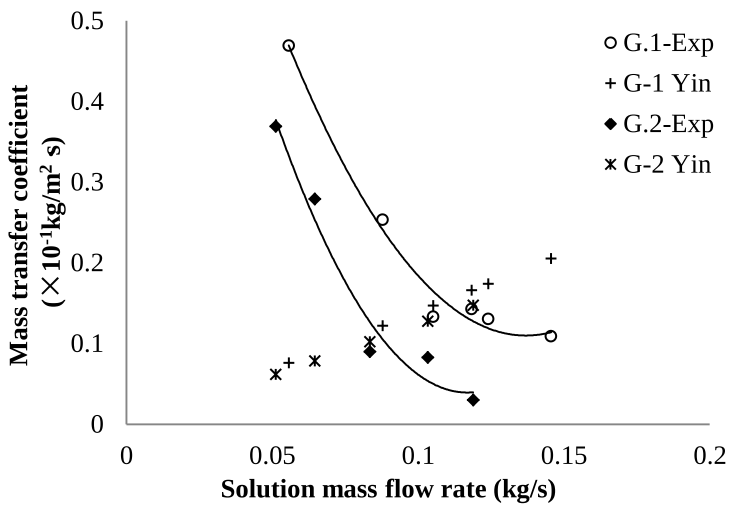

Fig. 5. 7 Comparison of mass transfer coefficient between experimental results and previous simulation results

The reason for this deviation is that the wetted area was assumed as a constant in previous researches, while the actual varied wetted area was employed for the calculation of mass transfer coefficient in our experiments. Therefore, when the solution mass flow rate was small, the actual wetted are was smaller than the assumed one, which led to an underestimation of the coefficient. With the increase of solution mass flow rate, the wetted area increased, so that an overestimation of the previous research occurred. Furthermore, as indicated in Fig. 5.1 (a), the moisture removal rate increased significantly with the solution mass flow rate. If the wetted area was set to be a constant, the rate was only expressed as the increase of the mass transfer coefficient. However, under insufficient wetting conditions, the wetted area actually also increased with the solution mass flow rate, and its rising rate was larger than that of the moisture removal rate. So, by using the actual wetted area in Eq. (5.3), the mass transfer coefficient in G. 1 and 2 was found to decrease with the solution mass flow rate. It should be noticed that the decrease of the coefficient only stands for the reduction of mass transfer per unit area, but could not indicate the mass exchange performance of the whole regenerator.

Therefore, both the mass transfer coefficient and wetted area influenced the mass transfer performance of the internally heated regenerator, and were varied with the operation parameters of solution and air. To evaluate and simulate the performance of liquid desiccant regenerator accurately, both the mass transfer coefficient and the wetted area under different conditions should be predicted by employing the newly developed models.

5.4 Summary

The mass transfer coefficient is an indispensable parameter for the performance evaluation and simulation of liquid desiccant system. In this chapter, the influencing factors affecting the coefficient under insufficient wetting conditions were investigated experimentally, with a single channel internally heated regenerator. By considering the actual wetted area, the mass transfer coefficient was found to decrease at a gradually reducing speed with the increase of solution mass flow rate. It also found to decrease with the increase of solution distributor thickness and solution temperature, and to increase with the mass flow rate of air. But, the influences of solution concentration and the working surface temperature were insignificant. Based on the experimental results, an empiric formula for insufficient wetted regenerator was developed with the multi linear regression. The predicted results were compared with those obtained from experiments, showing an acceptable error. Therefore, the mass transfer performance of internally heated regenerator is determined by both the mass transfer coefficient and wetted area. To describe the performance more accurately, the combined impacts of these two factors should be considered, by employing the derived equation in this chapter and the developed model in Chapter 4.

CHAPTER 6

3-D MODEL DEVELOPMENT FOR INTERNALLY COOLED/HEATED LIQUID DESICCANT SYSTEM

6.1 Introduction

In previous chapters, the influencing factors of the wetted area, film thickness and mass transfer coefficient of internally heated regeneration were studied experimentally and theoretically. A theoretical model with an analytical solution was developed for accurately calculating the wetted area of falling film, and an empiric formula of mass transfer coefficient was developed with acceptable errors comparing with the test data.

As summarized in Chapter 2, although there are several widely accepted theoretical models for predicting the performance of internally cooled/heated dehumidification/regeneration, some limitations have been observed. The main reason is that the actual dehumidification/regeneration process among the air, desiccant and extra fluid is three-dimensional, and the heat and mass transfer occurs in the direction of all three axes. However, most existing models only consider dimensions, assuming that either the heat and mass transfer in the thickness direction or the insufficient wetting condition on the working plate could be neglected. These assumptions may cause large deviations between simulations and actual experiment results.

Therefore, in this chapter, a 3-D model of internally heated regenerator was developed for describing the heat and mass transfer among the air, solution and extra hot water in all three directions. The insufficient wetting condition and change of film thickness due to the mass transfer and film deformation were taken into account. The numerical solution method of the model was also provided. To verify the model, the calculation results were compared with both those by existing theoretical models and our experimental results. With the new model, a parameter study has been done numerically to show the effect of inlet parameters on the moisture removal rate and regeneration efficiency.

6.2 3-D Model for internally cooled/heated liquid desiccant system

In the internally cooled/heated liquid desiccant system, by introducing the extra cool/hot fluid, the solution exchanges the moisture and heat with the air by direct contact and exchanges heat with the fluid by indirect contact simultaneously. The change of solution condition depends on the surface vapour pressure on the interface of liquid and air side. When the solution vapour pressure is greater than that of air, the desiccant releases the moisture to the process air, which is the regeneration process. In contrast, it is the dehumidification process. As the similar heat and mass transfer mechanism between these two processes of liquid desiccant, they could be described by the same theoretical model.

Generally, the internally cooled/heated dehumidifier/regenerator consists of several channels for the air/solution contacting. The composition of one channel is shown in Fig. 6.1. The solution film flows down along the working surface with the inclined angle of θ . The air could be blown into the channel with different flow patterns, i.e. counter flow, cross flow and parallel flow. For better system efficiency, the first two patterns are commonly used in practical applications. According to previous researches, due to the complexity of system, in our theoretical model, the distribution method of solution was simplified as the falling film, and the thermal and mass transfer between dispersed desiccant droplets and air was ignored. Additionally, although there are several types of practical internally cooled/heated units, for developing the model, the composition was simplified as the double plate.

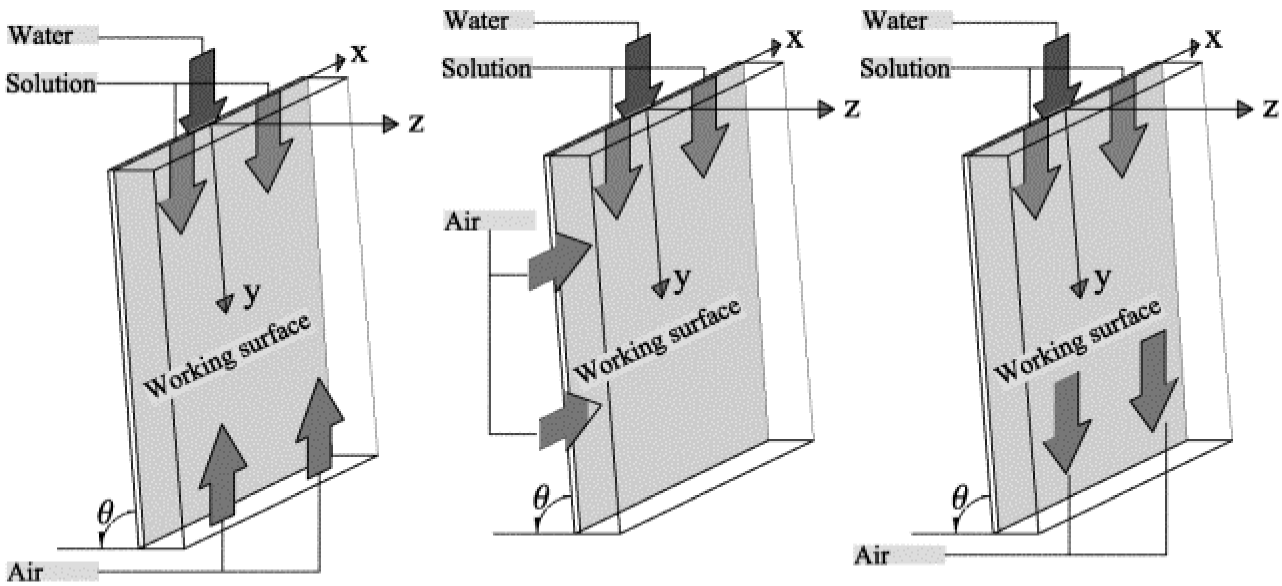

Fig. 6. 1 Schematic of one channel with different flow patterns of internally cooled/heated dehumidifier/regenerator

The following assumptions were made when building the model:

a) the flow is laminar and fully developed for the liquid desiccant and air, and there is thermodynamic equilibrium at the desiccant/air interface;

b) the desiccant film is smooth (not wavy);

c) the physical properties are constant, and no shear forces are exerted by the air on the desiccant;

d) the body force in the air, species thermo-diffusion and diffusion-thermo effects are negligible;

e) as the rim part of falling film is much narrow than the central part, its influence on the film thickness was neglected;

f) the velocity of desiccant in the transverse direction is negligible;

g) the change of the thickness of air due to the deformation of film thickness is negligible;

and

h) the latent heat of vapourization is assumed as a constant, and air thermal and moisture diffusivity in the flow direction are negligible.

The geometry of the channel is shown in Fig. 6.2.

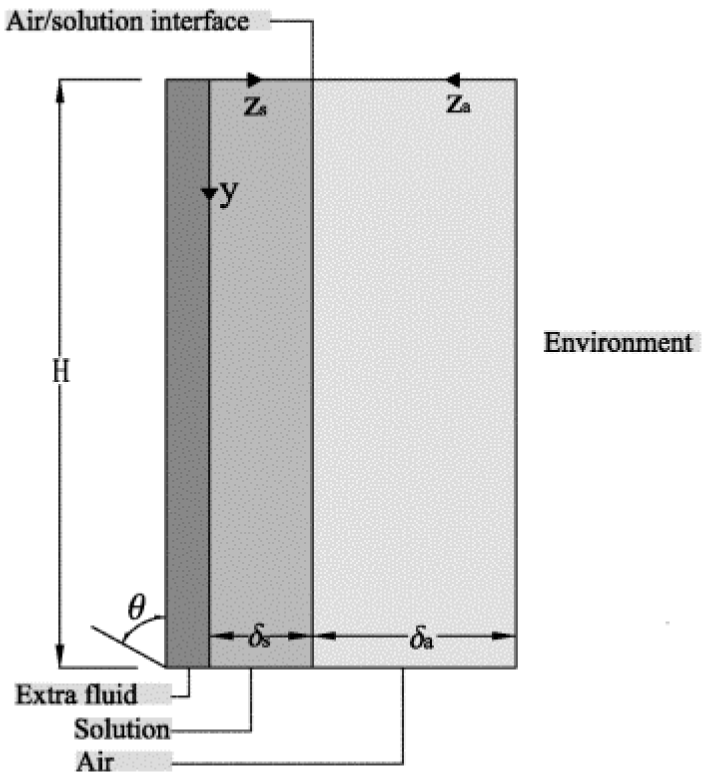

Fig. 6. 2 Geometry of one channel with notation

6.2.1 Governing equations and boundary conditions

Considering the assumptions above and the geometry, the N-S equation of the heat and mass transfer process is:

$$
\begin{aligned}
u_s \frac{\partial u_s}{\partial y} + v_s \frac{\partial v_s}{\partial z} &= -\frac{1}{\rho_s}\frac{\partial P}{\partial y} + \frac{\mu_s}{\rho_s}\left(\frac{\partial^2 u_s}{\partial y^2} + \frac{\partial^2 u_s}{\partial z^2}\right) + g\sin\theta \\
u_s \frac{\partial u_s}{\partial y} + v_s \frac{\partial v_s}{\partial z} &= -\frac{1}{\rho_s}\frac{\partial P}{\partial z} + \frac{\mu_s}{\rho_s}\left(\frac{\partial^2 v_s}{\partial y^2} + \frac{\partial^2 v_s}{\partial z^2}\right) - g\cos\theta
\end{aligned} \tag{6. 1}
$$

The continuity equation is:

$$\frac{\partial u_s}{\partial y}+\frac{\partial v_s}{\partial z}=0 \qquad (6.\ 2)$$

Therefore, the governing momentum, energy and species equations are:

For the liquid desiccant:

Energy equation: $$a_s\left(\frac{\partial^2 t_s}{\partial y^2}+\frac{\partial^2 t_s}{\partial {z_s}^2}\right)=u_s\frac{\partial t_s}{\partial y}+v_s\frac{\partial t_s}{\partial z_s} \qquad (6.\ 3)$$

Mass balance equation for species, LiCL: $$D_s\left(\frac{\partial^2 \zeta_s}{\partial y^2}+\frac{\partial^2 \zeta_s}{\partial {z_s}^2}\right)=u_s\frac{\partial \zeta_s}{\partial y}+v_s\frac{\partial \zeta_s}{\partial z_s} \qquad (6.\ 4)$$

For the process air:

For the counter-flow and parallel flow pattern of air:

Energy equation: $$a_a\frac{\partial^2 t_a}{\partial {z_a}^2}=u_a\frac{\partial t_a}{\partial y} \qquad (6.\ 5)$$

Mass balance equation for species, vapor: $$D_a\frac{\partial^2 \omega_a}{\partial {z_a}^2}=u_a\frac{\partial \omega_a}{\partial y} \qquad (6.\ 6)$$

Momentum equation: $$u_a\frac{\partial^2 u_a}{\partial {z_a}^2}=\frac{\partial P}{\partial y} \qquad (6.\ 7)$$

For the cross-flow pattern of air:

Energy equation: $$a_a\frac{\partial^2 t_a}{\partial {z_a}^2}=u_a\frac{\partial t_a}{\partial x} \qquad (6.\ 8)$$

Mass balance equation for species, vapor: $$D_a\frac{\partial^2 \omega_a}{\partial {z_a}^2}=u_a\frac{\partial \omega_a}{\partial x} \qquad (6.\ 9)$$

Momentum equation: $$u_a\frac{\partial^2 u_a}{\partial {z_a}^2}=\frac{\partial P}{\partial x} \qquad (6.\ 10)$$

As the solution falling film is very thin, it could be considered to exchange the heat with the extra cooling/heating fluid as a whole. So, for the extra fluid, the government equation is:

Energy equation: $$\frac{\partial t_f}{\partial y} = \frac{a_f H}{c_{p,f}}(\overline{t_s} - t_f) \qquad (6.\ 11)$$

where t means the temperature. a is the thermal diffusivity, and D is diffusion coefficient. ω is the moisture content and m is the mass flow rate. μ_s and ρ_s stand for the dynamic viscosity and density of solution respectively, which are decided by the solution temperature and concentration, ζ_s. u and v are the flow velocity. ω is the moisture content of air. H stands for the height of dehumidifier/regenerator. The subscripts *a, s, f* stand for the air, solution and extra fluid.

The boundary conditions are:

For the counter-flow pattern of air:

$$\begin{aligned}
&y = 0: \ \ t_s = t_{s,in}; \ \zeta_s = \zeta_{s,in}; \\
&y = H: \ t_a = t_{a,in}; \ \ \omega_a = \omega_{a,in}; \\
&z_s = 0: \ \frac{\partial \zeta}{\partial z_s} = 0; \ u_s = 0; \ v_s = 0; \\
&z_a = 0: \ \lambda_a \frac{\partial t_a}{\partial z_a} = K(t_a - t_{en}); \ \frac{\partial \omega_a}{\partial z_a} = 0; \ \frac{\partial u_a}{\partial z_a} = 0; \\
&z_s = \delta_s: \ t_s = t_a; \ u_s = -u_a; \ \omega_a = \omega_I; \ \frac{\partial u_s}{\partial z_s} = 0; \ \frac{\partial u_a}{\partial z_a} = 0;
\end{aligned} \qquad (6.\ 12)$$

For the parallel-flow pattern of air:

$$
\begin{aligned}
&y=0:\ \ t_s=t_{s,in};\ \zeta_s=\zeta_{s,in};t_a=t_{a,in};\ \ \omega_a=\omega_{a,in};\\
&z_s=0:\ \frac{\partial \zeta}{\partial z_s}=0;\ u_s=0;\ v_s=0;\\
&z_a=0:\ \lambda_a\frac{\partial t_a}{\partial z_a}=K(t_a-t_{en});\ \frac{\partial \omega_a}{\partial z_a}=0;\ \frac{\partial u_a}{\partial z_a}=0;\\
&z_s=\delta_s:\ t_s=t_a;\ u_s=u_a;\ \omega_a=\omega_I;\ \frac{\partial u_s}{\partial z_s}=0;\ \frac{\partial u_a}{\partial z_a}=0;
\end{aligned}
\tag{6. 13}
$$

For the cross-flow pattern of air:

$$
\begin{aligned}
&y=0:\ \ t_s=t_{s,in};\ \zeta_s=\zeta_{s,in};\\
&x=0:\ t_a=t_{a,in};\ \ \omega_a=\omega_{a,in};\\
&z_s=0:\ \frac{\partial \zeta}{\partial z_s}=0;\ u_s=0;\ v_s=0;\\
&z_a=0:\ \lambda_a\frac{\partial t_a}{\partial z_a}=h(t_a-t_{en});\ \frac{\partial \omega_a}{\partial z_a}=0;\ \frac{\partial w_a}{\partial z_a}=0;\\
&z_s=\delta_s:\ t_s=t_a;\ w_a=0;\ \omega_a=\omega_I;\ \frac{\partial u_s}{\partial z_s}=0;\ \frac{\partial w_a}{\partial z_a}=0;
\end{aligned}
\tag{6. 14}
$$

where δ_s is the thickness of liquid desiccant falling film and δ_a means the thickness of air channel. h is the convective heat transfer coefficient. The subscript *I* stands for the interface of air and solution, and *in* and *out* mean the inlet and outlet characteristics.

6.2.2 Required Equations of the model

To obtain the velocity profile for the solution, the film thickness should be calculated. The influences of insufficient wetting condition, film deformation due to the Marangoni effect and the mass transfer between air and solution are all taken into account. By integrating the Eq. (6.1) through the film thickness direction, it gives:

$$u_s = \frac{g\sin\theta}{\gamma_s}(\delta_s z - \frac{z^2}{2}) \quad (6.15)$$

According to our experimental and theoretical model in Chapter 3 and 4, the wetted width along the flow direction could be predicted under different operation conditions. Therefore, the solution mass flow rate could be expressed as:

$$\begin{aligned} m_s &= 2\int_0^{\frac{W_s(y)}{2}}\int_0^{\delta_s}\rho_s u_s dz\ dx \ (\text{if } W_s(y) \le W_d) \\ m_s &= 2\int_0^{\frac{W_d(y)}{2}}\int_0^{\delta_s}\rho_s u_s dz\ dx \ (\text{if } W_s(y) > W_d) \end{aligned} \quad (6.16)$$

where $W_s(y)$ is the wetted width changing with the flow distance due to the contraction or expansion of falling film. W_d is the design width of the internally heated/cooled dehumidifier/regenerator.

As the rim part of falling film is much narrow than the central part, its influence on the film thickness was neglected. So, the film thickness could be obtained the following equation:

$$\begin{aligned} \delta_s &= (\frac{3m_s(y)\gamma_s}{W_s(y)\rho_s g})^{1/3} \quad (\text{if } W_s(y) \le W_d) \\ \delta_s &= (\frac{3m_s(y)\gamma_s}{W_d\rho_s g})^{1/3} \quad (\text{if } W_s(y) > W_d) \end{aligned} \quad (6.17)$$

m_s is affected with the moisture exchange between solution and air, and would change with the flow distance, y, with the following equation:

$$m_s(y) = m_{s,in} \frac{1-\zeta_{s,in}}{1-\zeta_{s,y}} \tag{6. 18}$$

where $\zeta_{s,y}$ is the solution concentration in the position of y.

Therefore, by substituting Eq. (6.17) and (6.18) into (6.15) , the velocity profile for the solution could be calculated. The velocity profile for the process air could also be predicted through the momentum and continuity equations. As the change of film thickness is small compared to the thickness of air channel, its impact on the airflow velocity profile was neglected. Therefore, the mass flow rate of process air could be expressed as:

$$m_a = W_d \int_0^{\delta_a} \rho_a u_a dz_a \tag{6. 19}$$

So, for the counter-flow pattern of air:

$$\begin{aligned} u_a &= -u_{s,\max} + \frac{dp}{dy}\frac{1}{2\mu_a}(z_a{}^2 - \delta_a{}^2) \\ \frac{dp}{dy} &= -3\mu_a[\frac{u_s}{\delta_a{}^2} + \frac{m_a}{W_d \rho_a \delta_a{}^3}] \end{aligned} \tag{6. 20}$$

For the parallel-flow pattern of air:

$$u_a = u_{s,\max} + \frac{dp}{dy}\frac{1}{2\mu_a}(z_a{}^2 - \delta_a{}^2)$$
$$\frac{dp}{dy} = -3\mu_a[-\frac{u_s}{\delta_a{}^2} + \frac{m_a}{W_d \rho_a \delta_a{}^3}] \tag{6. 21}$$

For the cross-flow pattern of air:

$$w_a = \frac{dp}{dy}\frac{1}{2\mu_a}(z_a{}^2 - \delta_a{}^2)$$
$$\frac{dp}{dy} = -\frac{3\mu_a m_a}{W_d \rho_a \delta_a{}^3} \tag{6. 22}$$

where $u_{s,\max}$ means the solution velocity on the air/solution interface.

To solve the problem, the energy and species balances on the interface should be calculated by the additional equations.

$$\lambda_s \frac{\partial t_s}{\partial z} = \lambda_a \frac{\partial t_a}{\partial z} + \rho_a D_a h_{fg} \frac{\partial \omega_a}{\partial z}$$
$$\rho_s D_s \frac{\partial \zeta}{\partial y} = \rho_a D_a \frac{\partial \omega_a}{\partial y} \tag{6. 23}$$

where λ is the thermal conductivity coefficient.

By introducing the equations (6.15-6.23) into the government equations (6.1-6.11), the model could be solved with the boundary conditions using the numerical solution method.

6.2.3 Numerical solution of the model

In our investigation, the model is solved numerically with the finite-volume method. The simulation grids are shown in Fig. 6.3. The number of nodes in the thickness direction of the solution is much denser than that of air, and it varied in the flow direction according to the height of the channel.

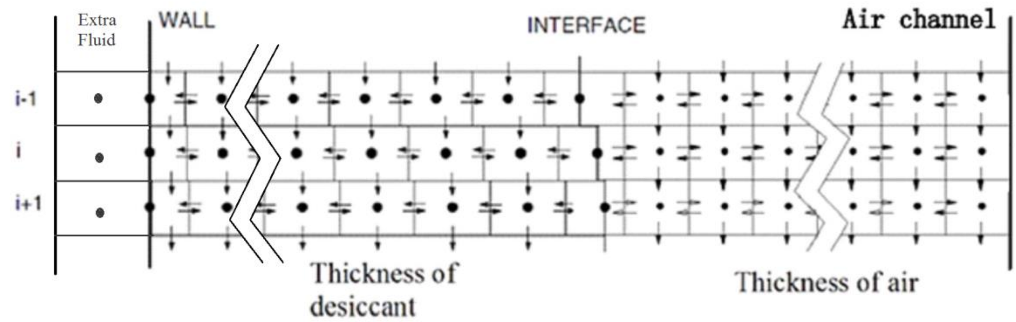

Fig. 6. 3 Schematic of simulation nodes in the flow direction

Firstly, the government equations should be discretized. In the steady state, the velocity of solution in the z-axis shows an insignificant effect, which could be neglected. As the Eq. (6. 3-6) has the similar formation, as shown in Eq. (6.24), the discretization could all be expressed with the Eq. (6.25). The discretization node is shown in Fig. 6.4.

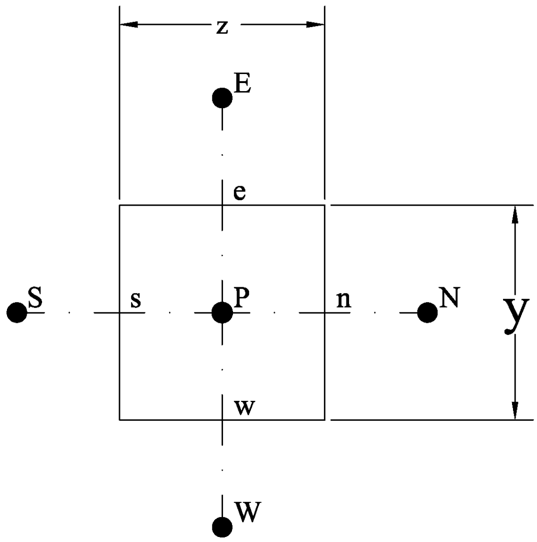

Fig. 6. 4 Schematic of an individual control element

$$u\frac{\partial\psi}{\partial y} = \Gamma\frac{\partial^2\psi}{\partial z^2} \tag{6. 24}$$

$$\psi_P = \frac{A_s\psi_S + A_n\psi_N + \frac{A_w}{2}\psi_W - \frac{A_e}{2}\psi_E}{A_s + A_n - \frac{A_w}{2} + \frac{A_e}{2}} \tag{6. 25}$$

where

$$\begin{aligned} A_s &= \frac{\Gamma_s\Delta y}{\Delta z} \\ A_n &= \frac{\Gamma_n\Delta y}{\Delta z} \\ A_e &= u_e\Delta z \\ A_w &= u_w\Delta z \end{aligned} \tag{6. 26}$$

It should be noticed that the interface between the last node in the desiccant side and the last node in the air sideways represented by an additional node. This interface node has a fixed volume, and provides heat and mass exchange between the air and desiccant. According to the previous studies (Zhou et al. 2006), the Two-Film Theory was employed to obtain the thickness of the interface node, as shown in the Eq. (6.27).

$$\delta_{inter} = \frac{D_s}{a_D} \tag{6. 27}$$

where δ_{inter} means the thickness of the hypothetical interface node. a_D is the local mass transfer coefficient between solution and air, which could be predicted by our investigation in the Chapter 5. Therefore, the energy and species balances on the interface could be expressed with the following equations.

$$\begin{aligned} &\lambda_s \frac{t_{s,interface} - t_{s,j_{max}}}{\delta_{inter,s}} = \lambda_a \frac{t_{a,interface} - t_{a,j_{max}}}{\delta_{inter,a}} + \rho_a D_a h_{fg} \frac{\omega_{a,interface} - \omega_{a,j_{max}}}{\delta_{inter,a}} \\ &\rho_s D_s \frac{\zeta_{s,interface} - \zeta_{s,j_{max}}}{\delta_{inter,s}} = \rho_a D_a \frac{\omega_{a,interface} - \omega_{a,j_{max}}}{\delta_{inter,a}} \end{aligned} \tag{6. 28}$$

where the subscript *interface* means the additional node, and j_{max} stands for the second last note of solution or air film.

Therefore, the model could be solved numerically with the following steps:

(1)Setting the inlet parameters for liquid desiccant, air and extra fluid, including the $t_{s,in}$, $t_{a,in}$, $t_{f,in}$, $m_{s,in}$, m_a, m_f, $\omega_{a,in}$, $\zeta_{s,in}$, and the design parameters, including H and W_d;

(2) Calculating the wetted width of solution film along the flow direction, $W(y)$, by using the model given in Chapter 5;

(3) Calculating the influence of extra cooling/heating fluid on the solution temperature with Eq. (6.11);

(4) Calculating the temperature profile of solution with Eq. (6.3) and (6.25). Firstly, the film thickness along the flow direction could be predicted with Eq. (6.17). Then, with the variable film thickness, by using Eq. (6.15), the velocity profile of solution could be calculated. As the Eq. (6.25) is an implicit format, to solve the equation, the iteration calculation is required.

(5) Updating the boundary condition of air with the result of step 4, and calculating the temperature profile of air with Eq. (6.5) and (6.25). The velocity profile of air could be estimated with Eq. (6.20), (6.21) or (6.22), depending on the different flow patterns.

(6) Calculating the moisture content of air interface with the solution temperature and initial solution concentration, with the boundary conditions.

(7) Calculating the profile of the moisture content of air with Eq. (6.6) and (6.25) ;

(8) Updating the solution concentration of the air/solution interface with Eq. (6.28), and calculating the profile of solution concentration with Eq. (6.4) and (6.25);

(9) Calculating the moisture content of air interface with the solution temperature and solution concentration obtained in the last step, and repeating steps (7)-(9) until the difference between the results of this time and those from last time is small enough, i.e. $\leq 10^{-5}$;

(10) Checking the heat and mass balance of air and solution with Eq. (6.28). If the error is small enough, i.e. $\leq 10^{-5}$, the results are acceptable; if not, the simulation procedure should be continued to the next step;

(11) Updating the solution temperature and concentration of the interface node with Eq. (6.28);

(12) Repeating steps (3) to (10) until the species and energy balance is approached.

The flow chart of the numerical solution is shown in Fig. 6.5, and the required iterations are also indicated.

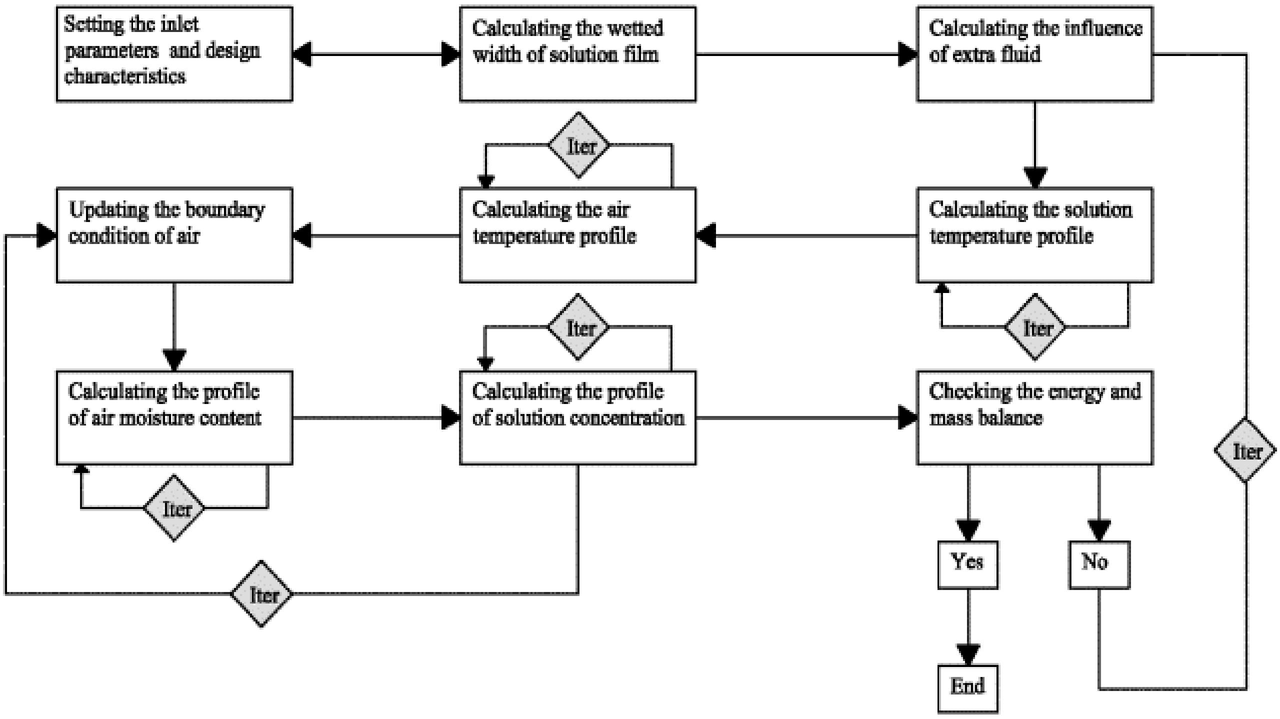

Fig. 6. 5 Flow chart of numerical solution of 3-D model

6.3 Verification and Comparison

By employing the simulation method introduced in the last section, the 3-D model for the internally heated regeneration could be solved numerically with the consideration of the insufficient wetting condition and the change of film thickness due to the mass transfer and film deformation . To verify the model, the calculation results were firstly compared with our experimental results. The moisture removal rate during the experiments and by our model under more than 100 different conditions were compared. The details of the experiments could refer to Chapter 3. The Average Relative Deviation (ARD) between our prediction results and experiment results could be calculated by the following equation.

$$ARD = \frac{1}{n}\sum_{i=1}^{n}\left|\frac{P_{\exp eriment,i} - P_{prediction,i}}{P_{prediction,i}}\right| \times 100\% \qquad (6.\ 29)$$

where n is the number of data set.

As shown in Fig. 6.6, the moisture removal rates under different operation conditions were calculated and compared with those recorded in our experiments. The majority of the simulation results showed an acceptable difference of less than ±25%, with an ARD of 14.9%. The errors may be caused by: 1) the slight irregularity or uneven roughness of the working surface due to the industrial processing; 2) the measurement uncertainties of the operation conditions during the experiments; 3) the assumptions made for developing the model, such as the employment of the two-film theory.

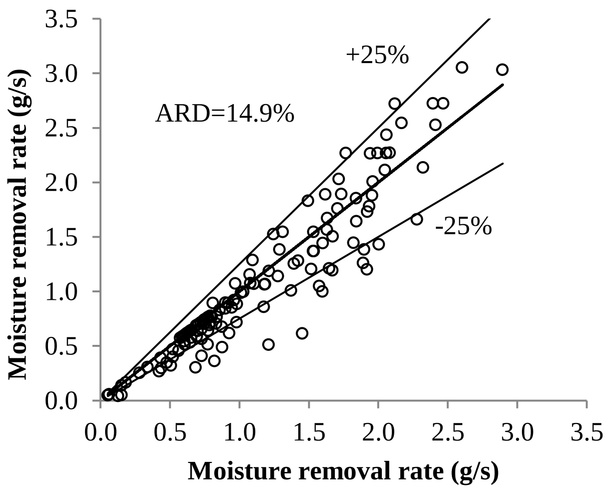

Fig. 6. 6 Comparison between calculation results with 3-D model and experimental results

Then, the simulation results were compared with the traditional theoretical model and the experimental data. The previous model employed in the comparison was developed by Khan (Khan, 1998) and Ren (Ren et al. 2007). It includes a set of steady-state differential equations and could be solved by dividing the whole heat/mass transfer plane into small differential elements. In the comparison, the experiments G.2, G.7, G.10 and 15 were selected to show the influences of significant parameters during the regeneration process, as described in Chapter 3. With the inlet parameters of solution, air and extra fluid and the design parameters in these experiments, the effect of different parameters on the regeneration performance could be simulated with the newly developed model and the existing model. Similar to the experiment, the LiCl and water were chosen as the solution and cooling/heating fluid, respectively, and the counter-flow pattern was adopted in this simulation.

As shown in Fig. 6.7, with the increase of solution mass flow rate, the moisture removal rate, which represents the mass transfer performance of the regenerator, increased significantly in the experiments. Both simulation results showed an increasing trend, but obviously, our newly developed model presented a much closer trend to the test data. With the increase of solution mass flow rate, as described in Chapter 3 and 4, the wetted area and width of the solution falling film increased almost proportionally, which effectively enhanced the heat and mass transfer area and time between the air and solution and improved the regeneration performance accordingly. Therefore, without considering the effect of wetted area and film thickness, the traditional model could not accurately predict the influence of solution mass flow rate. Furthermore, when the solution mass flow rate was small, the simulation results of the existing model were under-estimated as the actual wetting factor was smaller than the pre-set one, and the trend turned opposite with the increase of solution mass flow rate.

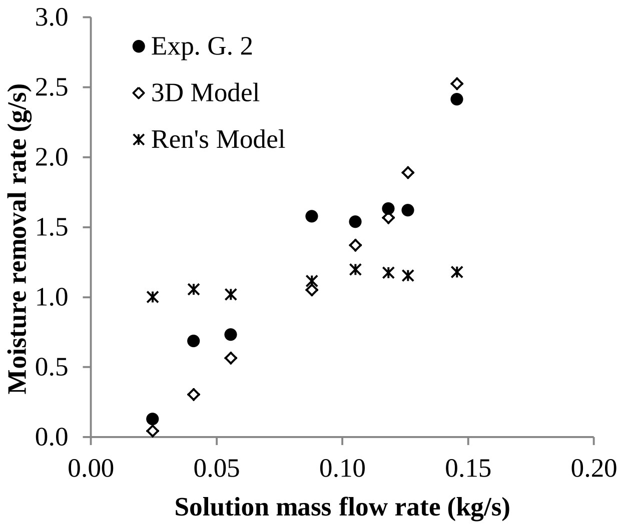

Fig. 6. 7 Comparison of experimental results, simulation results with 3-D model and with Ren's model under different solution mass flow rate

The influence of inlet temperature of extra hot water was shown in Fig. 6.8. When the water temperature increased, both the moisture removal rates in the experiment and with the 3-D model improved obviously, and their change trends were similar. But, the change with the traditional model were relatively small. As described in Chapter 4, the increase of water temperature could increase the solution temperature and also enlarge the wetted area and reduce the film thickness, which further improves the performance of internally heated regeneration. However, only the change of solution temperature were considered in the Ren's model, and the effect of the water temperature was seriously underestimated.

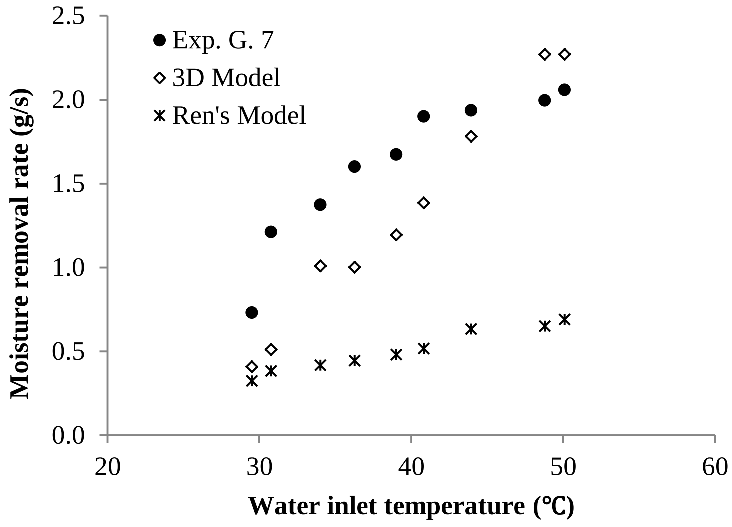

Fig. 6. 8 Comparison of experimental results, simulation results with 3-D model and with Ren’s model under different water inlet temperature

As found in Fig. 6.9, the moisture removal rates in the experiment, with the traditional model and our new model all increased with the solution inlet temperature. As the high temperature leads to a high equivalent humidity on the air/solution interface, the mass transfer could be enhanced due to the increasing mass gradient between air and solution. Furthermore, based on our previous research, the wetted area could be also improved as the initial wetted width increased with the solution temperature. Therefore, by calculating the enhanced mass transfer driving force and the increasing wetted area, the prediction with the 3-D model was more accurate compared with those by the 2-D model.

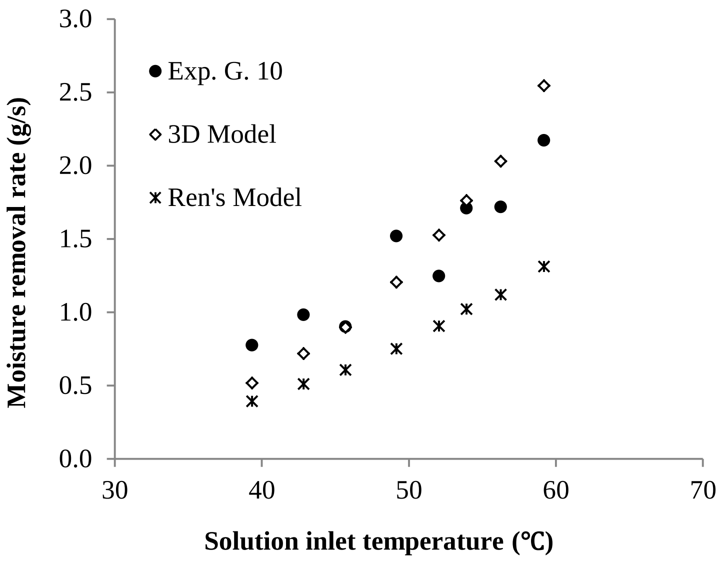

Fig. 6. 9 Comparison of experimental results, simulation results with 3-D model and with Ren's model under different solution inlet temperature

Based on the investigation in Section 3.4.4, the pre-wetting of working surface could effectively reduce the contact angle of solution and enlarge the wetted area accordingly. As shown in Fig. 6.10, the change of contact angle by making the surface hydrophilic was found to improve the moisture removal rate significantly in the experiments 14 and 15, and similar trend was also shown in the simulation results with the new 3-D model. The 3-D model is suitable for predicting the regeneration performance with different working surfaces, by taking the effect of solution contact angle into account. However, the contact angle of liquid desiccant was not included in the equations of the previous model, so the results were not listed in the figure.

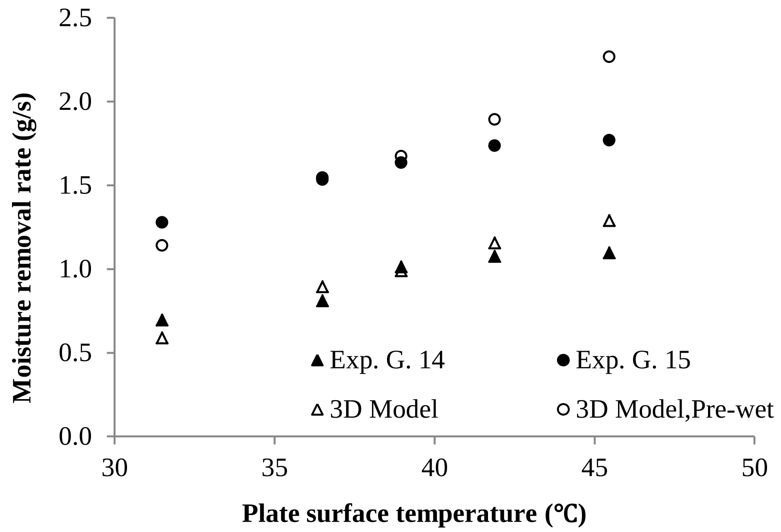

Fig. 6. 10 Comparison between simulation results with 3-D model and with Ren's model in pre-wetting and dry conditions

In terms of solution inlet concentration, the simulation results with the new model and Ren's 2-D model were similar, and both reduced with the decrease of interface equivalent humidity. But the change trend of the moisture removal rate with our model was a little smaller, as shown in Fig. 6.11. The difference is caused by the increase of wetted area with the solution concentration, which offsets part of performance reduction during the regeneration. However, the influence of concentration on the wetted area was not as obvious as other parameters, such as the solution temperature.

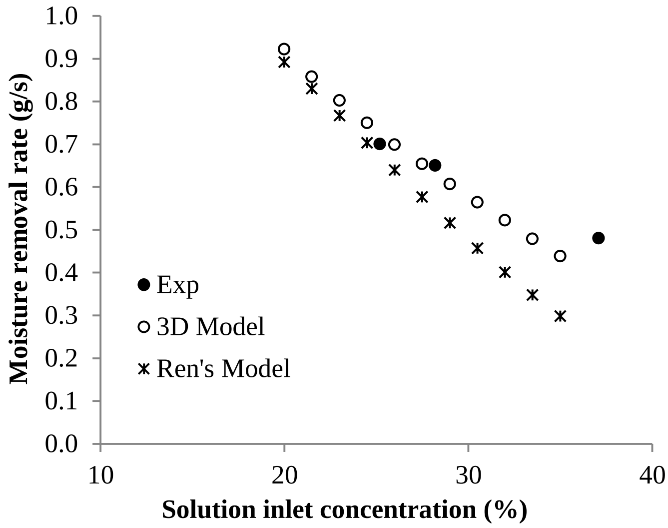

Fig. 6. 11 Comparison between simulation results with 3-D model and with Ren's model with different solution inlet concentration

Additionally, the influences of inlet parameters of air were simulated and compared. As shown in Fig. 6.12 (a), the results of moisture removal rates increased with both models as the increase of air temperature could avoid the temperature decrease of solution during the regeneration. With our investigation, the air temperature could also influence the plate surface temperature, and therefore influence the wetted area, but the effect was small compared to that of the hot water. So, comparing with the traditional model, the change trend with the new model was slightly obvious. However, as the mass flow rate of air shows slight impact on the wetted area and film thickness, as indicated in Fig. 6.12 (b), the simulation results with the existing and new models were almost the same.

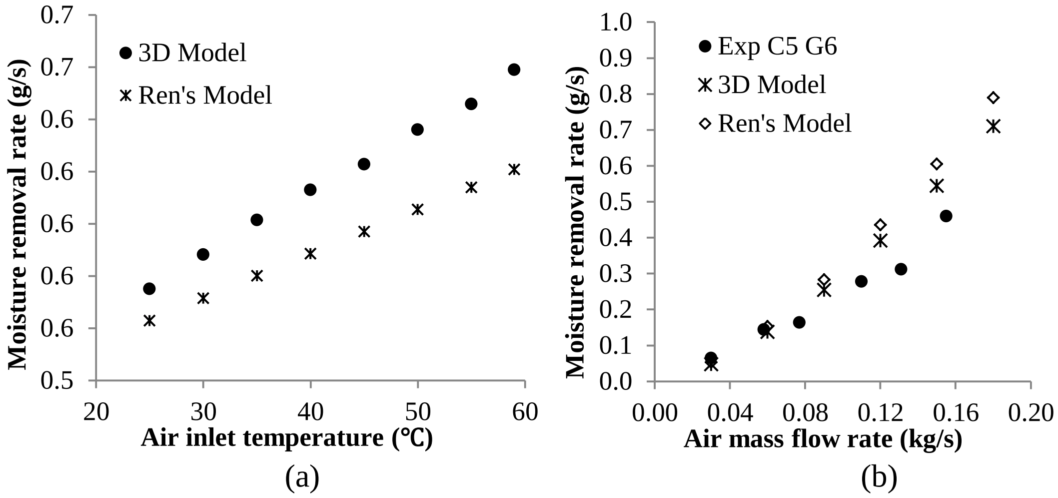

Fig. 6. 12 Comparison between simulation results with 3-D model and with Ren's model with (a) different air inlet temperature and (b) different air mass flow rate

Besides the outlet parameters and system performance, the film thickness in the y-z cross section along the flow direction and the surface temperature distribution in the x-y plate could also be calculated by the 3-D model. One test in G. 7 was chosen as an example, and the detailed experimental conditions were indicated in Fig. 6.13. As shown in Fig. 6.13 (a), due to the film contraction and the increase of solution mass flow rate, both the film thickness in the experiment and that predicted with the new model increased with the flow distance with a close trend. Compared with Fig. 6.13 (b) by the thermal camera and (c) by the simulation, it could be seen that the solution temperatures on the film surface were similar, which was higher in the central part and decreased with the increase of flow distance. As the change of thickness on the film edge was neglected in the new model, the surface temperatures of desiccant on the edge varied in different ways in Fig. 6.13 (b) and (c). However, as the area of the rim part was relatively small compared to the whole film, the difference was insignificant and would not influence the accuracy of the 3-D model.

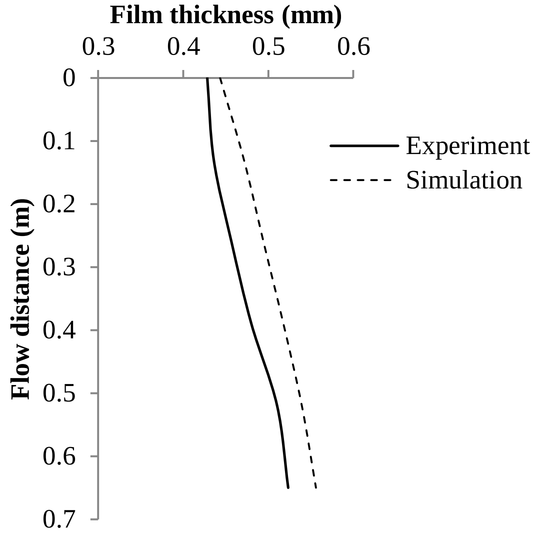

(a)

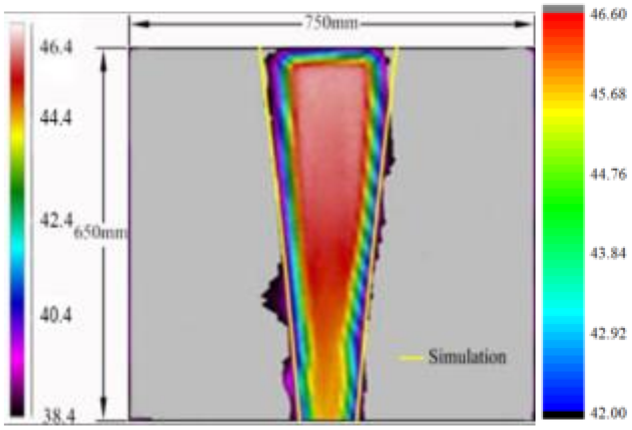

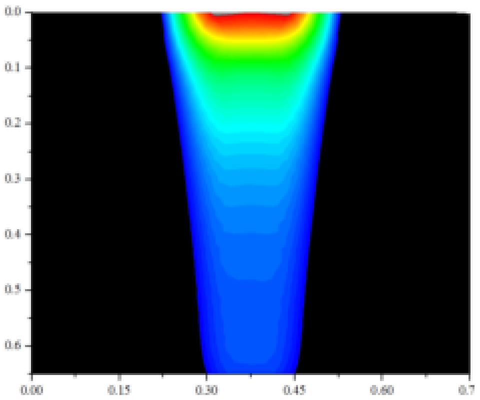

(b) (c)

m_s (kg/s)	$t_{s,in}$ (°C)	ζ_{in} (%)	t_p (°C)	$t_{w,in}$ (°C)	$m_{w,in}$ (kg/s)	$t_{a,in}$ (°C)	$\omega_{a,in}$ (g/kg)
0.034	46.6	30.0	40.8	51.2	0.131	24.1	9.34

Fig. 6. 13 Comparison between simulation results with 3-D model and experimental results: (a) film thickness along the flow direction; (b) thermal image of solution surface temperature in the experiment and (c) simulated solution surface temperature

Therefore, by comparing with the experimental data and existing theoretical model, the newly developed 3-D model, which considering the effect of wetted area, film thickness and contact angle of solution, was found to show more accurate estimation under different operation conditions. So, the model could be employed to predict the regeneration performance of the falling film liquid desiccant regeneration system. Although the model was developed based on the regeneration process, it could also be applied for the dehumidifier with the similar mechanism between dehumidification and regeneration.

6.4 Simulation result and parameter study

With the 3-D model, the influencing factors of mass transfer performance of internally heated regeneration could be investigated numerically, and the performance could be expressed as the regeneration efficiency and the moisture removal rate. The regeneration efficiency is defined as the ratio of the actual moisture change between air and desiccant to the maximum possible change under given operating condition, which could be calculated by the following equation:

$$\varepsilon_m = \frac{\omega_{a,in} - \omega_{a,out}}{\omega_{a,in} - \omega_{I,in}} \tag{6. 30}$$

where ω_a means the moisture content and $\omega_{I,in}$ is the moisture content of the air which is at equilibrium with the desiccant solution at the inlet concentration and temperature.

The moisture removal rate, which means the rate of moisture added to the air from the desiccant, could be calculated from Eq. (6.28).

$$\dot{m}_{removal} = \dot{m}_a(\omega_{a,out} - \omega_{a,in}) \tag{6. 31}$$

where $\dot{m}_a$ is the air flow rate.

The initial value of the parameters required in the simulation was set as: $m_s = 0.1kg/s$, $t_{s,in} = 55$℃ , $\zeta_{in} = 32\%$, $t_{w,in} = 60$℃ , $m_w = 0.5kg/s$, $m_a = 0.5kg/s$, $t_{a,in} = 25$℃ , $\omega_{a,in} = 9.87g/kg$ and $\delta_{\max,i} = 1mm$. According to the previous study (Liu et al. 2008), the air and heating/cooling fluid flow patterns showed little effect on the system performance. So, the common counter-flow pattern was adopted in this simulation. The widely used LiCl and water were chosen as the solution and cooling/heating fluid, respectively.

Firstly, in the initial condition, the changes of solution temperature and concentration in both the y-z section cross and the x-y plate during the internally heated regeneration process were simulated. As shown in Fig. 6.14 (a), in the thickness direction, due to the introduction of extra hot water, the temperature of working plate was increased and the solution was heated in the side near the plate. Synchronously, with the moisture and thermal exchange with the relative dry and cool air, the solution temperature in the side near the air firstly decreased and then increased due to the heat transfer inside the film thickness, which could also be found in Fig. 6.14 (b). As the film was very thin, the heat transfer was effective to heat up the solution.

Additionally, as the plate surface temperature was higher than the solution, based on our research in Chapter 4, the falling film was expanded along the flow direction.

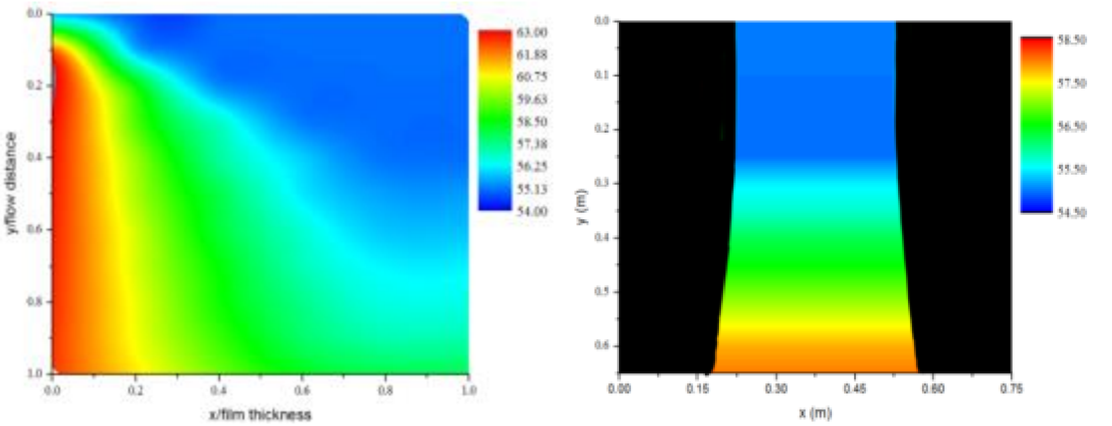

(a) (b)

Fig. 6. 14 Distribution of solution temperature during the internally heated regeneration process in (a) y-z cross section and (b) x-y plane

Furthermore, in Fig. 6.15 (a), unlike the temperature, in the thickness direction, only the concentration in the side near the air changed significantly due to the moisture transfer from solution to air, while that of the major part of film was almost unchanged. The main possible reasons are: a) the mass diffusion coefficient was relatively small compared to the thermal one (10^{-10} compared to 10^{-7}), so the mass transfer inside the solution film was slow; and b) the employment of Two-film theory in the development of the new model. It could be found that the solution concentration changed most dramatically in the right and bottom edge of Fig. 6.15 (a), because the hottest solution met the driest counter-flow air in this position. The similar phenomenon was seen in Fig. 6.15 (b). In this figure, with the exchange of moisture with the air, the solution concentration on the film surface increased gradually, and the peak occurred in the bottom of the channel.

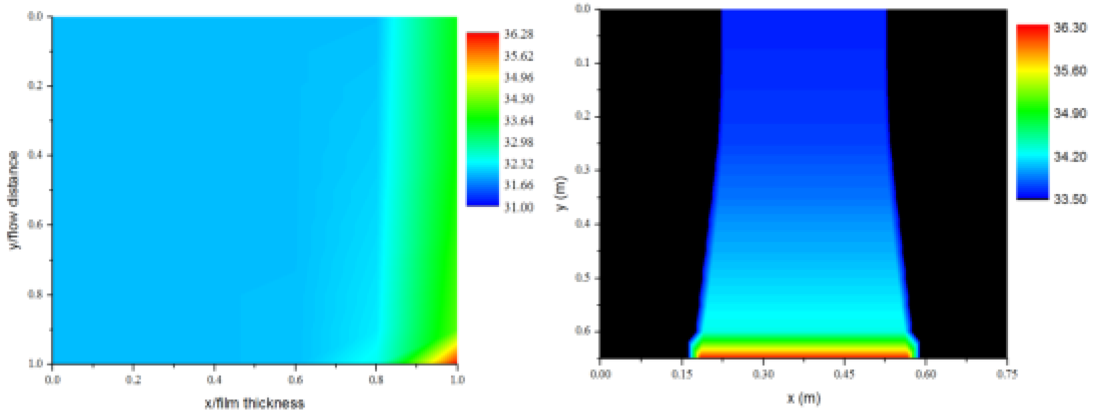

(a) (b)

Fig. 6. 15 Distribution of solution concentration during the internally heated regeneration process in (a) y-z cross section and (b) x-y plane

Then, by changing one parameter and keeping other parameters as constant, the impact of different factors on the moisture efficiency and moisture removal rate could be calculated. For each parameter, three conditions were simulated to make the analysis more accurate. The detailed operation parameters and changing range applied in the simulation were also listed in the figures.

As shown in Fig. 6.16, both the moisture removal rate and regeneration efficiency increased with the solution mass flow rate. When the solution mass flow rate was small, the wetted area increased significantly with the flow rate, which effectively enhanced the mass transfer between air and solution. However, when the wetted area was similar to the design area of the working surface, the increase of solution mass flow rate could only increase the thickness of solution film, and the growth rate of the moisture exchange became slower. That is why there existed a turning point in these curves. The position of the turning point was determined by the operation and design parameters of the internally heated regeneration. So, in our simulation, as the water temperature was higher in Condition 3 and the wetted area was larger accordingly, the turning point occurred in a relatively small solution mass flow rate compared with those in Condition 1 and 2.

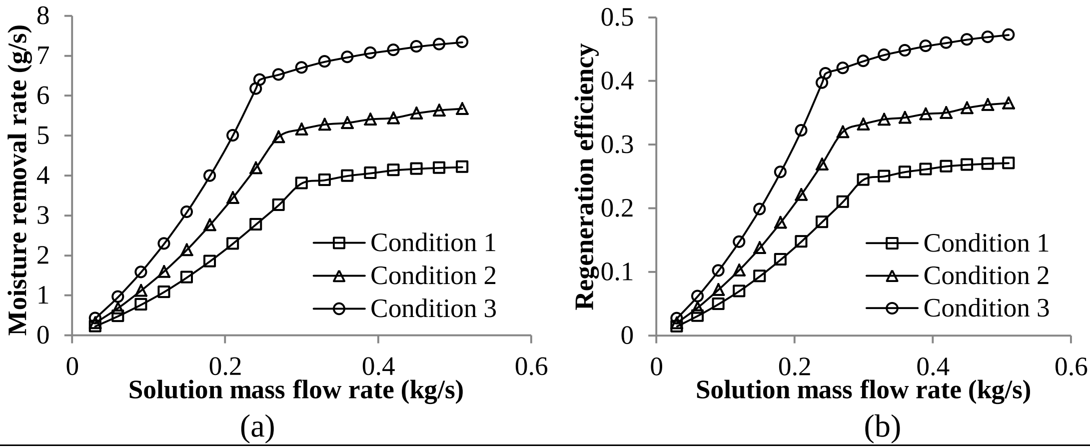

No.	m_s (kg/s)	$t_{s,in}$ (℃)	ζ_{in} (%)	$t_{w,in}$ (℃)	m_w (kg/s)	m_a (kg/s)	$t_{a,in}$ (℃)	$\omega_{a,in}$ (g/kg)
Condition 1	0.03-0.5	55	32.0	50	0.5	0.5	25	9.87
Condition 2	0.03-0.5	55	32.0	60	0.5	0.5	25	9.87
Condition 3	0.03-0.5	55	32.0	70	0.5	0.5	25	9.87

Fig. 6. 16 Influence of solution mass flow rate on (a) moisture removal rate and (b) regeneration efficiency

From Fig. 6.17, due to the increase of the equilibrium humidity on the liquid/air surface, the moisture removal rate was found to increase with the solution inlet temperature significantly. However, with the increase of solution temperature, the regeneration efficiency was firstly decreased dramatically, and then the decrease rate became slow gradually.

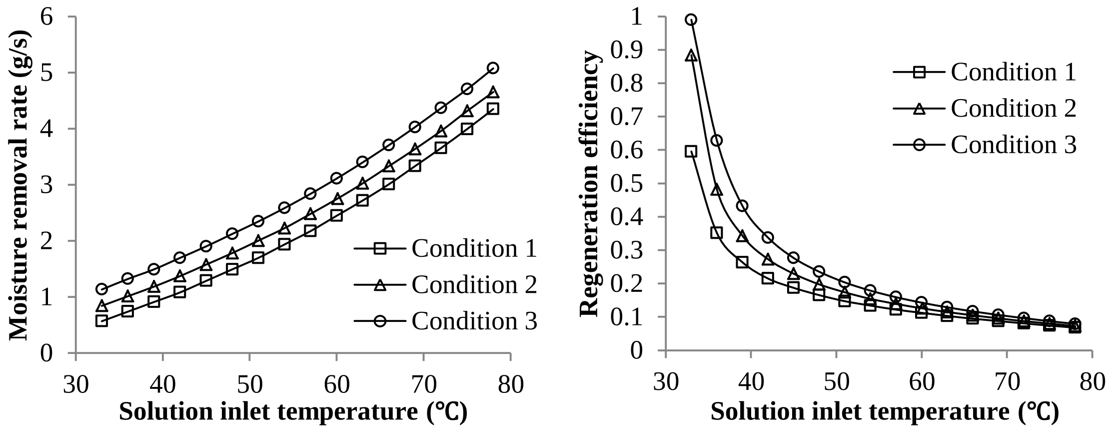

(a) (b)

No.	m_s (kg/s)	$t_{s,in}$ (℃)	ζ_{in} (%)	$t_{w,in}$ (℃)	m_w (kg/s)	m_a (kg/s)	$t_{a,in}$ (℃)	$\omega_{a,in}$ (g/kg)
Condition 1	0.1	33-78	32.0	50	0.5	0.5	25	9.87
Condition 2	0.1	33-78	32.0	60	0.5	0.5	25	9.87
Condition 3	0.1	33-78	32.0	70	0.5	0.5	25	9.87

Fig. 6. 17 Influence of solution inlet temperature on (a) moisture removal rate and (b) regeneration efficiency

As shown in Fig. 6.18, with the increase of solution inlet concentration, the mass transfer between air and solution decreased, while the moisture efficiency increased. However, the effect of solution concentration on the system performance was not as obvious as those of solution mass flow rate and temperature.

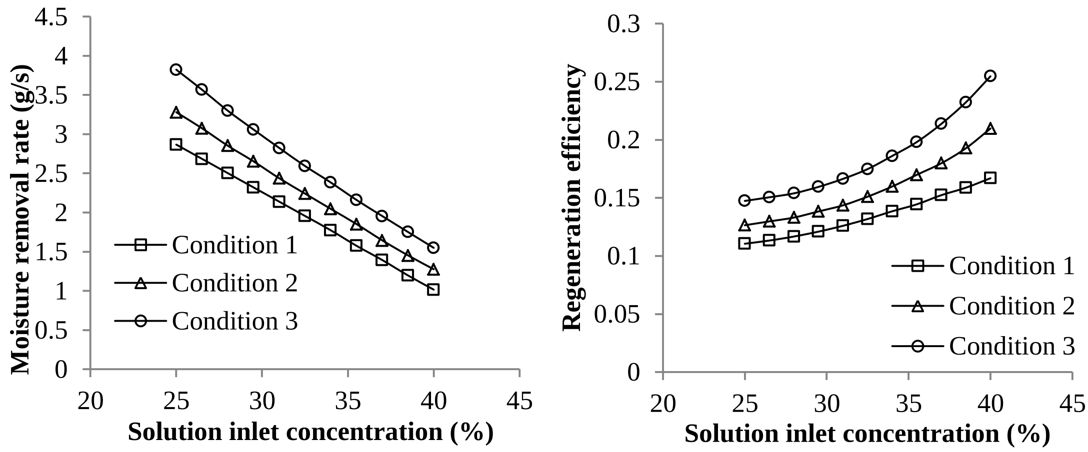

(a) (b)

No.	m_s	$t_{s,in}$	ζ_{in} (%)	$t_{w,in}$	m_w	m_a	$t_{a,in}$	$\omega_{a,in}$

	(kg/s)	(℃)		(℃)	(kg/s)	(kg/s)	(℃)	(g/kg)
Condition 1	0.1	55	25-40	50	0.5	0.5	25	9.87
Condition 2	0.1	55	25-40	60	0.5	0.5	25	9.87
Condition 3	0.1	55	25-40	70	0.5	0.5	25	9.87

Fig. 6. 18 Influence of solution inlet concentration on (a) moisture removal rate and (b) regeneration efficiency

The influences of parameters of extra hot water were shown in Fig. 6.19 and 20. With the increase of hot water temperature, based on our previous research, the solution temperature could be improved, and the plate surface temperature increased and the wetted area was enlarged accordingly. Therefore, as shown in Fig. 6.19, both the moisture removal rate and regeneration efficiency increased significantly with the water temperature. However, due to the small heat exchange efficiency between hot water and solution, the change of system mass performance with the hot water mass flow rate was slightly, and approached a steady state when the mass flow rate was high, as demonstrated in Fig. 6.20. So, in practical applications, the flow rate of hot water should be adjusted according to the simulation results, and the extravagant water mass flow rate would not benefit the system performance by increasing the pump energy use.

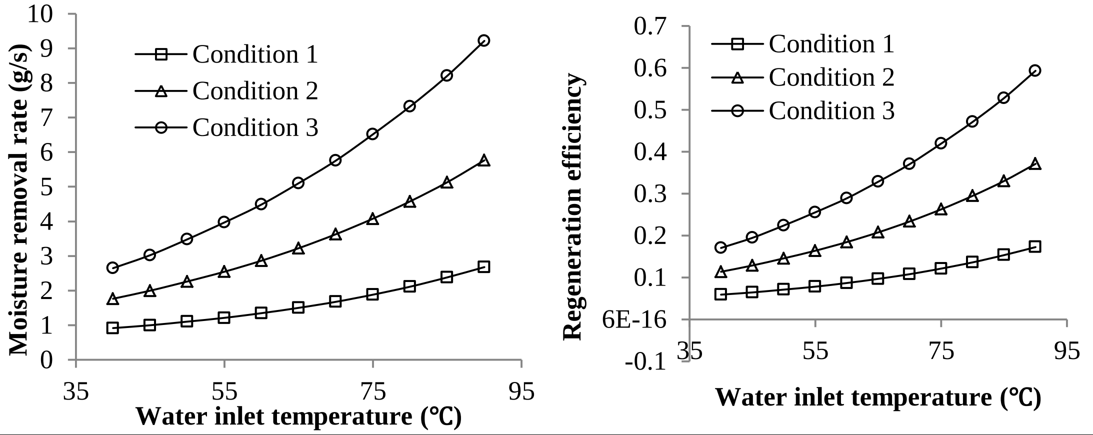

(a) (b)

No.	m_s (kg/s)	$t_{s,in}$ (°C)	ζ_{in} (%)	$t_{w,in}$ (°C)	m_w (kg/s)	m_a (kg/s)	$t_{a,in}$ (°C)	$\omega_{a,in}$ (g/kg)
Condition 1	0.1	55	32	40-90	0.5	0.5	25	9.87
Condition 2	0.1	55	32	40-90	0.5	0.5	25	9.87
Condition 3	0.1	55	32	40-90	0.5	0.5	25	9.87

Fig. 6. 19 Influence of hot water temperature on (a) moisture removal rate and (b) regeneration efficiency

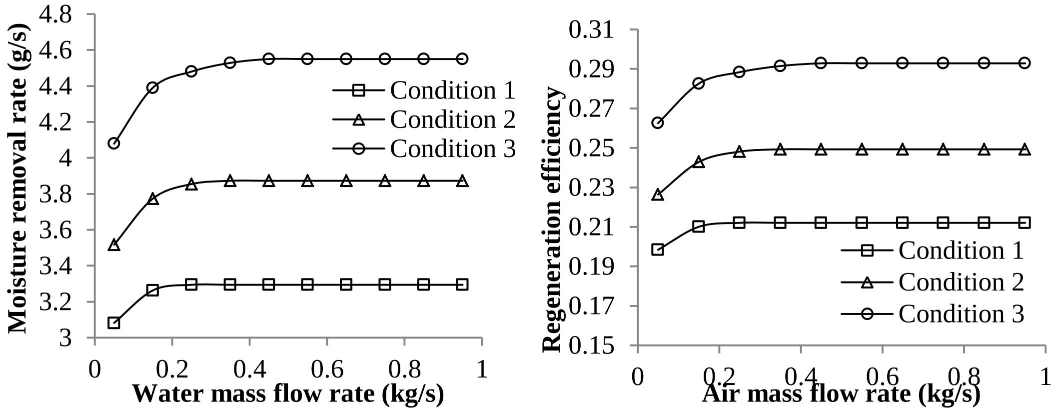

(a) (b)

No.	m_s (kg/s)	$t_{s,in}$ (°C)	ζ_{in} (%)	$t_{w,in}$ (°C)	m_w (kg/s)	m_a (kg/s)	$t_{a,in}$ (°C)	$\omega_{a,in}$ (g/kg)
Condition 1	0.1	55	32	50	0.05-0.95	0.5	25	9.87
Condition 2	0.1	55	32	60	0.05-0.95	0.5	25	9.87
Condition 3	0.1	55	32	70	0.05-0.95	0.5	25	9.87

Fig. 6. 20 Influence of hot water mass flow rate on (a) moisture removal rate and (b) regeneration efficiency

As shown in Fig. 6.21, the mass flow rate of air could benefit the mass transfer performance of regeneration significantly. But, when the flow rate was high, as the air could not exchange the heat and moisture with the solution sufficiently, the moisture removal rate increased slightly and the regeneration efficiency decreased seriously. Since higher air flow rate led to a higher energy consumption of fans in practical liquid desiccant systems, according to different operation conditions, there exists the maximum flow rate for air to avoid the energy waste.

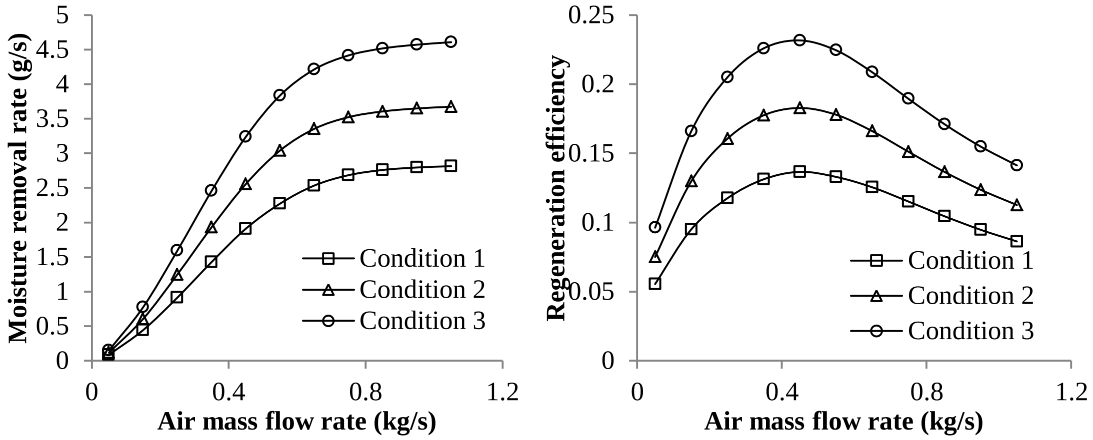

(a) (b)

No.	m_s (kg/s)	$t_{s,in}$ (°C)	ζ_{in} (%)	$t_{w,in}$ (°C)	m_w (kg/s)	m_a (kg/s)	$t_{a,in}$ (°C)	$\omega_{a,in}$ (g/kg)
Condition 1	0.1	55	32	50	0.5	0.05-1.05	25	9.87
Condition 2	0.1	55	32	60	0.5	0.05-1.05	25	9.87
Condition 3	0.1	55	32	70	0.5	0.05-1.05	25	9.87

Fig. 6. 21 Influence of air mass flow rate on (a) moisture removal rate and (b) regeneration efficiency

The influences of the air inlet temperature and moisture content on the system performance could be seen in Fig. 6.22 and 6.23. With the increase of the humidity inside the air, as shown in Fig. 6.23, the regeneration potential of the process air reduces seriously, and the moisture removal rate and efficiency decreased accordingly. When the air temperature was high, the mass performance of the regenerator increased, but the impact was not obvious as that of the air moisture content, as presented in Fig. 6.22.

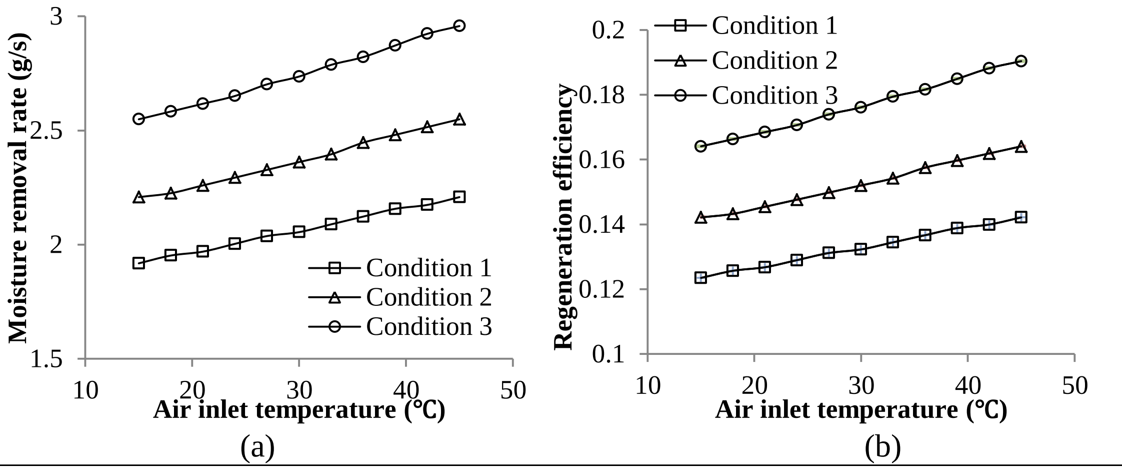

No.	m_s (kg/s)	$t_{s,in}$ (℃)	ζ_{in} (%)	$t_{w,in}$ (℃)	m_w (kg/s)	m_a (kg/s)	$t_{a,in}$ (℃)	$\omega_{a,in}$ (g/kg)
Condition 1	0.1	55	32	50	0.5	0.5	15-45	9.87
Condition 2	0.1	55	32	60	0.5	0.5	15-45	9.87
Condition 3	0.1	55	32	70	0.5	0.5	15-45	9.87

Fig. 6. 22 Influence of air inlet temperature on (a) moisture removal rate and (b) regeneration efficiency

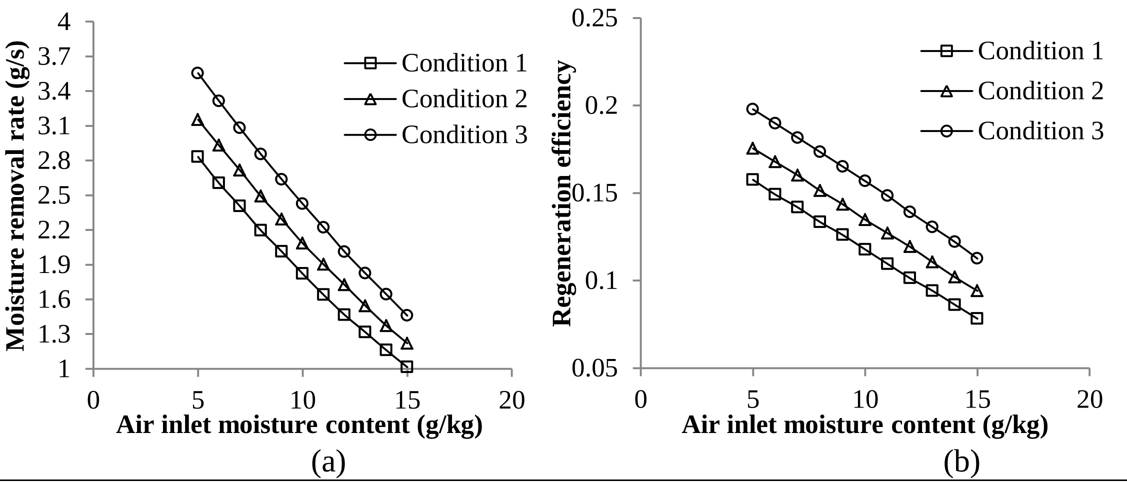

No.	m_s (kg/s)	$t_{s,in}$ (℃)	ζ_{in} (%)	$t_{w,in}$ (℃)	m_w (kg/s)	m_a (kg/s)	$t_{a,in}$ (℃)	$\omega_{a,in}$ (g/kg)
Condition 1	0.1	55	32	50	0.5	0.5	25	5-15
Condition 2	0.1	55	32	60	0.5	0.5	25	5-15
Condition 3	0.1	55	32	70	0.5	0.5	25	5-15

Fig. 6. 23 Influence of air inlet moisture content on (a) moisture removal rate and (b) regeneration efficiency

According to our previous research, as the thickness of solution distributor plays a significant role in the wetted area of falling film, it could also influence the mass transfer performance of the internally heated regeneration. As shown in Fig. 6.24, if the thickness of solution distributor is small enough, the falling film would cover the whole working plate, which may not occur in the practical systems as the solution may leak from the regenerator. With the increase of the solution distributor thickness, the wetted area decreased seriously, as well as the moisture removal rate and the regeneration efficiency. Furthermore, when the thickness was large, the form of falling desiccant would shrink from a film to a thick steam, and the heat and mass transfer between solution and air becomes poor.

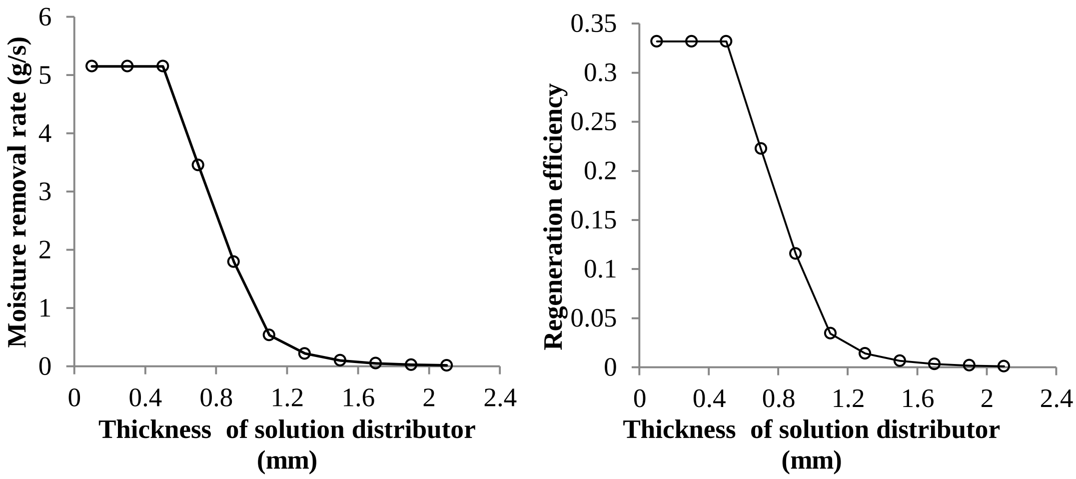

Fig. 6. 24 Influence of solution distributor thickness on (a) moisture removal rate and (b) regeneration efficiency

In the simulation of internally heated regenerator, the change trends of the moisture removal rate and regeneration efficiency with a particular variable are similar under different conditions, which means that the influence of one variable would not change even when other variables change. As variables have different influences on the mass transfer performance of regeneration, the values of maximum second derivative of different design and operation variables were developed, which revealed the maximum change rate of effectiveness with the change of a variable. As shown in Table 6.1, a larger value represents more significant influence while a smaller one means less impact. Furthermore, a positive value means that the effectiveness increased with the increase of the variable, while a negative one represents the opposite.

Table 6. 1 Values of maximum second derivative of variables

	$\dot{m}_{removal}$	ε_m
$t_{s,in}$	3.02	-6.78
$t_{a,in}$	0.24	0.24
$t_{f,in}$	2.05	2.05
$m_{s,in}$	1.46	1.46
$m_{a,in}$	1.38	-0.93
$m_{f,in}$	0.073	0.073
$\zeta_{s,in}$	-3.40	2.20
$\omega_{a,in}$	-1.72	-1.40
$\delta_{\max,i}$	-5.28	-5.28

From the table, the thickness of solution distributor is found to show the greatest impact on the moisture removal rate, and the change of inlet temperature of solution results in the most obvious change of regeneration efficiency. For the $\dot{m}_{removal}$, the changes of solution temperature and concentration also lead to significant change. As the increase of hot water temperature could improve the plate surface temperature and the wetted area effectively, it also has significant influence on the moisture removal rate. However, the effects of air temperature and hot water mass flow rate are much smaller. In terms of ε_m, besides the change of inlet temperature of solution, the solution distributor thickness has the second largest important influence. The concentration of solution shows significant influence on the regeneration efficiency, and the change of the hot water temperature, and the solution mass flow rate and the moisture content of air as well. Therefore, it provides a useful reference for researchers and engineers to improve or optimize the mass transfer performance of internally heated regeneration.

6.5 Summary

In this section, based on previous studies on the wetted area and mass transfer coefficient, a 3-D model of internally heated regenerator was developed for describing the heat and mass transfer among the air, solution and extra hot water. The insufficient wetting condition, the change of film thickness due to the mass transfer and film deformation and the effect of contact angle were taken into account. Using the finite-volume method, the numerical solution of the model and the simulation steps were provided.

To verify the model, the calculation results were compared with results by other existing theoretical models and our experimental results. With the consideration of the effect of wetted area and film thickness, compared to the experimental data, the newly developed model could accurately predict the influence of solution mass flow rate and extra hot water temperature, but the effects were found to be seriously underestimated in the traditional models. Furthermore, by taking the effect of contact angle of into account, the new model is proved to be suitable for predicting the regeneration performance with different working surfaces, while the contact angle was not included in the previous model. Additionally, the film thickness and the distribution of solution temperature on the film surface predicted by the 3-D model show a close trend to those recorded in our experiments of internally heated regeneration.

With the new model, a parameter study has been conducted numerically to show the effect of inlet parameters on the moisture removal rate and regeneration efficiency. As the film is very thin and the thermal diffusivity is relatively high, the heat transfer between the hot water and solution is effective to heat up the falling film. Meanwhile, with the low mass diffusivity, the change of solution concentration only occurs in the side close to air and the concentration of a large part of the falling film were almost unchanged. Furthermore, the thickness of solution distributor shows the greatest impact on the moisture removal rate, and the change of inlet temperature of solution results in the most obvious change of regeneration efficiency. The changes of solution concentration and hot water temperature also lead to significant changes on the system performance. Although the increase of the mass flow rates of solution, air and hot water benefit the mass transfer, the effect of the excessive mass flow rates are slight.

Therefore, it concludes that this new model is very useful for both researchers and engineers to predict the performance of internally heated regeneration accurately. The parameter study provides a useful reference to improve or optimize the practical regenerator applications. Although the model was developed based on the regeneration process, it could also be applied for the dehumidifier with the similar mechanism between dehumidification and regeneration.

CHAPTER 7

MODEL DEVELOPMENT FOR OPERATION PERFORMANCE OF INTERNALLY COOLED/HEATED SLDAC

7.1 Introduction

In previous chapters, the heat and mass transfer of internally cooled/heated dehumidifier/regenerator, which are the most critical components in LDAC system, were investigated experimentally, theoretically and numerically. Besides, the SLDAC has other components, such as the solar thermal system, heat recovery system, cooling system, energy storage system and auxiliary heating system. To evaluate the energy performance of the whole system, the operation performance and energy consumption should be simulated and compared with conventional systems.

The newly developed 3-D model is regarded as an accurate way to predict the system performance of dehumidifier/regenerator. However, due to a large number of variables involved, this method is complex and usually requires thousands of iterative calculations, which is inconvenient for researchers and engineers, especially for those investigating the dynamic operation performance of the system. In view of the previous approach, most studies investigated on the quick prediction model for the adiabatic liquid desiccant systems (Chung and Luo 1994, Abdul-Wahab et al. 2004, Gandhidasan 2004 and Gandhidasan 2005). Due to the complex configuration, research on internally cooled/heated systems is very limited (Yin et al. 2009, Gao et al. 2012). So it is necessary to find a quick and accurate way to calculate the outlet characteristics and the system performance, which the influences of all design variables and operation parameters should be considered.

Furthermore, referring to the review in Chapter 2, many previous research focused on the operation performance of packed-bed or solar collector/regenerator liquid desiccant systems (Khalid Ahmed et al. 1997, Rane et al. 2002, Chen et al. 2003, Liu et al. 2006). But the study on the solar-assisted internally cooled/heated system is limited due to its complexity. Therefore, an operation simulation model of the whole SLDAC system should be developed.

In this chapter, firstly, a new simplified numerical model for the internally cooled/heated dehumidifier/regenerator was developed, by defining three kinds of effectiveness. With this model, the system outlet parameters of all fluids (air, desiccant and heating/cooling fluid) under different design and operation conditions could be obtained accurately and directly without any iterative calculations, and the heat and mass transfer performance could also be assessed. To verify the model, the results by this prediction model were compared with the simulation results obtained by the theoretical model developed before.

Then, by linking the theoretical or numerical model of individual component with iteration loops, an operation simulation method of the SLDAC was developed. By assuming the initial parameters and solving the nested loops, the outlet parameters of all fluids and energy consumption under different operation conditions could be obtained. In this chapter, the heat and mass balance equations of different components, the initial parameters and the simulation procedures with the four iteration loops were described. The simulation results of the operation performance of SLDAC are shown in the next chapter.

7.2 Quick prediction model for internally cooled/heated LDAC

7.2.1 Simplified model development

To build the new quick prediction model for the internally cooled/heated dehumidifier/regenerator (ICHDR), three kinds of effectiveness are defined, as shown in Eq. (7.1), which are: ε_{ha}, enthalpy effectiveness, the ratio of the actual energy change of air to the maximum possible one; ε_{ma}, moisture effectiveness, the ratio of the actual mass change of air to the maximum possible one, which is also recognized as the mass transfer effectiveness; and ε_{tf}, temperature effectiveness, the ratio of the actual heat change of desiccant to the maximum possible one. These three kinds of effectiveness could represent the heat and mass transfer during the dehumidification and regeneration process.

$$\varepsilon_{ha} = \frac{h_{a,in} - h_{a,out}}{h_{a,in} - h_{I,in}}; \ \varepsilon_{ma} = \frac{\omega_{a,in} - \omega_{a,out}}{\omega_{a,in} - \omega_{I,in}}; \ \varepsilon_{tf} = \frac{t_{f,in} - t_{f,out}}{t_{f,in} - t_{s,in}} \tag{7. 1}$$

where h means the enthalpy, ω is the moisture content and t is the temperature. The subscripts a, s, f, I stand for the air, desiccant solution, cooling/heating fluid, and the interface between air and solution, respectively. The subscripts *in* and *out* mean the inlet and outlet characteristics.

Based on the energy and mass balances, a simplified model for ICHDR could be developed by applying these kinds of effectiveness, as demonstrated in Eq. (7.2).The following assumptions were made when building the model: a) the latent heat of vapourization were assumed as constants; b) air thermal and moisture diffusivity in the flow directions was assumed as zero; and c) no heat was transferred to the surroundings.

$$\begin{aligned}
h_{a,out} &= h_{a,in} - \varepsilon_{ha}(h_{a,in} - h_{I,in}) \\
\omega_{a,out} &= \omega_{a,in} - \varepsilon_{ma}(\omega_{a,in} - \omega_{I,in}) \\
t_{f,out} &= t_{f,in} - \varepsilon_{tf}(t_{f,in} - t_{s,in}) \\
\dot{m}_{s,out} &= \dot{m}_{s,in} + \dot{m}_a(\omega_{a,in} - \omega_{a,out}) \\
\zeta_{s,out} &= 1/((1/\zeta_{s,in})(1 + \varepsilon_{ma}\dot{m}_a(\omega_{a,in} - \omega_{I,in})/\dot{m}_{s,in})) \\
h_{s,out} &= \frac{\dot{m}_a(h_{a,in} - h_{a,out}) + \dot{m}_f c_{p,f}(t_{f,in} - t_{f,out})}{\dot{m}_{s,in}} + h_{s,in}
\end{aligned} \tag{7. 2}$$

where *m* stands for the mass flow rate and *t* means the temperature. ζ is the solution concentration.

With these equations, six outlet parameters of air, solution and heating/cooling fluid could be obtained directly. Other outlet characteristics, such as the outlet temperature of air and the outlet temperature of desiccant, could be also calculated by Eq. (7.3) and Eq. (7.4), respectively.

$$t_{a,out} = (h_{a,out} - r_{ab,I} \cdot \omega_{a,out})/(\mathrm{c}_{\mathrm{p,d}} + \mathrm{c}_{\mathrm{p,m}} \cdot \omega_{a,out}) \tag{7. 3}$$

$$A = -66.2324 + 1127.11\zeta_{s,out} - 7985.3\zeta_{s,out}{}^2 + 21534\zeta_{s,out}{}^3 - 16635.2\zeta_{s,out}{}^4$$
$$B = 4.5751 - 14.6924\zeta_{s,out} + 63.07226\zeta_{s,out}{}^2 - 138.054\zeta_{s,out}{}^3 + 106.69\zeta_{s,out}{}^4$$
$$C = -0.000809689 + 0.0218145\zeta_{s,out} - 0.136194\zeta_{s,out}{}^2 + 0.320998\zeta_{s,out}{}^3 - 0.264266\zeta_{s,out}{}^4$$
$$t_{s,out} = \frac{-B + \sqrt{B^2 - 4C(A - h_{s,out})}}{2C} \tag{7. 4}$$

where $r_{ab,I}$ is the latent heat of vapourization.

Furthermore, to reveal the heat and mass transfer performance of dehumidifiers and regenerators, two indicators, i.e. the moisture removal rate (the rate of moisture taken from the air in dehumidifiers or added to the air in regenerators) and heat exchange rate (the rate of energy obtain of the desiccant solution), are also significant in both theoretical studies and applications. They could be estimated by Eq. (7.5) and (7.6).

$$\dot{m}_{removal} = \dot{m}_a(\omega_{a,out} - \omega_{a,in}) = \varepsilon_{ma}\dot{m}_a(\omega_{I,in} - \omega_{a,in}) \tag{7. 5}$$

$$\dot{Q}_{energy} = \dot{m}_{s,out} h_{s,out} - \dot{m}_{s,in} h_{s,in} \tag{7. 6}$$

Therefore, without any iteration, the outlet parameters and performance indicators of ICHDR could be easily obtained with this simplified prediction model, when the three types of effectiveness could be calculated directly with the known design and operation variables.

7.2.2 Correlation development for three types of effectiveness

To obtain the correlations, the system performance under different design and operation variables were investigated numerically by employing the newly developed 3-D model. According to previous studies (Liu et al. 2009), the air and heating/cooling fluid flow patterns showed an insignificant effect on the system performance, so the common counter-flow pattern was adopted in this simulation. The widely used LiCl and water were chosen as the solution and cooling/heating fluid, respectively.

As listed in Table 7.1, the thirteen influencing variables could be divided into three groups; parameters of air, desiccant solution and cooling/heating fluid; heat and mass transfer property and configuration of dehumidifier/regenerator. According to the common working conditions of the ICHDR, the changing range of these parameters were chosen, which should be wider than the common ones. As extra heat is useful to improve the system performance during the regeneration process, the changing ranges of the inlet temperature of water, solution and process air for regenerators are higher compared to those for dehumidifiers. In addition, based on the previous studies (Kessling et al. 1995, Jain et al. 2000, Yin et al. 2008, Liu et al. 2009) and our experiments, the pre-set values for the numerical simulation are also listed. By keeping other parameters as constants with initial values and changing one parameter within the whole possible range, the effectiveness and system performance under different operation conditions could be calculated numerically.

Table 7. 1Summary of influencing parameters (including the changing ranges and initial values)

Type	Unit	Description	Range		Initial value	
			Dehumidifier	Regenerator	Dehumidifier	Regenerator
Parameters of Air	m_a(kg/s)	Mass flow rate of air across each channel	0.05-1.5	0.05-1.5	0.5	0.5
	$t_{a,in}$(°C)	Inlet temperature of air	15-45	25-90	33	25
	$\omega_{a,in}$	Inlet moisture content of air	5-25	5-25	20.7 (65%)	9.87 (50%)
Parameters of Solution	$m_{s,in}$(kg/s)	Inlet mass flow rate of solution	0.05-1.0	0.05-1.0	0.25	0.25
	$t_{s,in}$(°C)	Inlet temperature of solution	15-45	25-70	30	55
	$\zeta_{s,in}$(%)	Inlet concentration of solution	25-50	20-45	36	32
Parameters of Cooling/heating fluid	$m_{f,in}$(kg/s)	Inlet flow rate of cooling/heating fluid	0.05-1.50	0.05-1.50	0.5	0.5
	$t_{f,in}$(°C)	Inlet temperature of cooling/heating fluid	15-45	25-70	28	60
Heat and mass	a_w(kW/m^2•°C)	Heat transfer coefficient between desiccant and	0.1-2.5	0.1-2.5	0.17	0.17

transfer properties		cooling/heating fluid				
System design variables	H (m)	Height of dehumidifier/regenerator	0.1-1.5	0.1-1.5	0.5	0.5
	W_d (m)	Width of dehumidifier/regenerator	0.1-1.5	0.1-1.5	1.0	1.0
	δ_s (10^{-3} m)	Thickness of solution distributor	0.5-5.0	0.5-5.0	1.0	1.0
	δ_a (10^{-3} m)	Thickness of air channel	10-50	10-50	10.0	10.0

The three kinds of effectiveness, as the indicators of the mass and heat transfer performance, were found to be significantly influenced by the temperature, moisture and enthalpy gradients amongst the air, solution and cooling/heating fluid. The same conclusions were also previously drawn (Gandhidasan 2004, 2005). The temperature difference between the desiccant solution and cool/heating fluid induces the driving force of sensible heat transfer. The difference of moisture content between the air and air/desiccant interface makes the desiccant absorb the moisture or deliver it to the air. The enthalpy gradient results in the thermal energy exchange between the air and air/desiccant interface due to the heat and mass transfer. The enthalpy of air is the function of air temperature and moisture content, and the enthalpy of solution is decided by the solution temperature and concentration. In addition, the mass flow rate of fluids and system design parameters also affect the effectiveness.

Therefore, these kinds of effectiveness could be represented as the functions of mass and heat driving forces, mass flow rate of fluids, and system design parameters, as shown in Eq.(7.7).

$$\varepsilon = b_0 (h_{a,in} - h_{I,in})^{b_1} (\omega_{a,in} - \omega_{I,in})^{b_2} (t_{f,in} - t_{s,in})^{b_3} m_s^{b_4} m_a^{b_5} m_f^{b_6} a_w^{b_7} W_d^{b_8} H^{b_9} \delta_a^{b_{10}} \delta_s^{b_{11}} \tag{7. 7}$$

where b_0-b_{11} are constants which sate the degrees and directions of variables' influences.

The limits and signs of the effectiveness are defined by Eq. (7.8).

$$\begin{aligned} &0 \le \varepsilon_{ha} \le 1; \\ &0 \le \varepsilon_{ma} \le 1; \\ &\varepsilon_{tf} \begin{cases} \text{Dehumidifier} \begin{cases} \varepsilon_{tf} < 0 \text{ when } t_{s,in} < t_{f,in} \\ \varepsilon_{tf} \ge 0 \text{ when } t_{s,in} \ge t_{f,in} \end{cases} \\ \text{Regenerator} \begin{cases} \varepsilon_{tf} < 0 \text{ when } t_{s,in} > t_{f,in} \\ \varepsilon_{tf} \ge 0 \text{ when } t_{s,in} \ge t_{f,in} \end{cases} \end{cases} \end{aligned} \tag{7. 8}$$

With the statistical data of different dehumidification and regeneration conditions, the multiple linear regressions were employed to obtain the value of b_0-b_{11} for three kinds of effectiveness, with the steps described in the Section 5.2.2. To verify the coefficients obtained by linear regressions, an F test has to be conducted. As the accuracy of linear regressions would significantly increase with the quantity of independent statistical data, an adequate amount of data is necessary.

7.2.3 Correlations for ICHDR and Model verification

With the numerical simulation data, the correlations of the three kinds of effectiveness in dehumidifiers and regenerators could be developed by linear regressions, as shown in Eq. (7.9) - (7.12), respectively.

For $W_i \le W_d$

$$\varepsilon_{de,ha} = \frac{0.246 \cdot (|t_{f,in} - t_{s,in}|)^{0.027} (1000 \cdot (\omega_{a,in} - \omega_{I,in}))^{0.619} m_s^{0.865} a_w^{0.058} H^{0.399}}{(h_{a,in} - h_{I,in})^{0.658} \delta_a^{0.378} \delta_s^{0.309} m_a^{0.051} m_f^{0.016}}$$

$$\varepsilon_{de,ma} = \frac{0.109 \cdot (|h_{a,in} - h_{I,in}|)^{0.264} m_s^{0.878} a_w^{0.058} \mathrm{H}^{0.401} (|t_{f,in} - t_{s,in}|)^{0.029}}{(1000 \cdot (\omega_{a,in} - \omega_{I,in}))^{0.323} \delta_a^{0.375} \delta_s^{0.326} m_a^{0.054} m_f^{0.017}} \tag{7. 9}$$

$$\varepsilon_{de,tf} = \frac{0.0044 \cdot (1000 \cdot (\omega_{a,in} - \omega_{I,in}))^{0.576} a_w^{1.036} H^{1.225} m_s^{0.429} m_a^{0.557}}{(h_{a,in} - h_{I,in})^{0.324} m_f^{1.028} (|t_{f,in} - t_{s,in}|)^{0.744} \delta_a^{0.602} \delta_s^{0.850}} \cdot \frac{t_{f,in} - t_{s,in}}{|t_{f,in} - t_{s,in}|}$$

$$\varepsilon_{re,ha} = \frac{0.579 \cdot (1000 \cdot (\omega_{I,in} - \omega_{a,in}))^{1.156} m_s^{1.247} m_a^{0.231} a_w^{0.095} H^{0.145} (|t_{f,in} - t_{s,in}|)^{0.1367}}{\delta_s^{0.947} (|h_{a,in} - h_{I,in}|)^{1.915} m_f^{0.0231} \delta_a^{0.368}}$$

$$\varepsilon_{re,ma} = \frac{0.195 \cdot (1000 \cdot (\omega_{I,in} - \omega_{a,in}))^{0.554} m_s^{1.0392} m_a^{0.150} (|t_{f,in} - t_{s,in}|)^{0.1036} a_w^{0.0785} \delta_a^{0.0324} H^{0.0202}}{\delta_s^{0.858} (|h_{a,in} - h_{I,in}|)^{1.291} m_f^{0.011}}$$

$$\varepsilon_{re,tf} = \frac{1.232 \cdot (|h_{a,in} - h_{I,in}|)^{0.232} a_w^{0.758} \mathrm{H}^{0.932} m_a^{0.671} \delta_s^{0.046}}{(1000 \cdot (\omega_{I,in} - \omega_{a,in}))^{0.504} m_f^{1.028} (|t_{f,in} - t_{s,in}|)^{1.04} \delta_a^{0.480} m_s^{0.443}} \cdot \frac{t_{f,in} - t_{s,in}}{|t_{f,in} - t_{s,in}|} \tag{7. 10}$$

For $W_i > W_d$

$$\varepsilon_{de,ha} = \frac{10 \cdot (|t_{f,in} - t_{s,in}|)^{0.0486} (\omega_{a,in} - \omega_{I,in})^{0.525} (m_s / m_a)^{0.349} m_f^{0.0773} a_w^{0.0764} (-0.0022 \cdot W_d + 0.0102 \cdot H)^{0.0407}}{(h_{a,in} - h_{I,in})^{0.547} \delta_a^{0.378}}$$

$$\varepsilon_{de,ma} = \frac{0.0829 \cdot (|h_{a,in} - h_{I,in}|)^{0.195} (m_s / m_a)^{0.350} m_f^{0.0619} a_w^{0.07} (-0.0032 \cdot W_d + 0.0248 \cdot \mathrm{H})^{0.0854}}{(|t_{f,in} - t_{s,in}|)^{0.009} (\omega_{a,in} - \omega_{I,in})^{0.0441} \delta_a^{0.375}}$$

$$\varepsilon_{de,tf} = \frac{0.115 \cdot (h_{a,in} - h_{I,in})^{0.304} (\omega_{a,in} - \omega_{I,in})^{0.394} a_w^{0.757} (W_d \cdot H)^{0.754}}{m_f^{0.857} (m_s / m_a)^{0.261} (|t_{f,in} - t_{s,in}|)^{0.759} \delta_a^{0.602}} \cdot \frac{t_{f,in} - t_{s,in}}{|t_{f,in} - t_{s,in}|} \tag{7. 11}$$

$$\varepsilon_{re,ha}=\frac{27.061\cdot(1000\cdot(\omega_{I,in}-\omega_{a,in}))^{0.987}(m_s/m_a)^{0.770}a_w{}^{0.0838}(0.196\cdot W_d+0.287\cdot H)^{0.125}}{(\left|h_{a,in}-h_{I,in}\right|)^{1.532}(\left|t_{f,in}-t_{s,in}\right|)^{0.0038}m_f{}^{-0.012}\delta_a{}^{0.368}}$$

$$\varepsilon_{re,ma}=\frac{46.219\cdot(1000\cdot(\omega_{I,in}-\omega_{a,in}))^{0.728}(m_s/m_a)^{0.844}m_f{}^{0.001}a_w{}^{0.0691}\delta_a{}^{0.0324}(W_d\cdot H)^{0.0242}}{(\left|h_{a,in}-h_{I,in}\right|)^{1.332}(\left|t_{f,in}-t_{s,in}\right|)^{0.0168}}$$

$$\varepsilon_{re,tf}=\frac{0.0554\cdot(\left|h_{a,in}-h_{I,in}\right|)^{0.794}a_w{}^{0.622}((1.552\cdot W_d+0.118\cdot \mathrm{H}))^{0.896}(m_s/m_a)^{0.0032}}{(1000\cdot(\omega_{I,in}-\omega_{a,in}))^{0.636}m_f{}^{0.908}(\left|t_{f,in}-t_{s,in}\right|)^{1.07}\delta_a{}^{0.480}}\cdot\frac{t_{f,in}-t_{s,in}}{\left|t_{f,in}-t_{s,in}\right|} \tag{7. 12}$$

where subscripts *de* and *re* stand for the dehumidifiers and regenerators, respectively.

An F-test was required to check the significance of regression correlations, with the data set faithful at 0.01, 0.05 and 0.1 significance levels, respectively. The related Fa could be found in the F Distribution Tables. As shown in Table 7.2, the F-ratios are significantly larger than the Fa at all three levels, and the linear regressions are reliable.

Table 7. 2 Significance Test for Linear Regression

ε	n	F-ratio	Significance $F_a(m,n-m-2)$		
			0.1	0.05	0.01
$\varepsilon_{de,ha}$	271	41.6	1.70	1.976	2.59
$\varepsilon_{de,ma}$	271	30.4			
$\varepsilon_{de,tf}$	271	136.3			
$\varepsilon_{re,ha}$	257	178.6	1.72	1.98	2.6
$\varepsilon_{re,ma}$	257	184.7			
$\varepsilon_{re,tf}$	257	429.6			

Therefore, with the statistic correlations of three kinds of effectiveness, the simplified prediction model for internally cooled dehumidifiers and internally heated regenerators could be developed, by inserting Eq. (7.9) - (7.12) to Eq. (7.2).

To verify the newly developed simplified model, firstly, the outlet parameters of ICHDR by the quick prediction model with Eq. (7.2) and by the 3-D theoretical model under more than 250 different conditions were compared, as shown in Fig. 7.1. The detailed inlet parameters and design variables were also presented. The Average Relative Deviation (ARD) and Average Composite Deviation (ACD) between our prediction results and simulation results could be calculated by the following equations.

$$ARD = \frac{1}{n}\sum_{i=1}^{n}\left|\frac{P_{simulation,i} - P_{prediction,i}}{P_{simulation,i}}\right| \times 100\% \tag{7. 13}$$

$$ACD = \frac{1}{n}\sum_{i=1}^{n}\sqrt{\sum_{j=1}^{m}\left(\frac{P_{simulation,i,j} - P_{prediction,i,j}}{P_{simulation,i,j}} \times 100\%\right)^2} \tag{7. 14}$$

where n is the number of data. m is the number of outlet parameters, which is six in our simplified model. P stands for an individual outlet parameter, such as the outlet solution enthalpy and air moisture content.

As shown in Fig. 7.1(a), for dehumidifiers, the outlet parameters obtained by our quick prediction model are similar to the results obtained by the theoretical model. The greatest difference occurred in the outlet moisture content of air, which may be attributed to its relatively low level (10^{-3}) compared to the other parameters (enthalpy 10^{1}-10^{2}; mass flow rate 10^{-1}-10^{1}; and so on). But, the majority of the results of moisture content still showed an acceptable difference of less than ±20%, with an ARD of 11%. The errors for solution and air enthalpy are smaller, with an ARD of about 5%. The results of cooling water temperature, solution mass flow rate and concentration were found to be consistent with the simulation ones, with the ARDs about or even less than 1%. In terms of regenerators in Fig. 7.1(b), the distribution of deviations is similar to those of dehumidifiers. It should be noticed that the errors of the simplified model for regenerators are much smaller than for those of dehumidifiers. This may be caused by the temperature difference. In regenerators, the temperature of liquid (about 50 to 80°C) is much higher than that of the air (about 20 to 40°C), as well as their enthalpies. However, the temperatures and enthalpies of the three fluids are close to each other in the dehumidification process, which would reduce the accuracy of linear regressions and increase the errors of statistical correlations.

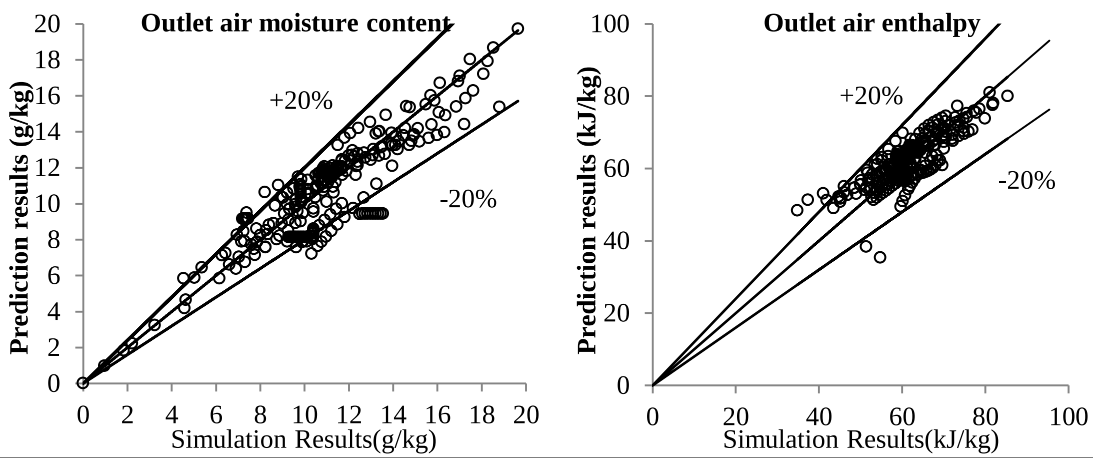

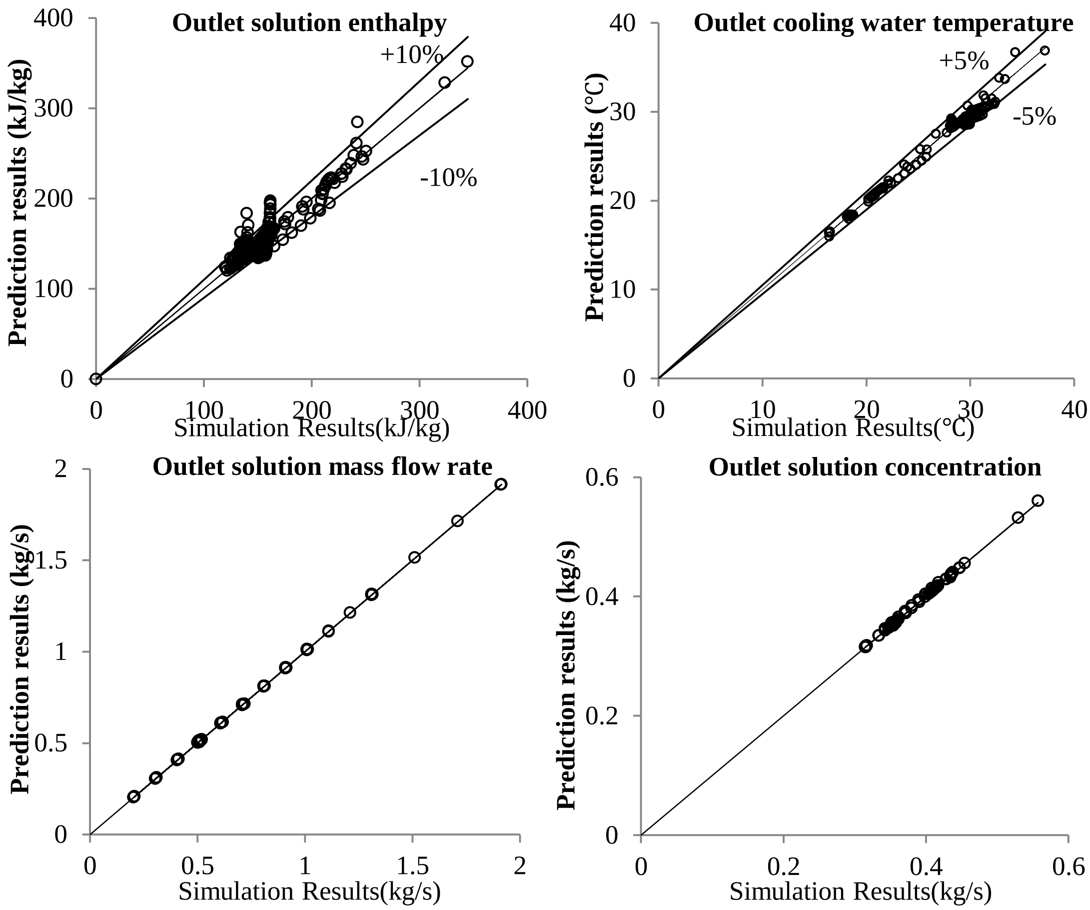

Condition amount 271	ARD (%)	Air moisture content	11.0%	Air enthalpy	5.90%	Solution enthalpy	4.58%
		Cooling water temperature	1.10%	Solution mass flow rate	0.27%	Solution concentration	0.30%

(a) Dehumidifier

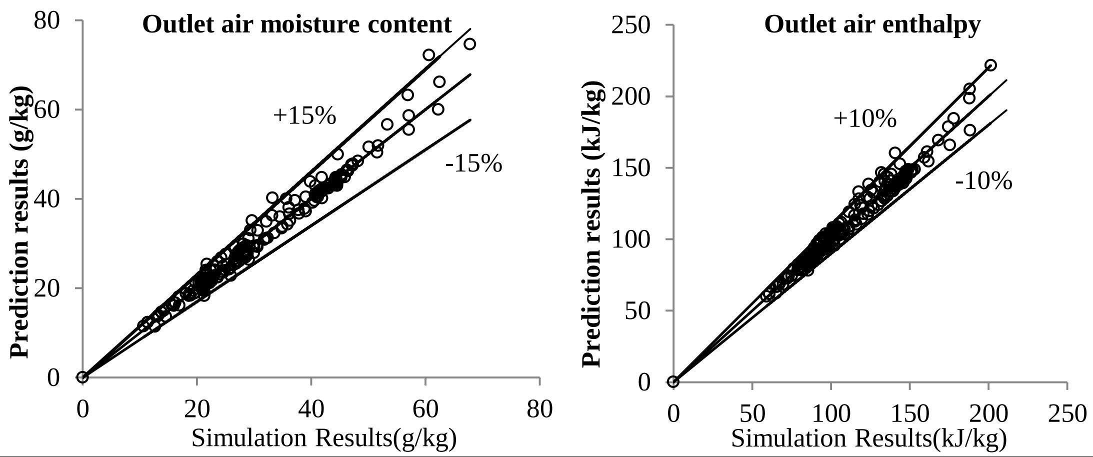

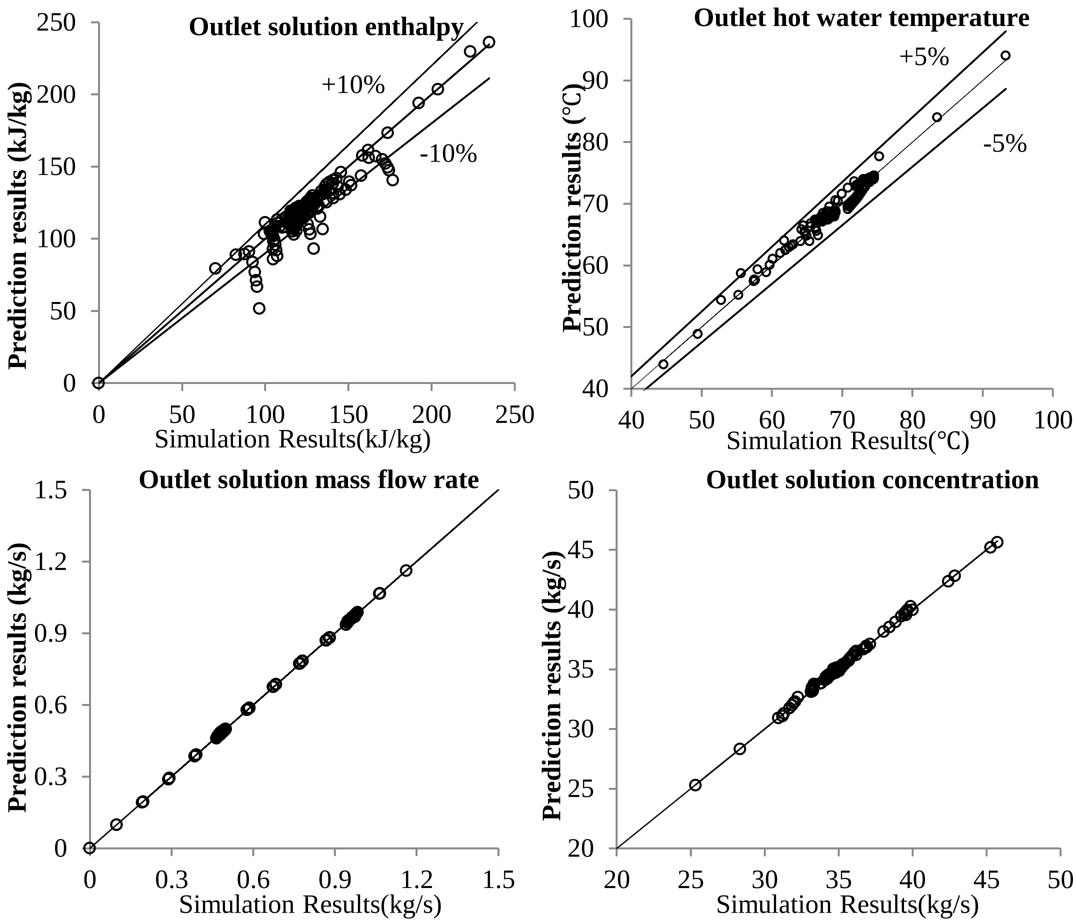

<table>
<tr><td rowspan="2">Condition amount 257</td><td rowspan="2">ARD (%)</td><td>Air moisture content</td><td>3.38%</td><td>Air enthalpy</td><td>2.85%</td><td>Solution enthalpy</td><td>4.11%</td></tr>
<tr><td>Cooling water temperature</td><td>0.66%</td><td>Solution mass flow rate</td><td>0.19%</td><td>Solution concentration</td><td>0.18%</td></tr>
</table>

(b) Regenerator

Fig. 7. 1 Comparison of six outlet parameters between prediction and simulation results

The composite errors of the six outlet parameters are compared, as shown in Fig. 7.2. Most differences are found within 20% for dehumidifiers and 15% for regenerators, with an acceptable ACD of 14.7% and 7.1%, respectively.

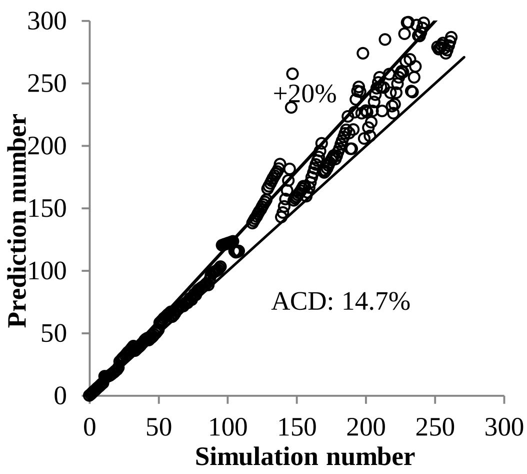

(a) Dehumidifier

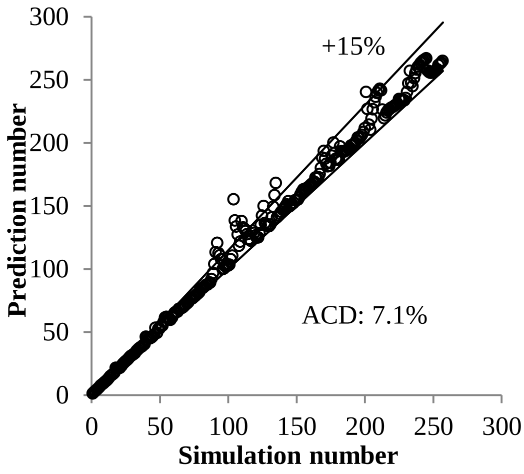

(b) Regenerator

Fig. 7. 2 Comparison of composite errors between prediction and simulation results

Therefore, this new simplified prediction model is suitable for evaluating the outlet parameters and system performance of ICHDR directly, especially for the dynamic operation performance of internally cooled/heated LDAC systems.

7.3 System modelling of internally cooled/heated SLDAC

7.3.1 Description of internally cooled/heated SLDAC

The proposed SLDAC system mainly consists of an internally cooled/heated liquid desiccant ventilation system and an all-air cooling system, for handling the latent and sensible air-conditioning (AC) load of buildings separately. The system includes a liquid desiccant loop (pink line), two water loops (blue line) and two air loops (green line), as shown in Fig. 7.3.

As shown in Fig. 7.3, after entering the ventilation system, the fresh air was first dehumidified by the dehumidifier and then pre-cooled by a heat exchanger which was connected to the cooling tower. Then, by mixing with the return air, the supply air was cooled to the indoor set point with the cooling coil driven by the vapour compressor. Therefore, under cooling conditions, most latent load and part sensible load were handled within the liquid desiccant ventilation system, while the rest of load was handled by the cooling coil.

For the better performance of dehumidification, the cool water from the cooling tower was introduced into the internally cooled dehumidifier. In order to utilize the desiccant repeatedly, the weak desiccant solution requires concentration in the regenerator with heat supply. For the energy saving and environment friendly purposes, solar energy is considered as a promising heating source. Therefore, in our system, the hot water required in the internally heated regenerator was mainly supplied by solar thermal collectors, and an electric heater was installed as a back up when the solar radiation is insufficient in cloudy or rainy days.

To improve the efficiency of liquid desiccant system, several heat exchangers were applied for pre-cooling or pre-heating the solution. With the heat exchanger #1, the concentrated solution was pre-cooled by exchanging heat with the cool water from the cooling tower. Then, after the dehumidification process, the solution was preheated by a solution-to-solution heat exchanger #2, as the diluted solution needs to be heated up before the regeneration process while the concentrated solution needs to be cooled down before the dehumidification. The temperature of diluted solution was further increased by heating with the hot water from solar collectors, with the heat exchanger #3.

Due to the lower thermal loss and higher efficiency, the evacuated-tube solar collector was employed in the SLDAC system. Additionally, the power consumptions of pumps and fans should also be considered.

7.3.2 Simulation Models of System Components

To simulate the energy consumption of SLDAC, the mass and energy balances of each component should be built. In this section, the mathematical models of different components, including the internally cooled/heated dehumidifier/ regenerator, the heat exchanger, the solar collector, the cooling tower, the vapour compression system and the pump, are discussed

1) Internally cooled/heated dehumidifier/ regenerator

For the ICHDR, the heat and mass transfer happens amongst the air, desiccant solution and cooling/heating fluid. The common counter-flow pattern was adopted, and the widely used LiCl and water were chosen as the solution and cooling/heating fluid, respectively.

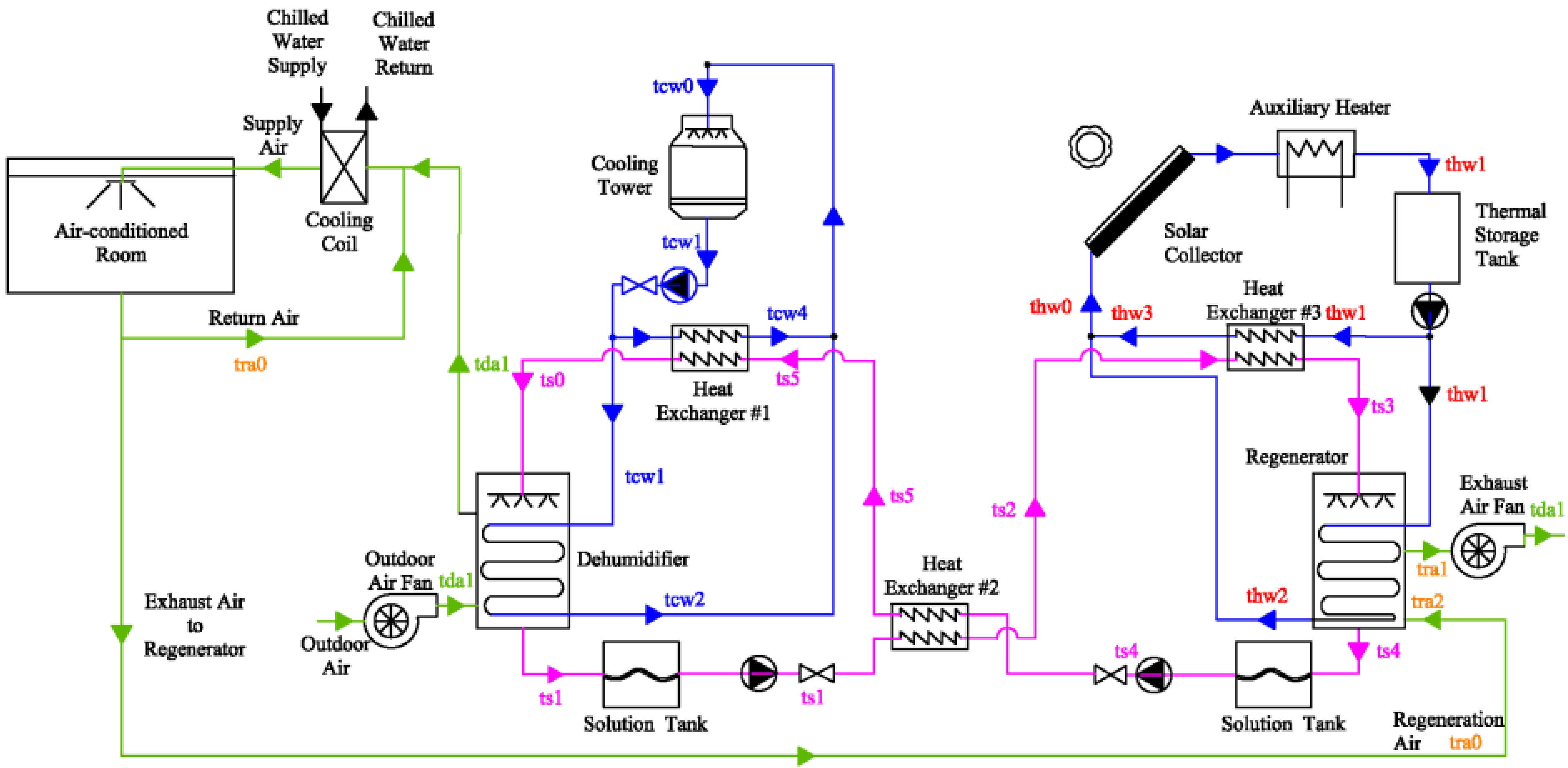

Fig. 7. 3 Schematic diagram of system components of SLDAC

With the quick prediction model developed in Section 7.2, the outlet parameters of air, solution and heating/cooling fluid could be obtained directly with the given inlet parameters, including the outlet temperature of air, cooling/heating water and desiccant solution, the outlet moisture content of air and the outlet concentration and mass flow rate of solution. For defining the amount of vapour removed from the fresh air to the desiccant solution, the moisture removal rate of dehumidification ($\dot{m}_{removal,de}$) could be calculated as follows:

$$\dot{m}_{removal,de} = m_{da}(\omega_{da,in} - \omega_{da,out}) \qquad (7.\ 15)$$

where m refers to the mass flow rate, and ω is the moisture content. The subscript *da* stands for the outdoor fresh air, and *in* and *out* mean the inlet and outlet characteristics.

Similarly, the regeneration rate ($\dot{m}_{removal,re}$), which is used to describe the amount of water evapourating from the solution to the air, could be expressed as:

$$\dot{m}_{removal,re} = m_{ra}(\omega_{ra,in} - \omega_{ra,out}) \qquad (7.\ 16)$$

where the subscript *ra* stands for the exhaust air from the air-conditioned rooms.

2) Solar Collector

The solar energy collected by the collector is mainly determined by the temperature of inlet water and ambient air, and the area and efficiency of the collector, which could be calculated by:

$$Q_{solar} = IA_c\eta_{solar} = \tau IA_c - U_cA_c(t_{in} - t_{amb}) \qquad (7.\ 17)$$

where τ is the transmissivity of the cover glass upon the solar collector. t_{in} refers to the inlet water temperature, and t_{amb} is the outdoor air temperature. I is the incident solar radiation on the plate surface, and A_c means the area of the collector. U_c is the overall thermal loss coefficient of the collector.

The efficiency of the solar collectors could be expressed as a quadratic efficiency curve:

$$\eta_{solar} = a_0 - a_1(T_{in} - T_{amb}) / I + a_2I[(T_{in} - T_{amb}) / I]^2 \qquad (7.\ 18)$$

For the evacuated-tube solar collector employed in this simulation, these coefficients are set to be 0.84, 2.02 and 0.0046, respectively (Walker et al. 2004).

3) Vapour compressor system

The cooling load handled with the cooling coil of SLDAC could be calculated as:

$$Q_{cc} = Q_c - m_{da}(h_{da} - h_{da,dc}) \tag{7. 19}$$

where Q_c is the total cooling load of the building, and m_{da} means the minimum outdoor airflow rate required in the building. h_{da} refers to the enthalpy of ambient air and $h_{da,dc}$ is the enthalpy of the process air entering the cooling coil.

When the cooling coil driven by the vapour compressor system is operated with the liquid desiccant system, the COP will increase. Based on previous research, the average COP of the vapour compressor system of buildings was found to be about 3.3, while it was estimated to be about 4.62 for the totally dry cooling coil condition (Li et al. 2010). Therefore, the energy consumption of the vapour compressor system in the proposed SLDAC and conventional system could be obtained.

4) Cooling tower

The efficiency of cooling tower can be defined as follows:

$$\eta_{ct} = \frac{T_{w,in} - T_{w,out}}{T_{w,in} - T_{a,wb}} \tag{7. 20}$$

where T_w and $T_{a,wb}$ represent the water temperature in the cooling tower and the wet-bulb temperature of ambient air, respectively. The subscripts *in* and *out* mean the inlet and outlet characteristics. From this equation, it reveals that the outlet temperature of the water leaving the cooling tower is limited by the wet-bulb temperature of the surrounding air.

5) Heat exchanger

In our proposed SLDAC system, there are different types of heat exchangers employed, including a solution-to-solution heat exchanger, a water-to-solution heat exchanger and an air-to-water heat exchanger. The general formula for calculating the efficiency for the counter-flow heat exchanger is expressed as:

$$\begin{aligned}\eta_{ex} &= \frac{m_{hot} c_{p,hot} (T_{hot,in} - T_{hot,out})}{\min(m_{hot} c_{p,hot}, m_{cold} c_{p,cold})(T_{hot,in} - T_{cold,in})} \\ &= \frac{m_{cold} c_{p,cold} (T_{cold,in} - T_{cold,out})}{\min(m_{hot} c_{p,hot}, m_{cold} c_{p,cold})(T_{hot,in} - T_{cold,in})}\end{aligned} \tag{7. 21}$$

where m and c_p refer to the mass flow rate and the specific heat, respectively. The subscripts *hot* and *cold* stand for the hot and cold fluid through the exchanger, and *in* and *out* mean the inlet and outlet characteristics.

6) Pump

The performance of pump is determined by its volumetric flow rate, pressure rise and efficiency, as shown in Eq. (7.22):

$$W_p = \frac{\rho_{water} gHQ}{\eta_p} \tag{7. 22}$$

where W_p is the total pump power. H stands for the pump head (m), and Q is the volume of fluid delivered by the pump per unit time. η_p refers to the efficiency of individual pump.

7.3.3 Input and output parameters

To simulate the operation performance of SLDAC, design and performance variables of the system and the simulated building were required. The input variables could be mainly divided into three categories: the initial assumed parameters of the system, the climatic data and the load profile of the building. The last two categories are related to the selected case for the simulation, which are described in the next chapter.

The initial assumed parameters mainly included: the assumed parameters of individual components, which were constant throughout the simulation; and the initial parameters of working fluids, which referred to the initial value of operation conditions and may change with the simulation steps. The settings of the assumed parameters of different components were based on the previous research, as summarized in Table 7.3.

Table 7. 3 Assumptions of individual component

Heat exchanger	Efficiency	1#: 0.93
		2#: 0.54

		3#: 0.93
Cooling tower	Efficiency	0.45
Solar collector	Thermal Efficiency	0.82
	Titled angle	22.5 ℃(facing south)
Electrical heater	Efficiency	0.9
Chiller	COP	3.3 (conventional AC system)
		4.62 (totally dry cooling coil)
Dehumidifier/Regenerator	Height × Weight	0.55 m × 0.5 m
	Air channel thickness	0.02 m

According to the common operation conditions of the solar-assisted system and liquid desiccant system, the initial parameters of working fluids were assumed, as listed in the Table 7.4. During the simulation, the initial parameters may change due to the iteration loop of thermal and mass energy transfer.

Table 7. 4 Assumptions of initial parameters of working fluids

Initial parameter	Working fluid	Component	Value
Mass flow rate (kg/s)	Desiccant	Dehumidifier/Regenerator	0.5
	Cooling water	Heat exchanger 1#	0.5
		Dehumidifier	0.5
	Heating water	Heat exchanger 3#	0.5
		Regenerator	0.5
	Air	Dehumidifier	Ventilation rate of the building
		Regenerator	Exhaust rate of the building
Temperature (℃)	Desiccant	Dehumidifier	25

	Cooling water	Cooling tower	30
	Heating water	Solar collector	60
Concentration (%)	Desiccant	Dehumidifier	34.5

The input and output variables for every component in the proposed SLDAC were summarized in Table 7.5. The variables of the working fluids (i.e. water, air and desiccant solution) were indicated in Fig. 7.4.

Table 7. 5 Summary of input and output variables of each component

Component	Parameter	Input variable	Output variable
Dehumidifier	Process air	$t_{da,0}, \omega_{da,0}, h_{da,0}$	$t_{da,1}, \omega_{da,1}, h_{da,1}$
	Desiccant solution	$t_{s,0}$, $\zeta_{s,0}$	$t_{s,1}$, $\zeta_{s,1}$
	Cooling water	$t_{cw,1}$	$t_{cw,2}$
	Moisture removal rate		$\dot{m}_{removal,de}$
Regenerator	Process air	$t_{ra,2}, \omega_{ra,2}, h_{ra,2}$	$t_{ra,4}, \omega_{ra,4}, h_{ra,4}$
	Desiccant solution	$t_{s,3}$, $\zeta_{s,3}$	$t_{s,4}$, $\zeta_{s,4}$
	Heating water	$t_{hw,1}$	$t_{hw,2}$
	Moisture removal rate		$\dot{m}_{removal,re}$
Solar Collector	Water	$t_{hw,0}$	$t_{hw,4}$
Cooling Tower	Water	$t_{cw,0}$	$t_{cw,1}$
	Ambient air	$t_{a,wb}$	
Cooling Coil	Chilled water	$t_{cdw,i}$	$t_{cdw,o}$

Heat Exchanger #1	Desiccant solution	$t_{s,5}$, $\zeta_{s,5}$	$t_{s,8}$, $\zeta_{s,8}$
	Water	$t_{cw,1}$	$t_{cw,4}$
Heat Exchanger #2	Desiccant solution	$t_{s,1}$, $\zeta_{s,1}$	$t_{s,2}$, $\zeta_{s,2}$
	Desiccant solution	$t_{s,4}$, $\zeta_{s,4}$	$t_{s,5}$, $\zeta_{s,5}$
Heat Exchanger #3	Desiccant solution	$t_{s,6}$, $\zeta_{s,6}$	$t_{s,7}$, $\zeta_{s,7}$
	Water	$t_{hw,1}$	$t_{hw,3}$
Auxiliary Heater	Water	$t_{s,7}$, $\zeta_{s,7}$	$t_{s,3}$, $\zeta_{s,3}$

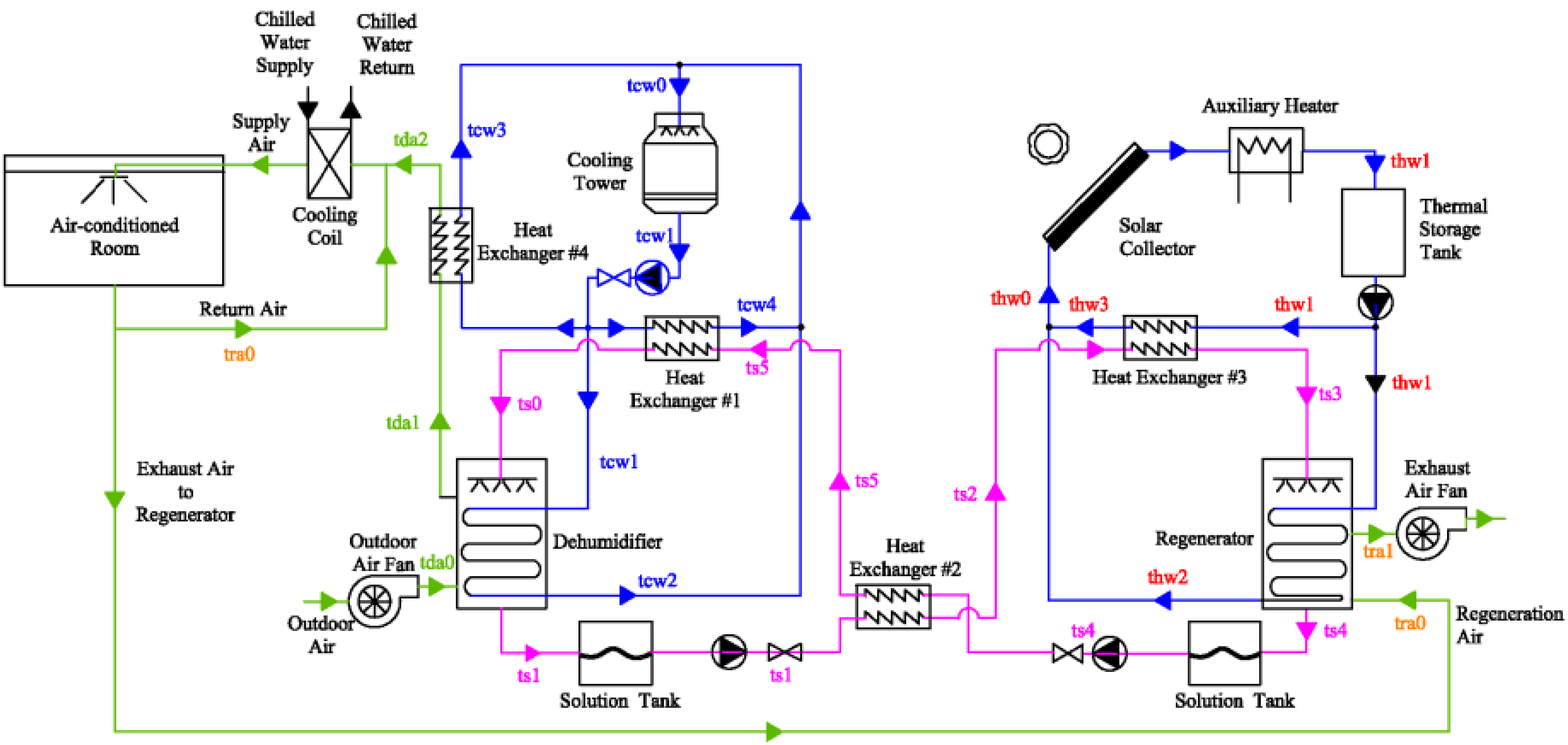

Fig. 7. 4 Schematic diagram of the links of the fluid temperatures

7.3.4 Iteration Loops

As mentioned earlier, the inlet parameters, such as the inlet temperature of solution and water, were valued by assumption. However, under the given operation conditions, the actual inlet parameters may differ from the assumed ones. Therefore, the iteration loop was required, and the calculation process was repeated until the small error between the current and previous result was approached. To build the dynamic operation model of SLDAC, four main iteration loops were employed, including the loop for the desiccant inlet temperature of regenerator, the hot water temperature, the cooling water temperature and the desiccant inlet temperature of dehumidifier. The four loops were introduced in details as below:

1) Loop for the solution inlet temperature of regenerator

This loop was to find out the required solution temperature at the inlet of the regenerator, and ensure the regeneration capacity matching the dehumidification requirement of the case building. For maintaining the solution concentration and applying the desiccant repeatedly, the moisture absorbed by the strong solution in the dehumidifier should be totally desorbed in the regenerator. Therefore, the iteration loop was set to stop until the regeneration capacity was just slightly larger than the dehumidification requirement (The safety factor for the regeneration capacity is 1.1.).

2) Loop for the heating water temperature

To maintain the system performance of the internally heated regenerator, the hot water from the heat source (the solar collector or secondary electrical heater) was applied to flow through the regenerator. Simultaneously, the hot water was also delivered to increase the solution temperature before the regenerator in the heat exchanger #3. After passing through the regenerator and exchanger, the return water was mixed and sent back to the solar collector. Therefore, the outlet temperature from the heat source should be the same as the inlet one of regenerator and exchanger, which means that the iteration calculation was required. It should be noticed that if the hot water temperature was re-valued, the loop #1 had to start again since the required regeneration temperature was influenced by the hot water temperature.

3) Loop for the cooling water temperature

The cooling water from the cooling tower was delivered to the internally cooled dehumidifier for improving the dehumidification efficiency and to the heat exchanger #1 for pre-cooling the solution. The mixed return water was evaporative cooled simultaneously, so the water temperature from the cooling tower should be the same as the entering water temperature before the dehumidifier and exchanger. Similarly, the change of cooling water temperature would influence the first and second loops. Therefore, the third loop should be re-valued until the prerequisites in all three loops were fulfilled.

4) Loop for the inlet solution temperature of dehumidifier

As shown in Fig. 7.4, the desiccant solution flowed circularly through the dehumidifier, regenerator and several heat exchangers and then back to the dehumidifier. According to the physical principle, the solution temperature entering the dehumidifier should be similar to that of the return solution passing through the components along the flow way. So, the iteration loop was required to obtain the solution temperature. It should be noticed that if the inlet solution temperature changed, all the temperatures in the first three loops changed accordingly, which means that all the loops should be re-started and re-approached.

The four iteration loops were indicated in Fig. 7.5. To obtain the accurate result in these loops, the difference between the current calculated value and the previous one should be small enough. The accepted error was set to be 0.1℃, since the uncertainty of the common measurement method of the temperature, i.e. by the Pt-RTD, is ± 0.1℃.

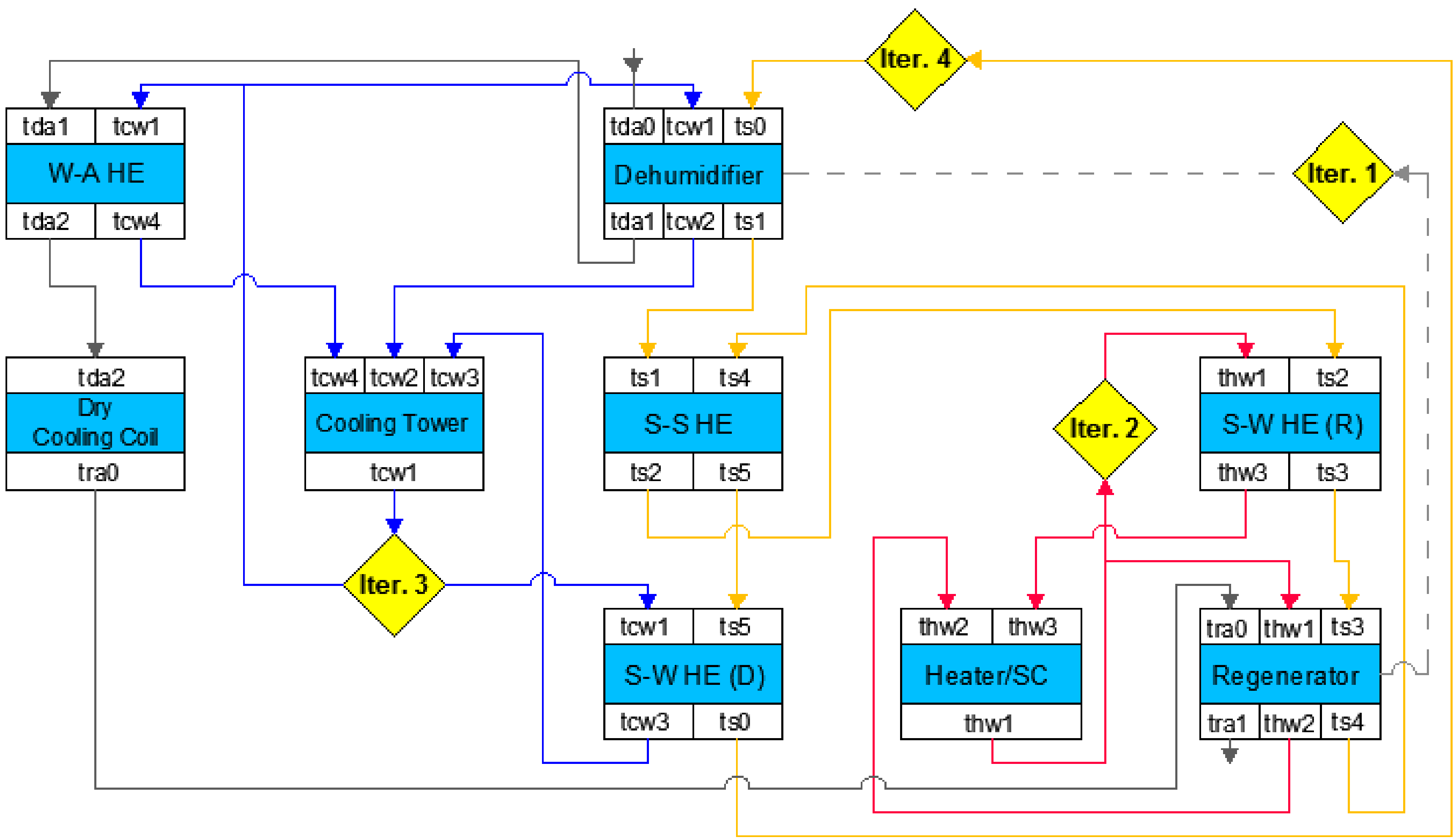

Fig. 7. 5 Iteration loops used in the simulation of SLDAC

7.3.5 Simulation Procedure

Firstly, the climate weather data, i.e. the dry/wet bulb temperature of ambient air and the solar radiation, and the load profile of the simulated building, i.e. the minimum outdoor air flow rate, the indoor set point and the cooling/dehumidification demands, should be imported. To obtain the data, a case building locating in a certain area should be selected, as described in next chapter. Afterwards, the initial parameters of the solution desiccant and cooling/heating water were assumed, including the solution temperature before the dehumidifier, the cooling water temperature after the cooling tower and heating water temperature after the heat source.

Then, with the equations described in Section 7.3.2, the outlet parameters of the desiccant solution and cooling water leaving the dehumidifier could be calculated. After exchanging heat with the return solution and hot water from the heat source, the weak solution was sent into the regenerator, which was internally heated with the hot water. The first loop was started to calculate the inlet solution temperature of the regenerator, and then the hot water temperature of the solar collector and auxiliary heater could be obtained with the second loop. Therefore, with the quick prediction model of internally heated regenerator, the outlet parameters of the solution were derived. With the cooling water from the cooling tower, the temperature of solution was further reduced, and the third loop was applied to calculate the cooling water temperature. Finally, the fourth iteration loop was required to check whether the difference between the temperature of desiccant solution after the heat exchanger and that of the inlet solution before the dehumidifier was small enough.

Due to the large number of variables involved in the process, being coupled with four iteration loops makes the simulation become increasingly complex and time-consuming. To accelerate the simulation speed of the programme, the values of temperatures required in four loops were firstly re-valued from a large range (i.e. ±5, ±1), and then, when a suitable range was found, a smaller range (i.e. ±0.5, ±0.1) was applied for re-valuing the temperatures. The flow chart of the simulation procedure including the four iteration loops was shown in Fig. 7.6.

If all errors of four iteration loops were reduced under the set value, the simulation was considered as convergence, and all the inlet and outlet parameters of the desiccant solution, cooling/heating water and air could be obtained. Therefore, with the outlet parameters of the processed ventilation air, the energy consumption to drive the cooling coil could be calculated. The energy required in the solar collector or auxiliary heater for heating the solution and water could also be derived. Besides, with the equations in Section 7.3.2, the energy consumption of the pumps and fans in the system could be obtained. The detailed results of operation and energy performance of SLDAC are listed in Chapter 8.

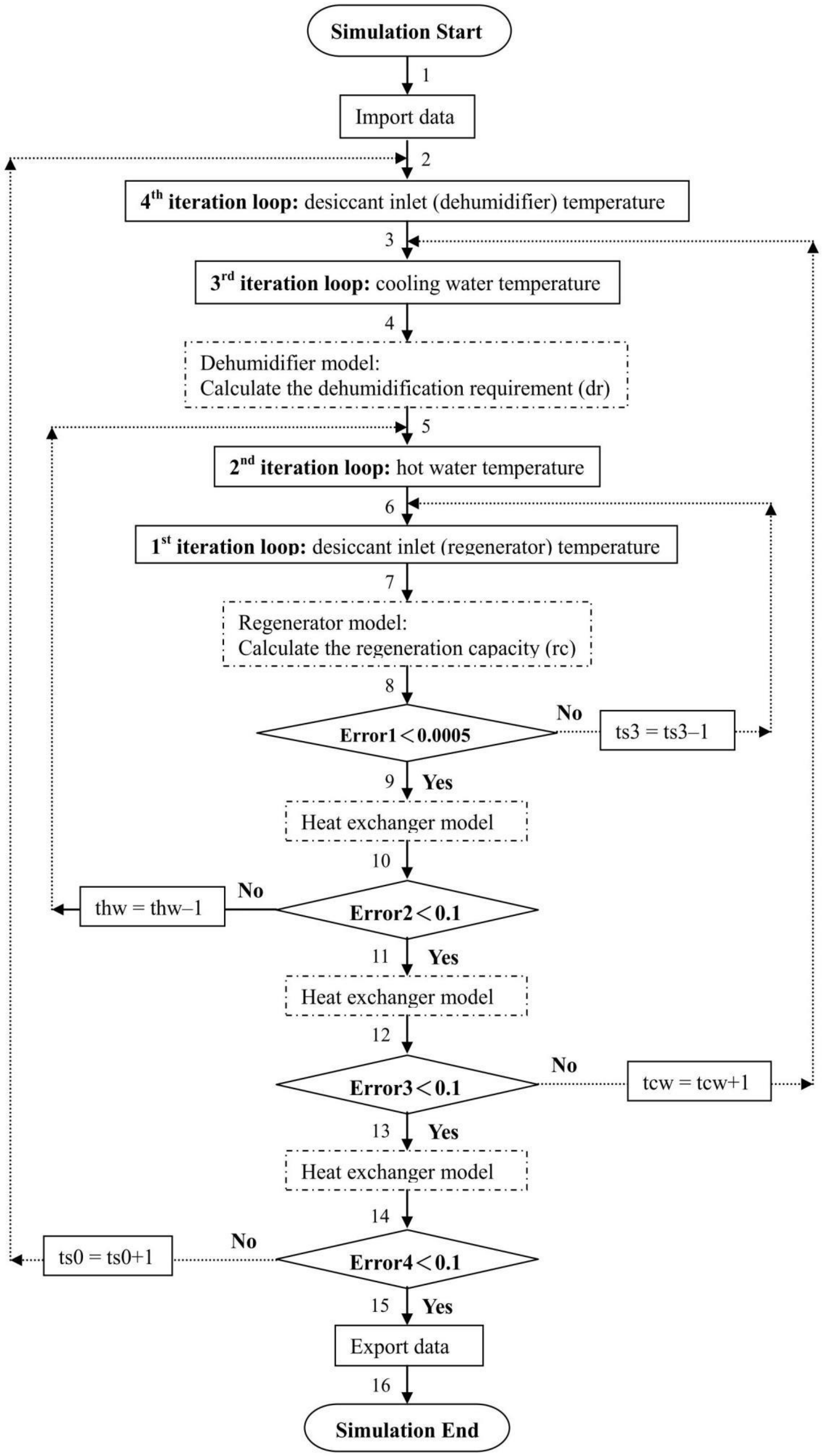

Fig. 7. 6 Flow chart of the simulation procedure

7.4 Summary

In this chapter, firstly, we developed a simplified prediction model for the internally cooled/heated dehumidifier/regenerator. With this model, the outlet parameters of solution, air and cooling/heating water could be obtained accurately and directly without any iteration. In this model, three kinds of effectiveness were defined, i.e. enthalpy effectiveness, moisture effectiveness and temperature effectiveness. LiCl and water were chosen as the solution and cooling/heating fluid, respectively. With the linear regressions, the statistical correlations of three kinds of effectiveness for internally cooled dehumidifier and internally heated regenerator were developed by using the mass and heat driving forces and other related parameters as variables. The required F-test was conducted and showed that these regressions are reliable. The composite differences between our prediction results and those obtained by the theoretical model under more than 250 operation conditions were compared, showing an ACD of 14.7% for dehumidifier and 7.1% for regenerator. Therefore, this new simplified prediction model is very useful for both researchers and engineers, especially for evaluating the dynamic operation performance of the LDAC system.

Then, with this numerical model of dehumidifier/regenerator and equations of other components, the operation performance simulation of the SLDAC, which includes the internally cooled dehumidifier, internally heated regenerator, solar thermal collector, cooling coil driven by the vapour compression, auxiliary electricity heater, three heat exchangers fans and pumps, were conducted. To obtain the real temperature of solution and cooling/heating water, four iteration calculation loops were employed; i.e. the loop for the solution inlet temperature of regenerator, for the heating water temperature, for the cooling water temperature and for the inlet solution temperature of dehumidifier. These four loops were nested, which means that if the parameter of the outer loop changed, the inter loop had to be re-started and re-valued. Therefore, after setting the operation conditions and assuming the initial values, the four loops should be solved by the iteration calculation, and then the outlet parameters of air, solution and heating/cooling fluid under different design and operation conditions could be obtained. Furthermore, the climatic data and load profiles of a selected building are required for the dynamic operation performance simulation of SLDAC, which are described in Chapter 8.

CHAPTER 8

AIR-CONDITIONING LOAD ANALYSIS AND ENERGY PERFORMANCE OF SLDAC OF BUILDINGS IN HONG KONG

8.1 Introduction

As mentioned earlier, to evaluate the dynamic operation performance of SLDAC, a case building in a certain area should be selected to obtain the required climatic data and building's air-conditioning (AC) load profile. Hong Kong, as a high density city locating in a subtropical offshore region, is generally warm and humid throughout the whole year. Due to the significant improvement of local living and working standards, the number of air-conditioned commercial buildings has increased greatly in recent years, and the annual energy consumption increased from 45% to 60% of the total use in Hong Kong from 1990 to 2000. About 30-50% of this energy consumption is consumed by AC systems. Besides, the climate change is also a vital reason for the ever-growing energy consumption in Hong Kong. Fortunately, with the long cooling seasons, the subtropical area is suitable for developing the solar energy applications because of its abundant solar radiation.

Therefore, the commercial buildings in Hong Kong were regarded to be a suitable case to investigate the dynamic operation performance of SLDAC. Accordingly, understanding the characteristics of the AC load profile of these buildings is pre-requested, and analysing how their loads respond to the local climate change is also important. Then, with the weather data and load profiles, the operation performance and energy consumption of the SLDAC could be studied and compared with the traditional ones.

Referring to the literature review in Chapter 2, the load profile of buildings in Hong Kong has been investigated by many local researchers, including Yu et al. (2001), Deng et al. (2003), Yik et al. (2001), Zhang et al. (2001), Bojić et al. (2005) and Lam et al. (2010). However, most previous studies investigated on the total or part of AC load in buildings, and there is little research on the comprehensive load profile analysis of commercial buildings in Hong Kong. Furthermore, although many researchers investigated on the energy performance of LDAC or SLDAC in buildings (Lowenstein et al. 1995, Khalid Ahmed et al. 1997, Rane et al. 2002, Liu et al. 2006 and Chen et al. 2003), most of them concerned the packed-bed or solar collector/regenerator liquid desiccant system, and the research on the internally cooled/heated liquid desiccant system is limited. Additionally, only several researchers have been conducted on the operation performance of LDAC applied in buildings under the hot climate like Hong Kong (Li et al. (2007), Alizadeh et al. (2007), Judah et al. (2011)).

This chapter firstly investigated the AC load profiles of three typical commercial buildings in Hong Kong, i.e. office, hotel and retail buildings, and addressed the main problem of the application of traditional AC system in these buildings. The impact of climate change on the ventilation load during last six decades in Hong Kong was also investigated. Then, the dynamic operation performance and energy consumption of the SLDAC employed in these buildings was simulated and compared with the conventional system. To minimize the consumption, several optimization methods of the SLDAC were provided and compared.

8.2 Air-conditioning load analysis for commercial buildings in Hong Kong

This section firstly investigated the load profiles of three typical commercial buildings (office, hotel and retail) in Hong Kong, focusing on the latent load due to the humid local weather condition. The main limitation of conventional air-conditioning systems in Hong Kong was also analysed. Then, the impact of climate change on the ventilation load during last six decades in Hong Kong was investigated. The response of ventilation load to the climate change, including the sensible and latent cooling load in daytimes and nighttimes, was investigated.

8.2.1 Research method of load profile of commercial buildings

The load profile was simulated with the ASHRAE Heat Balance Method. Three types of typical commercial buildings in Hong Kong were chosen, i.e. office, hotel and retail buildings. The input parameters of the load profile simulation were derived from the energy codes for commercial buildings, which are specified by the Hong Kong government (Hong Kong Government, 2005). The details of building construction, including materials and *U* values of wall, roof, ceiling, floor and window, were found from Appendix A of OTTV (Overall Thermal Transfer Value, 1995). The default parameters of occupant density, the minimum outdoor air requirement, lighting power density and equipment power density were found from Tables A2 and A3 in Appendix 2 of the Hong Kong Building Energy Code (Hong Kong Government, 2005). The schedules of occupancy, lighting, small power and AC system were found in Tables A4 to A7.

The floor layouts and building façades of the hotel building are shown in Table 8.1. It should be specially noted that the typical hotel building has four kinds of zones: guestroom (4-40/F, 62 per floor), corridor (4-40/F), lobby (1-2/F) and restaurant (3/F). The different occupancy densities, ventilation rates, operation modes and internal load schedules of different zones were considered.

Table 8. 1 Floor layouts and building façade of hotel building

Building	Typical Floor Plans

Façade	1-2F	3F	4-39F
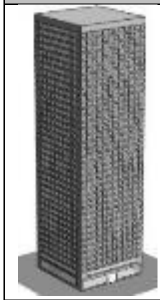	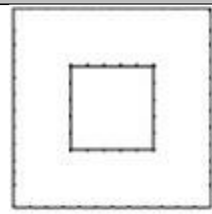	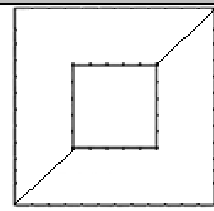	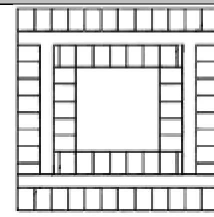

The weather data of typical weather year 1989, which has been specified in the Hong Kong Performance-based Building Energy Code for building energy simulation purpose (EMSD, 2003), is applied in the simulation. A summary of key simulation variables for the three types of buildings are shown in Table 8.2.

Table 8. 2 Summary of weather data and simulation design variables of commercial buildings

Variables	**Building Type**		
	Hotel	**Office**	**Retail**
Number of floors	40	40	5
Total air-conditioned floor area (m^2) (%GFA)	42,219 (81%)	42,840(83%)	5355(83%)
Window to wall ratio	0.5	0.5	0.5
U values of external wall/glass/roof/ceiling	2.30/5.67/0.73/3.56	2.30/5.67/0.73/3.56	2.30/5.67/0.73/3.56
Summer/winter indoor temperature set point (^oC)	23/20	23/20	23/20
RH set point (%)	54	54	54
Air-conditioning system	24/24	13/7(Sat)/0(Sun)	16/16

operation hours per weekday/weekend(h)			
Room/Zone Types	Guestroom/Corridor/Lobby/Restaurant	Perimeter/interior	Single zone
Occupancy density (m^2/person)	2/guestroom[a]	8	8
Minimum Outdoor Air (L/s/person)	30 L/s/guestroom[a]	8	8
Infiltration (ach) ventilation system off/on	0.5/0.1	0.5/0.1	0.5/0.1

[a] only the data for guestroom are listed, and the other data could be found in Appendix 3 of Hong Kong Building Energy Code.

The simulation time step was set as one hour. The total AC load (Q_t) includes the sensible and latent parts, and each part is consisted by three components: space load (load caused by the envelope, lighting, equipment and occupants), ventilation load (load caused by handling fresh air in AC system) and infiltration load (load caused by handling fresh air leaking from doors and windows).

In terms of the impact of climate change, the hourly meteorological data from 1950 to 2007 recorded by the Hong Kong Observatory, including the external dry-bulb temperature and relative humidity, were employed. As shown in Fig. 8.1, the annual average external dry-bulb temperature from the Hong Kong Observatory presents an obvious increase from 1950 to 2007, at a rate of about 0.03℃ per year. The increasing outdoor temperature, as known as the global climate warming, would result in higher heat gain in buildings.

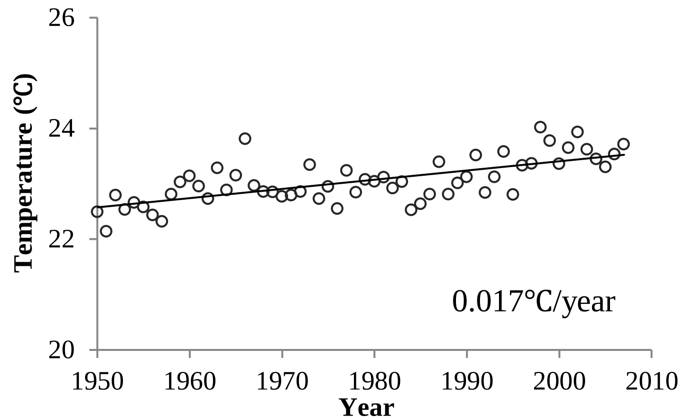

Fig. 8. 1 Annual average external dry-bulb temperature from 1950 to 2007

The ventilation loads per flow volume at time *t*, including the total, sensible and latent load, are calculated by:

$$
\begin{aligned}
q_{v,t} &= \rho(h_{o,t} - h_{i,t}) \\
q_{s,t} &= c\rho(t_{o,t} - t_{i,t}) \\
q_{l,t} &= \rho h_{fg}(d_{o,t} - d_{i,t})
\end{aligned}
\qquad (8.\ 1)
$$

where *c* is the specific heat capacity of air, ρ means the air density, and h_{fg} stands for the latent heat of vapourization. The subscripts *t*, *s*, *l* stand for the total, sensible and latent ventilation load, respectively. To indicate the effect of UHI, the ventilation load during the daytimes (8:00-18:00) and nighttimes (19:00-7:00 tomorrow) is also calculated.

To demonstrate the results of climate change by local meteorological data, the mentioned hotel building was selected as a respective building to simulate the ventilation load change. With 24-hour AC operation all over the year, it could reveal the trend of ventilation load during a long period. The simulation period was set from 1950 to 2007 and the time interval was one hour.

8.2.2 Annual AC load profiles and reheating ratio

To verify the results, the simulated load profiles of commercial buildings were compared with those obtained from simulations or surveys of previous studies, as shown in Fig. 8.3, and similar trends were found. Because the heat loss in heat exchangers and transportation systems in existing buildings were not considered, our simulation results were relatively lower than the average survey results. However, the difference was insignificant in the load profile analysis.

Table 8. 3 Comparison of related researches

Data source	**Building type**	**Method**	**Amount of Samples**	**Annual Energy Consumption per area MJ/m^2**
Yik et al. (2001)	Office building	Simulation	1	1048
	Hotels	Survey	6	1570-2950 Average: 2100
	Mixed retail/office buildings	Survey	10	950-2340 Average: 1657
Deng et al. (2003)	Hotels	Survey	7	1650-2100 Average:1933

This study	Office	Simulation	1	891
	Hotel	Simulation	1	1749
	Retail	Simulation	1	936-977

As shown in Fig. 8.2, the cooling load, including sensible and latent (dehumidification) parts, took a dominant proportion of the total annual load in all buildings, which was more than 98%. The dehumidification load occupied a high portion of the cooling load, which was about 50% (Hotel), 30% (Office) and 40% (Retail). The heating and humidification loads took insignificant portions in the annual total load. These load profiles are caused by the local subtropical offshore climate which is generally warm and humid throughout the whole year. Both cooling sensible and dehumidification loads of hotel buildings are much higher than those of other buildings, especially the dehumidification load, mainly due to its longest 24h operation period and highest ventilation rate of fresh air.

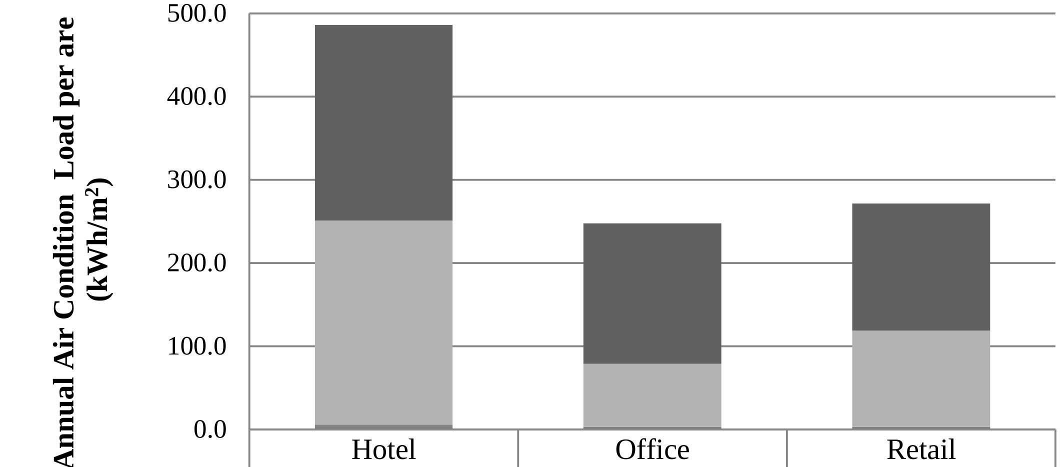

	Hotel	Office	Retail
cooling (sensible)	234.7	168.7	152.8
dehumidification	245.5	75.9	115.5
heating	5.5	3.0	3.1
humidification	0.1	0.0	0.0

Fig. 8. 2 Total air-conditioning load per area of three typical commercial buildings

As shown in Fig. 8.3, the latent load proportion of the total cooling load keeps high and steady from March to September for all typical buildings. Hotel buildings showed the highest latent load proportion, which was above 25% all over the year and even above 50% for 7 months. Retail buildings had the second highest proportion, above 40% from March to September. The lowest proportion occurred in office buildings, but the latent load still contributed more than 30% of the total load. The difference of latent load proportions is mainly caused by the different operation and occupancy schedules of these buildings.

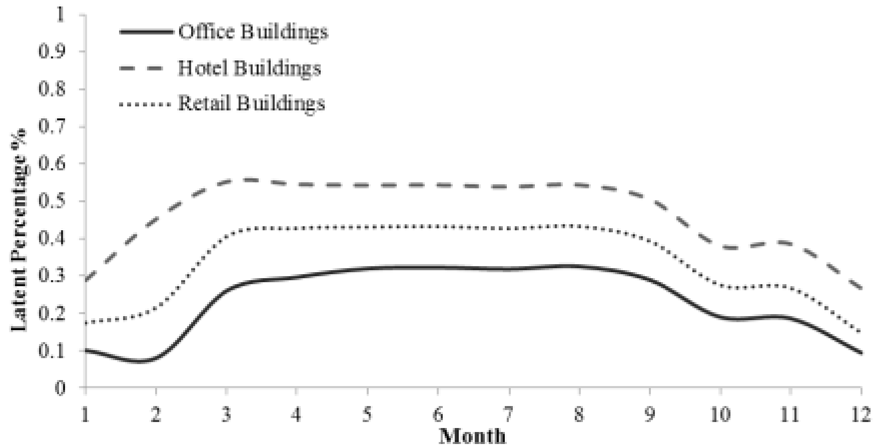

Fig. 8. 3 Annual proportion of latent load for three commercial buildings

Then, the detailed components of sensible and latent cooling loads in these buildings through the whole year were investigated. Both sensible and latent parts of the cooling load include three components: space load, ventilation load and infiltration load. Due to the similar occupancy, ventilation and operation characteristics in office and retail buildings, only results of hotel and office buildings were listed. For the sensible cooling load, as shown in Fig. 8.4 (a), the space load took a dominant percentage in most time of the year, especially for office buildings. Hotel buildings had lower space load ratio due to its higher fresh air requirement, but the trends of two typical buildings were similar. The space load percentage reached 70-90% during most time of the year with the peak occurring in May and November. With little infiltration load (less than 5%), the rest of sensible load was the ventilation load with a percentage of 15-25%.

For the latent cooling load, as shown in Fig. 8.4 (b), the ventilation latent load was the major component, especially in hotel buildings. The ratio of the ventilation latent load to the total latent load keeps high all over the year, with an annual average value of 81.8% for the hotel and 67.5% for the office building. The peak period of ventilation load for hotel and office building appeared from June to October (about 90%) and May to September (about 80%), respectively. The infiltration load had a small contribution to the latent load (less than 7%), and the rest was the space load, which contributed more in winter and less in other seasons.

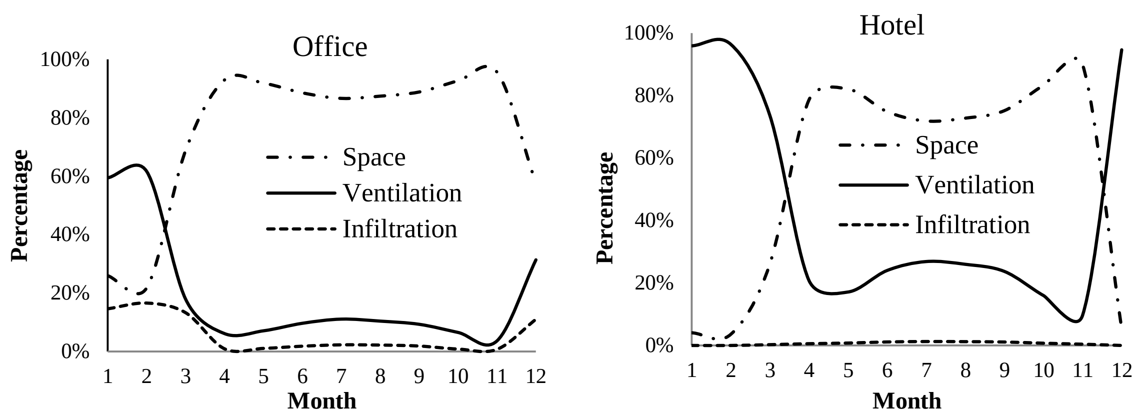

(a) Proportion of sensible cooling load components

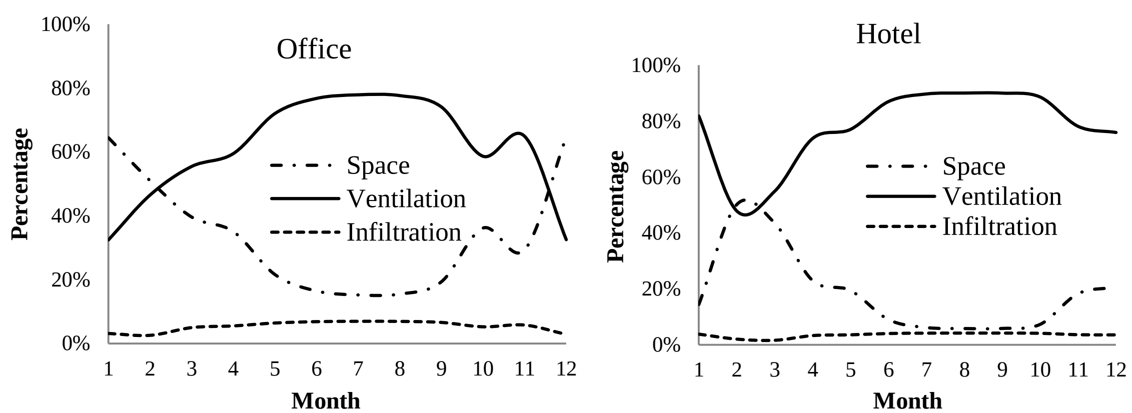

b) Proportion of latent cooling load components

Fig. 8. 4 Proportions of load components in hotel and office buildings

Due to the high dehumidification load proportion in local buildings, the mismatch of space sensible load and latent load would lead to a low temperature of indoor air. To investigate the problem, a parameter, namely reheating ratio, was defined, which stands for the percentage of hours required for reheating in total operation hours.

According to the ASHRAE handbook and local regulations, the indoor air set point is 23℃ and 54% RH, and the optimal comfort zone is 22 to 25.5℃ for temperature and 30-60% for RH in Hong Kong commercial buildings (ASHRAE Handbook, 2009). In order to calculate the reheating ratio, several assumptions of the conventional vapour compressor AC system and indoor air conditions were made: a) the temperature difference between indoor and supply air set point is 9℃, and the RH of the off coil air is 90%; b) the maximum indoor RH is set at 54% and 60% for condition A and B, respectively; and c) the chosen design indoor air temperatures for the calculation are 25.5, 24, 23 and 22℃.

To calculate the reheating ratio, first, the sensible-total heat ratio (SHR) at specific time *t*, $SHR_{a,t}$, and the SHR of the indoor air set point, SHR_s, should be derived. The logistic to decide whether reheat is needed or not is as following. Therefore, the reheating ratio could be calculated by the ratio of hours required for reheating to the total operation hours.

$$\begin{aligned} &if\ SHR_{a,t} \geq SHR_s,\ reheat\ is\ not\ needed\ at\ time\ t; \\ &if\ SHR_{a,t} < SHR_s,\ reheat\ is\ needed\ at\ time\ t; \end{aligned}$$

Table 8.4 provides the reheating ratio in terms of the indoor RH and temperature set points. If the required maximum indoor RH was below 54%, the reheating ratio in commercial buildings was quite high, up to about 90% in the hotel building. The lowest value, in office buildings, also reached 60% to 80%. With the upper limitation of RH of 60%, the reheating ratio could be greatly reduced. However, reheating was still necessary in 10% to 20% operation hours for the retail and office buildings. The reheating ratio also decreased slightly with the temperature set point in most cases. However, low temperature set point leads to higher energy use in AC system and draft feeling of occupants. Reducing the temperature set point may not be a proper solution to the high reheating ratio in Hong Kong.

Table 8. 4 Summary of reheat ratio in three typical buildings

Condition	Indoor air set point		SHR_s	Reheat Ratio (%)		
	Temperature(℃)	Relative humidity (%)		Office	Retail	Hotel
A	25.5	54	0.89	80.7	91.4	91.5
	24	54	0.88	72.7	90.7	87.5
	23	54	0.88	66.6	89.7	94.3
	22	54	0.88	60.3	89.1	92.1
B	25.5	60	0.68	12.0	20.6	6.2
	24	60	0.70	11.4	17.1	7.8
	23	60	0.70	10.9	14.8	5.2
	22	60	0.71	10.6	12.5	5.1

The high reheating ratio shows that in most operation hours, in order to deal with the high SHR conditions in commercial buildings, the traditional AC system has to overcool the supply air and then reheat it. However, because reheating is a waste of energy which should be avoided, most buildings in Hong Kong do not have a reheating system. That is why the supply air temperature is quite low, which leads to critical thermal discomfort for occupants.

8.2.3 Impact of climate change on ventilation load in buildings of Hong Kong

To analyse the change trend of ventilation load in sixty years, the average hourly ventilation load per flow volume in summer (from May to September) is chosen as a representative parameter, namely *V*. The different *V* values in daytimes and nighttimes were also calculated.

From Fig. 8.5, it is found that the average hourly ventilation load increases with a rate of 0.028 kW per year through the period from 1950 to 2007. The rising rates of the sensible and latent loads are quite different during the last six decades. The latent part, V_l, which takes about 80% of the total *V*, presents a higher upward trend (about 1.8 times) compared to that of the sensible cooling load V_s.

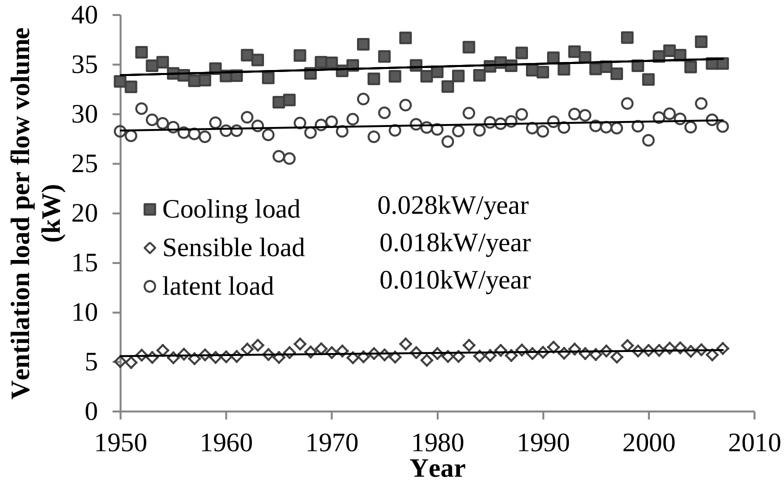

Fig. 8. 5 Change of cooling ventilation load from 1950 to 2007

As shown in Fig. 8.6 (a), for the sensible cooling load, the V_s at night during these years is smaller (about 75% of that in daytimes), but its increasing rate is much higher, about ten times, than that in daytimes. It means that due to the climate change in Hong Kong, the difference between outdoor air temperatures at night and in daytimes will be gradually narrowed in the future. As shown in Fig. 8.6 (b), before 1970s, the latent load during the nighttimes was smaller than that in daytimes, but the relationship changed because of the climate change. After 1970s, the gap between latent loads was widened due to its high increase speed at night. Therefore, although the hourly ventilation load is higher in daytimes currently, due to the higher upward rate at night (about 3 times of those in daytimes), the load difference between daytimes and nighttimes becomes continually smaller. It reveals that the latent cooling ventilation load at night responds to the climate change more sensitive than others.

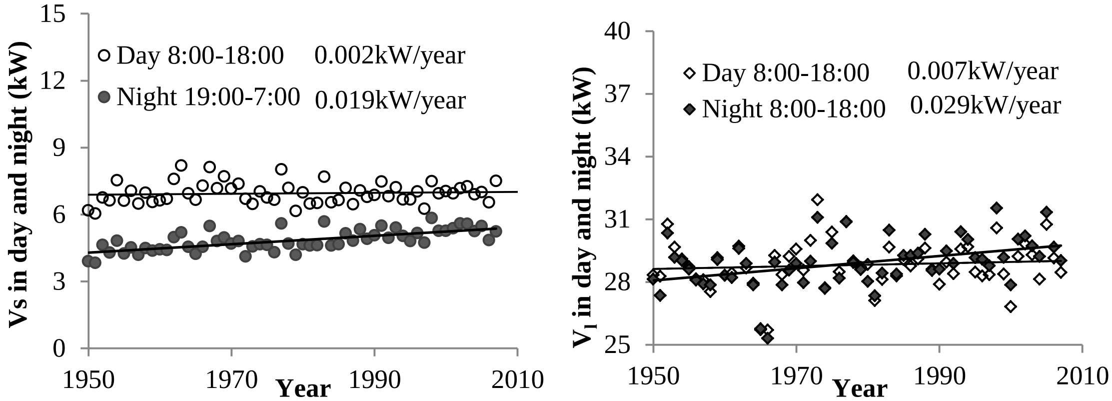

Fig. 8. 6 V_l and V_s in daytimes and nighttimes from 1950 to 2007

With the weather data from 1950 to 2007, the change trend of annual cooling ventilation load of the hotel building was investigated. As shown in Fig. 8.7, both the sensible and latent parts of the annual ventilation load per area have been increasing these years, and the change trends were similar to the previous results. The latent one, which takes a dominated position in the annual load (more than 80%), has a higher increasing rate compared to that of the cooling load.

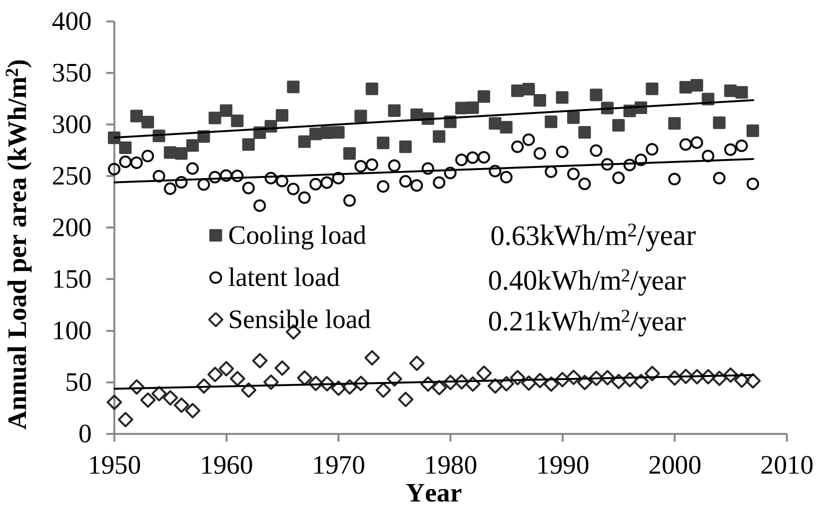

Fig. 8. 7 Annual cooling load of the hotel building per area from 1950 to 2007

As shown in Fig. 8.8 (a), the sensible load at night, which increases at higher rate, is getting closer to that in daytimes during the 60-year period. In terms of latent part, in Fig. 8.8 (b), the load at night, which has been already 30-40% higher, has a much larger upward rate compared to that in daytimes.

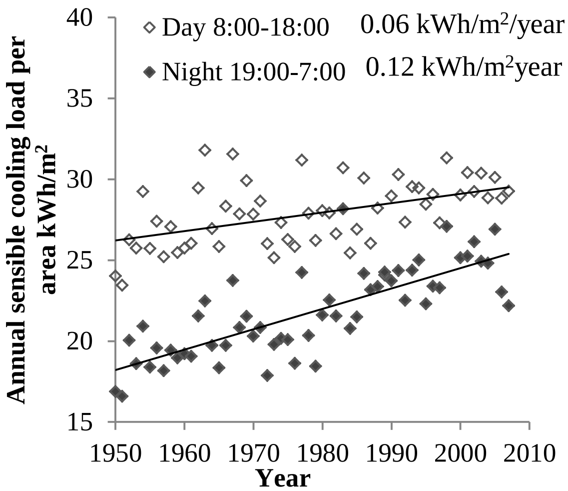

(a)Annual sensible cooling load

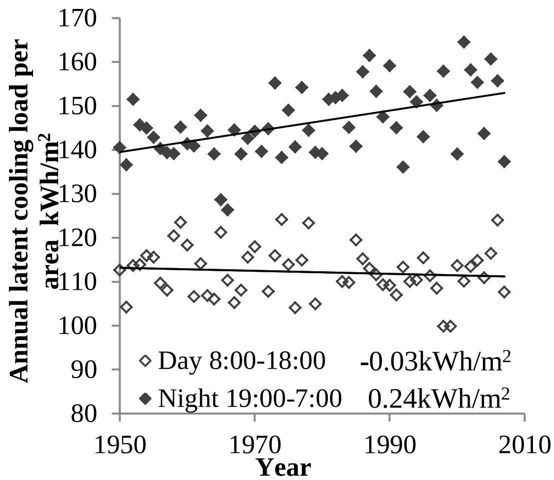

(b) Annual latent cooling load

Fig. 8. 8 Annual sensible and latent cooling load in daytimes and nighttimes

The change trends of electricity consumption and CO_2 emission of this hotel building were developed. As shown in Fig. 8.9 (a), the general trend of electricity consumption to process the fresh air has been growing in the past 60 years. Similar to the trends of ventilation load, the increase of electricity consumption at nighttimes is considered as the main reason of the total increase, with a rate of 0.3kWh/m^2 compared to 0.1kWh/m^2 in daytimes. The CO_2 emission from 1950 to 2007 caused by the power generation and ventilation system operation is shown in Fig. 8.9 (b).

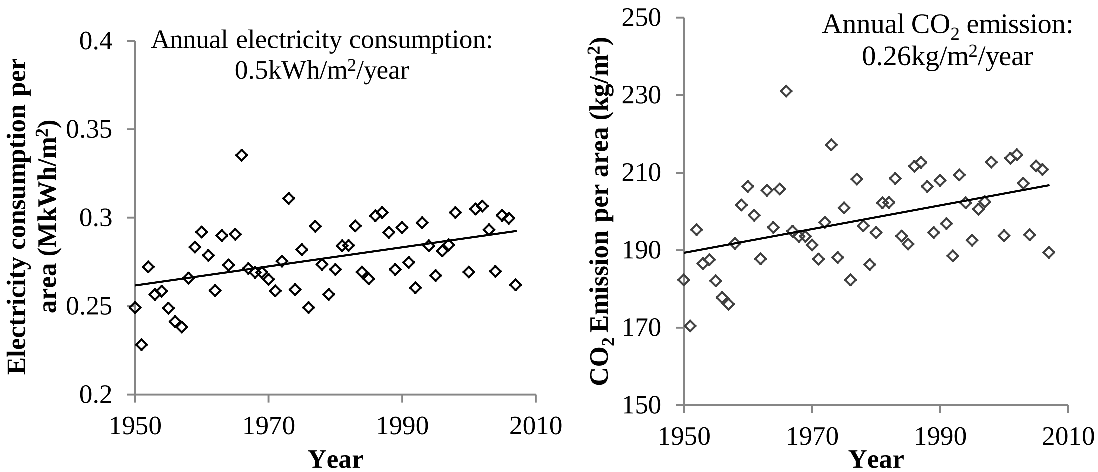

Fig. 8. 9 Change trend of (a) Electricity Consumption and (b) CO_2 emission from 1950 to 2007

From 1950 to 2007, both the sensible part and latent part of cooling load show an increasing trend, and the latter reveals a higher growth rate. The growing rate at night is much larger than that in daytimes. The local climate warming and UHI effect, caused by the unique urban location and environment of Hong Kong, play an important role in the different change trends of different loads. As located in a coastline, the moisture of outdoor air is directly related to the moisture of air upon the surrounding sea level. As shown in Fig. 8.10, the moisture content of outdoor air increases at a rate about 0.02 g/kg per year, and the RH keeps steady. When the air temperature increases due to the climate warming, to keep the equilibrium humidity of the air upon the air-sea interface, evapouration from surrounding sea water will be speeded up, which leads to moisture content increase of the air. Therefore, more moisture content from the fresh air should be removed. To compare the change trend, the load change rate due to the outdoor air condition could be calculated as follow.

$$\begin{aligned} dq_t &= c\rho v_t \\ dq_m &= \rho h_{fg} v_m \end{aligned} \tag{8. 2}$$

where dq stands for the load change rate, v means the growing rate discussed before, and subscript t and m represent temperature and moisture content of outdoor air, respectively.

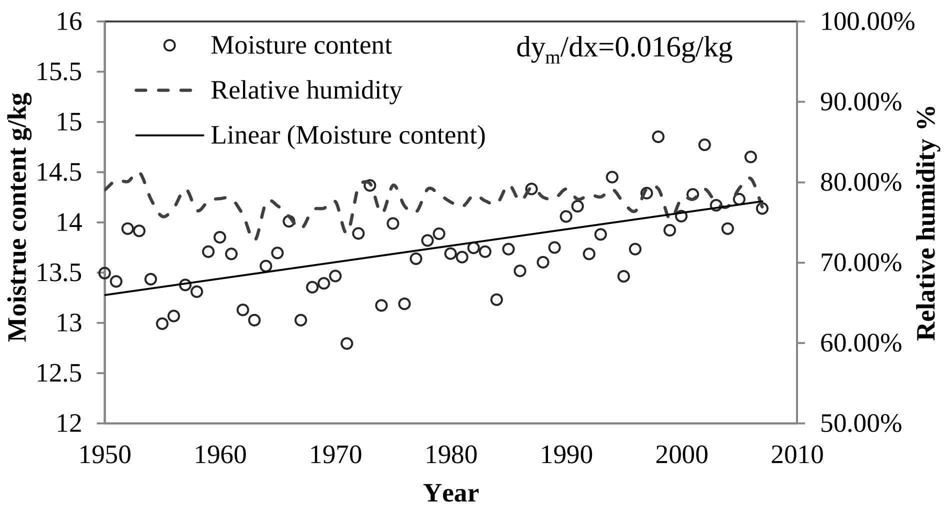

Fig. 8. 10 Annual average moisture content and RH of outdoor air from 1950 to 2007

As shown in Table 8.5, the load change rate caused by the increase of moisture content is higher than that of temperature, which leads to higher increasing rate of dehumidification load.

Table 8. 5 Increasing rate and load change rate of external air temperature and moisture

	External air temperature	External air moisture content
Increasing rate per year	0.017℃	0.016 g/kg
Load change rate (kW/year)	0.021	0.048

In terms of the trend difference in daytimes and nighttimes, the serious UHI effect in Hong Kong is considered as the main reason. From researches by Giridharan and Memon (2009, 2011), it is clear that the sky view factor has been greatly reduced due to the extensive construction programs and high-rise & high-density urban plan in Hong Kong, especially in recent decades. The low sky view factor significantly reduces the nocturnal cooling, including the long-wave radiation and wind speed in nighttimes, but the daytimes shadow effect is enhanced. Therefore, it actually offsets part of the global warming in daytimes, but leads to sharp temperature increase in nighttimes.

8.2.4 Summary

This section investigated the AC load profiles of three typical commercial buildings in Hong Kong, i.e. office, hotel and retail buildings. Then, the impact of climate change on the ventilation load of buildings in Hong Kong during the period from 1950 to 2007 was analysed.

Results show that the cooling load contributes to more than 98% of the total annual load, with high latent (dehumidification) load proportion from March to September. The high reheating ratio, i.e. from 60%-90%, is found to be the main reason for the poor indoor thermal comfort in these buildings. In the cooling AC load, the ventilation load occupies a large percentage of the latent load, while the major component of sensible load is the space load. Therefore, applying the conventional AC system is not a good choice as it will lead to several problems such as energy waste and low system COP. Furthermore, the latent load, which already occupies about 80% of the total load, increases with a much higher rate due to the climate warming. The serious UHI effect in Hong Kong causes a higher growing rate of ventilation load in nighttimes, which is about three times compared to that in daytimes. For the buildings requiring long period air-conditioning, the latent load in nighttimes is the most sensitive component responding to the climate change, and plays the most significant role in the increase of energy consumption accordingly.

Therefore, to solve the problem, the independent sensible/latent control AC system is proposed as the best solution for local buildings.

8.3 Operation performance of internally cooled/heated SLDAC in Hong Kong

By inputting the weather data from the Hong Kong Observatory and the load profiles of commercial buildings in Hong Kong, the dynamic operation performance of the internally cooled/heated SLDAC could be evaluated with the simulation method developed in Chapter 7. The time interval in the simulation was set as 1 hour. Due to the location of Hong Kong, the solar collectors in the simulation were set to be installed facing the south, with a tilted angle of 22.5°. Because of the similar characteristics of office and retail buildings, only results of office buildings were introduced.

Although the occupancy schedule of office started from 7am to 7 pm every day, the ventilation latent load was quite low at the 7am and 7 pm due to the small number of occupants. In our simulation, the proposed system was operated from 8 am to 6 pm every day. Furthermore, the simulation period of the system was set as the cooling season, which is April to October according to the Guideline from the Hong Kong Government.

8.3.1 Energy performance of internally cooled/heated SLDAC in Hong Kong

Firstly, the annual primary energy requirement of the LDAC, without the introduction of solar thermal energy, was discussed. As shown in Fig. 8.11, as about 10% energy used for regenerating the desiccant solution, the primary energy consumption of the LDAC was around 4.7% higher than that of the conventional vapour compression cooling system (CVCS).

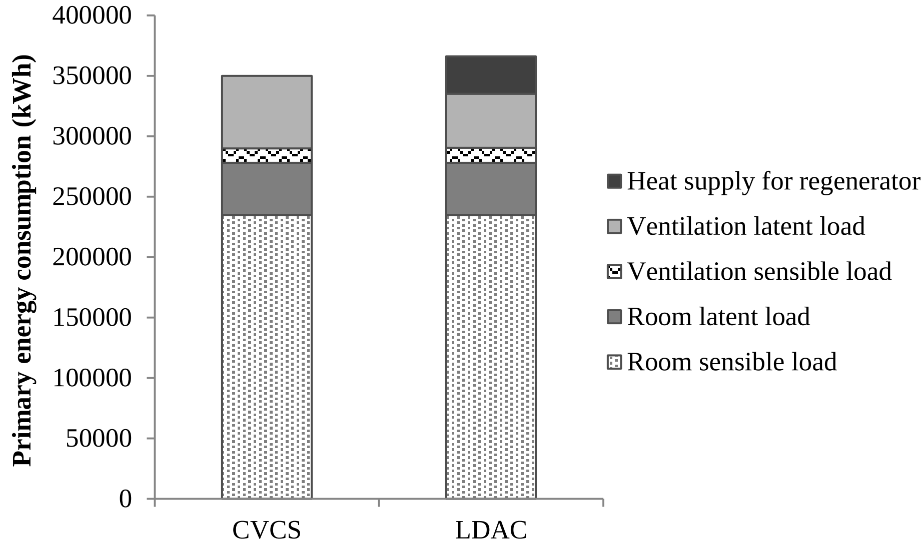

Fig. 8. 11 Annual primary energy consumption of CVCS and LDAC

As shown in Fig. 8.12, if the electric heater was applied as the heat source, the annual electricity consumption of LDAC was much higher than that of conventional system of the office. The main reason is that the heating efficiency of electricity (less than 1) is much lower than its cooling efficiency (about 3-4). In order to handle the high dehumidification load in commercial buildings, more electricity would be used to heat the liquid desiccant before entering the regenerator. Therefore, in commercial buildings in Hong Kong, the AC system with liquid desiccant ventilation system should not be driven by high grade energy, such as the electricity.

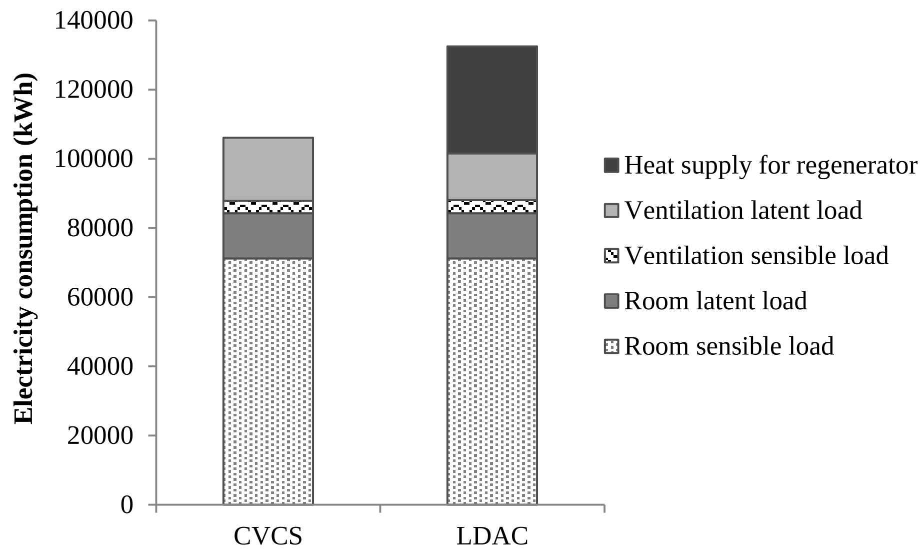

Fig. 8. 12 Annual electricity consumption of CVCS and LDAC

To reduce the energy use, solar energy applications are necessary for the LDAC. It should be noticed that the energy consumption of the solar-assisted systems is affected by the installation area of solar thermal collectors. Therefore, if the LDAC is expected to save energy, it has the required minimum installation area for solar collectors. As shown in Fig. 8.13, with the increase of installation area, the electricity consumption of LDAC applied in office buildings decreased. But, the energy saving percentage had an upper limitation, which means that all the energy required by the liquid desiccant regenerator was supplied by the solar thermal energy. So, by applying the SLDAC in the office building, up to 7.9% of total electricity consumption for AC system could be saved with solar collectors. By adding the thermal storage, the saving percentage would improve to 12.5%.

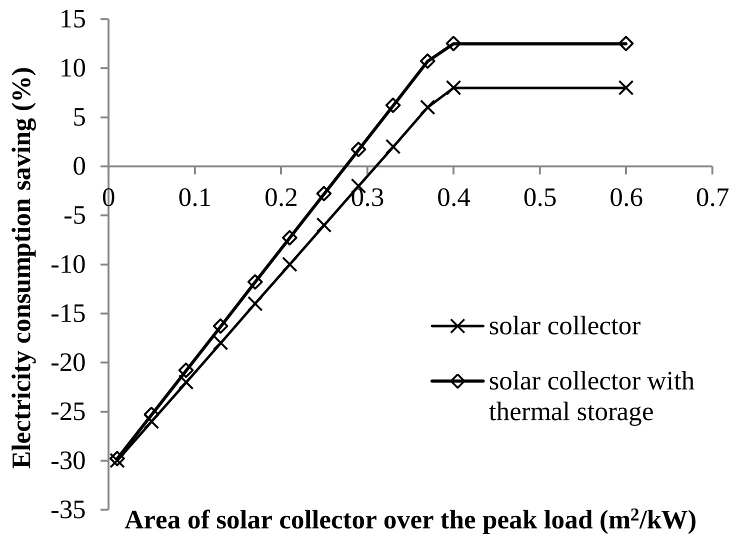

Fig. 8. 13 Energy saving percentages of LDAC with different solar collector areas

8.3.2 Problems of SLDAC applied in buildings of Hong Kong

The energy saving percentage of the proposed SLDAC, around 7.9%-12.5%, is not high when it was employed in the office building in Hong Kong. The main reason is that the liquid desiccant system was originally designed to handle the entire ventilation latent load for improving the COP of the cooling system which only deals with the sensible load. However, as shown in Fig. 8.14, during our simulation, the actual removal rate of dehumidifier in LDAC was found lower than the required one, which led to an unimproved COP of the cooling coil compared the CVCS. Due to the higher fresh air temperature and humidity in summer, the actual moisture removal rate of the ventilation air showed a peak in July. However, the actual dehumidification capacity almost kept the same during these months, which led to a large gap compared to the required one. This problem seriously impacted the performance and energy potential of LDAC applied in the office building.

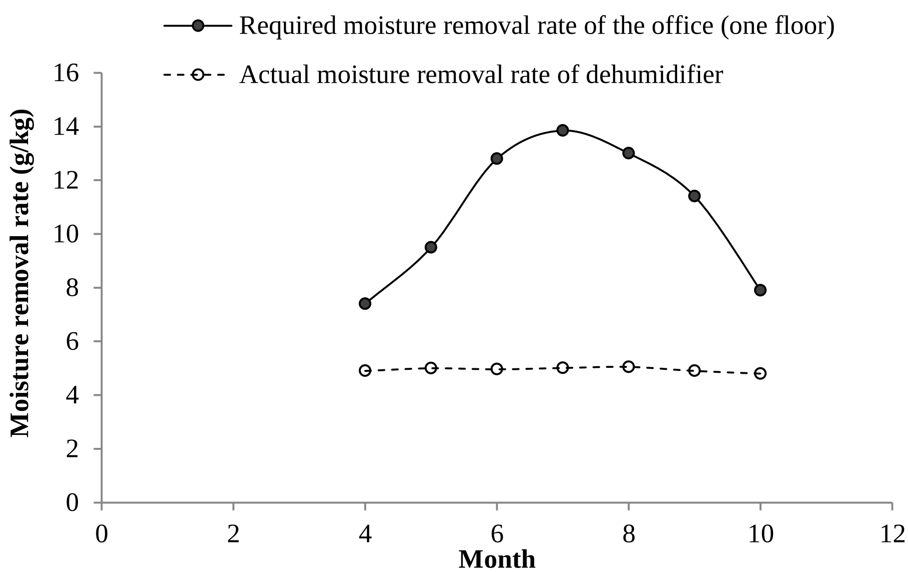

Fig. 8. 14 Comparison between the required dehumidification rate and actual one by LDAC

The main reason of this problem is that the only cooling source of our proposed liquid desiccant system was the cooling tower, for removing the extra heat produced in the regeneration process and providing the cool water for the dehumidification process. According to the physical model in Chapter 7, the capacity of the cooling tower is limited by the wet-bulb temperature of the surrounding air. However, the outdoor air in summer is humid and hot of Hong Kong. For example, in a typical day in July, the wet-bulb temperature of ambient air is around 28 to 31℃, and the lowest temperature of the cooling water could be calculated as about 30℃. So, the desiccant solution was only cooled to around 31 to 34℃. The increase of the desiccant temperature and cooling water temperature would seriously reduce the performance of dehumidifier. Therefore, if the cooling tower is chosen as the only cooling source, the dehumidification capacity of the LDAC could not satisfy the requirement of commercial buildings in Hong Kong.

To improve the energy saving potential of the SLDAC system, the system should be optimized by introducing extra cooling source or by adjusting the operation conditions, which are discussed in the next section.

8.4 Performance optimization of internally cooled/heated SLDAC in Hong Kong

8.4.1 Optimization of the addition of extra cooling coil

For the originally designed SLDAC system, due to the limitation of cooling tower, the dehumidification capacity was far under expectation, which led to a low COP of the chiller driven by the vapour compression system. To solve the problem, as shown in Fig. 8.15, an auxiliary cooler was introduced, to maintain the desiccant solution temperature entering the dehumidifier and to adjust the moisture removal rate. The cooling water used in the auxiliary cooling coil was also supplied by the chiller. Therefore, in this situation, as the entire latent load of the ventilation load and the space load was handled by the dehumidifier, the cooling coils could be considered as totally dry and the COP of the chiller could be improved to 4.62.

To handle all the latent load of the office building, the temperature of desiccant entering the dehumidification could be calculated with the numerical prediction model developed in Chapter 7, as the required moisture removal rate of dehumidifier and parameters of air and water were known. It should be noticed that the solution temperature during the operation should be higher than the crystallization point of the desiccant. The crystallization point of LiCl could be predicted with the following equation (Conde, 2004):

$$T_{LiCl} = T_{c,H_2O} \, (A_0 + A_1\zeta + A_2\zeta^{2.5}) \tag{8. 3}$$

where T is the absolute temperature, K. The parameters of A_0, A_1 and A_2 are -0.56036, 4.72308 and -5.81105 for LiCl-3H_2O and -0.315220, 2.88248 and -2.62433 for LiCl-2H_2O, respectively.

As the solution temperature was reduced, the efficiency of the dehumidifier was effectively enhanced. Taking a typical day in July as an example, with the addition of extra cooling coil, the average efficiency of dehumidifier increased from 0.25 to 0.57. Since only the sensible load of the building was dealt with the chiller, its required primary energy, including it to cool the supply air and to cool the desiccant, decreased.

Therefore, with the reduced energy demand and higher COP of the chiller, the electricity consumption significantly decreased, as shown in Fig. 8.16. Annually, the electricity used for driving the chiller in this optimization method was around 44% smaller compared to that of the conventional AC system. As the COP of chiller increased, the design size of the refrigeration system could be downsized, and the initial cost of the whole system could be reduced.

Furthermore, from Fig. 8.17 we could found, due to low solution temperature in the dehumidifier, the thermal energy required to regenerate the desiccant in the regenerator increased significantly. Fortunately, with the introduction of solar energy applications, the energy required in the regenerator could be supplied by the solar collector, which is depended on the installation area of thermal collectors. As shown in Fig. 8.18, compared with the conventional system, if all the energy required in the regenerator could be supplied by the solar energy, the saving percentage could approach up to 28.5% of the total electricity demand. However, since the energy used for regenerating the solution was higher, the minimum installation area of solar collectors for the optimized SLDAC was also higher, which was about 0.45 m^2/kW compared to 0.28 m^2/ kW in the base case (with the thermal storage). According to the peak load of the office building selected in our simulation, the minimum required area of solar collectors was about 147 m^2 in this optimization method.

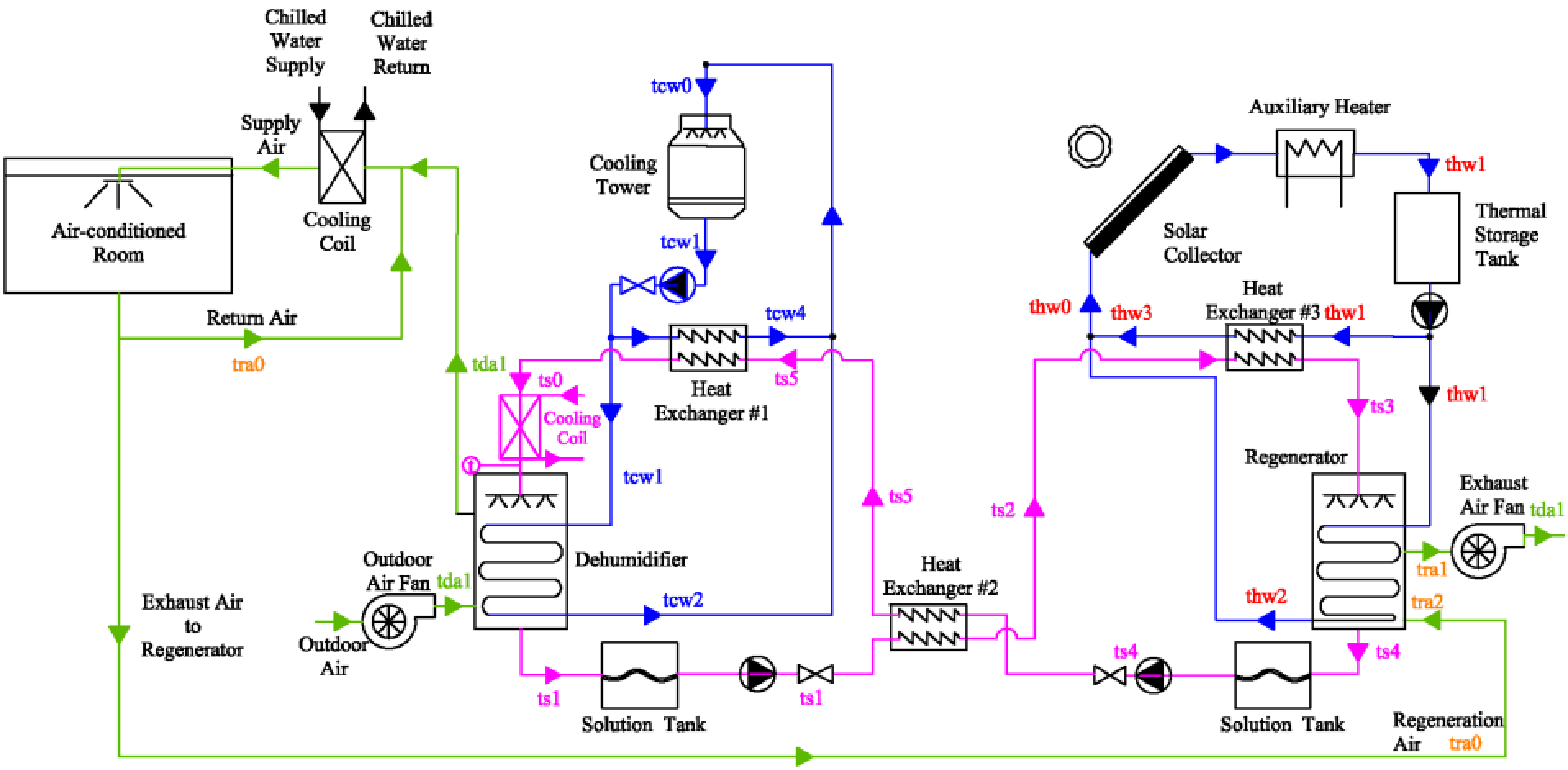

Fig. 8. 15 Schematic diagram of optimized SLDAC: Case 1

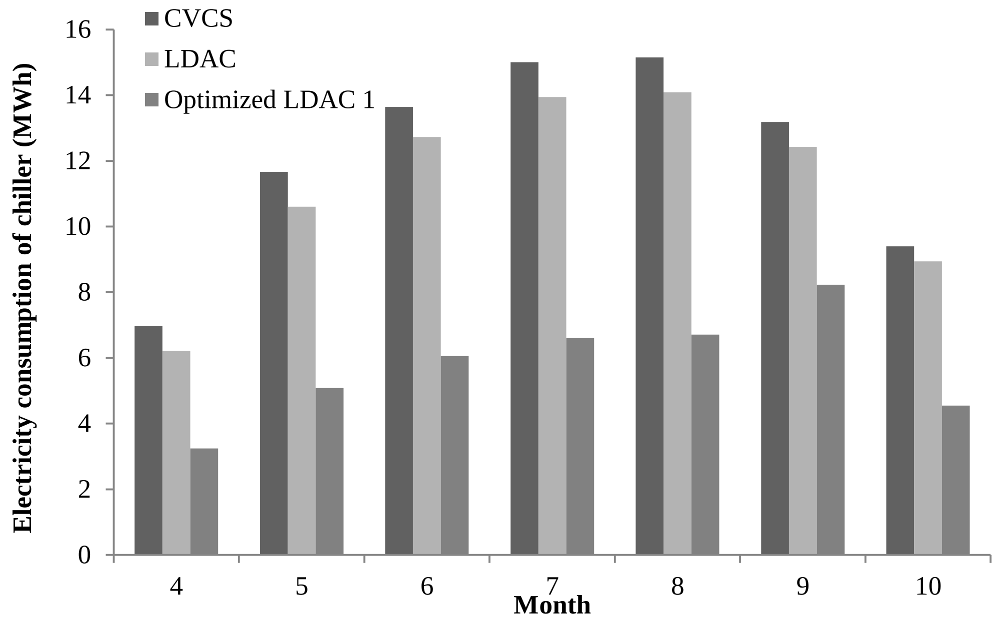

Fig. 8. 16 Monthly electricity consumption of the chiller in CVCS, LDAC and optimized LDAC

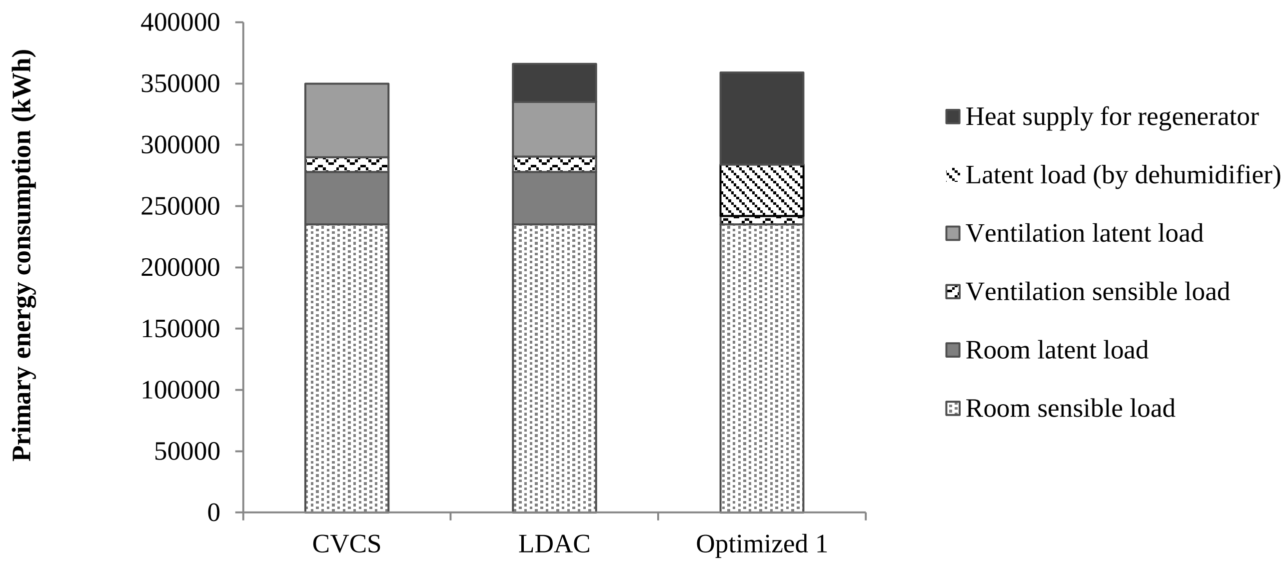

Fig. 8. 17 Annual primary energy consumption of CVCS, LDAC and optimized LDAC 1

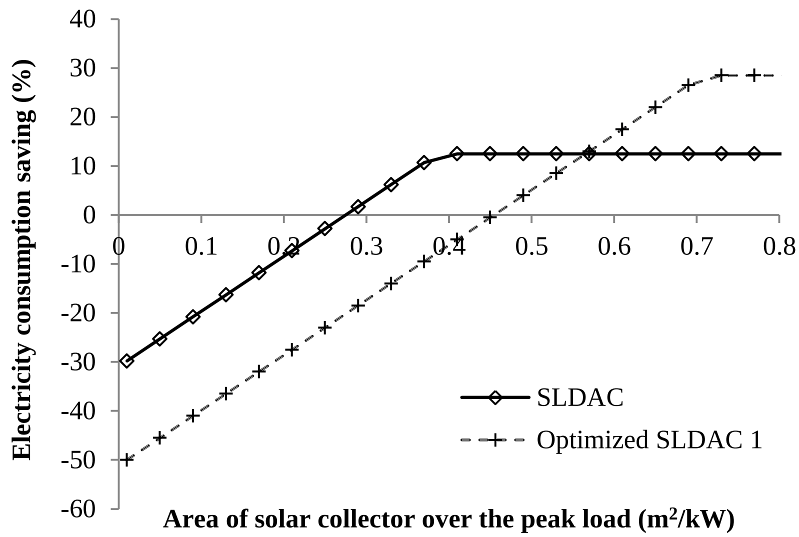

Fig. 8. 18 Energy saving percentages of optimized SLDAC with different installed solar collector areas

8.4.2 Optimization of the addition of auxiliary heat exchanger

By introducing an extra cooling coil to reduce the inlet solution temperature of the dehumidifier, the electricity energy consumption of the SLDAC system could be significantly reduced. But, the minimum installation area of solar collectors increased about 60% due to the enlargement of thermal energy required during the regeneration process. To solve this problem, an auxiliary heat exchanger was added to the system, which was indicated as the heat exchanger #4 in Fig. 8.19.

With this heat exchanger, the desiccant temperature entering the internally heated regenerator could be improved with the hot water leaving the regenerator, and the regeneration efficiency could be enhanced. Furthermore, the lower temperature water leaving the exchanger also benefits the efficiency of solar collectors. Taking a typical day in July as an example, compared to the situation without the heat exchanger #4, the water temperature entering the solar collector decreased from 47.3 to 37.6℃, and the collector efficiency was enhanced by around 17.1%.

As shown in Fig. 8.20, compared to the optimized LDAC case 1, the primary energy demand was 4.4% lower in this system with the extra heat exchanger. Although the primary energy saving ratio was not large, with the combined impact of less energy demand and higher solar collector efficiency, the performance of the solar-assisted system could be effectively improved. The saving percentage of electricity consumption of the optimized case 2 could be found in Fig. 8.21. With the introduction of the heat exchanger #4, the minimum installation area of solar collectors could be effectively decreased, from 0.45 m^2 /kW of case 1 to 0.22 m^2 /kW, and the minimum required area of solar collectors of the office building could be calculated as 72 m^2. Besides saving the installation spaces, the reduction of solar collector area could also further decrease the initial cost of the solar-assisted system.

Furthermore, in this optimization, the maximum energy saving percentage was around 36.7% compared to the conventional vapour compression AC system. If the area of solar collectors is large enough to meet all the heat requirement of the regeneration, the annual electricity consumption of the optimized system case 2 could be 44.6 MWh lower than the CVCS. High energy saving potential could be achieved. According to the electricity tariff of CLP in Hong Kong (HK$ 1.045/ kWh), for this typical office building, around HK$ 468,000 of operation cost for air-conditioning could be saved yearly. Therefore, the optimized SLDAC system is suitable for commercial buildings in Hong Kong.

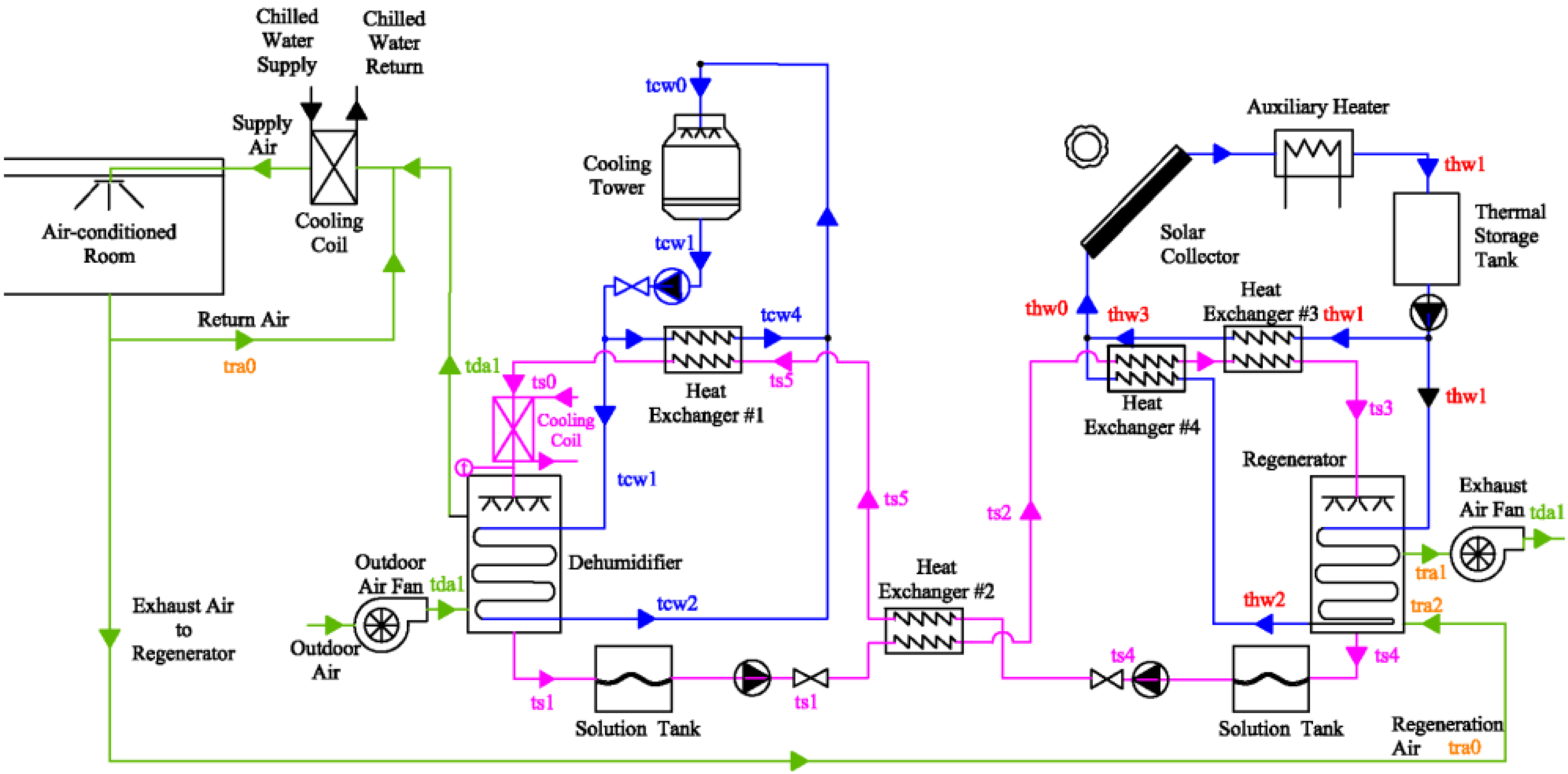

Fig. 8. 19 Schematic diagram of optimized SLDAC: Case 2

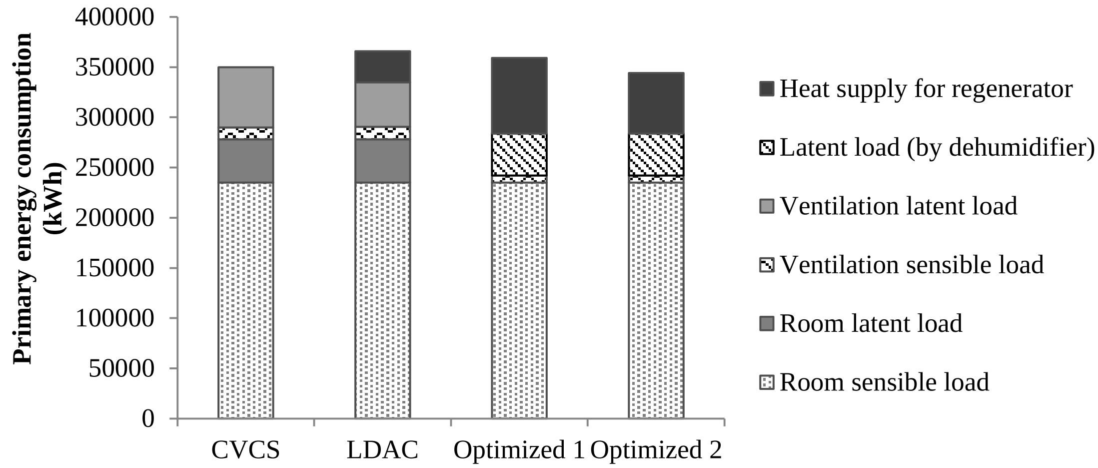

Fig. 8. 20 Annual primary energy consumption of CVCS, optimized LDAC 1 and 2

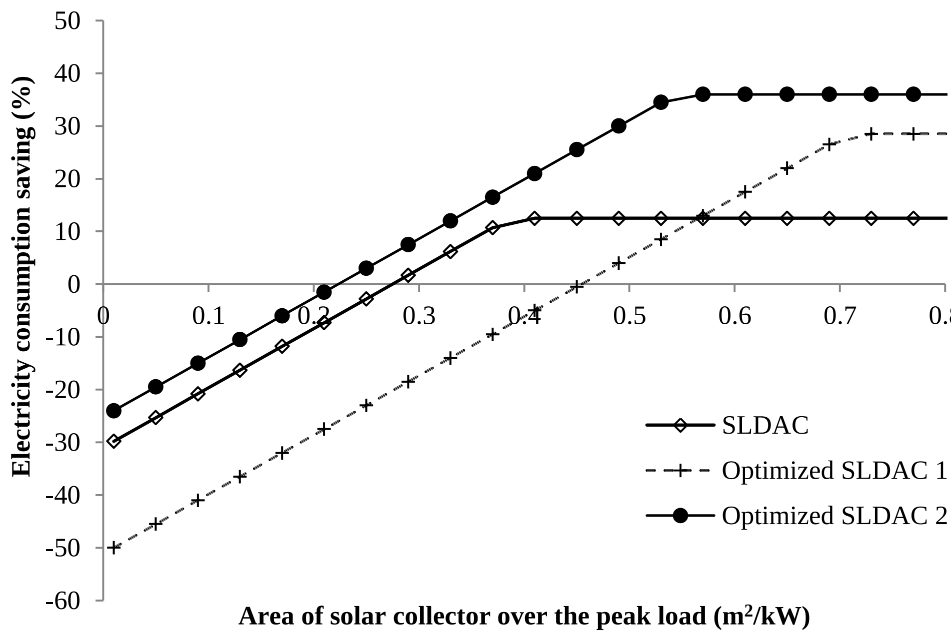

Fig. 8. 21 Energy saving percentage of two optimized SLDAC with different installed solar collector areas

8.4.3 Other optimization methods

Several other optimization methods were also investigated in our research, as shown in Fig. 8.22 and 8.23.

In the optimized system case 3, an indirect heat exchanger #5 was introduced between the outdoor fresh air entering the dehumidifier and the exhaust air entering the regenerator. With the exchanger, the temperature of fresh air could be decreased, which could improve the efficiency of the dehumidifier. Synchronously, the cool exhaust air could be heated to improve the performance of regeneration. In terms of case 4, another heat exchanger #6 was applied to further improve the temperature of exhaust air for the regeneration. The temperature of the process air leaving the dehumidifier could be decreased accordingly. Therefore, the energy consumed in the cooling coil to cool the supply air could be saved.

However, the effects of these two optimization methods were not as obvious as those of the case 1 and 2. As shown in Fig. 8.24, by employing the heat exchanger #5, only 0.66% of thermal energy required for the regeneration could be saved by the improvement of exhaust air temperature. Synchronously, due to the increase of fresh air temperature, around 2.1% of primary energy consumed in the dehumidifier was reduced. Furthermore, in the case 4, as the heat exchange #6 was used, around 0.65% of the regeneration heat consumption could be further saved. As the process air leaving the dehumidifier was cooled by the relative cooler exhaust air from the room, the primary energy demanded by the cooling coil to deal with the sensible load could be decreased about 1.8%.

Therefore, for the optimized system case 3 and 4, the total primary energy consumption was only 0.36% and 0.51% lower than the case 2, respectively. Assuming that all the thermal energy consumed in the regenerator could be supplied with the solar energy, compared with the optimized case 2, around 450 kWh and 594 kWh of electricity consumption could be further reduced annually for case 3 and 4, respectively. With these two optimization methods, the annual operation expense for the air-conditioning system in the office could be reduced by only HK$470 and HK$620. So, these two optimization methods are not recommended.

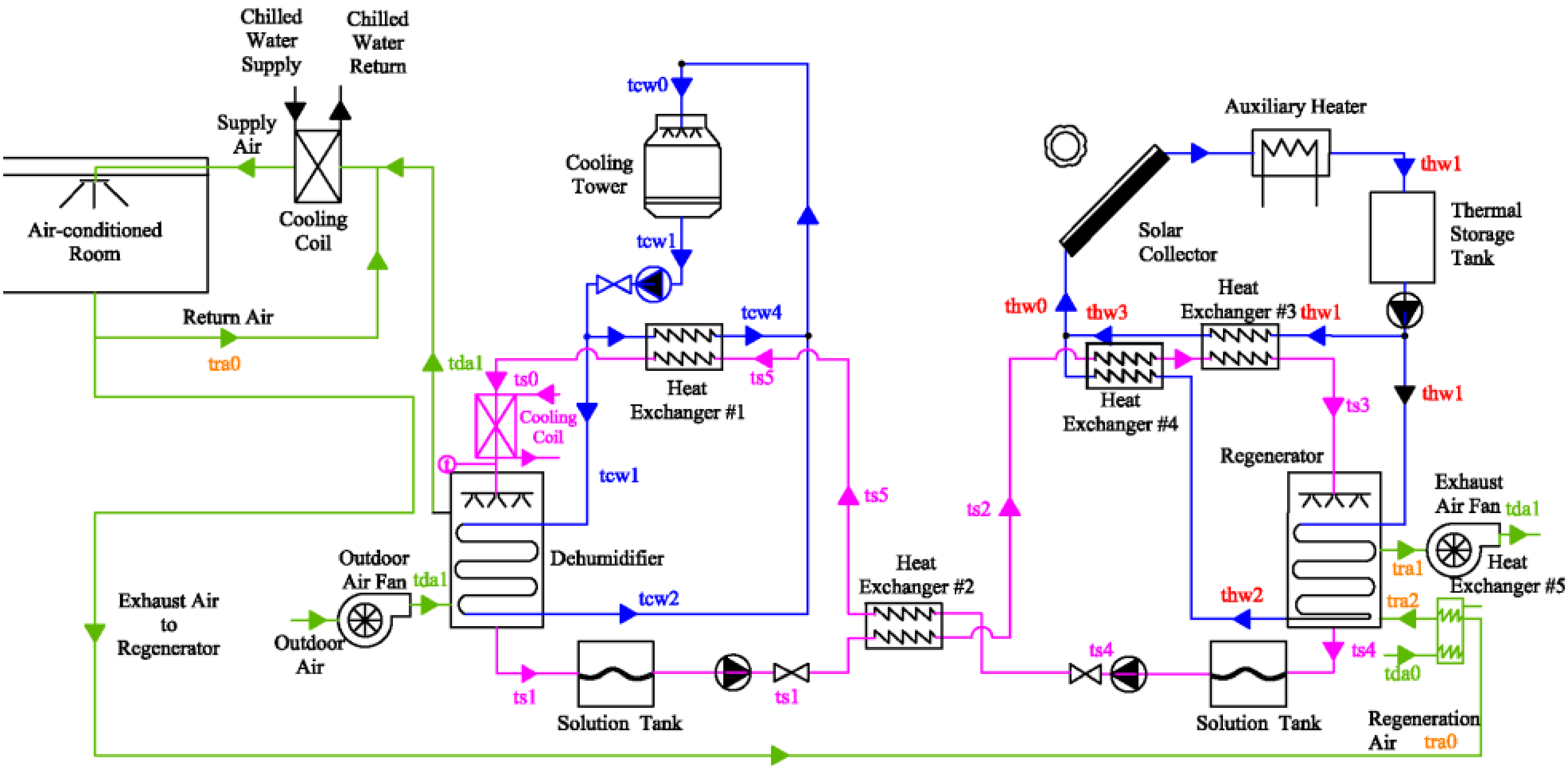

Fig. 8. 22 Schematic diagram of optimized SLDAC: Case 3

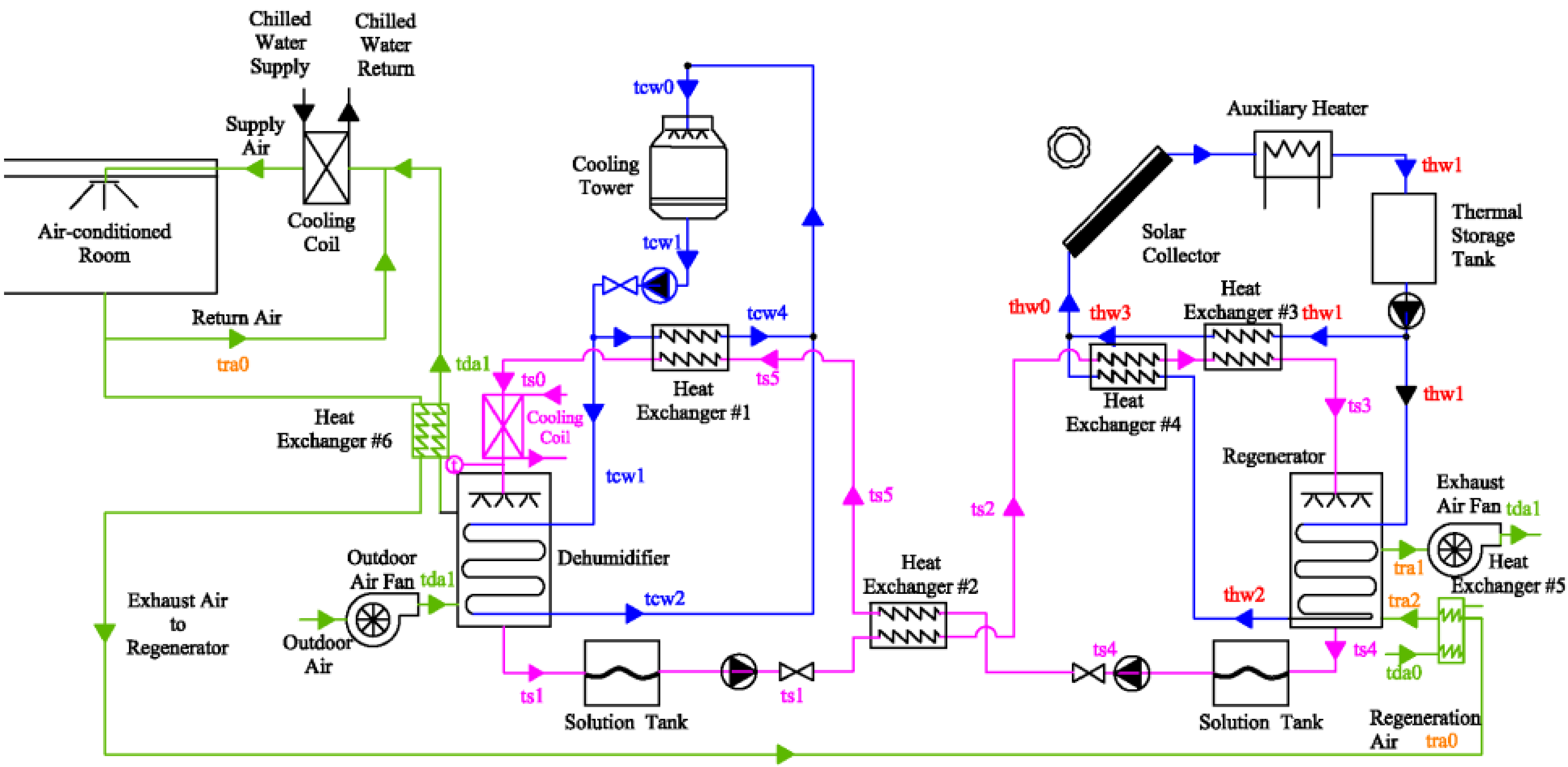

Fig. 8. 23 Schematic diagram of optimized SLDAC: Case 4

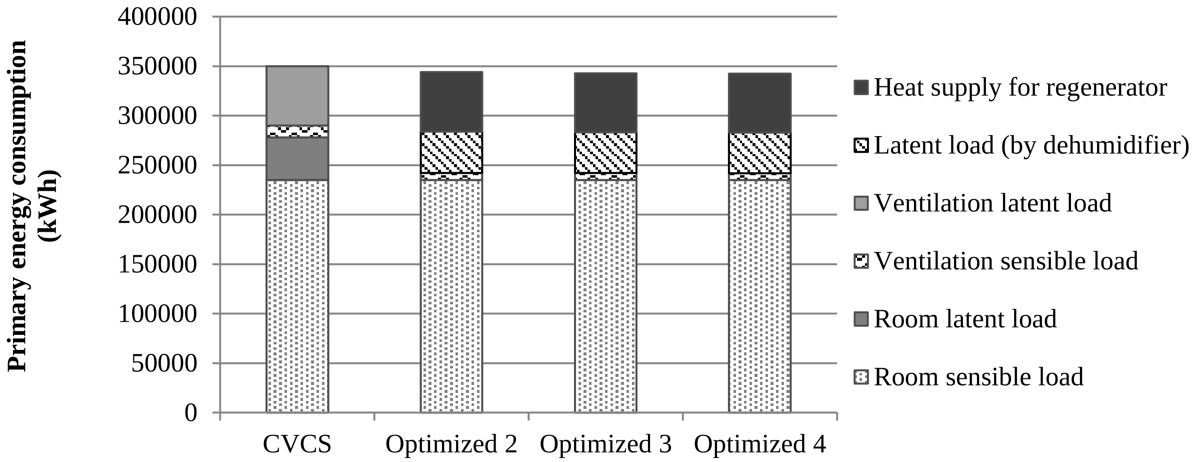

Fig. 8. 24 Annual primary energy consumption of CVCS, optimized LDAC 2, 3 and 4

8.4.4 Discussion

In this section, the energy use performance and saving percentage of different SLDAC systems in the typical commercial office building in Hong Kong were investigated. With the application of the optimized liquid desiccant dehumidification and solar collector, compared to the traditional vapour compression AC system, up to around 37% of total electricity consumption could be saved annually. The electricity saving percentage is affected by the installation area of solar thermal collectors, and there is a minimum installation area for the energy saving.

The graph of electricity saving percentage is a useful reference for designers and engineers to design the SLDAC system and determine the related solar collector installation area in both new and existing commercial buildings in Hong Kong. For example, if the traditional AC system of an office building is planned to be retrofitted to the solar-assisted liquid desiccant dehumidification system for energy saving, according to the peak cooling load, it should be assessed first whether the minimum required installation area for solar thermal collectors could be satisfied. According to Fig. 8.21, assuming the optimized case 2 of SLDAC as the new system, the minimum required area is 0.22 m^2/kW(peak load). If the minimum area cannot be provided, the AC system retrofitting will lead to more energy consumption. If yes, the engineers could determine the design area for solar collectors based on the energy saving target, or calculate the energy saving rate easily with the set area for solar collectors. For example, according to Fig. 8.21, if the energy saving aim was 30%, the required area could be obtained to be about 0.49 m^2/kW(peak load) for the office building.

8.5 Summary

In this chapter, firstly, to evaluate the dynamic operation performance of SLDAC, the AC load profiles of three typical commercial buildings in Hong Kong, i.e. office, hotel and retail buildings, were investigated. With the AC load profiles and local weather data, the operation performance and energy use potential of the SLDAC was investigated and compared with the conventional system. Several optimization methods of the system were provided for energy saving. Additionally, we also studied the impact of climate change on the ventilation load of buildings in Hong Kong during the period from 1950 to 2007.

Results show that the cooling load contributes to more than 98% of the total annual load, with a high latent load proportion from March to September. The high reheating ratio, i.e. from 60%-

90%, is found to be the main reason for the poor indoor thermal comfort, such as the overcool supply air, in these buildings. In the cooling AC load, the ventilation load occupies a large percentage of the latent load, while the major component of sensible load is the space load. Furthermore, due to climate warming, both sensible and latent parts of ventilation load in buildings present an increasing trend, and the latter shows a much higher rate. The serious UHI effect in Hong Kong causes a higher growth rate of the ventilation load at nighttimes, which is about three times compared with that in the daytimes.

Then, by simulating the dynamic operation of the internally cooled/heated SLDAC, due to the high energy demand in the regeneration, the electricity driven LDAC is not suitable for the commercial building, while the solar-assisted system with thermal storage could provide promising energy saving potential. However, with the cooling tower as the only cooling source of the dehumidifier, the dehumidification capacity could not satisfy the requirement and only up to 12.5% of electricity consumption could be saved annually compared to traditional systems. So, several optimization methods were proposed and investigated. By introducing an extra cooling coil for the dehumidifier and a heat exchanger for the regenerator, the electricity saving percentage could be significantly improved to 36.7%. But, the effect of employing two air-air heat exchangers was minor. Furthermore, the energy consumption of the solar-assisted systems is affected by the installation area of solar thermal collectors, and the energy saving could not be achieved until the roof area for solar collector installation is larger than the minimum required value. For our optimized system, the minimum installation area is 0.22 m^2/kW(peak load) for office buildings.

Therefore, the SLDAC system could benefit the commercial buildings locating in warm or hot and humid area most because of the high latent load proportion and abundant solar radiation, and the solar thermal storage and optimization system are strongly suggested. The results and conclusions can be useful for researchers, and for local engineers and designers to design or retrofit the AC system for both new and existing commercial buildings.

CHAPTER 9

CONCLUSIONS AND RECOMMENDATIONS FOR FUTURE WORK

This research investigated the heat and mass transfer of the internally heated liquid desiccant regenerator experimentally and theoretically, focusing on the change of wetted area, film thickness and mass transfer coefficient under the insufficient wetting condition. A 3-D theoretical model was developed for evaluating the system performance more accurately. Based on the new model, a simplified model of the liquid desiccant system and a simulation model of the solar-assisted air-conditioning system with desiccant dehumidification were developed, to evaluate the dynamic operation performance numerically under actual conditions. The outcomes of this thesis can effectively help researchers and engineers to predict and evaluate the dehumidification/regeneration process more accurately. The observations, main conclusions and recommendations for future work are summarized in this chapter.

9.1 Conclusions of Experimental Investigations

In practical falling film liquid desiccant systems, the working surface is usually found to be wetted very incompletely by the desiccant. The wetted area and film thickness are key parameters affecting the system performance, and indispensable parameters in the system evaluation and simulation. Furthermore, without the actual wetted area under different conditions, the mass transfer coefficient could not be obtained accurately.

In our experiments, by building and testing a single channel internally heated regenerator, the influencing factors of the wetted area and film thickness were investigated experimentally, as well as their effects on the mass transfer performance. The film area and size under different operation parameters were recorded by a thermal camera, and LiCl was chosen as the solution. It was found that the increase of wetted area benefits the mass transfer performance greatly, while the performance reduced with the increase of solution film thickness. In incomplete wetting conditions, the typical flow shape of solution falling film was a symmetrical tongue type, and the film was contracted along the flow direction. The film area was mainly decided by two parameters: the initial film width and the wetted width along the flow direction. The initial width was affected by the thickness of solution distributor most greatly, and also changed with the contact angle, mass flow rate and temperature of solution desiccant. Furthermore, when the surface was pre-wetted to make it hydrophilic, the contraction of falling film could be effectively weakened, so the film width along the flow direction increased significantly. The increase of plate surface temperature could also reduce the film contraction in the transverse direction, especially for the low solution mass flow rate. The contraction was found to be aggravated with higher solution temperature, but the impact was relatively small. Additionally, the contact angle of solution was experimentally found to be determined by the surface roughness, solution concentration and temperature.

Then, with the single channel regenerator, the influencing factors affecting the mass transfer coefficient under insufficient wetting conditions were investigated. By considering the actual wetted area, although the increase of solution mass flow rate benefited the moisture removal rate, the mass transfer coefficient decreased with a gradually reducing speed. The coefficient also decreased with the increase of solution distributor thickness and solution temperature, and increased with the mass flow rate of air. An empiric formula was developed with the multi linear regression, showing acceptable error with the experiments results

9.2 Conclusions of Theoretical Investigations

Based on the experimental results, for accurately calculating the wetted area of internally heated regeneration, a theoretical model with an analytical solution was developed, by describing the transverse flow caused by the Marangoni effect. The model could be divided into three parts, including the models for initial wetted width, for contact angle and for contraction distance along the flow direction. The calculation results were validated and compared with the experimental ones, and small average errors of 8.8%, 12.3% and 10.8% were reported for the three parts . It was found that the film thickness, plate surface temperature, and the temperature, concentration and contact angle of solution showed significant influences on the wetted area.

Then, a 3-D model of internally heated regeneration was developed for describing the heat and mass transfer among the air, solution and extra hot water in all three directions. The model could solved numerically using the finite-volume method. The insufficient wetting condition, the change of film thickness due to the mass transfer and film deformation, and the effect of contact angle were taken into account. The calculation results were compared with those obtained by other existing theoretical models, and showed a closer trend to the experimental data, especially in the prediction of the influences of solution mass flow rate, hot water temperature and different working surfaces. Besides the outlet parameters of fluids, the film thickness and parameter distribution in the y-z and x-y cross sections could also be calculated in the new model.

The parameter study with the new model showed that the thickness of solution distributor shows the greatest impact on the moisture removal rate, and the change of inlet temperature of solution results in the most obvious change of regeneration efficiency. The changes of solution concentration and hot water temperature also significantly affect the system performance. Although the increase of the mass flow rates of solution, air and hot water benefit the mass transfer, the effect of excessive rates are slight and the energy consumed to deliver the fluids may be wasted. Some suggestions were given for improving the wetted area and optimizing the system performance.

Although the model was developed based on the internally heated regeneration, as the introduction of plate surface temperature, our result are also suitable for the adiabatic liquid desiccant system. Furthermore, considering the similar heat and mass transfer mechanism between the dehumidification and regeneration of liquid desiccant, the newly developed model could also be applied for the dehumidification process.

9.3 Conclusions of Numerical Investigations

Although the 3-D model could predict the system performance more accurately, it is complex and inconvenient for investigating the dynamic operation performance. A simplified prediction model for internally cooled/heated dehumidifier/regenerator was developed numerically by defining three kinds of effectiveness, i.e. enthalpy effectiveness, moisture effectiveness and temperature effectiveness. With the multi linear regressions, the statistical correlations of three kinds of effectiveness were developed, by setting the mass and heat driving forces and other related parameters as variables. The composite differences between our prediction results and those obtained by the theoretical model under more than 250 operation conditions were compared, showing an ACD of 14.7% for dehumidifier and 7.1% for regenerator. With this model, the outlet parameters of solution, air and cooling/heating water could be obtained accurately and directly, without any iteration.

Then, an operation performance simulation model of the whole SLDAC was developed by employing four iteration calculation loops. For obtaining the real temperature of solution and water of the system, the four loops were nested, which means that if the parameter of the outer loop changed, the inter loop had to be re-started and re-valued. For a case study, the AC load profiles of typical commercial buildings in Hong Kong were investigated. With the AC load profiles and local weather data, the operation performance and energy potential of the SLDAC were evaluated and compared with the conventional system.

Results showed that due to the high dehumidification demand in summer, if the cooling tower is used as the only cooling source of the dehumidifier, the dehumidification capacity could not satisfy the requirement and only up to 12.5% of electricity consumption could be saved annually compared to traditional systems. But, by introducing an extra cooling coil for the dehumidifier and a heat exchanger for the regenerator, the electricity saving percentage could be significantly improved to 36.7%. The energy consumption of solar-assisted system is affected by the installation area of solar thermal collectors, and the energy saving could not be achieved until the available roof area for solar collector installation is larger than the minimum required value. For the case study, the minimum installation area is 0.22 m^2/kW (peak load) for office buildings.

Academically, this research developed a 3-D theoretical model for predicting the heat and mass transfer of falling film liquid desiccant system more accurately. The newly developed models for calculating the wetted area, film thickness and mass transfer coefficient during the dehumidification/regeneration process in the internally cooled/heated and adiabatic systems were also proposed. This provides a useful reference for researchers and engineers to improve the wetted area and optimize the system performance, such as changing the working surface property and adding additive into the desiccant to enhance the heat and mass transfer. Furthermore, as the falling liquid film are widely employed in many industrial applications, such as vertical condensers, film evaporators, absorption towers and heat exchangers, our results could be also applied for the performance evaluation and optimization in these areas.

9.4 Recommendations for Future Work

It must be recognized that there is some insufficiency in this study due to time limitation. The heat and mass transfer of falling film systems applies widely in engineering projects and scientific applications. It is worthwhile and necessary to do further research on this topic.

During our experiments, it was observed that the surface of falling film was not smooth but had many small waves due to the gradients of surface temperature and concentration. The waves would change the film thickness, and may significantly influence the heat and mass transfer performance of liquid desiccant systems (Killion and Garimella, 2001; Chang and Demekhin, 2002). However, because of the limitation of present experiments, the waves and unstable film thickness under different operation conditions were seldom reported, and its influence was neglected in the development of the theoretical model of wetted area, formula of mass transfer coefficient and the 3-D model for the falling film regeneration. Therefore, to understand the falling film liquid desiccant system more accurately, it is recommended to improve an experimental rig for investigating the dynamic change of waves on the film surface and the dynamic film deformation under different operation parameters. The heat and mass transfer performance and coefficients during the dehumidification/regeneration process would also be observed and calculated.

As the inherent instability on the film surface in both transverse and flow directions should be considered, the 3-D theoretical model is suggested to be improved from the existing steady-state form into the unsteady-state one, and the change of parameters with the time should be solved. The liquid velocities in all flow, thickness and transverse directions inside the falling film should also be calculated. Additionally, the impacts of the fluctuation of the inlet parameters should be also considered in the new model.

Furthermore, although there are several types of practical internally cooled/heated units, for developing the model, the composition was simplified as the double plate in this research. For the future study, the heat and mass transfer during the dehumidification/regeneration process of other types can be studied, such as fin exchangers, tubes and corrugated surfaces. In addition, in our research, the distribution method of solution was simplified as the falling film, and the thermal and mass transfer between dispersed desiccant droplets and air was ignored. This should also be studied, especially for liquid desiccant systems with spray nozzles.

Additionally, for the solar-assisted air-conditioning system with the desiccant dehumidification, an actual system should be built to investigate its performance under the actual operation conditions. Different system operation control strategies and optimization methods for the SLDAC system should be numerically simulated for improving its feasibility in practical applications.

REFERENCES

A. Ali, K. Vafai, A.-R.A. Khaled. Analysis of heat and mass transfer between air and falling film in a cross flow configuration. International Journal of Heat and Mass Transfer, 47(4) (2004): 743-55.

A. Ertas, P. Gandhidasan, et al. Experimental study on the performance of a regeneration tower for various climatic conditions. Solar Energy, 53(1) (1994): 125-130.

A. Kakabayev, Absorption solar regeneration unit with open regeneration of solution. Applied Solar Energy, 5(4) (1969): 69-72.

A. Lowenstein, D. Novosel, The seasonal performance of a liquiddesiccant air conditioner, ASHRAE Transactions, 101 (1) (1995): 679-685.

A. Miyara. Numerical simulation of wavy liquid film flowing down on a vertical wall and an inclined wall. International Journal of Thermal Science, 39 (2000): 1015-27.

A. Shahab. Performance of a solar liquid desiccant air conditioner - An experimental and theoretical approach. Solar Energy, 2008, 82(6): 563-572.

A.A. Chowdhury, M.G. Rasul, M.M.K. Khan. Thermal-comfort analysis and simulation for various low-energy cooling-technologies applied to an office building in a subtropical climate. Applied Energy, 85 (6) (2008): 449-462.

A.A. Farayedhi, A.P. Gandhidasan, et al. Regeneration of liquid desiccants using membrane technology. Energy Conversion and Management, 40(13) (1999): 1405-1411.

A.E. Kabeel, Augmentation of the performance of solar regenerator of open absorption cooling system, Renewable Energy, 30 (3) (2005): 327-338.

A.G. Queiroz, A.F. Orlando, et al. Performance Analysis of an Air Drier for a Liquid Dehumidifier Solar Air Conditioning System. Journal of Solar Energy Engineering , 110(2) (1998): 120-124

A.M. Wu, H.F. Zhang. Mathematical model and performance analysis of an internally cooled liquid desiccant dehumidifier. Acta Energiae Solaris Sinica, 29 (7) (2008): 843-848 [in Chinese].

A.Y. Khan, Cooling and dehumidification performance analysis of internally-cooled liquid desiccant absorbers, Applied Thermal Engineering, 18(5) (1998): 265-281.

A.Y. Khan. J.L. Martinez. Modelling and parametric analysis of heat and mass transfer performance of a hybrid liquid desiccant absorber. Energy Conversion and Management, 1998, 39(10): 1095-1112.

ASHRAE Handbook, Volume Fundamentals, 2009.

C.D. Park, T. Nosoko, S. Gima, S.T. Ro. Wave-augmented mass transfer in a liquid film falling inside a vertical tube. International Journal of Heat and Mass Transfer, 47(2004): 2587-2598.

C.H. Liang, L.Z. Zhang, L.X. Pei. Independent air dehumidification with membrane-based total heat recovery: modeling and experimental validation. International Journal of Refrigeration, 33(2) (2010): 398-408.

C.Q. Ren, M. Tu, H.H. Wang. An analytical model for heat and mass transfer processes in internally cooled or heated liquid desiccant-air contact units. International Journal of Heat and Mass Transfer, 50(17) (2007): 3545-3555.

C.S.K. Ahmed, P. Gandhisan, A.A. Al-Farayedhi, Simulation of a hybrid liquid desiccant based air-conditioning system, Applied Thermal Engineering, 17 (2) (1997): 125-134.

C.S.P. Peng, J.R. Howell. Analysis and Design of Efficient Absorbers for Low-Temperature Desiccant Air Conditioners. Journal of Solar Energy Engineering, 103(1) (1981): 67-74.

D. Pietruschka, U. Eicker, M. Huber, Schumacher J. Experimental performance analysis and modelling of liquid desiccant cooling systems for air conditioning in residential buildings. International Journal of Refrigeration, 29(1) (2006): 110-124.

D.A. Goussis, R.E. Kelly, Effects of viscosity variation on the stability of a liquid film flow down heated or cooled inclined surfaces: Finite wavelength analysis, Physics of Fluids 30(1987): 974-982.

F.Xiao, G.M. Ge, X.F. Niu, Control performance of a dedicated outdoor air system adopting liquid desiccant dehumidification, Applied Energy, 88 (1) (2011): 143-149.

F. Zhang, D.L. Tang, J. Geng, Z.X. Wang, Z.B. Zhang. Study on the temperature distribution of heated falling liquid films. Physica D: Nonlinear Phenomena, 237(7) (2008): 867-872.

F. Zhang, Z.B. Zhang, J. Geng. Study on shrinkage characteristics of heated falling liquid films. AIChE Journal, 51(11) (2005): 2899-2907.

F.A.Al-Sulaiman, Gandhidasan P, et al. Liquid desiccant based two-stage evapourative cooling system using reverse osmosis (RO) process for regeneration. Applied Thermal Engineering, 27(14-15) (2007): 2449-2454.

F.K. Wasden, A. E. Dukler, A numerical study of mass transfer in free falling wavy films, AIChE Journal, 36 (9) (1990): 1379-1390.

F.W.H. Yik, J. Burnett, et al., Predicting air-conditioning energy consumption of a group of buildings using different heat rejection methods, Energy and Buildings, 33(2) (2001): 151-166.

G. Lychnos, P.A. Davies, Modelling and experimental verification of a solar-powered liquid desiccant cooling system for greenhouse food production in hot climates, Energy, 40(2012): 116-130.

G. Scalabrin, G. Scaltriti. A Liquid Sorption-Desorption System for Air Conditioning With Heat at Lower Temperature. Journal of Solar Energy Engineering, 112(2) (1990): 70-75.

G.M. Ge, F. Xiao, X.F. Niu, Control strategies for a liquid desiccant air-conditioning system, Energy and buildings, 43(6) (2011): 1499-1507.

G.M. Ge, F. Xiao, X.H. Xu, Model-based optimal control of a dedicated outdoor air-chilled ceiling system using liquid desiccant and membrane-based total heat recovery, Applied Energy, 88 (11) (2011): 4180-4190.

H.-C. Chang, E. A. Demekhin, Complex Wave Dynamics on Thin Films, Elsevier, New York (2002), Vol. 402.

H.M. Factor, G. Grossman. A packed bed dehumidifier/regenerator for solar air conditioning with liquid desiccants. Solar Energy, 24(6) (1980): 541-550.

H.M. Hellmann, G. Grossman. Simulation and analysis of an open-cycle dehumidifier-evapourator-regenerator (DER) absorption chiller for low-grade heat utilization. International Journal of Refrigeration, 18(3) (1995): 177-189.

H.M.Henning, Solar assisted air conditioning of buildings - an overview, Applied Thermal Engineering, 27 (10) (2007): 1734-1749.

Hong Kong Government, Hong Kong Energy Statistics, Census and Statistics Department, 1989-2000.

Hong Kong Government, Code of Practice for overall thermal transfer value in buildings, 1995.

Hong Kong Government, Hong Kong Building Energy Code, 2005 Edition, 2005.

Hong Kong Government, Hong Kong energy statistics annual report, Census and Statistics Department, 1979-2009.

Hong Kong Government, Performance-based Building Energy Code, 2003 edition, Electrical and Mechanical Services Department, 2003.

Hong Kong Government, Hong Kong Energy Statistics. Census and Statistics Department, 1989-2000.

Hong Kong Government, Hong Kong Monthly Dig. of Statistics. Census and Statistics Department, 1989-2000.

J. Geng. Influence of Marangoni Effect on Distillation in Packing Tower. PhD Dissertation. Nanjing, China: Nanjing University; 2002.

J.C. Lam, Building envelope loads and commercial sector electricity use in HongKong, Energy, 20(3) (1995): 189-194.

J.C. Lam, K.K.W Wan, et al. Long-term trends of heat stress and energy use implications in subtropical climates. Applied Energy, 87(2) (2010): 608-612.

J.C. Lam, K.K.W. Wan, T.N.T. Lam. An analysis of future building energy use in subtropical Hong Kong, Energy, 35(3) (2010): 1482-1490.

J.R. Howell, E.C.H. Bantel, Design of liquid desiccant dehumidification and cooling systems. In: Solar Energy Utilization, NATO Advanced Science Institute Series, Martinus Nijhoff Publishers (1987): 374-386.

J.V. Kaudinya, S.C. Kaushik. Experimental validation of theoretical studies on open and forced flow solar regenerator. International Journal of Solar Energy, 4 (1986): 13-33.

K.F. Fong, C.K. Lee, T.T. Chow, et al., Investigation on solar hybrid desiccant cooling system for commercial premises with high latent cooling load in subtropical Hong Kong, Applied Thermal Engineering, 31(16) (2011): 3393-3401.

K.K.W. Wan, D.H.W. Li, et al. Assessment of climate change impact on building energy use and mitigation measures in subtropical climates. Energy, 36(3) (2011): 1404-1414.

K.K.W. Wan, D.H.W. Li, et al., Future trends of building heating and cooling loads and energy consumption in different climates, Building and Environment, 46(1) (2011): 223-234.

K.L.M. Moran. Experimental study of laminar liquid films Falling on an inclined plate. Master Dissertation. Toronto, Canada: University of Toronto; 1997.

K.R. Morison, Q.A.G. Worth, N.P. O'dea, Minimum Wetting and Distribution Rates in Falling Film Evapourators, Food and Bioproducts Processing, 84 (4) (2006): 302-310.

K.W. Mui, L.T. Wong, L.Y. Law. An energy benchmarking model for ventilation systems of air-conditioned offices in subtropical climates. Applied Energy, 84 (1) (2007): 89-98.

L.C.S. Mesquita. S.J. Harrison, D. Thomey. Modeling of heat and mass transfer in parallel plate liquid-desiccant dehumidifiers. Solar Energy, 80 (2006): 1475-1482.

L.T. Wong, K.W. Mui. A transient ventilation demand model for air-conditioned offices, Applied Energy, 85(7) (2008): 545-554.

L.Z. Zhang, Energy performance of independent air dehumidification systems with energy recovery measures, Energy, 31 (8-9) (2006): 1228-1242.

L.Z. Zhang, J.L. Niu, Energy requirements for conditioning fresh air and the long-term savings with a membrane-based energy recovery ventilator in Hong Kong, Energy, 26(2) (2001): 119-135.

L. Zhang, E.Hihara, F.Matsuoka, C.B. Dang, Experimental analysis of mass transfer in adiabatic structured packing dehumidifier/regenerator with liquid desiccant, International Journal of Heat and Mass Transfer, 53 (13–14) (2010): 2856-2863.

M. Bojic, F. Yik. Cooling energy evaluation for high-rise residential buildings in Hong Kong. Energy and Buildings, 2005, 37(4): 345-351.

M.R. Conde, Properties of aqueous solutions of lithium and calcium chlorides: formulations for use in air conditioning equipment design, International Journal of Thermal Sciences, 43(4) (2004): 367-382.

M.S. Park, J.R. Howell, G.C. Vliet, J. Peterson, Numerical and experimental results for coupled heat and mass transfer between a desiccant film and air in cross-flow, International Journal of Heat and Mass Transfer, 37 (1994): 395-402.

M.V. Rane, M.V. Kota Reddy, J.S. Bajaj, Cooling and dehumidification using liquid desiccant, in: Proceedings of the International Sorption Heat Pump Conference, Shanghai, China, 2002: 414-418.

N. Audah, N. Ghaddar, et al. Optimized solar-powered liquid desiccant system to supply building fresh water and cooling needs. Applied Energy, 88(11) (2011): 3726-3736.

O.A. Kabov, B. Scheid, I.A. Sharina, J.C. Legros. Heat transfer and rivulet structures formation in a falling thin liquid film locally heated. International Journal of thermal science, 427 (2002): 664-672.

P. Gandhidasan, A simplified model for air dehumidification with liquid desiccant, Solar Energy, 76 (4) (2004): 409-416.

P. Gandhidasan, Quick performance prediction of liquid desiccant regeneration in a packed bed, Solar Energy, 79 (1) (2005): 47-55.

P. Gandhidasan, Reconcentration of aqueous solutions in a packed bed: a simple approach, Transactions of the ASME Journal of Solar Energy Engineering, 112 (1990): 268-272.

P.C.H. Yu, W.K. Chow, Energy use in commercial buildings in Hong Kong, Applied Energy, 69(4) (2001): 243-255.

P.N. Yoshimura, T. Nosoko, T. Nagata, Enhancement of mass transfer into a falling laminar liquid film by two-dimensional surface waves—some experimental observations and modeling, Chemical Engineering Science, 51(8) (1996) 1231-1240

Q.Y. Zhang, C.Z. Lou, H.X. Yang. Trends of Climate Change and Air-Conditioning Load of Residential Buildings in China. Journal of Asian Architecture and Building Engineering, 5(2) (2006): 435-441 .

R. Giridharan, S. Ganesan, et al. Daytimes urban heat island effect in high-rise and high-density residential developments in Hong Kong. Energy and Buildings, 36(6) (2004): 525-534.

R. Giridharan,S.S.Y Lau, et al. Nocturnal heat island effect in urban residential developments of Hong Kong. Energy and Buildings, 37(9) (2005): 964-971.

R. Giridharan,S.S.Y Lau, et al. Urban design factors influencing heat island intensity in high-rise high-density environments of Hong Kong. Building and Environment, 42(10) (2007): 3669-3684.

R.A. Memon, D.Y.C. Leung, et al. An investigation of urban heat island intensity (UHI) as an indicator of urban heating. Atmospheric Research, 94(3) (2009): 491-500.

R.A. Memon, D.Y.C. Leung. Impacts of environmental factors on urban heating. Journal of Environmental Sciences, 22(12) (2010): 1903-1909.

R.A. Memon, S. Chirarattananon,P. Vangtook, Thermal comfort assessment and application of radiant cooling: A case study, Building and Environment, 43 (7) (2008): 1185-1196.

S. Alizadeh, W.Y. Saman. An experimental study of a forced flow solar collector/regenerator using liquid desiccant. Solar Energy, 73(5) (2002): 345-362.

S. C. M.Hui. Solar Hong Kong - present applications and future prospects. Renewable Energy World, 3(1) (2000): 76-83.

S. Jain, P.K. Bansal. Performance analysis of liquid desiccant dehumidification systems.International Journal of Refrigeration, 30(5) (2007): 861-872.

S. Jain, P.L. Dhar, S.C. Kaushik, Experimental studies on the dehumidifier and regenerator of a liquid desiccant cooling system, Applied Thermal Engineering, 20 (2000): 253-267.

S. Lang, Current situation and progress of energy efficiency design standards in buildings in China. Refrigeration Air Conditioning & Electric Power Machinery, 23 (2002): 1-6 [in Chinese].

S.A. Abdul-Wahab, Y.H. Zurigat, M.K. Abu-Arabi, Predictions of moisture removal rate and dehumidification effectiveness for structured liquid desiccant air dehumidifier, Energy, 29 (1) (2004): 19-34.

S.A. Al-Sanea, M.F. Zedan. Optimized monthly-fixed thermostat-setting scheme for maximum energy-savings and thermal comfort in air-conditioned spaces. Applied Energy, 85(5) (2008): 326-46.

S.K. Chaudhari,K.R. Patil. Thermodynamic properties of aqueous solutions of lithium chloride. Physics and Chemistry of Liquids, 40(3) (2002): 317-325.

S.K. Wilson, B.R. Duffy, On the gravity-driven draining of a rivulet of fluid with temperature-dependent viscosity down a uniformly heated or cooled substrate, Journal of Engineering Mathematics, 42(2002): 359-372.

S.L. Wong, K.K.W. Wan, et al. Impact of climate change on residential building envelope cooling loads in subtropical climates. Energy and Buildings, 42(11) (2010): 2098-2103.

S.M. Deng, Energy and water uses and their performance explanatory indicators in hotels in Hong Kong, Energy and Buildings, 35(8) (2003): 775-784.

S.R. Broome, Liquid Distribution And Falling Film Wetting In Dairy Evapourators. Master Dissertation. Christchurch, New Zealand: University of Canterbury; 2005.

S.V. Potniz, T.G. Lenz. Dimensionless mass transfer correlations for packed-bed liquid-desiccant contactors. Industrial and Engineering Chemistry Research, 35 (1996): 4185-4419.

T. Katejanekarn, S. Chirarattananon, et al. An experimental study of a solar-regenerated liquid desiccant ventilation pre-conditioning system. Solar Energy, 83(6) (2009): 920-933.

T. Katejanekarn, S. Kumar. Performance of a solar-regenerated liquid desiccant ventilation pre-conditioning system. Energy and Buildings, 40(7) (2008): 1252-1267.

T.N.T Lam, K.K.W. Wan, et al. Impact of climate change on commercial sector air conditioning energy consumption in subtropical Hong Kong. Applied Energy, 87(7) (2010): 2321-2327.

T.T. Chow, A.L.S. Chan, K.F. Fong, Lin Z, Hong Kong solar radiation on building facades evaluated by numerical models, Applied Thermal Engineering, 25 (13) (2005): 1908-1921.

T.W. Chung, C.M. Luo, Vapour pressures of the aqueous desiccants, Journal of Chemical and Engineering, 44(1999) 1024-1027.

T.W. Chung, T.K. Ghosh, A.L. Hines, et al., Dehumidification of moist air with simultaneous removal of selected indoor pollutants by triethylene glycol solutions in a packed-bed absorber, Separation Science and Technology, 30(7-9) (1995):1809-1832.

T.W. Chung. Predictions of moisture removal efficiencies for packed-bed dehumidification systems. Gas Separation & Purification, 8 (4) (1994): 265-268.

U. Eicker, D. Schneider, J. Schumacher, et al., Operational experiences with solar air collector driven desiccant cooling systems. Applied Energy, 87 (12) (2010): 3735-3747.

V. Martin, D.Y. Goswami. Heat and mass transfer in packed bed liquid desiccant regenerators-an experimental investigation. Transactions of the ASME Journal of Solar Energy Engineering, 121(1990): 162-170.

W. Kessling, E. Laevemann, C. Kapfhammer, Energy storage for desiccant cooling systems component development, Solar Energy, 64(4-6) (1998): 209-221.

W.Y. Fung, K.S. Lam, et al. Impact of urban temperature on energy consumption of Hong Kong. Energy, 31(14) (2006): 2623-2637.

W.Y. Saman, S. Alizadeh, An experimental study on a cross-flow type plate heat exchanger for dehumidification/cooling, Solar Energy, 73 (2002): 59-71.

W.Z. Gao, J.H. Liu, Z.M. Wu, et al., Experimental Analyse of Regeneration Performance of Solar Liquid Desiccant Air-Conditioning System, Acta Energiae Solaris Sinica, 30(6) (2009): 744-748 [In Chinese].

X.H. Liu, X.M. Chang, J.J. Xia, Y. Jiang. Performance analysis on the internally cooled dehumidifier using liquid desiccant. Building and Environment, 44(2) (2009): 299-308.

X.H. Liu, Y. Jiang, et al., Experimental investigation of the heat and mass transfer between air and liquid desiccant in a cross-flow regenerator, Renewable Energy, 32(10) (2007): 1623-1636.

X.H. Liu, Y. Jiang, K.Y. Qu, Heat and mass transfer model of cross flow liquid desiccant air dehumidifier/regenerator, Energy Conversion and Management, 48 (2)(2007) 546-554.

X.H. Liu, Z. Li, Y. Jiang, B.R. Lin. Annual performance of liquid desiccant based independent humidity control HVAC system. Applied Thermal Engineering: 26(11-12) (2006): 1198-207.

X.W. Li, X.S. Zhang. Photovoltaic-electrodialysis regeneration method for liquid desiccant cooling system. Solar Energy, 83(12) (2009): 2195-2204.

X.Y. Chen, Y. Jiang,Z. Li, et al., An introduction of independent humidity control system with liquid desiccant air conditioner, in: Proceedings of the 4th International Symposium on HVAC, Beijing, China, October, 2003: 1042-1049.

Y. Gao, H. Zhang, S.J. You, et al., Experiment of mass transfer coefficient in regeneration of liquid desiccant using evapourative condenser, Journal of HV&AC, 42(1) (2012): 65-68. [In Chinese].

Y. Huang, J.L. Niu, T.M. Chung, Energy and carbon emission payback analysis for energy-efficient retrofitting in buildings—Overhang shading option, Energy and Buildings, 44 (2012): 94-103.

Y.G. Yin, X.S. Zhang, Comparative study on internally heated and adiabatic regenerators in liquid desiccant air conditioning system, Building and Environment, 45(8) (2010): 1799-1807.

Y.G. Yin, X.S. Zhang, D.G. Peng, X.W. Li. Model validation and case study on internally cooled/heated dehumidifier/regenerator of liquid desiccant systems. International Journal of Thermal Sciences, 48(8)(2009): 1664-1671.

Y.G. Yin, X.S. Zhang, G. Wang, et al., Experimental study on a new internally cooled/heated dehumidifier/regenerator of liquid desiccant systems, International Journal of Refrigeration, 31 (5) (2008): 857-866.

Y.G. Yin, X.S. Zhang, Z.Q. Chen, Experimental study on dehumidifier and regenerator of liquid desiccant cooling air conditioning system, Building and Environment, 42 (2007): 2505-2511.

Y.J. Dai, R.Z. Wang, H.F. Zhang, et al., Use of liquid desiccant cooling to improve the performance of vapour compression air conditioning, Applied Thermal Engineering, 21(12)(2001): 1185-1202.

Y.T. Li, H.X. Yang. Investigation on solar desiccant dehumidification process for energy conservation of central air-conditioning systems. Applied Thermal Engineering, 28(10) (2008): 1118-1126.

Y.T. Li, L. Lu, H.X. Yang, Energy and economic performance analysis of an open cycle solar desiccant dehumidification air-conditioning system for application in Hong Kong, Solar Energy, 84 (12) (2010): 2085-2095.

Y.T. Li, Study on Solar Liquid Desiccant Dehumidification and Regeneration for Central Air-Conditioning Applications, PhD Thesis, The Hong Kong Polytechnic University, 2008.

Y.M. Luo, S.Q. Shao, F. Qin, C.Q. Tian, H.X. Yang, Investigation on feasibility of ionic liquids used in solar liquid desiccant air conditioning system, Solar Energy, 86 (9) (2012) :2718-2724.

Z.J. Ma, S.W. Wang, Building energy research in Hong Kong: A review, Renewable and Sustainable Energy Reviews, 13 (8) (2009):1870-1883.